THE UNIVERSITY OF CHICAGO

EMERGENT 3D GENOME REORGANIZATION FROM THE STEPWISE ASSEMBLY OF TRANSCRIPTIONAL CONDENSATES IN THE HEAT SHOCK RESPONSE

A DISSERTATION SUBMITTED TO
THE FACULTY OF THE DIVISION OF THE BIOLOGICAL SCIENCES
AND THE PRITZKER SCHOOL OF MEDICINE
IN CANDIDACY FOR THE DEGREE OF
DOCTOR OF PHILOSOPHY

GRADUATE PROGRAM IN CELL AND MOLECULAR BIOLOGY

BY

SARAH PARACHA

CHICAGO, ILLINOIS

DECEMBER 2024

Copyright © 2024 by Sarah Paracha

All rights reserved

TABLE OF CONTENTS

LIST OF FIGURES

ACKNOWLEDGEMENTS

I am deeply grateful to my thesis committee members—Ilaria Rebay, Edwin (Chip) Ferguson, D. Allan Drummond, and Michael Glotzer—for their invaluable guidance and insights throughout this project. My heartfelt thanks go to my advisor, David Pincus, for his steadfast support and mentorship. I am especially thankful to Surabhi Chowdhary for her remarkable contributions and unwavering assistance, which were instrumental in bringing this work to fruition.

I also wish to express my profound gratitude to my husband, Scott, my siblings, and my parents. Their love, encouragement, and support have been the foundation of my journey, making this accomplishment possible.

ABSTRACT

The heat shock response (HSR) is a cellular stress pathway primarily regulated by the transcription factor Hsf1. Traditionally, Hsf1 activation has been viewed as a simple on/off switch, controlled by the chaperone protein Hsp70. However, in this study, I demonstrate that Hsf1 activation is more nuanced: it can function as a graded, tuneable response, modulated by both multivalent interactions with Hsp70 and phosphorylation. During thermal stress, I observed that Hsf1 forms biophysically dynamic clusters with Mediator and RNA Polymerase II (Pol II). These clusters, or condensates, serve as membrane-less hubs that concentrate transcriptional machinery, promoting the efficient expression of HSR target genes. Notably, these condensates facilitate the spatial reorganization of HSR target genes, effectively bringing them together during stress. In mammalian systems, transcriptional condensates are known to enable high-level gene expression, particularly in genes involved in development and cell identity, however, it was unclear whether these condensates are evolutionarily conserved or play a role in 3D genome organization. In this thesis, I identify transcriptional condensates within the yeast HSR, suggesting that they may represent an ancient, adaptable strategy in eukaryotic gene regulation. I also describe the stepwise process of condensate assembly: it begins with Hsf1 partially dissociating from Hsp70, allowing Mediator to bind. Further Hsp70 dissociation and Hsf1 hyperphosphorylation then expose multivalent binding sites that enhance this assembly. However, Hsf1-Mediator condensates alone do not recruit Pol II; Pol II condensation only occurs in response to a separate environmental signal, providing an additional layer of control over Hsf1-regulated genes. These findings highlight the role of HSR transcriptional condensates as flexible regulatory hubs, with full assembly and Pol II recruitment enabling active, long-range interactions across the genome in response to thermal stress. This dynamic, modular process underscores the sophisticated regulation possible within eukaryotic stress responses.

CHAPTER 1

INTRODUCTION

1.1 Condensates, Hsf1, and the HSR

The heat shock response (HSR) is a cellular stress pathway controlled by the transcription factor Hsf1. Under heat stress, Hsf1 forms transcriptional condensates with Mediator and RNA Polymerase II (Pol II), creating clusters that gather key transcriptional machinery and reposition HSR target genes (Chowdhary et al., 2022). This spatial organization facilitates gene expression and suggests that transcriptional condensates are evolutionarily conserved structures. In this thesis, I have determined that condensate assembly is sequential: Hsf1 first partially dissociates from Hsp70, allowing Mediator recruitment, with further Hsp70 dissociation and Hsf1 phosphorylation exposing binding sites for enhanced condensate formation. However, Pol II recruitment requires an additional environmental signal, introducing another layer of gene control. This research proposes that HSR transcriptional condensates function as dynamic, adaptable hubs, with full condensate formation and Pol II recruitment enabling genome-wide reorganization during stress responses.

In this chapter, I will outline the biological concepts, pathways, and molecules that are involved in understanding my research. I will begin by introducing biomolecular condensates, discussing their components, assembly mechanisms, and functional significance. I will then focus on transcriptional condensates, emphasizing their roles in eukaryotic transcription regulation as documented in current literature. Following this, I will provide an overview of the heat shock response (HSR) across different organisms. Finally, I will delve into the regulation and function of Hsf1 in both mammals and yeast, establishing a foundation for this pivotal protein that underpins my thesis research.

1.2 Biomolecular condensates

The cell is a densely packed environment where numerous complex biochemical reactions must occur quickly and consistently. To enhance control over reaction timing and location, cells concentrate specific components, influencing reaction rates and spatiotemporal regulation. Often, these processes are confined to organelles, which are subcellular compartments enclosed by a lipid bilayer membrane. This membrane allows for selective transport and separation from the cell's cytoplasm, creating specialized "factories" for particular functions—like mitochondria for respiration or the endoplasmic reticulum for protein synthesis.

In addition to membrane-bound organelles, cells also contain membrane-less structures called biomolecular condensates, which form through selective clustering of proteins and nucleic acids with shared functions (Banani et al., 2017). Despite their diverse contents, these condensates share several defining features. They are dynamic and heterogeneous (e.g., the nucleolus, which contains three distinct regions), and they concentrate nonstoichiometric assemblies of related biomolecules (Sabari et al., 2020). They exchange components rapidly with their surroundings (Phair & Misteli, 2000) and can merge or split with others of the same type (Altmeyer et al., 2015; Brangwynne et al., 2009; Hyman et al., 2014). Unlike membrane-bound organelles, biomolecular condensates are typically held together by weak, multivalent interactions among their components (Brangwynne et al., 2015; Mulyasasmita et al., 2011; Wong Po Foo et al., 2009).

This section will explore the formation, regulation, and functional roles of biomolecular condensates in cellular organization and gene regulation, highlighting their evolutionary significance and adaptability across eukaryotes. I will further focus on transcriptional condensates and their role in eukaryotic transcriptional regulation, how these condensates are thought to be regulated, and their role in chromatin rearrangement.

1.2.1 Molecular interactions that drive the formation of biomolecular condensates

Multivalent molecules, that is molecules which can undergo inter- and intra-molecular interactions with at least three other factors simultaneously, promote and enrich biomolecular condensates (Banjade & Rosen, 2014; Nott et al., 2015). This multivalence is important because when these biomolecules engage, they undergo a prompt transition from small complexes to large polymeric assemblies with an increase in protein concentration and a decrease in the solubility (Li et al., 2012). Such molecules include proteins and other biopolymers with intrinsically disordered regions (IDRs) (Wong Po Foo et al., 2009) (Figure 1) and structured, repeated modular interaction domains (Mulyasasmita et al., 2011; Sabari et al., 2020) (Figure 1) that can then selectively partition to form condensates.

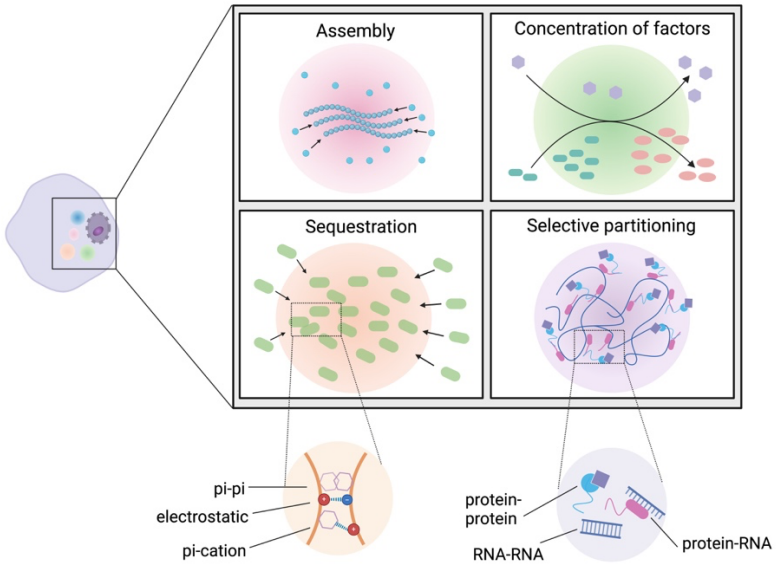

Figure 1.1 *Traits associated with biomolecular condensates and the types of multivalent interactions that contribute to their formation.* **(Top)** Features common to condensates that contribute to their functions. **(Bottom)** Multivalent interactions between the IDRs (left) or the modular domains (right) of proteins and nucleic acids drive the formation of liquid-like condensates in cells. Figure from (Wang et al., 2021).

Proteins with modular domains that can form condensates can be distinguished from proteins that are high affinity and low valence: when the latter interact, this can lead to strong, specific

networks that may result in solid-like precipitations rather than the dynamic, liquid-like polymer assemblies associated with condensates. Modular domain proteins that are involved in condensation within a cell are usually characterized by high valency, modest affinity, and long, flexible connections between binding elements (Jin et al., 2009), (Li et al., 2012). For example, in P-bodies, foci consisting of mRNA degradation machinery, a folded domain of enhancer of mRNA-decapping protein 3 (EDC3) interacts with 10 helical leucine rich motifs in disordered regions of mRNA-decapping enzyme subunit 2 (DCP2) to promote clustering behavior (Fromm et al., 2014).

Conversely, biomolecules with IDRs lack a defined 3D structure in these regions, but often contain repeated sequence elements that enable the establishment of dynamic, weak, non-covalent interactions that promote condensation. IDRs tend to be enriched in few amino acids: glycine, serine, glutamine, asparagine, phenylalanine, and tyrosine, though charged amino acid residues can also be occasionally found (Gilks et al., 2004; Kato et al., 2012; Reijns et al., 2008). Because there is little diversity in sequence, repeated motifs and charge blocks are present in these regions of condensate-promoting molecules (Banjade & Rosen, 2014; Decker et al., 2007; Lin et al., 2015; Pak et al., 2016).

Noncovalent pi-pi interactions can occur within two aromatic residues and pi-cation interactions can occur between an aromatic residue and a cation present on charged amino acids within the IDR or with other IDRs to encourage condensation (Mitrea et al., 2016) (Figure 1). Inter- or intramolecular interactions between oppositely charged blocks in the IDRs of biomolecules can also occur to induce selective partitioning. The patterning of charged residues is important in these cases: for the same net molecular charge, when the charge is evenly distributed condensate formation is suppressed, but when charged residues are grouped together condensation is encouraged (Das & Pappu, 2013; Molliex et al., 2015).

In disease states, such as cancer and neurodegenerative diseases like Alzheimer's and ALS, these multivalent interactions between specific molecules are manipulated so that the condensates take on a more aberrant nature, where the biomolecules can aggregate and solidify, becoming toxic for the cells rather than behaving as an adaptive process that aids in the cell's efficiency and fitness (Guillén-Boixet et al., 2020).

Of course, there are many other interactions that are important in condensate assembly, ranging from base pairing of nucleic acids to post-translational modifications of proteins, that can determine entry or exit from a condensate, but for this thesis I will focus on IDRs and modular proteins as they are the most relevant to my project.

1.2.2 Regulation of condensate assembly

Though condensates may contain hundreds of different types of molecules, their composition can be simplified into two main components, the scaffold and the clients (Banani et al., 2016). Scaffolds behave as regulatory elements which tend to have high valencies, undergoing many interactions with multiple partners to drive the formation of foci. They also behave as the initiating factor for condensate establishment, as the scaffold molecules govern the threshold concentration at which condensates form, and the removal of these molecules is likely to prevent condensate assembly altogether (Ditlev et al., 2018). Scaffolds can form by modular domain interactions, or interactions between the IDRs of these molecules. RNA has also been reported as a scaffold molecule, so the term is not just limited to proteins (Sharp et al., 2022).

Clients are molecules that transiently associate with the condensate without being an integral structural component. They interact in a more peripheral or transient manner, typically participating in the specific biochemical activities occurring within the condensate or serving functional roles, such as catalysing reactions, or participating in signalling pathways. (Alberti & Hyman, 2021).

Modifications that regulate scaffold proteins indirectly also regulate condensate assembly. For example, in the formation of stress granules (a type of condensate), the translation initiation factor eIF2α is phosphorylated upon stress, inhibiting translation (Pavitt, 2005). This releases mRNAs from polysomes and allows the RNA-binding protein G3BP1, which phase separates in the presence of free and unfolded mRNA, to become scaffolds for condensate formation. (Yang et al., 2020). Dephosphorylation of eIF2α allows mRNA translation to resume once the stress has subsided, allowing the stress granules to dissociate (Anderson & Kedersha, 2002). Similarly, binding of a client to a scaffold protein can also determine whether it is able to partition into a condensate or not. When the fusion in sarcoma (FUS) protein, mentioned previously, is bound to its RNA ligand, it remains in a soluble state, but when RNA is depleted from the nucleus, FUS phase separates (Maharana et al., 2018). Chromatin modifications also regulate condensate function, as methylation of histones can lead to the recruitment of heterochromatin factors, while acetylation of histones can expose TF binding sites and the recruitment of transcriptional machinery (Sabari et al., 2020) (Figure 2).

Post-translational modifications of condensate components can regulate condensate formation. In T-cell receptor transduction, phosphorylation of the signaling molecules must first occur to allow their assembly into clusters (Su et al., 2016). Similarly, FUS, an RNA-binding protein involved in transcriptional regulation, can be methylated or phosphorylated to disrupt its ability to form condensates (Hofweber et al., 2018; Monahan et al., 2017). In the nucleus, RNA Polymerase II is involved in two different types of condensates, transcriptional condensates and splicing condensates. The phosphorylation of the C-terminal domain of RNA Pol II by cyclin dependent kinases (CDKs) behaves like a switch, allowing the Pol II to exchange condensates, with hypo-phosphorylated Pol II incorporated into transcriptional foci and hyper-phosphorylated Pol II integrated into the splicing clusters (Guo et al., 2019).

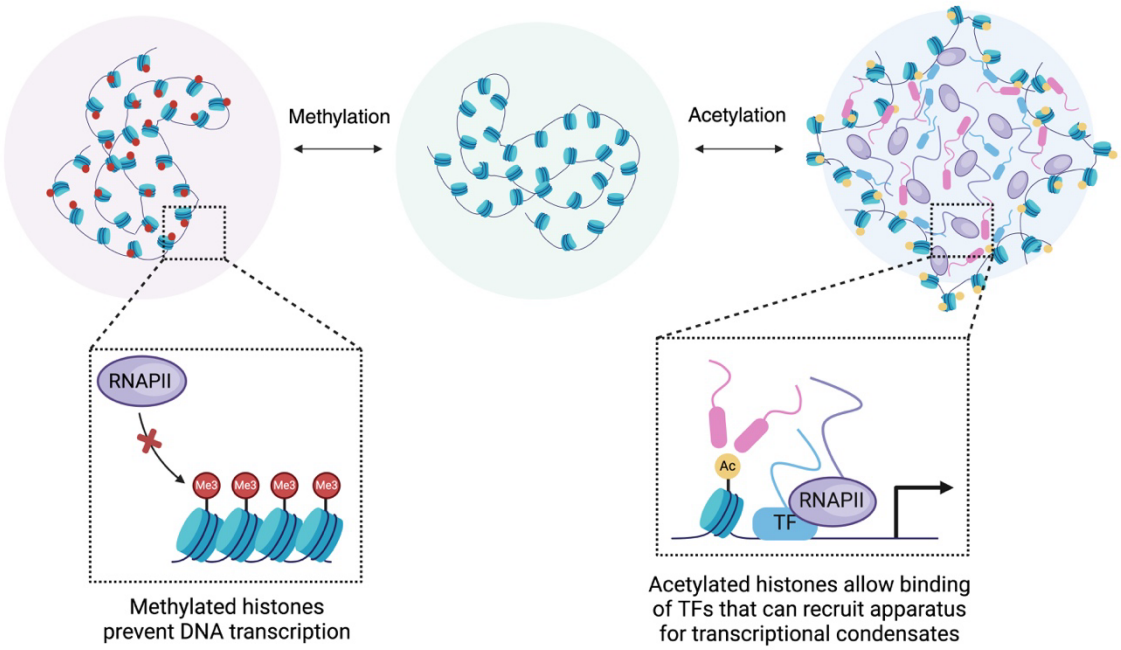

Figure 1.2 *Regulating chromatin state by PTMs on histones in nucleosomes.* Condensation is a common occurrence in the nucleus where PTMs can dictate their formation and functional state. Here, methylation of nucleosomal histones leads to heterochromatin formation (Wang et al., 2019), while acetylation of the same histones can drive the formation of active transcriptional condensates by recruiting transcriptional machinery (Sabari et al., 2018). Figure adapted from (Sabari et al., 2020).

Lastly, changes in conditions within a cell can affect protein behavior. Changes in pH, temperature, protein concentration, ions, osmolytes and metabolites may all affect the phase of a protein. Therefore, when a cell is under stress and there are pH changes, certain proteins may be triggered to selectively partition into condensates. Similarly, during nutrient deprivation, if metabolite concentration changes, this could shift the phase behavior of specific proteins. This area of condensate regulation has not been examined very thoroughly but could prove to be an exciting window into condensate function.

1.2.3 Functions of biomolecular condensates

Condensates are primarily thought to function as a means of concentrating their components to enhance reaction rates within the cell (Lyon et al., 2021). But the condensate can also behave as a holding stage, preventing biochemical reactions from moving forward. Under acute heat

shock, the nucleolus, a type of biomolecular condensate, gathers chaperone proteins such as Hsp70 and Hsp90, along with newly synthesized proteins that cannot fold properly under stress. This concentration of chaperones and unfolded proteins allows these proteins to be held in a state that facilitates rapid and accurate folding once the stress subsides (Frottin et al., 2019). During thermal stress in yeast cells when ribosome biogenesis is paused, orphan ribosomal proteins (oRPs) that do not have rRNA to complete their construction, are sequestered into condensates with the J-domain protein, Sis1, until the stress has transpired and the oRPs can be used for rapid ribosome production (Ali et al., 2023). When yeast cells are heat shocked, poly-A binding protein (Pab1) releases its substrate of mRNAs with rich 5' UTRs, while concentrating and forming condensates itself. Pab1 senses the change in temperature in the cell and extricates its cargo, which includes many mRNAs for heat shock proteins, augmenting their translation when under heat stress. Mutations in Pab1 that prevent condensation led to a loss in cellular fitness (Riback et al., 2017; Yoo et al., 2022). These examples support the idea that condensate formation may be an adaptive response to environmental stress and necessary for optimal cellular function.

Condensates have exhibited structural roles on a larger scale as well. Distal DNA damage sites have been shown to be brought together in condensate form to aid the proficiency of Rad52 DNA repair proteins in yeast cells (Oshidari et al., 2020). When proteins in the cell are targeted for autophagy by ubiquitination, the polyubiquitin chains on these marked proteins form multivalent interactions with the filaments on the scaffold protein p62, leading to the formation of condensates containing proteins marked for degradation that can then be targeted by the autophagosome more efficiently (Zaffagnini et al., 2018). Condensate formation has even been shown to restructure chromatin, with liquid condensates mechanically excluding chromatin in euchromatic regions *in vitro*, demonstrating that nuclear condensates may function in transcriptional regulation by physically pulling in targeted genomic loci and pushing out genes

that are not induced (Shin et al., 2018). In mouse embryonic cells and *Drosophila* cells, heterochromatin domains have exhibited the biophysical properties of liquid-like condensation, with heterochromatin proteins nucleating into foci at these sites (Guthmann et al., 2023; Strom et al., 2017), suggesting that condensates may be involved in transcriptional repression as well as activation.

1.2.4 Transcriptional condensates: composition and function

Transcriptional condensates are assemblies that concentrate transcription factors (TFs), co-activators, and RNA Polymerase II to target genes, allowing the efficient and robust transcription of these genes (Boija et al., 2018; Guo et al., 2019; Sabari et al., 2018). TFs typically have a structured DNA binding domain that binds, with a high affinity, to enhancers and promoters of specific genes (the scaffold) to recruit transcriptional machinery (the clients) and trigger their expression. TFs may also comprise an unstructured activation domain consisting of IDRs (or other condensate-promoting domains) that can interact with the IDRs of other TFs, co-activator proteins like Mediator, and Pol II, or transcriptional repression proteins, to form dynamic assemblies with transcriptional regulatory abilities at specific regions of the genome (Boija et al., 2018; Chong et al., 2018; Guo et al., 2019; Rawat et al., 2021; Sabari et al., 2018; Shin & Brangwynne, 2017; Wei et al., 2020).

One study determined that the IDR interactions of TFs and co-activators can crowd specific enhancer and promoter sites in the nucleus of cells and form condensates. The formation of these clusters stimulates transcription, and so, unless a specific threshold of TF and co-activator concentration is reached that allows partitioning into a condensate, these assemblies do not activate transcription (Shrinivas et al., 2019). Yet another study determined that activation of transcription can occur at a range of TF concentrations, where intermediate concentrations of the low complexity domains of transactivational machinery can interact to form smaller

transcription hubs that can eventually mature into condensates. The transcriptional activators do not need to be fully partitioned for the target genes to be expressed (Chong et al., 2018). Congruently, altering the concentration of IDR interactions at these hubs can tune transcription at these sites (Chong et al., 2022), possibly by increasing the amount of time a TF spends in a DNA-bound state, enabling the enlistment of co-activators and thus, enhancing the activity of this TF, without phase separation being a requirement (Trojanowski et al., 2022). Together, these findings suggest that transcriptional condensates provide a flexible and tunable mechanism for gene regulation, where the dynamics of TF and co-activator concentration and interaction fine-tune transcriptional activity, even without full phase separation.

1.2.5 Transcriptional condensates: regulation

The formation of transcriptional condensates is controlled by many of the same principals as those of general biomolecular condensates. IDR interactions are extremely important, and without their presence not only do condensates not form, but in some cases gene activation does not occur either (Boehning et al., 2018). Consequently, the composition of these condensates plays a role in their function, and only condensates with specific components will enhance transcription (Wei et al., 2020).

In transcriptional condensates, the binding of transcription factors (TFs) to their specific DNA motifs serves as a nucleation point for condensate formation, enabling the recruitment of additional transcriptional machinery to complete the condensate and activate transcription (Ryu et al., 2024; Wei et al., 2020). The TF's specificity for its binding site provides a regulatory layer for this selective partitioning of transcriptional components at the target site. Consequently, any modifications or activations of the TF, such as ligand binding or covalent changes like phosphorylation, can influence condensate assembly. These modifications often trigger TF nuclear localization, conformational changes, or activation in response to signalling

pathways. All this can lead to transcriptional condensate formation, as seen with ligand binding to estrogen and glucocorticoid receptors in mammalian cells (Nair et al., 2019; Stortz et al., 2020).

One mechanism by which the components of a transcriptional condensate are selected is dependent on the IDRs of the molecules involved. In mammalian adipocytes, a recent study reported that the pattern of charge blocks of amino acids in the IDRs of Mediator and Pol II is required for not only the specificity of selective partitioning of these molecules but for gene activation at these sites as well (Lyons et al., 2023). The charge pattern is both necessary and sufficient for the partitioning of functionally active transcriptional condensates in these cells. Proteins with similar functions exhibit similar charge patterns, indicating that the amino acid sequences in the low complexity domains of these proteins provide an additional layer of regulation to the assembly of transcriptional condensates, and that specific transcriptional programs segregate within specific condensates (Lyons et al., 2023).

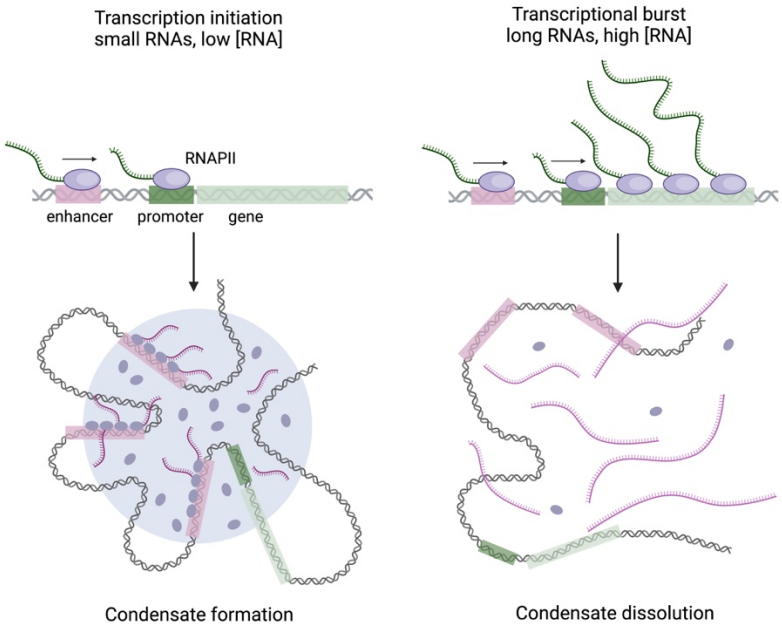

Figure 1.3 *Regulation of transcriptional condensate formation by RNA feedback mechanism.* Low levels of RNA at promoters and enhancers promotes condensate assembly, while high levels of RNA from transcriptional elongation leads to condensate dissolution. Figure adapted from (Henninger et al., 2021).

Finally, concentrating long RNA molecules has been implicated in the generation of a number of nuclear condensates, from the nucleolus to Cajal bodies. However, in transcriptional condensates RNA performs a different type of regulation. Both enhancers and promoters perform divergent transcription, that is the production of short, unstable, or temporary RNA like eRNA, long non-coding RNA (lncRNA) and upstream anti-sense RNA (uaRNA), concentrating these molecules at the enhancer/promoter positions within the genome (Core et al., 2008; Field & Adelman, 2020). A low concentration of interactions between these RNA molecules and the IDRs of the other components of the transcriptional condensate stimulates their selective partitioning at these sites. Once Pol II reaches the elongation phase, the increase in RNA levels precedes the dissolution of the condensates (Henninger et al., 2021). Thus, RNA production behaves as a negative feedback loop in the assembly of transcriptional condensates (Figure 3).

1.2.6 Transcriptional regulation in condensates

Transcriptional initiation and the release of RNA polymerase II from promoter-proximal pausing are widely considered to be the primary rate-limiting steps in transcription, especially in genes with complex regulatory requirements. In transcriptional condensates, the precise rate-limiting step remains unclear. With all components of the transcriptional machinery concentrated in close proximity, the question arises: what exactly dictates the speed of transcription within these structures?

The rate-limiting step of transcription in condensates is likely to be the recruitment and retention of essential transcriptional machinery, specifically the transition from initiation to productive elongation within the condensate's dense molecular environment. This process begins with the assembly and maturation of the condensates themselves. This initial assembly

phase, in which a high local concentration of transcriptional machinery is established, is most likely the critical rate-limiting step that sets the stage for transcriptional initiation.

Within the condensate, the recruitment of RNA polymerase II and the Mediator complex to enhancers or promoters is essential for transcription to proceed. These molecules must navigate specific molecular interactions and sometimes undergo conformational changes within the condensate to initiate productive transcription. As in typical transcription, a major rate-limiting step occurs as Pol II transitions from promoter-proximal pausing to productive elongation. This transition, regulated by pause-release factors like P-TEFb (which are often enriched within condensates), is crucial for releasing Pol II from pausing and facilitating its entry into elongation.

Transcriptional condensates are inherently dynamic, continuously remodeling in response to cellular signals or environmental stresses. These structural changes can introduce delays or promote efficient transcription depending on the condensate's state and regulatory needs. Thus, within transcriptional condensates, the process is often limited by the assembly and maturation of the condensate itself, followed by the efficient recruitment and regulated release of Pol II from pausing, which together enable a robust and coordinated transcriptional response.

1.2.7 Transcriptional condensates and 3D genome architecture

Super enhancers and other regions involved in coordinated transcriptional control, like cell-type-specific genes or those at the endpoints of complex signaling pathways (e.g., the Hippo pathway and olfactory receptors), show significant 3D genomic restructuring when active. This includes the formation of enhancer-promoter loops, promoter-terminator interactions, and connections between regulatory elements and their coding regions (Bashkirova & Lomvardas, 2019; Cai et al., 2019; Dekker, 2014; Wendt & Grosveld, 2014). These structural changes bring

distant genomic elements into close proximity, enabling efficient transcriptional regulation. This intricate 3D reorganization underscores the dynamic nature of the genome, highlighting how spatial architecture is intimately linked to the precise regulation of genes essential for cellular identity and function.

Transcriptional condensates are thought to form at these enhancer-rich regions of the genome like SEs (Dukler et al., 2016; Gosselin et al., 2014; Hnisz et al., 2013). Therefore, they not only concentrate transcriptional machinery at regulatory sites but must also actively reshape genome topology. This restructuring has been observed in various regulatory contexts, suggesting that 3D genome reorganization is an inherent consequence of condensate formation (Bashkirova & Lomvardas, 2019; Cai et al., 2019; Ramasamy et al., 2023; Sharma et al., 2021). Experiments using optogenetic techniques to induce condensation show that this process can rearrange chromatin interactions and modulate transcriptional activity (Kim et al., 2023). Furthermore, chromatin adaptor proteins are frequently found within transcriptional condensates, and in some instances, the condensation of Mediator alone can drive chromosome reorganization (Chowdhary et al., 2022; Ramasamy et al., 2023; Zamudio et al., 2019).

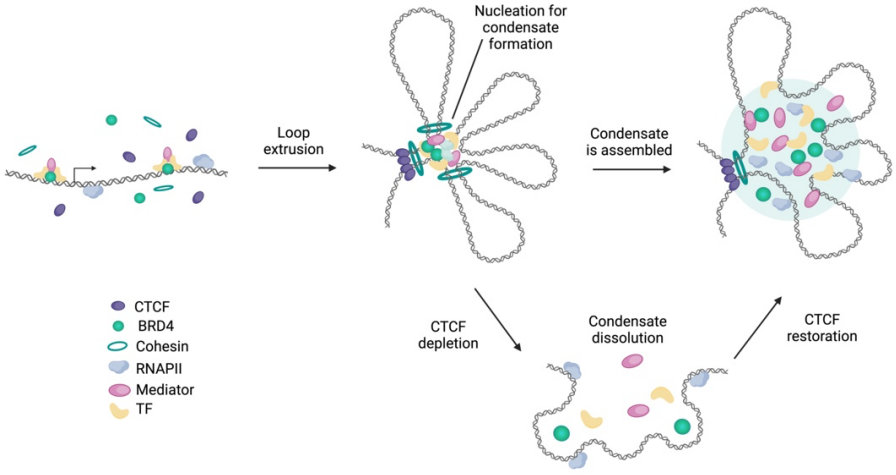

Figure 1.4 *Chromatin looping executed by CTCF and cohesin sets the stage for transcriptional condensate assembly.* CTCF and cohesin can mediate chromatin looping, bringing together distal regulatory sites of genes that are related in function. This provides the scaffolding to recruit the transcriptional apparatus, promoting the concentration of these molecules to form transcriptional condensate hubs. Figure from (Lee et al., 2021).

Interestingly, not all studies agree on causality. While some suggest that condensates induce chromatin looping, others report the opposite: chromatin looping may act as the foundational structure for condensates, with pre-existing genomic interactions guiding condensate formation (Lee et al., 2021) (Figure 4). This bidirectional relationship underscores the complex interplay between genome architecture and transcriptional condensates, with both capable of influencing each other under various cellular contexts.

Transcriptional condensates, regardless of their specific components or target gene locations, cluster transcriptional regulatory factors at sites of high transcriptional activity and coordinate the simultaneous activation of multiple genes. These condensates often exhibit spatiotemporal control over gene regulation. While most reported transcriptional condensates have been observed in mammalian cells, similar transcriptional programs may exist in yeast. The heat shock response in *S. cerevisiae* is one such program and serves as the focus of this study.

1.3 The heat shock response

Proteins play a central role in nearly all biological processes, relying on correct folding and the maintenance of their dynamic three-dimensional structures for proper function. To uphold this, cells have evolved mechanisms to maintain protein homeostasis, or "proteostasis," through a complex network of molecular chaperones and degradation systems known collectively as the proteostasis network (PN). The PN ensures a delicate balance between synthesizing new proteins, managing proper protein folding, maintaining physiological conformations, and degrading damaged or excess polypeptides (Powers et al., 2009). Cells can dynamically regulate components of the PN in response to changes in the environment, metabolic shifts, or transcriptional signals, often by activating specific stress responses (Richter et al., 2010).

The heat shock response (HSR) is one such stress response—a rapid, evolutionarily conserved gene expression program that supports proteostasis. First observed in *Drosophila* as chromosomal "puffs" triggered by temperature increases, these puffs hinted at heightened transcriptional activity at specific loci (Jamrich et al., 1977; Ritossa, 1962). Further studies linking the HSR to the proteostasis network identified many transcriptional targets encoding key components of either the ubiquitin-proteasome degradation pathway or heat shock proteins (HSPs), essential molecular chaperones for correct protein folding and aggregate prevention. While the HSR also upregulates factors involved in various cellular processes, including cell cycle regulation and nuclear import, its primary role remains proteome maintenance (Anckar & Sistonen, 2011; Voellmy & Boellmann, 2007).

Even a slight increase in temperature can trigger the HSR, leading to profound cellular effects. Acute heat shock halts global protein synthesis as HSR targets take precedence (Ashburner & Bonner, 1979). RNA splicing and translation pause, while unprocessed ribosomal RNA (rRNA) and newly synthesized orphan ribosomal proteins (lacking rRNA partners) form condensates in the nucleus (further discussed in Chapter 3) (Ali et al., 2023; Boulon et al., 2010). Meanwhile, cytosolic RNA, translation initiation factors, and other mRNA-related components gather in stress granules (SGs) until the stress resolves (Buchan & Parker, 2009). In eukaryotes, actin filament reorganization generates stress fibres, which alter the cytoskeleton and impair cellular transport (Toivola et al., 2010). In yeast, brief heat exposure uncouples oxidative phosphorylation from mitochondrial electron transport, reducing ATP production (Patriarca & Maresca, 1990). Additionally, disruptions in the lipid-protein ratio of the cell membrane increase permeability, lowering pH and altering the cytosolic electrostatic balance (Richter et al., 2010; Vigh et al., 2007).

Collectively, these changes result in cell cycle arrest and growth quiescence, which, though halting proliferation, can be adaptive depending on the stress duration. Short exposures to mild

heat stress can confer thermotolerance, enhancing the cell's resilience to future, more severe stresses. In fact, HSP production from one stress type can protect cells from other stressors as well (Lindquist, 1986). In *C. elegans*, mild, transient HSR activation reduces mutation penetrance, essentially boosting cellular fitness and providing a protective effect (Casanueva et al., 2012). Therefore, the HSR is involved in not only stabilizing the cell during acute stress, but also in cellular fitness. Thus, beyond stabilizing the cell during acute stress, the HSR plays a critical role in promoting cellular resilience and fitness.

1.3.1 The HSR regulon: the HSP family of molecular chaperones

The HSP gene family is among the most significantly upregulated targets of the HSR across species. Although these proteins are already present in high concentrations under non-heat shock (NHS) conditions, their elevated expression during heat shock (HS) underscores the cell's need to halt general protein synthesis and prioritize proteome maintenance under stress. Chaperones are crucial in this role, as they must maintain stoichiometric ratios with their client proteins to effectively prevent protein misfolding and aggregation (Kiefhaber et al., 1991).

Chaperones are broadly categorized into six families: Hsp100s, Hsp90s, Hsp70s, Hsp60s, Hsp40s, and small heat shock proteins (sHsps), that are conserved across species, although certain chaperones may be specific to individual species (Mayer, 2010). Lacking specificity for individual client proteins, chaperones transiently interact with a broad range of non-native proteins through exposed hydrophobic amino acid patches or structural motifs. Their primary function is to prevent unwanted intermolecular interactions by precisely controlling the binding and release of their clients. This cycle is chiefly driven by ATP hydrolysis, facilitated by nucleotide exchange factors (NEFs) and Hsp40/J-domain proteins (Richter et al., 2010). Together, these chaperones maintain proteostasis under both NHS and stress conditions, ensuring cellular stability and functionality across diverse organisms.

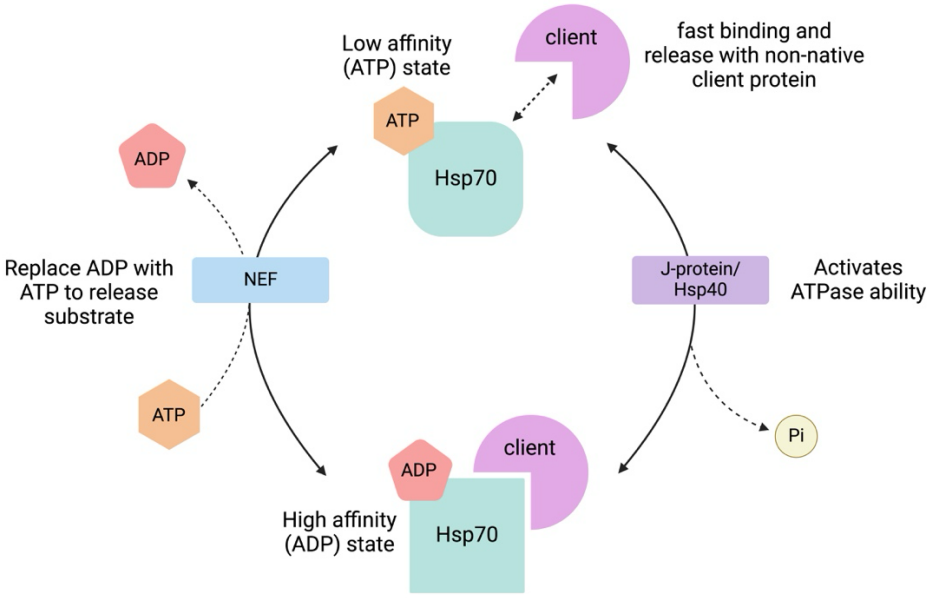

Figure 1.5 *Chaperone cycle of Hsp70.* Binding of the substrate to Hsp70-ATP substrate binding domain (SBD in blue) is mediated by J-domain proteins (JDP). This triggers ATP hydrolysis transitioning the Hsp70-ADP to its high affinity state. Nucleotide exchange factors (NEFs) then exchange the ADP to ATP, converting Hsp70 back to low affinity state and driving substrate release. Figure adapted from (Rosenzweig et al., 2019).

Hsp70

Hsp70 chaperones are among the most highly conserved, playing essential roles in a variety of housekeeping and stress-related cellular processes. Not only are these ATPases expressed across species, but they also have specialized versions within cellular organelles, such as the endoplasmic reticulum, mitochondria, and nucleus. All Hsp70 family members contain a nucleotide-binding domain (NBD) and a substrate-binding domain (SBD) (Rosenzweig et al., 2019). Hsp70 chaperones are among the most highly conserved, playing essential roles in a variety of housekeeping and stress-related cellular processes. Not only are these ATPases expressed across species, but they also have specialized versions within cellular organelles, such as the endoplasmic reticulum, mitochondria, and nucleus. All Hsp70 family members contain a nucleotide-binding domain (NBD) and a substrate-binding domain (SBD) (Zuiderweg et al., 2017).

The activity of Hsp70 involves rapid binding and dissociation from its substrates. When ATP is bound at the NBD, Hsp70 exists in a low-affinity state, loosely attached to its substrate and with low ATPase activity (Mayer et al., 2000). Binding of a J-domain protein induces ATP hydrolysis, triggering an allosteric shift that transforms Hsp70 into its high-affinity state (Kityk et al., 2015). For substrate release, a nucleotide exchange factor (NEF) interacts with the NBD to replace ADP with a new ATP molecule, thereby freeing the client protein to proceed with its next cellular role (Bracher & Verghese, 2015).

The primary role of Hsp70 proteins is to interact with nascent polypeptides co-translationally, preventing non-native interactions until the full sequence required for proper folding has been synthesized, thereby reducing the risk of aggregation in newly formed proteins (Frydman, 2001). Additionally, Hsp70 facilitates the handover of substrates to other chaperones, such as Hsp90, or even to the ubiquitin-proteasome system, which manage the later stages of the protein lifecycle (Mayer & Bukau, 2005). Hsp70 is also essential for dismantling large molecular assemblies, most notably aiding in the disassembly of clathrin coats in eukaryotic cells (Sousa & Lafer, 2015). Moreover, Hsp70 supports the disaggregase function of Hsp100s by activating their ATP hydrolysis-driven mechanism, enabling Hsp100 to disassemble aggregated proteins (Oguchi et al., 2012). A similar role is observed during the heat shock response (HSR), where Hsp70 helps in the condensation of orphan ribosomal proteins (oRPs). In this case, Hsp70 preserves the reversibility of the condensates, holding the oRPs to prevent aggregation until the cell returns to steady-state conditions (Ali et al., 2023).

Hsp90

Hsp90 proteins are among the most conserved chaperones across species, present in cells at high concentrations under normal conditions and further upregulated during stress. Unlike other chaperones, Hsp90 is more selective in its substrate binding, primarily working with

metastable signal transducers that regulate critical biological processes, such as steroid hormone receptors and regulatory kinases. Hsp90 also possesses ATPase activity and typically binds proteins in near-native states, awaiting final maturation. Acting as a "holdase," Hsp90 transiently binds its clients through continuous cycles of chaperoning, preventing aggregation until the proteins are properly folded (Karras et al., 2017). Hsp90 plays a unique role in the heat shock response (HSR), linking environmental changes to the evolution of new traits in organisms. By buffering genetic mutations and rendering them phenotypically silent under stable conditions, Hsp90 can act as a "capacitor." During environmental stress, however, when the chaperone system is overwhelmed, these hidden mutations may become phenotypically expressed, potentially revealing new traits (Lindquist, 2009). Similarly, Hsp90 can stabilize certain unstable mutations in its substrates, allowing their phenotypic expression under regular conditions, only to reveal modified traits upon heat stress (Cowen & Lindquist, 2005).

Hsp100

Hsp100 chaperones belong to the family of conserved AAA+ ATPases, forming dynamic hexameric ring structures with two nucleotide-binding sites per monomer, although some Hsp100s may contain only one (Barends et al., 2010). In conjunction with Hsp70 and Hsp40, Hsp100 chaperones act as powerful disaggregases, preventing protein aggregation under stress by dispersing heat-induced condensates through the ATPase-driven activity of their hexameric rings, keeping the rescued polypeptides in a soluble state (Mogk et al., 2015; Yoo et al., 2022). This function provides cells with stress tolerance, allowing rapid reactivation of heat-affected proteins once the stress subsides. Additionally, Hsp100 can facilitate protein degradation by collaborating with proteolytic components to unfold substrates and direct them into degradation machinery (Doyle & Wickner, 2009). Notably, higher eukaryotes, including mammals, lack Hsp100 chaperones or related proteins with disaggregation capabilities (Richter et al., 2010).

Small Hsps

Small Hsps are low-molecular-weight, ATP-independent chaperones that contain a conserved α-crystallin domain. They form large, polydisperse oligomers through weak interactions between their disordered N- and C-terminal domains (Riedl et al., 2020). Due to sequence variability and flexible oligomerization, small Hsps accommodate a diverse range of client proteins within the cell. Under stress, inactive oligomers dissociate, exposing substrate-binding sites within their α-crystallin domains and allowing small Hsps to sequester their clients in large sHsp-substrate complexes, alleviating the load on the broader proteostasis network (Specht et al., 2011; Ungelenk et al., 2016). Hsp70 and Hsp100 chaperones subsequently release small Hsp clients once the cell stabilizes, or alternatively, their substrates may be targeted for degradation via the proteasome (Reinle et al., 2022).

J-proteins/Hsp40 and NEFs

J-proteins are defined by the presence of a J-domain, a conserved region of approximately 70 amino acids forming four α-helices. These proteins are indispensable for Hsp70 function, as they not only enhance Hsp70 ATPase activity but also play a crucial role in initial substrate recognition. By providing specificity to Hsp70, different classes of J-proteins direct Hsp70 to particular organelles and clients, tailoring interactions to the needs of each context (Kampinga & Craig, 2010).

Similarly, NEFs are essential for Hsp70 activity, responsible for exchanging ADP for ATP and subsequently releasing the Hsp70 client. Unlike J-proteins, NEFs lack homology; although they all interact with the Hsp70 nucleotide-binding domain (NBD), each family of NEFs uses distinct mechanisms to fulfill this function. NEFs are often localized to specific subcellular regions, ensuring precise timing for substrate release and transfer from Hsp70 to downstream proteins, thus optimizing the chaperone's role in proteostasis (Faust & Rosenzweig, 2020).

Hsp60s

Hsp60s, also known as chaperonins, are widely conserved across prokaryotes and eukaryotes. These proteins typically form large, barrel-shaped complexes made of multiple subunits, often assembling into double-ring structures (Singh et al., 2024). The Hsp60 complex provides an isolated environment for substrate proteins, shielding them from aggregation-prone interactions. Substrates enter the central cavity of the chaperonin complex, where they bind and undergo ATP-driven conformational changes that facilitate proper folding. In mitochondria, Hsp60 works closely with Hsp10, a smaller co-chaperone that caps the Hsp60 barrel during folding cycles (Ishida et al., 2018). This partnership is crucial for the accurate and efficient folding of mitochondrial proteins, which are particularly susceptible to misfolding due to the unique mitochondrial environment.

1.4 HSF1: the master transcriptional regulator of the HSR

The rapid transcriptional upregulation of all the targets of the HSR requires activation machinery that is responsive to environmental stressors, specifically a transcription factor that can stimulate the expression of the HSR regulome quickly and efficiently upon sensing stress. In eukaryotes, a conserved family of heat shock transcription factors (HSFs) were identified as the critical regulators of the HSR (Sorger et al., 1987; Sorger & Pelham, 1987). *Drosophila* and *Caenorhabditis elegans* possess a single HSF, HSF1/HSF-1 respectively. Yeast cells have a single HSF, Hsf1, that is essential for their survival, while mammalian cells have HSF1, HSF2, and tissue-specific paralogs essential for development (Anckar & Sistonen, 2011). All HSFs bind to preserved DNA motifs called heat shock elements (HSEs), present in multiple copies in the promoters and enhancers of their target genes (Bienz & Pelham, 1987; Pelham, 1982; Tuite et al., 1988). For the purposes of this study, I will be focusing on HSF1 and its orthologs, as it is the most widely studied HSF in the field.

Many genes are repressed during acute stress, and this downregulation of highly expressed genes has been termed stress-induced transcriptional attenuation (SITA) (Anckar & Sistonen, 2011; Sawarkar, 2022). While this is an important property of the transcriptional response to stress, many studies have determined that this repressive activity is Hsf1-independent across cell types (Duarte et al., 2016; Gasch & Werner-Washburne, 2002; Mahat et al., 2016). Therefore, I will largely be concentrating on the transcriptional activation capabilities of Hsf1.

1.4.1 Hsf1 in the context of other cellular stresses

In addition to heat stress, a number of other environmental stressors have been identified that activate the HSR or work alongside it. A shared effect of all these different stress conditions is the imbalance in proteostasis that they cause, thus activating the genes encoding Hsps that can then aid with bringing the cell back to a stable state (Figure 6). The unfolded protein response (UPR) is the stress pathway involved in ER proteostasis and is activated when there is an accumulation of newly synthesized proteins that cannot be folded correctly. This buildup can be due to changes in ER homeostasis caused by a number of factors such as calcium ion depletion, oxidative stress, or even viral infection (Cao & Kaufman, 2012). In yeast, the UPR upregulates the production of a protein, Sir2, that activates the HSR, which in turn can induce an increase in the expression of ER chaperones that aid in the removal or folding of the accumulated protein in the ER (Weindling & Bar-Nun, 2015).

The oxidative stress response and the HSR exhibit an overlap in their downstream effects. In fact, the key transcription factor of the oxidative stress response, Nrf2, shares several transcriptional targets with HSF1, suggesting a collaboration between these two stress-induced TFs (Barna et al., 2018). Since the presence of reactive oxygen species triggers a change in protein homeostasis, oxidative stress is also likely to trigger the HSR to provide an increase in chaperones and their co-factors. In fact, the sHsp hsp27, is essential in reducing the levels of

ROS and the maintenance of the cellular redox state by mediating the glutathione levels in these cells during stress (Mehlen et al., 1996).

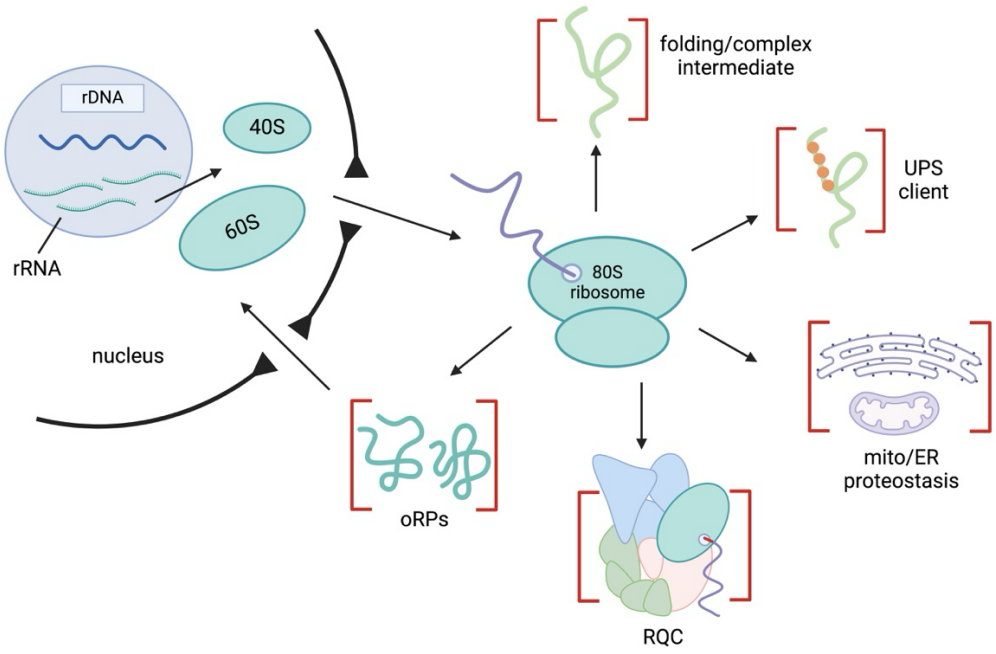

Figure 1.6 *Sources of the ligands of the HSR*. Many activities within the cell can result in the induction of the HSR: nascent protein folding complexes, orphan ribosomal proteins (oRPs) formed during nutrient deprivation, ribosome quality control (RQC), ER and mitochondrial stress responses, and the ubiquitin degradation machinery. All these processes cause an impairment of proteostasis in the cell, thus prompting the HSR. Figure adapted from (Pincus, 2020).

When a ribosome stalls in yeast cells, it may form truncated proteins that are toxic to the cell. The ribosome quality control complex (RQC) binds to these stalled ribosomes and target them for degradation by the ubiquitin proteasome (Brandman et al., 2012). In addition, the RQC stimulates the addition of alanine and threonine residues at the C-terminus of the truncated protein (CAT tails) (Shen et al., 2015). The accumulation of CAT tails activates the HSR, which in turn, stimulates the upregulation of protein degradation machinery that can aid in clearing these stalled ribosomes and their cargo (Sitron et al., 2020). Similarly, if the degradation machinery is compromised, that will lead to an accumulation of unwanted proteins in the cell, which will in turn trigger the HSR.

The mTOR pathway, essential in nutrient sensing and growth in eukaryotes, regulates ribosome biogenesis. When the cell is subjected to nutrient deprivation, ribosome biogenesis is halted which can lead to a pausing of rRNA production and the accumulation of newly synthesized ribosomal proteins. These "orphan" ribosomal proteins (oRPs) behave as signal for the HSR, upregulating chaperone proteins to aid in "holding" the oRPs until nutrient stress is relieved, therefore ensuring rapid production of ribosomes once rRNA manufacture commences.

In mammalian cells, the Ras/MAPK pathway couples signals from cell surface receptors to gene expression. Depending on the signal, this pathway can interpret it as a stimulus for apoptosis, cell cycle progression, proliferation, or even cytokine production, by phosphorylation down a kinase cascade that ends in the nucleus at specific transcription factors (McCubrey et al., 2007). In mammalian cells, MEK kinase can phosphorylate HSF1, promoting activation of the TF (Tang et al., 2015). This suggests that cell proliferation signals and the cell cycle can also act as triggers for HSF1 activity. In tumor cells, when MEK activity is blocked, the HSR is also repressed, resulting in protein destabilization, aggregation, and amyloidogenesis.

1.4.2 The role of HSF1 beyond stress

HSF1 activity can be triggered by signals beyond stress, playing diverse roles across developmental and physiological processes. In *C. elegans*, for instance, HSF-1 mediates larval development by regulating approximately 70 target genes essential for this process. The promoters of these genes contain partial heat shock elements (HSEs) and GC-rich motifs, suggesting that HSF-1 coordinates this developmental program in conjunction with a co-factor (Li et al., 2016). Similarly, in *Drosophila*, HSF1 loss leads to developmental arrest at the L2-L3 larval transition (Jedlicka et al., 1997) while in mice, HSF1 influences neuronal development,

with some target genes involved in synapse formation (Uchida et al., 2011), and the growth and differentiation of olfactory neurons (Takaki et al., 2006).

HSF1 also plays a significant role in gametogenesis. In male mice, HSF1 is involved in the elimination of defective spermatocytes (Izu et al., 2004), the survival of immature germ cells (Widłak et al., 2003), and the proper packaging of DNA in developing sperm (Aligue et al., 1994). In females, HSF1 regulates genes required for oocyte meiosis, as evidenced by HSF1 knockout mice, which experience cell cycle arrest at phases I or II of meiosis (Metchat et al., 2009). *Drosophila* HSF1 also impacts oogenesis and maternal effect sterility, underscoring HSF1's role in gamete development (Jedlicka et al., 1997).

Beyond development, HSF1 is a major player in disease onset and progression. By enhancing cellular stress tolerance, increased HSF1 activity is often linked to cancers, as it supports the oncogenic proteome and facilitates tumour malignancy (Dai & Sampson, 2016). The HSR regulome contributes to preserving the functional structure of oncoproteins as they are inherently unstable, partially folded, or prone to aggregation, requiring a robust proteostasis network to maintain their active and functional conformations. The HSF1 targets drive signalling pathways that support tumour angiogenesis and other processes involved in cancer progression (Mendillo et al., 2012; Semenza, 2003). In tumour cells and cancer lines, HSF1 can be constitutively active, promoting rapid growth despite deleterious mutations, and leading to proteostasis disruptions that can result in proteomic instability and amyloidogenesis (Dai & Sampson, 2016). Consequently, HSF1 inhibition has emerged as a promising target for anticancer therapies.

Conversely, HSF1 activation has therapeutic potential as well. Progressive protein accumulation is a common issue in aging organisms (Vellai & Takács-Vellai, 2010) and protein aggregation in neuronal cells in the brain is a hallmark of neurodegenerative diseases such as

Alzheimer's, Parkinson's, and Huntington's (Soto, 2003). In both cases, proteostasis becomes compromised as stress response pathways diminish with age or disease progression. Activating HSF1 may counter protein aggregation, thereby reducing neurodegeneration and supporting proteostasis mechanisms to extend cellular longevity (Billes et al., 2016; Hsu et al., 2003; Neef et al., 2011).

1.4.3 Hsf1: structure, function, and mode of action

Hsf1 structure

Eukaryotic Hsf1 is a multidomain protein comprising an N-terminal DNA binding domain (DBD), a trimerization domain (3mer) and a C-terminal activation domain (CTA), with higher eukaryotes possessing a separate 160 amino acid regulatory domain (RD) as well. The RD is a highly flexible intrinsically disordered region (IDR) and is involved in the control of HSF1 trimerization (Hentze et al., 2016; Rabindran et al., 1993), as well as its transactivational capabilities and any interactions HSF1 may have with various partners (Green et al., 1995). Meanwhile, in yeast, the N-terminal domain (NTA) and the CTA are both intrinsically disordered and contain sites for Hsp70 binding, behaving as a regulatory domain for this ortholog (more on this later) (Krakowiak et al., 2018; Zheng et al., 2016) (Figure 9A).

The DBD of HSF1 is the most structured region of the protein, consisting of a winged helix-loop-helix architecture that can interact with HSEs (Neudegger et al., 2016). All three DBDs of the HSF1 trimer are necessary for efficient binding to DNA (Kim et al., 1994). The trimerization domain is made up of a coiled-coil, and during thermal stress a conformational change in the RD leads to a tightening of this coil, which in turn favours the cooperative trimerization of the leucine zipper of HSF1 (Hentze et al., 2016).

Though the HSR is conserved across organisms, yeast Hsf1 and human HSF1 share only 17% sequence homology, and their domain structure is moderately different as well, as yeast Hsf1 has an extra disordered region at its N-terminal, and its DNA binding domain is present towards the centre of the protein. Though yeast Hsf1 maintains the winged helix-loop-helix structure with a coiled-coil trimerization domain, it does not have an RD. Therefore, yeast Hsf1 trimerization is not regulated by a conformational change in the RD that triggers the formation of the triple leucine zipper. In fact, if human HSF1 is expressed as the only copy of Hsf1 in yeast cells, the RD must be deleted for the cells to be viable. This is likely due to the observation that yeast Hsf1 is constitutively trimerized and present in the nucleus of these cells, so this cannot be used a means of modulation for TF activity.

Function

A recent study showed the essential function of yeast Hsf1 by showing that its primary role under NHS conditions is to drive the co-expression of Hsp70 and Hsp90. Remarkably, when Hsf1 is removed from the nucleus, yeast cells continue to grow robustly if provided with external Hsp70 and Hsp90, which prevent protein aggregation and associated toxicity (Solís et al., 2016). Without nuclear Hsf1, the heat shock response (HSR) remains largely functional, likely due to an overlap in genetic targets between Hsf1 and other environmental stress response transcription factors, such as Msn2/4 (Solís et al., 2016). This finding suggests that, while the majority of Hsf1's heat-induced targets can be regulated by Msn2/4, certain genes still specifically require Hsf1 for their transcription.

Similarly, in mouse embryonic stem cells (mESCs) and mouse embryonic fibroblasts (MEFs), both HSF1 and HSF2 – the only HSF paralogs in these cells – can be deleted without impacting the basal expression of their target genes, indicating that mESCs and MEFs may regulate HSF1's NHS expression program through alternative mechanisms. However, under heat shock

conditions, HSF1 becomes essential for the transcription of nine core genes, including Hsp40, Hsp70, and Hsp90, and HSF2 alone cannot compensate for the absence of HSF1 in these stress-responsive roles (Mahat et al., 2016; Solís et al., 2016).

Mode of action

HSF trimers bind to HSEs, which comprise alternating inverted repeats of the sequence nGAAn. To stimulate transcription, a TF must be able to access the DNA it binds. Histone-modifying enzymes and chromatin remodelling factors facilitate the reshaping of the chromatin landscape by using epigenetic changes that can reorganize the genome. Though the HSR is an inducible response, surprisingly, in *Drosophila* and mammalian cells, most HSEs for heat-inducible genes are present at sites of open, active chromatin (Guertin & Lis, 2010; Sullivan et al., 2001). The HSE sites of heat-inducible HSF1 genes are maintained in a nucleosome-free state during NHS conditions by utilizing a variety of factors, like the SWI/SNF complex, that interact with and recruit chromatin remodelling proteins, while the onset of stress also stimulates the acetylation of histone H3 and H4 to keep the chromatin in an active transcriptional state (Duarte et al., 2016; Fujimoto et al., 2012; Mueller et al., 2017). Though the chromatin is present in an operational conformation, HSF1 occupancy of these HSE sites remains heat inducible. The chromatin is likely present in an active and open configuration because HSF1 is absent from the nucleus in these cells unless it is heat-activated and trimerized. As a result, when HSF1 is stimulated and translocated to the nucleus during HS, the induced gene transcription can occur as rapidly as possible.

However, in yeast cells, while Hsf1 occupies the HSEs of its core targets that are constitutively active, even during NHS conditions, many of its unoccupied, non-induced targets possess nucleosome marks that indicate an inactive chromatin conformation (Pincus et al., 2018). When the cells are exposed to an acute thermal stress, there is Hsf1 occupancy of 31 more

targets, in addition to an increased occupancy of the core targets as well (Pincus et al., 2018). Consequently, multiple studies have also revealed that HSF1 cooperatively binds to promoter regions of its target genes which possess more than one HSE site. The primary HSE element, HSE1, has a stronger affinity for Hsf1, and only when HSE1 is occupied will the secondary sites be employed, most likely during HS, as this cooperativity is required for full inducibility of the gene (Amin et al., 1994; Erkine et al., 1999; Jaeger et al., 2014; Schmauder et al., 2022). This evidence further supports that HSF1 is constitutively active at some of its target genes.

Similar to *Drosophila* and mammalian cells, core targets sites bound by Hsf1 in NHS conditions in yeast cells are enriched in pioneer factors, proteins that allow the chromatin to maintain a nucleosome-free, open conformation for easy access by transcriptional machinery (Pincus et al., 2018). For inducibly-occupied Hsf1 sites, the chromatin remodelling complex, RSC, plays a role in aiding Hsf1 to remodel nucleosomes during HS (Pincus et al., 2018). RSC and SWI/SNF, one of the protein complexes reported to be involved in maintaining open chromatin at HSE sites in flies and mammals (Sullivan et al., 2001), are considered homologues, which provides some evidence for evolutionary consistency in this process (Cairns et al., 1996). The status of the chromatin at HSF1 inducible gene targets in yeast, compared to that of higher eukaryotes, may be due to Hsf1 being constitutively present in a trimerized and activated state in the nucleus of yeast cells (Sorger & Nelson, 1989). By ensuring the heat-inducible sites are present in an accessible state until necessary, yeast Hsf1 cannot bind and upregulate these genes in NHS conditions, adding another layer of regulation in HSR gene activation.

1.4.4 Regulating Hsf1 and the HSR: a simple question with a complicated answer

The HSR is a conserved process across species, the regulation of HSF1 varies significantly. Although the concept of an autoregulatory feedback loop involving Hsp expression appears consistent, the complexity of HSF1 regulation tends to increase with the organism's complexity.

Certain regulatory mechanisms are better understood in mammalian cells, while others are clearer in simpler organisms like yeast. In this section, I will explore the known mechanisms governing HSF1 and HSR regulation in mammals and yeast. This is a critical area of study, as HSF1 represents a promising therapeutic target in various diseases; thus, understanding its cellular modulation could reveal new opportunities for drug development.

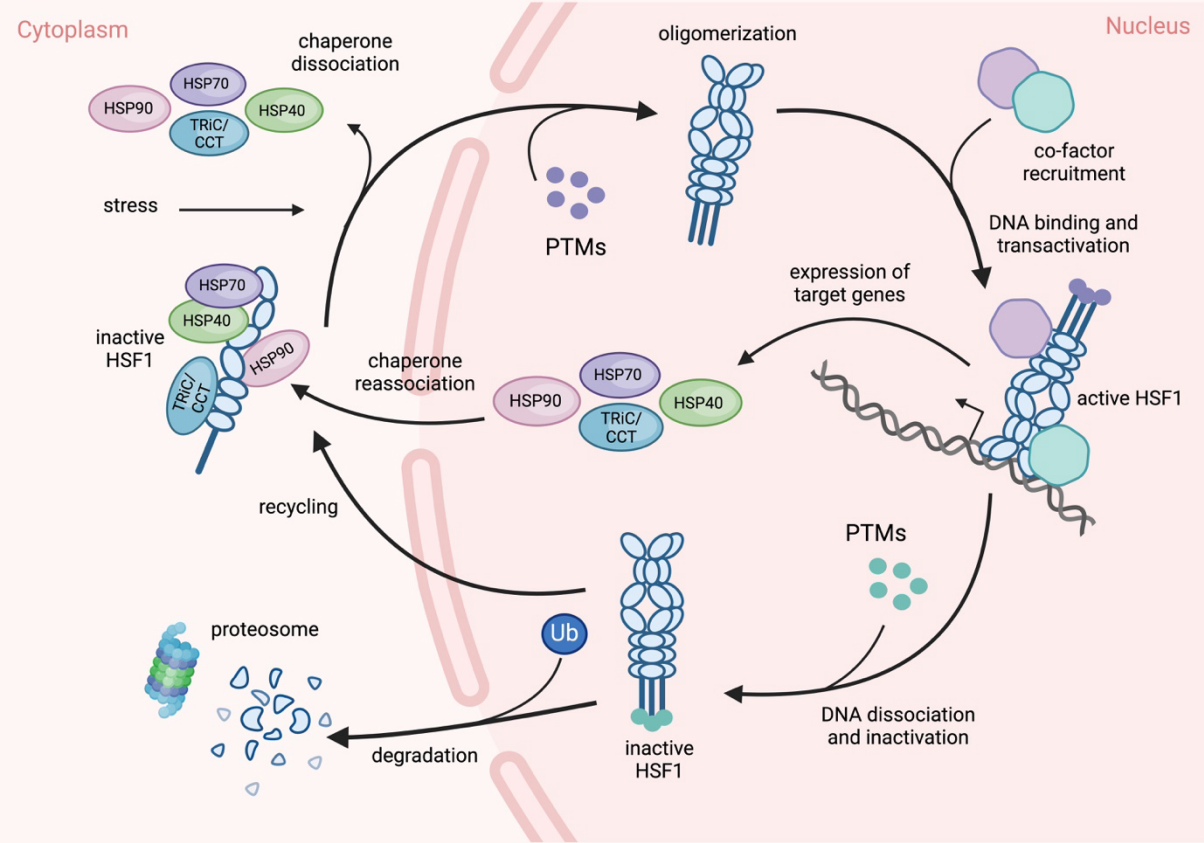

Figure 1.7 *The activation-attenuation cycle of mammalian Hsf1.* In response to stress, monomeric Hsf1 is released from inhibitory binding by chaperones and shuttled to the nucleus where it can trimerize and bind to HSEs to induce transcription of the HSR regulon. When Hsf1 is no longer needed, it is modified by phosphorylation and sumoylation that will mark it for degradation, or it will be recycled into monomeric form and bound to chaperones again. Figure adapted from (Gomez-Pastor et al., 2018).

Modulating HSF1 in mammalian cells

In mammalian cells, HSF1 partakes in an activation-attenuation cycle in which it is stimulated via a multistep pathway leading to HSF1 transcriptional activation capacity, and once it is no longer needed, is then marked for degradation or recycling. HSF1 is present in an inactive,

monomeric form and shuttles between the nucleus and the cytosol, unable to bind DNA (Baler et al., 1993; Vujanac et al., 2005) (Figure 7). Upon stress, HSF1 is then rapidly accumulated in the nucleus where it can bind to HSEs near its gene targets and induce their expression once it is activated (Sarge et al., 1993). Whether HSF1 trimerizes in the cytosol or the nucleus is still unclear, but it does not have DNA binding capability unless it is in a trimeric state. Furthermore, trimeric HSF1 can be maintained in an inactive state when bound by a chaperone complex made up of HSP90, p23, and FKBP4 (Bharadwaj et al., 1999). The monomeric iteration of HSF1 can be preserved when in complex with Hsp70, Hsp90, and TRiC/CCT (an HSF1-independent chaperone), in the cytosol (Shi et al., 1998), while the transactivation capacity of activated trimeric HSF1 can be suppressed when it interacts with HSP70 and HSP40 (DNAJB1) (Abravaya et al., 1992; Shi et al., 1998). These chaperone interactions depict a negative feedback mechanism that serves to regulate the intensity and duration of the HSR depending on the levels of excess chaperones present in the cell to inhibit HSF1 (Figure 7).

Post-translational modifications (PTMs), including phosphorylation, acetylation, and sumoylation, can also modulate HSF1 activation. Two phosphorylation sites, Ser230 and Ser326, in the regulatory domain (RD) of human HSF1 facilitate its transactivation capability (Guettouche et al., 2005). Upon HS, phosphorylation of Ser303 can mediate the addition of a small ubiquitin-related modifier (SUMO) to Lys298 in the RD of HSF1 (Hietakangas et al., 2003). Sumoylation occurs when HSF1 is in a trimeric state, however, how it affects HSF1 activity is yet to be determined. Evidence suggests that sumoylation may be involved in recruiting transcriptional repressors, or it affects the interaction of HSF1 with transcriptional machinery (Kmiecik et al., 2021; Kmiecik & Mayer, 2022). Acetylation of HSF1 occurs in the attenuation stage of the HSF1 regulatory cycle (Figure 7). HSF1 is maintained in a deacetylated state by SIRT1, which increases the stabilization and dwell time of DNA-bound HSF1.

However, when the HSR is over, SIRT1 is depleted allowing acetylation by p300/CBP to promote the attenuation of excess HSF1 by marking it for the ubiquitin proteosome system (Åkerfelt et al., 2010; Li et al., 2017) (Figure 7).

The chaperone titration model

As mentioned earlier, a number of molecular chaperones are involved in the regulation of HSF1 in mammalian cells, many of which are also under the transcriptional control of this TF. Therefore, it has been suggested that HSF1 interacts with these chaperones and is kept in an inactive form in NHS conditions. When the cell undergoes HS, these chaperones are sequestered away to deal with the influx of newly synthesized, non-native proteins that require aid in folding while proteostasis is imbalanced (Tye & Churchman, 2021). This releases HSF1, activating the HSR and the translation of a surplus of chaperone proteins that can then restore the cell to a steady state, while concomitantly, or subsequently, regulate HSF1 in a negative feedback loop (Masser et al., 2019). This putative regulatory mechanism is termed the chaperone titration model.

Several lines of evidence support this model: downregulation of Hsp90 or TRiC/CCT triggers HSF1 activity (Neef et al., 2014; Zou et al., 1998) while an increase in Hsp90 exhibits HSF1 repression (Prince et al., 2015). Hsp90 has since been shown to favour the trimeric conformation of HSF1 (Hentze et al., 2016), and accordingly more evidence has been reported that claims there is no interaction between HSF1 and Hsp90 unless there is cross-linking (Guo et al., 2001). Therefore, Hsp90's ability to suppress HSF1 trimerization has been called into question, suggesting the chaperone might play a distinctive role in HSR modulation instead.

HSF1 was found to co-precipitate with Hsp70 in mammalian cells and multiple Hsp70 binding sites have been identified in human HSF1 (Abravaya et al., 1992; Kmiecik et al., 2020). Overexpression of Hsp70 has exhibited a suppression of Hsf1 activity as well (Baler et al., 1996;

Shi et al., 1998), further establishing a role for Hsp70 in regulation of HSF1. In fact, a recent study uncovered a potential mechanism for Hsp70 repression: the binding of multiple Hsp70s to HSF1 *in vitro*, in association with the Hsp40 DNAJB1 and ATP, leads to the unzipping of the triple leucine zipper of the HSF1 trimer by entropic pulling, monomerizing the TF and dislodging it from DNA, thus inactivating it (Kmiecik et al., 2020). This process is sensitive to the concentration of Hsp70, as the more chaperones that are bound to the HSF1 trimer, the quicker it will unzip (Kmiecik & Mayer, 2022). This mechanism of Hsp70 suppression also supports the chaperone titration model, exhibiting a direct link to Hsp70 concentration and the quelling of HSF1 activity.

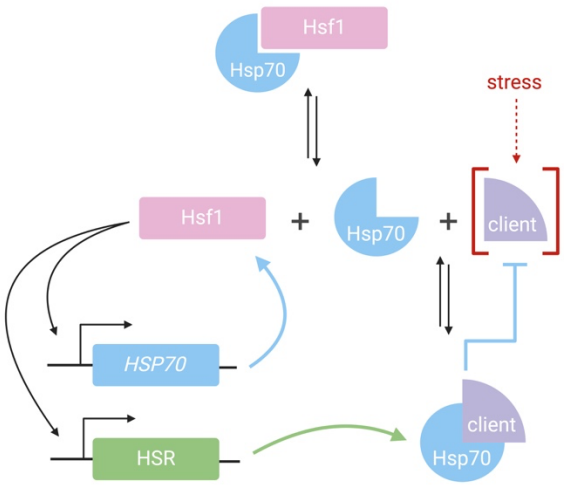

Figure 1.8 *The chaperone titration model.* In yeast, Hsp70 binds and represses Hsf1 activity during NHS conditions in the cell. During HS, the Hsp70 titrates away from Hsf1 to bind to stressed-induced clients, allowing Hsf1 to activate and drive expression of HSR genes. Hsp70 forms a negative feedback loop, as when it is produced in excess, or when the cell has reached steady state, it binds to Hsf1 again, repressing its activity and ending the HSR. Figure adapted from (Pincus, 2020).

Furthermore, it has been recently reported that purified HSF1-Hsp70 complexes are able to bind to HSE DNA at NHS conditions, and that increasing concentrations of Hsp70 hindered this binding (Ciccarelli & Andréasson, 2024). Using HEK293T cells, it was determined that Hsp70 binds to HSF1 via its substrate binding domain, and this interaction is reduced after exposure to thermal stress, though specific sites on Hsf1 for this molecular association were not

identified. Perturbing proteostasis by impairing protein folding using the drug AzC also triggered the release of Hsf1 (Ciccarelli & Andréasson, 2024). This establishes Hsp70 as a key regulator of Hsf1 activity and supports the chaperone titration model by displaying the sensitivity of Hsp70 to imbalances in proteostasis.

While this model is largely accepted in the field, it is important to mention that the endogenous molecular ratio between HSF1:Hsp70 is 1:1000, which makes it difficult to reconcile how much Hsp70 must be titrated away for HSF1 to be activated. As previously mentioned, J-proteins are necessary for Hsp70 ATPase activity and client binding (Kampinga & Craig, 2010). Because Hsf1 binds to Hsp70 via its substrate binding domain in yeast cells, it is considered to be an Hsp70 client (Masser et al., 2019). And so, the J-protein Sis1 has recently been identified to promote and maintain the binding interaction of this client protein with Hsp70, with a 5-fold decrease in binding when Sis1 is depleted from the nucleus, and an increase in Hsf1 activity. During HS in yeast, Sis1 is sequestered to the nucleolus and to condensates present in the cytosol. These regions are notably devoid of Hsf1, thereby implying that Sis1 is needed for efficient interaction of Hsf1 with Hsp70 and once it is absent, Hsf1 is activated (Feder et al., 2021). The ratio of Sis1:Hsf1 is more comparable within a cell, and so it would make more sense that the J-protein being titrated away is what induces Hsf1.

In mammalian cells, the J-protein DNAJB1, homologous to Sis1, is essential for an entropic pulling and unzipping mechanism that likely mediates Hsp70-dependent repression of HSF1 (Kmiecik et al., 2020). This supports the idea that the sequestration of J-proteins away from sites of HSF1 inhibition may be the key factor driving HSF1 activation.

Regulation of Hsf1 in yeast

In yeast cells, it is unclear if Hsf1 is ever present in a monomeric form, existing as a perpetual trimer largely in the nucleus of these cells (Sorger et al., 1987; Sorger & Nelson, 1989). As

mentioned previously, under NHS conditions in yeast, certain Hsf1 target genes are already occupied by the TF, but once the cell is subjected to HS, the occupancy of these constitutively active genes increases, while the promoters of HS-specific genes are also populated (Hahn et al., 2004; Pincus et al., 2018; Sorger et al., 1987; Zheng et al., 2016). And so, it makes sense that these two HSF1 orthologs would be controlled by somewhat dissimilar mechanisms.

The pool of available Hsp70 and Hsp90 within a cell has been shown to mediate Hsf1 activity: an escalation in the chaperone concentrations leads to suppression of the transcriptional activity of the TF, while depletion or impairment of the Hsps results in a hyperactive Hsf1 (Baler et al., 1996; Zhao et al., 2002; Zou et al., 1998). However, similar to mammalian HSF1, no Hsp90 binding sites have been identified on the Hsf1 protein and thus no protein-protein interactions have been established between the two proteins, unless they are crosslinked (Guo et al., 2001). Though no clear modes of regulation have been reported so far, Hsp90 has been identified as one of the essential Hsf1 target genes, with the cell succumbing to proteotoxicity and death if it is not transcribed (Solís et al., 2016). Since it is also required for the stabilization of many essential proteins within the cell (Karras et al., 2017), Hsp90 must play a managing role in the stress response pathway or modulation of proteostasis in general, but we have yet to provide compelling evidence for direct Hsf1 regulation.

However, like human HSF1, yeast Hsf1 also exhibits direct Hsp70 regulation. Two Hsp70 binding sites have been identified on Hsf1: the NE1 site and the CE2 site, present in the IDRs of the NTA and CTA of Hsf1, respectively (Krakowiak et al., 2018; Peffer et al., 2019) (Figure 9B). Both sites form stable complexes with Hsp70 under basal conditions, and that interaction is lost once the cell undergoes acute HS, though with sustained HS the interaction is restored. The CE2 site alone is essential for Hsf1 suppression under NHS conditions and inactivation after HS has subsided, even when the entire NTA has been deleted (Krakowiak et al., 2018). When either site is deleted or mutated, Hsf1 exhibits a loss in Hsp70 binding, as well as an

increase in Hsf1 transcriptional activity (Peffer et al., 2019; Zheng et al., 2016). Hsp70 binds Hsf1 via its substrate binding domain, and Sis1 is necessary for an effective interaction (Feder et al., 2021; Masser et al., 2019). Both Sis1 and Hsp70 are under the transcriptional control of Hsf1, but only Hsp70 and Hsf1 form the core feedback loop, dependent on the expression of Hsp70 (Garde et al., 2024).

Yeast Hsf1 does not exhibit the same PTMs as human HSF1. In fact, only phosphorylation has been identified as a modulator of Hsf1 activity so far. However, the exact sites have yet to be determined as different residues of Hsf1 are phosphorylated depending on cell-to-cell variation and environmental conditions (Zheng et al., 2018). Additionally, in both yeast and human cells, phosphorylation is dispensable for acute Hsf1 activation after thermal stress (Budzyński et al., 2015; Zheng et al., 2016). To understand the role of phosphorylation in yeast Hsf1 regulation, our lab designed a phosphomimetic mutant Hsf1, Hsf1-PO_4*, that replaces 116 serine/threonine residues with aspartate to mimic the negative charge of a phosphate group. Conversely, we also designed a phospho-null mutant Hsf1, Δpo_4, whereby 152 S/T residues were converted to alanine (Zheng et al., 2016). Interestingly, hyperphosphorylation escalates Hsf1 activity in both NHS and HS conditions, while hypophosphorylation exhibits a somewhat attenuated Hsf1 activity in both NHS and HS settings. Moreover, phosphorylation also enables sustained activity of Hsf1 during prolonged HS (Zheng et al., 2016). And so, rather than being a key form of regulation for Hsf1, like Hsp70 binding, phosphorylation exhibits a more nuanced and complex role in the fine-tuning of Hsf1 activity. This, along with the CE2 and NE1 sites, intimates that the cell may be able to modify Hsf1 activity depending on the stress or extracellular signal.

But how does Hsp70 and phosphorylation regulate Hsf1 activity in yeast? Unfortunately, yeast Hsp70 does not exhibit an ability for entropic pulling like its human counterpart. The obvious

answer, considering Hsf1 is a TF, is that Hsp70 modulates Hsf1's ability to bind DNA. However, while it has been reported that purified complexes of Hsp70-bound Hsf1 can bind HSEs, with excess Hsp70 impeding DNA binding (Masser et al., 2019), the specific sites on Hsf1 responsible for this have not yet been determined so this may still be a path worth exploring. Another mechanism by which Hsp70 can inhibit Hsf1 activity is by impairing the recruitment of transcriptional machinery, such as the Mediator complex and RNA Pol II, to sites of Hsf1 gene expression. It is also possible that all the Hsp70 binding sites have not yet been elucidated, and that multivalent nature of Hsp70 binding might provide more answers on its mechanism of action for Hsf1 regulation. This question is a central theme of this study and will be discussed further in the next chapters.

1.4.5 Transcriptional condensates in the HSR: Aims of the study

The HSR has long been a model system to explore eukaryotic gene transcription as: it is triggered by a specific environmental cue, gene transcription is regulated by one central transcription factor, Hsf1, and it exhibits a robust and dynamic induction of its target genes. And so, studying transcriptional condensates as a mode of eukaryotic transcriptional modulation by using this gene expression program is a logical direction to explore. Though these condensates have only been identified at super-enhancer-regulated cell-identity genes in mammalian cells, there is sufficient evidence to conclude that yeast cells may also form transcriptional condensates at the sites of Hsf1 target genes during HS.

Hsf1 induction triggers the remodelling of the 3D architecture of the yeast genome. Gene coalescence of transcriptionally activated Hsf1 genes occurs across and between chromosomes once the stress response is initiated (Chowdhary et al., 2017). This is consistent with the presence of clusters of regulatory elements at SEs in mammalian cells. This genetic interaction is ablated when the binding of Hsf1 to target HSEs is prevented, and can only occur between

HSR genes, excluding any other expressed genes, even those present punctuated between the Hsf1 targets (Chowdhary et al., 2019). The conformational rearrangement is specific to the Hsf1-mediated stress pathway, as Msn2/4-regulated genes do not exhibit this trait. Again, this matches the observation that the induction of a transcriptional condensate occurs once a TF binds to its specific DNA motif at the SE site and only involves the relative functional genes, as described earlier.

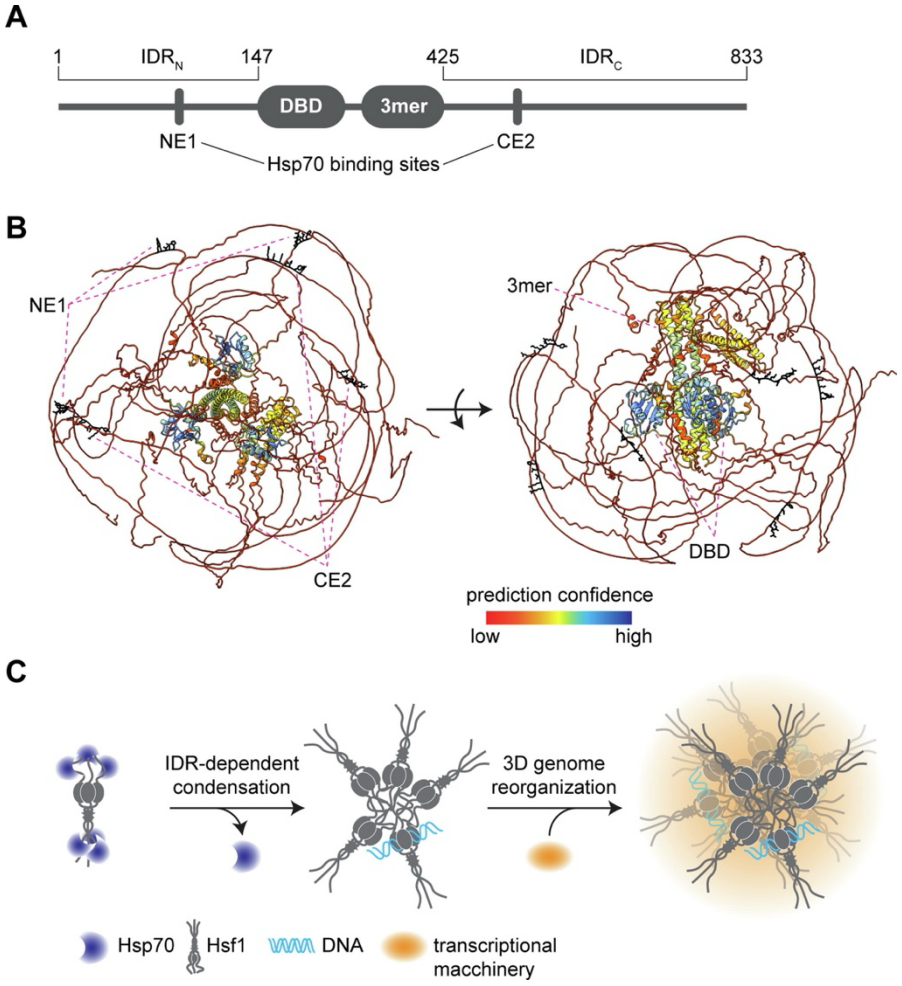

Figure 1.9 *The structure and mechanism of induction for Hsf1 in budding yeast.* **(A)** Domain architecture of yeast Hsf1 **(B)** Predicted structure of yeast Hsf1 using CollabFold **(C)** During acute HS, Hsf1 is released by Hsp70, allowing Hsf1 IDRs to interact with other Hsf1 molecules and transcriptional machinery to assemble transcriptionally active condensates. Figure from (Dea & Pincus, 2024).

Moreover, Hsf1 forms discrete nuclear puncta during HS that disperse simultaneously with the attenuation of the HSR, mirroring the dynamics of HSR gene coalescence and dissolution

(Chowdhary et al., 2019). Transcriptional condensates in mammalian cells have also been associated with dynamic and regulated gene clustering (SEs). Mediator and RNA Pol II have been shown to be recruited to sites of Hsf1 gene transcription, consistent with their presence in mammalian transcriptional condensates, and these interactions tend to occur via the IDRs of these molecules in both species, further providing evidence that these nuclear puncta are in fact transcriptional condensates (Figure 9C).

In this study, I show that Hsf1 does in fact form transcriptional condensates in yeast cells, and that these condensates behave as yet another layer of regulation of the HSR. I explore the properties of these condensates, linking gene coalescence to condensate formation, and investigate how Mediator and RNA Pol II may be recruited to these structures. I examine the ways in which these condensates are induced and modulated in cells, primarily by probing Hsf1 regulation and the manner in which transcriptional condensates form. I determine that gene coalescence occurs after condensate formation rather than the other way round, elucidating an emergent property of HSR condensates. Lastly, I provide a mechanism for Hsp70 and phosphorylation regulation of Hsf1, determining that Mediator and Pol II recruitment can be decoupled from transcriptional activation, exhibiting the tunability of Hsf1 activity in response to stress rather than it being an on/off switch.

REFERENCES:

Abravaya, K., Myers, M. P., Murphy, S. P., & Morimoto, R. I. (1992). The human heat shock protein hsp70 interacts with HSF, the transcription factor that regulates heat shock gene expression. *Genes Dev*, *6*(7), 1153-1164. https://doi.org/10.1101/gad.6.7.1153

Åkerfelt, M., Morimoto, R. I., & Sistonen, L. (2010). Heat shock factors: integrators of cell stress, development and lifespan. *Nature Reviews Molecular Cell Biology*, *11*(8), 545-555. https://doi.org/10.1038/nrm2938

Alberti, S., & Hyman, A. A. (2021). Biomolecular condensates at the nexus of cellular stress, protein aggregation disease and ageing. *Nature Reviews Molecular Cell Biology*, *22*(3), 196-213. https://doi.org/10.1038/s41580-020-00326-6

Ali, A., Garde, R., Schaffer, O. C., Bard, J. A. M., Husain, K., Kik, S. K., Davis, K. A., Luengo-Woods, S., Igarashi, M. G., Drummond, D. A., Squires, A. H., & Pincus, D. (2023). Adaptive preservation of orphan ribosomal proteins in chaperone-dispersed condensates. *Nat Cell Biol*, *25*(11), 1691-1703. https://doi.org/10.1038/s41556-023-01253-2

Aligue, R., Akhavan-Niak, H., & Russell, P. (1994). A role for Hsp90 in cell cycle control: Wee1 tyrosine kinase activity requires interaction with Hsp90. *Embo j*, *13*(24), 6099-6106. https://doi.org/10.1002/j.1460-2075.1994.tb06956.x

Altmeyer, M., Neelsen, K. J., Teloni, F., Pozdnyakova, I., Pellegrino, S., Grøfte, M., Rask, M. D., Streicher, W., Jungmichel, S., Nielsen, M. L., & Lukas, J. (2015). Liquid demixing of intrinsically disordered proteins is seeded by poly(ADP-ribose). *Nat Commun*, *6*, 8088. https://doi.org/10.1038/ncomms9088

Amin, J., Fernandez, M., Ananthan, J., Lis, J. T., & Voellmy, R. (1994). Cooperative binding of heat shock transcription factor to the Hsp70 promoter in vivo and in vitro. *J Biol Chem*, *269*(7), 4804-4811.

Anckar, J., & Sistonen, L. (2011). Regulation of HSF1 function in the heat stress response: implications in aging and disease. *Annu Rev Biochem*, *80*, 1089-1115. https://doi.org/10.1146/annurev-biochem-060809-095203

Anderson, P., & Kedersha, N. (2002). Visibly stressed: the role of eIF2, TIA-1, and stress granules in protein translation. *Cell Stress Chaperones*, *7*(2), 213-221. https://doi.org/10.1379/1466-1268(2002)007<0213:vstroe>2.0.co;2

Ashburner, M., & Bonner, J. J. (1979). The induction of gene activity in drosophilia by heat shock. *Cell*, *17*(2), 241-254. https://doi.org/10.1016/0092-8674(79)90150-8

Baler, R., Dahl, G., & Voellmy, R. (1993). Activation of human heat shock genes is accompanied by oligomerization, modification, and rapid translocation of heat shock transcription factor HSF1. *Molecular and cellular biology*, *13*(4), 2486-2496.

Baler, R., Zou, J., & Voellmy, R. (1996). Evidence for a role of Hsp70 in the regulation of the heat shock response in mammalian cells. *Cell Stress Chaperones*, *1*(1), 33-39. https://doi.org/10.1379/1466-1268(1996)001<0033:efaroh>2.3.co;2

Banani, S. F., Lee, H. O., Hyman, A. A., & Rosen, M. K. (2017). Biomolecular condensates: organizers of cellular biochemistry. *Nat Rev Mol Cell Biol*, *18*(5), 285-298. https://doi.org/10.1038/nrm.2017.7

Banani, S. F., Rice, A. M., Peeples, W. B., Lin, Y., Jain, S., Parker, R., & Rosen, M. K. (2016). Compositional Control of Phase-Separated Cellular Bodies. *Cell*, *166*(3), 651-663. https://doi.org/10.1016/j.cell.2016.06.010

Banjade, S., & Rosen, M. K. (2014). Phase transitions of multivalent proteins can promote clustering of membrane receptors. *Elife*, *3*. https://doi.org/10.7554/eLife.04123

Barends, T. R., Werbeck, N. D., & Reinstein, J. (2010). Disaggregases in 4 dimensions. *Curr Opin Struct Biol*, *20*(1), 46-53. https://doi.org/10.1016/j.sbi.2009.12.014

Barna, J., Csermely, P., & Vellai, T. (2018). Roles of heat shock factor 1 beyond the heat shock response. *Cellular and Molecular Life Sciences*, *75*(16), 2897-2916. https://doi.org/10.1007/s00018-018-2836-6

Bashkirova, E., & Lomvardas, S. (2019). Olfactory receptor genes make the case for inter-chromosomal interactions. *Current Opinion in Genetics & Development*, *55*, 106-113. https://doi.org/https://doi.org/10.1016/j.gde.2019.07.004

Bharadwaj, S., Ali, A., & Ovsenek, N. (1999). Multiple components of the HSP90 chaperone complex function in regulation of heat shock factor 1 In vivo. *Mol Cell Biol*, *19*(12), 8033-8041. https://doi.org/10.1128/mcb.19.12.8033

Bienz, M., & Pelham, H. R. B. (1987). Mechanisms of Heat-Shock Gene Activation in Higher Eukaryotes. In J. G. Scandalios & E. W. Caspari (Eds.), *Advances in Genetics* (Vol. 24, pp. 31-72). Academic Press. https://doi.org/https://doi.org/10.1016/S0065-2660(08)60006-1

Billes, V., Kovács, T., Hotzi, B., Manzéger, A., Tagscherer, K., Komlós, M., Tarnóci, A., Pádár, Z., Erdős, A., Bjelik, A., Legradi, A., Gulya, K., Gulyás, B., & Vellai, T. (2016). AUTEN-67 (Autophagy Enhancer-67) Hampers the Progression of Neurodegenerative Symptoms in a Drosophila model of Huntington's Disease. *J Huntingtons Dis*, *5*(2), 133-147. https://doi.org/10.3233/jhd-150180

Boehning, M., Dugast-Darzacq, C., Rankovic, M., Hansen, A. S., Yu, T., Marie-Nelly, H., McSwiggen, D. T., Kokic, G., Dailey, G. M., Cramer, P., Darzacq, X., & Zweckstetter, M. (2018). RNA polymerase II clustering through carboxy-terminal domain phase separation. *Nat Struct Mol Biol*, *25*(9), 833-840. https://doi.org/10.1038/s41594-018-0112-y

Boija, A., Klein, I. A., Sabari, B. R., Dall'Agnese, A., Coffey, E. L., Zamudio, A. V., Li, C. H., Shrinivas, K., Manteiga, J. C., Hannett, N. M., Abraham, B. J., Afeyan, L. K., Guo, Y. E., Rimel, J. K., Fant, C. B., Schuijers, J., Lee, T. I., Taatjes, D. J., & Young, R. A. (2018). Transcription Factors Activate Genes through the Phase-Separation Capacity of Their Activation Domains. *Cell*, *175*(7), 1842-1855.e1816. https://doi.org/10.1016/j.cell.2018.10.042

Boulon, S., Westman, B. J., Hutten, S., Boisvert, F. M., & Lamond, A. I. (2010). The nucleolus under stress. *Mol Cell*, *40*(2), 216-227. https://doi.org/10.1016/j.molcel.2010.09.024

Bracher, A., & Verghese, J. (2015). The nucleotide exchange factors of Hsp70 molecular chaperones. *Front Mol Biosci*, *2*, 10. https://doi.org/10.3389/fmolb.2015.00010

Brandman, O., Stewart-Ornstein, J., Wong, D., Larson, A., Williams, C. C., Li, G. W., Zhou, S., King, D., Shen, P. S., Weibezahn, J., Dunn, J. G., Rouskin, S., Inada, T., Frost, A., & Weissman, J. S. (2012). A ribosome-bound quality control complex triggers degradation of nascent peptides and signals translation stress. *Cell*, *151*(5), 1042-1054. https://doi.org/10.1016/j.cell.2012.10.044

Brangwynne, C. P., Eckmann, C. R., Courson, D. S., Rybarska, A., Hoege, C., Gharakhani, J., Jülicher, F., & Hyman, A. A. (2009). Germline P granules are liquid droplets that localize by controlled dissolution/condensation. *Science*, *324*(5935), 1729-1732. https://doi.org/10.1126/science.1172046

Brangwynne, Clifford P., Tompa, P., & Pappu, Rohit V. (2015). Polymer physics of intracellular phase transitions. *Nature Physics*, *11*(11), 899-904. https://doi.org/10.1038/nphys3532

Buchan, J. R., & Parker, R. (2009). Eukaryotic stress granules: the ins and outs of translation. *Mol Cell*, *36*(6), 932-941. https://doi.org/10.1016/j.molcel.2009.11.020

Budzyński, M. A., Puustinen, M. C., Joutsen, J., & Sistonen, L. (2015). Uncoupling Stress-Inducible Phosphorylation of Heat Shock Factor 1 from Its Activation. *Mol Cell Biol*, *35*(14), 2530-2540. https://doi.org/10.1128/mcb.00816-14

Cai, D., Feliciano, D., Dong, P., Flores, E., Gruebele, M., Porat-Shliom, N., Sukenik, S., Liu, Z., & Lippincott-Schwartz, J. (2019). Phase separation of YAP reorganizes genome topology for long-term YAP target gene expression. *Nat Cell Biol*, *21*(12), 1578-1589. https://doi.org/10.1038/s41556-019-0433-z

Cairns, B. R., Lorch, Y., Li, Y., Zhang, M., Lacomis, L., Erdjument-Bromage, H., Tempst, P., Du, J., Laurent, B., & Kornberg, R. D. (1996). RSC, an Essential, Abundant Chromatin-Remodeling Complex. *Cell*, *87*(7), 1249-1260. https://doi.org/10.1016/S0092-8674(00)81820-6

Cao, S. S., & Kaufman, R. J. (2012). Unfolded protein response. *Current Biology*, *22*(16), R622-R626. https://doi.org/10.1016/j.cub.2012.07.004

Casanueva, M. O., Burga, A., & Lehner, B. (2012). Fitness Trade-Offs and Environmentally Induced Mutation Buffering in Isogenic C. elegans. *Science*, *335*(6064), 82-85. https://doi.org/doi:10.1126/science.1213491

Chong, S., Dugast-Darzacq, C., Liu, Z., Dong, P., Dailey, G. M., Cattoglio, C., Heckert, A., Banala, S., Lavis, L., Darzacq, X., & Tjian, R. (2018). Imaging dynamic and selective low-complexity domain interactions that control gene transcription. *Science*, *361*(6400). https://doi.org/10.1126/science.aar2555

Chong, S., Graham, T. G. W., Dugast-Darzacq, C., Dailey, G. M., Darzacq, X., & Tjian, R. (2022). Tuning levels of low-complexity domain interactions to modulate endogenous oncogenic transcription. *Mol Cell*, *82*(11), 2084-2097.e2085. https://doi.org/10.1016/j.molcel.2022.04.007

Chowdhary, S., Kainth, A. S., & Gross, D. S. (2017). Heat Shock Protein Genes Undergo Dynamic Alteration in Their Three-Dimensional Structure and Genome Organization in Response to Thermal Stress. *Mol Cell Biol*, *37*(24). https://doi.org/10.1128/mcb.00292-17

Chowdhary, S., Kainth, A. S., Paracha, S., Gross, D. S., & Pincus, D. (2022). Inducible transcriptional condensates drive 3D genome reorganization in the heat shock response. *Mol Cell*, *82*(22), 4386-4399.e4387. https://doi.org/10.1016/j.molcel.2022.10.013

Chowdhary, S., Kainth, A. S., Pincus, D., & Gross, D. S. (2019). Heat Shock Factor 1 Drives Intergenic Association of Its Target Gene Loci upon Heat Shock. *Cell Rep*, *26*(1), 18-28.e15. https://doi.org/10.1016/j.celrep.2018.12.034

Ciccarelli, M., & Andréasson, C. (2024). Protein Misfolding Releases Human HSF1 from HSP70 Latency Control. *Journal of Molecular Biology*, *436*(20), 168740. https://doi.org/https://doi.org/10.1016/j.jmb.2024.168740

Core, L. J., Waterfall, J. J., & Lis, J. T. (2008). Nascent RNA sequencing reveals widespread pausing and divergent initiation at human promoters. *Science*, *322*(5909), 1845-1848. https://doi.org/10.1126/science.1162228

Cowen, L. E., & Lindquist, S. (2005). Hsp90 potentiates the rapid evolution of new traits: drug resistance in diverse fungi. *Science*, *309*(5744), 2185-2189. https://doi.org/10.1126/science.1118370

Dai, C., & Sampson, S. B. (2016). HSF1: Guardian of Proteostasis in Cancer. *Trends in Cell Biology*, *26*(1), 17-28. https://doi.org/https://doi.org/10.1016/j.tcb.2015.10.011

Das, R. K., & Pappu, R. V. (2013). Conformations of intrinsically disordered proteins are influenced by linear sequence distributions of oppositely charged residues. *Proc Natl Acad Sci U S A*, *110*(33), 13392-13397. https://doi.org/10.1073/pnas.1304749110

Dea, A., & Pincus, D. (2024). The Heat Shock Response as a Condensate Cascade. *Journal of Molecular Biology*, *436*(14), 168642. https://doi.org/https://doi.org/10.1016/j.jmb.2024.168642

Decker, C. J., Teixeira, D., & Parker, R. (2007). Edc3p and a glutamine/asparagine-rich domain of Lsm4p function in processing body assembly in Saccharomyces cerevisiae. *J Cell Biol*, *179*(3), 437-449. https://doi.org/10.1083/jcb.200704147

Dekker, J. (2014). Two ways to fold the genome during the cell cycle: insights obtained with chromosome conformation capture. *Epigenetics & Chromatin*, *7*(1), 25. https://doi.org/10.1186/1756-8935-7-25

Ditlev, J. A., Case, L. B., & Rosen, M. K. (2018). Who's In and Who's Out-Compositional Control of Biomolecular Condensates. *J Mol Biol*, *430*(23), 4666-4684. https://doi.org/10.1016/j.jmb.2018.08.003

Doyle, S. M., & Wickner, S. (2009). Hsp104 and ClpB: protein disaggregating machines. *Trends in Biochemical Sciences*, *34*(1), 40-48. https://doi.org/10.1016/j.tibs.2008.09.010

Duarte, F. M., Fuda, N. J., Mahat, D. B., Core, L. J., Guertin, M. J., & Lis, J. T. (2016). Transcription factors GAF and HSF act at distinct regulatory steps to modulate stress-induced gene activation. *Genes Dev*, *30*(15), 1731-1746. https://doi.org/10.1101/gad.284430.116

Dukler, N., Gulko, B., Huang, Y. F., & Siepel, A. (2016). Is a super-enhancer greater than the sum of its parts? *Nat Genet*, *49*(1), 2-3. https://doi.org/10.1038/ng.3759

Erkine, A. M., Magrogan, S. F., Sekinger, E. A., & Gross, D. S. (1999). Cooperative binding of heat shock factor to the yeast HSP82 promoter in vivo and in vitro. *Mol Cell Biol*, *19*(3), 1627-1639. https://doi.org/10.1128/mcb.19.3.1627

Faust, O., & Rosenzweig, R. (2020). Structural and Biochemical Properties of Hsp40/Hsp70 Chaperone System. In M. L. Mendillo, D. Pincus, & R. Scherz-Shouval (Eds.), *HSF1 and Molecular Chaperones in Biology and Cancer* (pp. 3-20). Springer International Publishing. https://doi.org/10.1007/978-3-030-40204-4_1

Feder, Z. A., Ali, A., Singh, A., Krakowiak, J., Zheng, X., Bindokas, V. P., Wolfgeher, D., Kron, S. J., & Pincus, D. (2021). Subcellular localization of the J-protein Sis1 regulates the heat shock response. *J Cell Biol*, *220*(1). https://doi.org/10.1083/jcb.202005165

Field, A., & Adelman, K. (2020). Evaluating Enhancer Function and Transcription. *Annu Rev Biochem*, *89*, 213-234. https://doi.org/10.1146/annurev-biochem-011420-095916

Fromm, S. A., Kamenz, J., Nöldeke, E. R., Neu, A., Zocher, G., & Sprangers, R. (2014). In vitro reconstitution of a cellular phase-transition process that involves the mRNA decapping machinery. *Angew Chem Int Ed Engl*, *53*(28), 7354-7359. https://doi.org/10.1002/anie.201402885

Frottin, F., Schueder, F., Tiwary, S., Gupta, R., Körner, R., Schlichthaerle, T., Cox, J., Jungmann, R., Hartl, F. U., & Hipp, M. S. (2019). The nucleolus functions as a phase-separated protein quality control compartment. *Science*, *365*(6451), 342-347. https://doi.org/10.1126/science.aaw9157

Frydman, J. (2001). Folding of newly translated proteins in vivo: the role of molecular chaperones. *Annu Rev Biochem*, *70*, 603-647. https://doi.org/10.1146/annurev.biochem.70.1.603

Fujimoto, M., Takaki, E., Takii, R., Tan, K., Prakasam, R., Hayashida, N., Iemura, S., Natsume, T., & Nakai, A. (2012). RPA assists HSF1 access to nucleosomal DNA by recruiting histone chaperone FACT. *Mol Cell*, *48*(2), 182-194. https://doi.org/10.1016/j.molcel.2012.07.026

Garde, R., Dea, A., Herwig, M. F., Ali, A., & Pincus, D. (2024). Feedback control of the heat shock response by spatiotemporal regulation of Hsp70. *Journal of Cell Biology*, *223*(12). https://doi.org/10.1083/jcb.202401082

Gasch, A. P., & Werner-Washburne, M. (2002). The genomics of yeast responses to environmental stress and starvation. *Funct Integr Genomics*, *2*(4-5), 181-192. https://doi.org/10.1007/s10142-002-0058-2

Gilks, N., Kedersha, N., Ayodele, M., Shen, L., Stoecklin, G., Dember, L. M., & Anderson, P. (2004). Stress granule assembly is mediated by prion-like aggregation of TIA-1. *Mol Biol Cell*, *15*(12), 5383-5398. https://doi.org/10.1091/mbc.e04-08-0715

Gomez-Pastor, R., Burchfiel, E. T., & Thiele, D. J. (2018). Regulation of heat shock transcription factors and their roles in physiology and disease. *Nature Reviews Molecular Cell Biology*, *19*(1), 4-19. https://doi.org/10.1038/nrm.2017.73

Gosselin, D., Link, V. M., Romanoski, C. E., Fonseca, G. J., Eichenfield, D. Z., Spann, N. J., Stender, J. D., Chun, H. B., Garner, H., Geissmann, F., & Glass, C. K. (2014). Environment drives selection and function of enhancers controlling tissue-specific macrophage identities. *Cell*, *159*(6), 1327-1340. https://doi.org/10.1016/j.cell.2014.11.023

Green, M., Schuetz, T. J., Sullivan, E. K., & Kingston, R. E. (1995). A heat shock-responsive domain of human HSF1 that regulates transcription activation domain function. *Mol Cell Biol*, *15*(6), 3354-3362. https://doi.org/10.1128/mcb.15.6.3354

Guertin, M. J., & Lis, J. T. (2010). Chromatin landscape dictates HSF binding to target DNA elements. *PLoS Genet*, *6*(9), e1001114. https://doi.org/10.1371/journal.pgen.1001114

Guettouche, T., Boellmann, F., Lane, W. S., & Voellmy, R. (2005). Analysis of phosphorylation of human heat shock factor 1 in cells experiencing a stress. *BMC Biochem*, *6*, 4. https://doi.org/10.1186/1471-2091-6-4

Guillén-Boixet, J., Kopach, A., Holehouse, A. S., Wittmann, S., Jahnel, M., Schlüßler, R., Kim, K., Trussina, I., Wang, J., Mateju, D., Poser, I., Maharana, S., Ruer-Gruß, M., Richter, D., Zhang, X., Chang, Y. T., Guck, J., Honigmann, A., Mahamid, J.,…Franzmann, T. M. (2020). RNA-Induced Conformational Switching and Clustering of G3BP Drive Stress Granule Assembly by Condensation. *Cell*, *181*(2), 346-361.e317. https://doi.org/10.1016/j.cell.2020.03.049

Guo, Y., Guettouche, T., Fenna, M., Boellmann, F., Pratt, W. B., Toft, D. O., Smith, D. F., & Voellmy, R. (2001). Evidence for a mechanism of repression of heat shock factor 1 transcriptional activity by a multichaperone complex. *Journal of Biological Chemistry*, *276*(49), 45791-45799.

Guo, Y. E., Manteiga, J. C., Henninger, J. E., Sabari, B. R., Dall'Agnese, A., Hannett, N. M., Spille, J. H., Afeyan, L. K., Zamudio, A. V., Shrinivas, K., Abraham, B. J., Boija, A., Decker, T. M., Rimel, J. K., Fant, C. B., Lee, T. I., Cisse, II, Sharp, P. A., Taatjes, D. J., & Young, R. A. (2019). Pol II phosphorylation regulates a switch between transcriptional and splicing condensates. *Nature*, *572*(7770), 543-548. https://doi.org/10.1038/s41586-019-1464-0

Guthmann, M., Qian, C., Gialdini, I., Nakatani, T., Ettinger, A., Schauer, T., Kukhtevich, I., Schneider, R., Lamb, D. C., Burton, A., & Torres-Padilla, M. E. (2023). A change in biophysical properties accompanies heterochromatin formation in mouse embryos. *Genes Dev*, *37*(7-8), 336-350. https://doi.org/10.1101/gad.350353.122

Hahn, J. S., Hu, Z., Thiele, D. J., & Iyer, V. R. (2004). Genome-wide analysis of the biology of stress responses through heat shock transcription factor. *Mol Cell Biol*, *24*(12), 5249-5256. https://doi.org/10.1128/mcb.24.12.5249-5256.2004

Henninger, J. E., Oksuz, O., Shrinivas, K., Sagi, I., LeRoy, G., Zheng, M. M., Andrews, J. O., Zamudio, A. V., Lazaris, C., Hannett, N. M., Lee, T. I., Sharp, P. A., Cissé, II, Chakraborty, A. K., & Young, R. A. (2021). RNA-Mediated Feedback Control of Transcriptional Condensates. *Cell*, *184*(1), 207-225.e224. https://doi.org/10.1016/j.cell.2020.11.030

Hentze, N., Le Breton, L., Wiesner, J., Kempf, G., & Mayer, M. P. (2016). Molecular mechanism of thermosensory function of human heat shock transcription factor Hsf1. *Elife*, *5*. https://doi.org/10.7554/eLife.11576

Hietakangas, V., Ahlskog, J. K., Jakobsson, A. M., Hellesuo, M., Sahlberg, N. M., Holmberg, C. I., Mikhailov, A., Palvimo, J. J., Pirkkala, L., & Sistonen, L. (2003). Phosphorylation of serine 303 is a prerequisite for the stress-inducible SUMO modification of heat shock factor 1. *Mol Cell Biol*, *23*(8), 2953-2968. https://doi.org/10.1128/mcb.23.8.2953-2968.2003

Hnisz, D., Abraham, B. J., Lee, T. I., Lau, A., Saint-André, V., Sigova, A. A., Hoke, H. A., & Young, R. A. (2013). Super-enhancers in the control of cell identity and disease. *Cell*, *155*(4), 934-947. https://doi.org/10.1016/j.cell.2013.09.053

Hofweber, M., Hutten, S., Bourgeois, B., Spreitzer, E., Niedner-Boblenz, A., Schifferer, M., Ruepp, M. D., Simons, M., Niessing, D., Madl, T., & Dormann, D. (2018). Phase Separation of FUS Is Suppressed by Its Nuclear Import Receptor and Arginine Methylation. *Cell*, *173*(3), 706-719.e713. https://doi.org/10.1016/j.cell.2018.03.004

Hsu, A. L., Murphy, C. T., & Kenyon, C. (2003). Regulation of aging and age-related disease by DAF-16 and heat-shock factor. *Science*, *300*(5622), 1142-1145. https://doi.org/10.1126/science.1083701

Hyman, A. A., Weber, C. A., & Jülicher, F. (2014). Liquid-liquid phase separation in biology. *Annu Rev Cell Dev Biol*, *30*, 39-58. https://doi.org/10.1146/annurev-cellbio-100913-013325

Ishida, R., Okamoto, T., Motojima, F., Kubota, H., Takahashi, H., Tanabe, M., Oka, T., Kitamura, A., Kinjo, M., Yoshida, M., Otaka, M., Grave, E., & Itoh, H. (2018). Physicochemical Properties of the Mammalian Molecular Chaperone HSP60. *Int J Mol Sci*, *19*(2). https://doi.org/10.3390/ijms19020489

Izu, H., Inouye, S., Fujimoto, M., Shiraishi, K., Naito, K., & Nakai, A. (2004). Heat shock transcription factor 1 is involved in quality-control mechanisms in male germ cells. *Biology of reproduction*, *70*(1), 18-24.

Jaeger, A. M., Makley, L. N., Gestwicki, J. E., & Thiele, D. J. (2014). Genomic heat shock element sequences drive cooperative human heat shock factor 1 DNA binding and selectivity. *J Biol Chem*, *289*(44), 30459-30469. https://doi.org/10.1074/jbc.M114.591578

Jamrich, M., Greenleaf, A. L., & Bautz, E. K. (1977). Localization of RNA polymerase in polytene chromosomes of Drosophila melanogaster. *Proc Natl Acad Sci U S A*, *74*(5), 2079-2083. https://doi.org/10.1073/pnas.74.5.2079

Jedlicka, P., Mortin, M. A., & Wu, C. (1997). Multiple functions of Drosophila heat shock transcription factor in vivo. *Embo j*, *16*(9), 2452-2462. https://doi.org/10.1093/emboj/16.9.2452

Jin, J., Xie, X., Chen, C., Park, J. G., Stark, C., James, D. A., Olhovsky, M., Linding, R., Mao, Y., & Pawson, T. (2009). Eukaryotic protein domains as functional units of cellular evolution. *Sci Signal*, *2*(98), ra76. https://doi.org/10.1126/scisignal.2000546

Kampinga, H. H., & Craig, E. A. (2010). The HSP70 chaperone machinery: J proteins as drivers of functional specificity. *Nat Rev Mol Cell Biol*, *11*(8), 579-592. https://doi.org/10.1038/nrm2941

Karras, G. I., Yi, S., Sahni, N., Fischer, M., Xie, J., Vidal, M., D'Andrea, A. D., Whitesell, L., & Lindquist, S. (2017). HSP90 Shapes the Consequences of Human Genetic Variation. *Cell*, *168*(5), 856-866.e812. https://doi.org/10.1016/j.cell.2017.01.023

Kato, M., Han, Tina W., Xie, S., Shi, K., Du, X., Wu, Leeju C., Mirzaei, H., Goldsmith, Elizabeth J., Longgood, J., Pei, J., Grishin, Nick V., Frantz, Douglas E., Schneider, Jay W., Chen, S., Li, L., Sawaya, Michael R., Eisenberg, D., Tycko, R., & McKnight, Steven L. (2012). Cell-free Formation of RNA Granules: Low Complexity Sequence Domains Form Dynamic Fibers within Hydrogels. *Cell*, *149*(4), 753-767. https://doi.org/10.1016/j.cell.2012.04.017

Kiefhaber, T., Rudolph, R., Kohler, H. H., & Buchner, J. (1991). Protein aggregation in vitro and in vivo: a quantitative model of the kinetic competition between folding and aggregation. *Biotechnology (N Y)*, *9*(9), 825-829. https://doi.org/10.1038/nbt0991-825

Kim, S. J., Tsukiyama, T., Lewis, M. S., & Wu, C. (1994). Interaction of the DNA-binding domain of Drosophila heat shock factor with its cognate DNA site: a thermodynamic analysis using analytical ultracentrifugation. *Protein Sci*, *3*(7), 1040-1051. https://doi.org/10.1002/pro.5560030706

Kim, Y. J., Lee Jr, M., Lee, Y.-T., Jing, J., Sanders, J. T., Botten, G. A., He, L., Lyu, J., Zhang, Y., & Mettlen, M. (2023). Light-activated macromolecular phase separation modulates transcription by reconfiguring chromatin interactions. *Science Advances*, *9*(13), eadg1123.

Kityk, R., Vogel, M., Schlecht, R., Bukau, B., & Mayer, M. P. (2015). Pathways of allosteric regulation in Hsp70 chaperones. *Nat Commun*, *6*, 8308. https://doi.org/10.1038/ncomms9308

Kmiecik, S. W., Drzewicka, K., Melchior, F., & Mayer, M. P. (2021). Heat shock transcription factor 1 is SUMOylated in the activated trimeric state. *J Biol Chem*, *296*, 100324. https://doi.org/10.1016/j.jbc.2021.100324

Kmiecik, S. W., Le Breton, L., & Mayer, M. P. (2020). Feedback regulation of heat shock factor 1 (Hsf1) activity by Hsp70‐mediated trimer unzipping and dissociation from DNA. *The EMBO Journal*, *39*(14), e104096. https://doi.org/https://doi.org/10.15252/embj.2019104096

Kmiecik, S. W., & Mayer, M. P. (2022). Molecular mechanisms of heat shock factor 1 regulation. *Trends in Biochemical Sciences*, *47*(3), 218-234. https://doi.org/10.1016/j.tibs.2021.10.004

Krakowiak, J., Zheng, X., Patel, N., Feder, Z. A., Anandhakumar, J., Valerius, K., Gross, D. S., Khalil, A. S., & Pincus, D. (2018). Hsf1 and Hsp70 constitute a two-component feedback loop that regulates the yeast heat shock response. *Elife*, *7*. https://doi.org/10.7554/eLife.31668

Lee, R., Kang, M.-K., Kim, Y.-J., Yang, B., Shim, H., Kim, S., Kim, K., Yang, C. M., Min, B.-g., Jung, W.-J., Lee, E.-C., Joo, J.-S., Park, G., Cho, W.-K., & Kim, H.-P. (2021). CTCF-mediated chromatin looping provides a topological framework for the formation of phase-separated transcriptional condensates. *Nucleic Acids Research*, *50*(1), 207-226. https://doi.org/10.1093/nar/gkab1242

Li, J., Chauve, L., Phelps, G., Brielmann, R. M., & Morimoto, R. I. (2016). E2F coregulates an essential HSF developmental program that is distinct from the heat-shock response. *Genes Dev*, *30*(18), 2062-2075. https://doi.org/10.1101/gad.283317.116

Li, J., Labbadia, J., & Morimoto, R. I. (2017). Rethinking HSF1 in Stress, Development, and Organismal Health. *Trends Cell Biol*, *27*(12), 895-905. https://doi.org/10.1016/j.tcb.2017.08.002

Li, P., Banjade, S., Cheng, H.-C., Kim, S., Chen, B., Guo, L., Llaguno, M., Hollingsworth, J. V., King, D. S., Banani, S. F., Russo, P. S., Jiang, Q.-X., Nixon, B. T., & Rosen, M. K. (2012). Phase transitions in the assembly of multivalent signalling proteins. *Nature*, *483*(7389), 336-340. https://doi.org/10.1038/nature10879

Lin, Y., Protter, D. S., Rosen, M. K., & Parker, R. (2015). Formation and Maturation of Phase-Separated Liquid Droplets by RNA-Binding Proteins. *Mol Cell*, *60*(2), 208-219. https://doi.org/10.1016/j.molcel.2015.08.018

Lindquist, S. (1986). THE HEAT-SHOCK RESPONSE. *Annual Review of Biochemistry*, *55*(Volume 55, 1986), 1151-1191. https://doi.org/https://doi.org/10.1146/annurev.bi.55.070186.005443

Lindquist, S. (2009). Protein folding sculpting evolutionary change. *Cold Spring Harb Symp Quant Biol*, *74*, 103-108. https://doi.org/10.1101/sqb.2009.74.043

Lyon, A. S., Peeples, W. B., & Rosen, M. K. (2021). A framework for understanding the functions of biomolecular condensates across scales. *Nat Rev Mol Cell Biol*, *22*(3), 215-235. https://doi.org/10.1038/s41580-020-00303-z

Lyons, H., Veettil, R. T., Pradhan, P., Fornero, C., De La Cruz, N., Ito, K., Eppert, M., Roeder, R. G., & Sabari, B. R. (2023). Functional partitioning of transcriptional regulators by patterned charge blocks. *Cell*, *186*(2), 327-345.e328. https://doi.org/10.1016/j.cell.2022.12.013

Maharana, S., Wang, J., Papadopoulos, D. K., Richter, D., Pozniakovsky, A., Poser, I., Bickle, M., Rizk, S., Guillén-Boixet, J., Franzmann, T. M., Jahnel, M., Marrone, L., Chang, Y.-T., Sterneckert, J., Tomancak, P., Hyman, A. A., & Alberti, S. (2018). RNA buffers the phase separation behavior of prion-like RNA binding proteins. *Science*, *360*(6391), 918-921. https://doi.org/doi:10.1126/science.aar7366

Mahat, D. B., Salamanca, H. H., Duarte, F. M., Danko, C. G., & Lis, J. T. (2016). Mammalian Heat Shock Response and Mechanisms Underlying Its Genome-wide Transcriptional Regulation. *Mol Cell*, *62*(1), 63-78. https://doi.org/10.1016/j.molcel.2016.02.025

Masser, A. E., Kang, W., Roy, J., Mohanakrishnan Kaimal, J., Quintana-Cordero, J., Friedländer, M. R., & Andréasson, C. (2019). Cytoplasmic protein misfolding titrates Hsp70 to activate nuclear Hsf1. *Elife*, *8*, e47791.

Mayer, M. P. (2010). Gymnastics of molecular chaperones. *Mol Cell*, *39*(3), 321-331. https://doi.org/10.1016/j.molcel.2010.07.012

Mayer, M. P., & Bukau, B. (2005). Hsp70 chaperones: cellular functions and molecular mechanism. *Cell Mol Life Sci*, *62*(6), 670-684. https://doi.org/10.1007/s00018-004-4464-6

Mayer, M. P., Schröder, H., Rüdiger, S., Paal, K., Laufen, T., & Bukau, B. (2000). Multistep mechanism of substrate binding determines chaperone activity of Hsp70. *Nat Struct Biol*, *7*(7), 586-593. https://doi.org/10.1038/76819

McCubrey, J. A., Steelman, L. S., Chappell, W. H., Abrams, S. L., Wong, E. W., Chang, F., Lehmann, B., Terrian, D. M., Milella, M., Tafuri, A., Stivala, F., Libra, M., Basecke, J., Evangelisti, C., Martelli, A. M., & Franklin, R. A. (2007). Roles of the Raf/MEK/ERK pathway in cell growth, malignant transformation and drug resistance. *Biochim Biophys Acta*, *1773*(8), 1263-1284. https://doi.org/10.1016/j.bbamcr.2006.10.001

Mehlen, P., Kretz-Remy, C., Préville, X., & Arrigo, A. P. (1996). Human hsp27, Drosophila hsp27 and human alphaB-crystallin expression-mediated increase in glutathione is essential for the protective activity of these proteins against TNFalpha-induced cell death. *Embo j*, *15*(11), 2695-2706.

Mendillo, M. L., Santagata, S., Koeva, M., Bell, G. W., Hu, R., Tamimi, R. M., Fraenkel, E., Ince, T. A., Whitesell, L., & Lindquist, S. (2012). HSF1 drives a transcriptional program distinct from heat shock to support highly malignant human cancers. *Cell*, *150*(3), 549-562. https://doi.org/10.1016/j.cell.2012.06.031

Metchat, A., Akerfelt, M., Bierkamp, C., Delsinne, V., Sistonen, L., Alexandre, H., & Christians, E. S. (2009). Mammalian heat shock factor 1 is essential for oocyte meiosis and directly regulates Hsp90alpha expression. *J Biol Chem*, *284*(14), 9521-9528. https://doi.org/10.1074/jbc.M808819200

Mitrea, D. M., Cika, J. A., Guy, C. S., Ban, D., Banerjee, P. R., Stanley, C. B., Nourse, A., Deniz, A. A., & Kriwacki, R. W. (2016). Nucleophosmin integrates within the nucleolus via multi-modal interactions with proteins displaying R-rich linear motifs and rRNA. *Elife*, *5*. https://doi.org/10.7554/eLife.13571

Mogk, A., Kummer, E., & Bukau, B. (2015). Cooperation of Hsp70 and Hsp100 chaperone machines in protein disaggregation. *Front Mol Biosci*, *2*, 22. https://doi.org/10.3389/fmolb.2015.00022

Molliex, A., Temirov, J., Lee, J., Coughlin, M., Kanagaraj, A. P., Kim, H. J., Mittag, T., & Taylor, J. P. (2015). Phase separation by low complexity domains promotes stress granule assembly and drives pathological fibrillization. *Cell*, *163*(1), 123-133. https://doi.org/10.1016/j.cell.2015.09.015

Monahan, Z., Ryan, V. H., Janke, A. M., Burke, K. A., Rhoads, S. N., Zerze, G. H., O'Meally, R., Dignon, G. L., Conicella, A. E., Zheng, W., Best, R. B., Cole, R. N., Mittal, J., Shewmaker, F., & Fawzi, N. L. (2017). Phosphorylation of the FUS low-complexity domain disrupts phase separation, aggregation, and toxicity. *Embo j*, *36*(20), 2951-2967. https://doi.org/10.15252/embj.201696394

Mueller, B., Mieczkowski, J., Kundu, S., Wang, P., Sadreyev, R., Tolstorukov, M. Y., & Kingston, R. E. (2017). Widespread changes in nucleosome accessibility without changes in nucleosome occupancy during a rapid transcriptional induction. *Genes Dev*, *31*(5), 451-462. https://doi.org/10.1101/gad.293118.116

Mulyasasmita, W., Lee, J. S., & Heilshorn, S. C. (2011). Molecular-level engineering of protein physical hydrogels for predictive sol-gel phase behavior. *Biomacromolecules*, *12*(10), 3406-3411. https://doi.org/10.1021/bm200959e

Nair, S. J., Yang, L., Meluzzi, D., Oh, S., Yang, F., Friedman, M. J., Wang, S., Suter, T., Alshareedah, I., Gamliel, A., Ma, Q., Zhang, J., Hu, Y., Tan, Y., Ohgi, K. A., Jayani, R. S., Banerjee, P. R., Aggarwal, A. K., & Rosenfeld, M. G. (2019). Phase separation of ligand-activated enhancers licenses cooperative chromosomal enhancer assembly. *Nat Struct Mol Biol*, *26*(3), 193-203. https://doi.org/10.1038/s41594-019-0190-5

Neef, D. W., Jaeger, A. M., Gomez-Pastor, R., Willmund, F., Frydman, J., & Thiele, D. J. (2014). A direct regulatory interaction between chaperonin TRiC and stress-responsive transcription factor HSF1. *Cell Rep*, *9*(3), 955-966. https://doi.org/10.1016/j.celrep.2014.09.056

Neef, D. W., Jaeger, A. M., & Thiele, D. J. (2011). Heat shock transcription factor 1 as a therapeutic target in neurodegenerative diseases. *Nat Rev Drug Discov*, *10*(12), 930-944. https://doi.org/10.1038/nrd3453

Neudegger, T., Verghese, J., Hayer-Hartl, M., Hartl, F. U., & Bracher, A. (2016). Structure of human heat-shock transcription factor 1 in complex with DNA. *Nat Struct Mol Biol*, *23*(2), 140-146. https://doi.org/10.1038/nsmb.3149

Nott, T. J., Petsalaki, E., Farber, P., Jervis, D., Fussner, E., Plochowietz, A., Craggs, T. D., Bazett-Jones, D. P., Pawson, T., Forman-Kay, J. D., & Baldwin, A. J. (2015). Phase transition of a disordered nuage protein generates environmentally responsive membraneless organelles. *Mol Cell*, *57*(5), 936-947. https://doi.org/10.1016/j.molcel.2015.01.013

Oguchi, Y., Kummer, E., Seyffer, F., Berynskyy, M., Anstett, B., Zahn, R., Wade, R. C., Mogk, A., & Bukau, B. (2012). A tightly regulated molecular toggle controls AAA+ disaggregase. *Nat Struct Mol Biol*, *19*(12), 1338-1346. https://doi.org/10.1038/nsmb.2441

Oshidari, R., Huang, R., Medghalchi, M., Tse, E. Y. W., Ashgriz, N., Lee, H. O., Wyatt, H., & Mekhail, K. (2020). DNA repair by Rad52 liquid droplets. *Nat Commun*, *11*(1), 695. https://doi.org/10.1038/s41467-020-14546-z

Pak, C. W., Kosno, M., Holehouse, A. S., Padrick, S. B., Mittal, A., Ali, R., Yunus, A. A., Liu, D. R., Pappu, R. V., & Rosen, M. K. (2016). Sequence Determinants of Intracellular Phase Separation by Complex Coacervation of a Disordered Protein. *Mol Cell*, *63*(1), 72-85. https://doi.org/10.1016/j.molcel.2016.05.042

Patriarca, E. J., & Maresca, B. (1990). Acquired thermotolerance following heat shock protein synthesis prevents impairment of mitochondrial ATPase activity at elevated temperatures in Saccharomyces cerevisiae. *Exp Cell Res*, *190*(1), 57-64. https://doi.org/10.1016/0014-4827(90)90143-x

Pavitt, G. D. (2005). eIF2B, a mediator of general and gene-specific translational control. *Biochem Soc Trans*, *33*(Pt 6), 1487-1492. https://doi.org/10.1042/bst0331487

Peffer, S., Gonçalves, D., & Morano, K. A. (2019). Regulation of the Hsf1-dependent transcriptome via conserved bipartite contacts with Hsp70 promotes survival in yeast. *J Biol Chem*, *294*(32), 12191-12202. https://doi.org/10.1074/jbc.RA119.008822

Pelham, H. R. (1982). A regulatory upstream promoter element in the Drosophila hsp 70 heat-shock gene. *Cell*, *30*(2), 517-528. https://doi.org/10.1016/0092-8674(82)90249-5

Phair, R. D., & Misteli, T. (2000). High mobility of proteins in the mammalian cell nucleus. *Nature*, *404*(6778), 604-609. https://doi.org/10.1038/35007077

Pincus, D. (2020). Regulation of Hsf1 and the Heat Shock Response. In M. L. Mendillo, D. Pincus, & R. Scherz-Shouval (Eds.), *HSF1 and Molecular Chaperones in Biology and Cancer* (pp. 41-50). Springer International Publishing. https://doi.org/10.1007/978-3-030-40204-4_3

Pincus, D., Anandhakumar, J., Thiru, P., Guertin, M. J., Erkine, A. M., & Gross, D. S. (2018). Genetic and epigenetic determinants establish a continuum of Hsf1 occupancy and activity across the yeast genome. *Molecular Biology of the Cell*, *29*(26), 3168-3182. https://doi.org/10.1091/mbc.E18-06-0353

Powers, E. T., Morimoto, R. I., Dillin, A., Kelly, J. W., & Balch, W. E. (2009). Biological and chemical approaches to diseases of proteostasis deficiency. *Annu Rev Biochem*, *78*, 959-991. https://doi.org/10.1146/annurev.biochem.052308.114844

Prince, T. L., Kijima, T., Tatokoro, M., Lee, S., Tsutsumi, S., Yim, K., Rivas, C., Alarcon, S., Schwartz, H., Khamit-Kush, K., Scroggins, B. T., Beebe, K., Trepel, J. B., & Neckers, L. (2015). Client Proteins and Small Molecule Inhibitors Display Distinct Binding Preferences for Constitutive and Stress-Induced HSP90 Isoforms and Their Conformationally Restricted Mutants. *PLoS One*, *10*(10), e0141786. https://doi.org/10.1371/journal.pone.0141786

Rabindran, S. K., Haroun, R. I., Clos, J., Wisniewski, J., & Wu, C. (1993). Regulation of heat shock factor trimer formation: role of a conserved leucine zipper. *Science*, *259*(5092), 230-234.

Ramasamy, S., Aljahani, A., Karpinska, M. A., Cao, T. B. N., Velychko, T., Cruz, J. N., Lidschreiber, M., & Oudelaar, A. M. (2023). The Mediator complex regulates enhancer-promoter interactions. *Nat Struct Mol Biol*, *30*(7), 991-1000. https://doi.org/10.1038/s41594-023-01027-2

Rawat, P., Boehning, M., Hummel, B., Aprile-Garcia, F., Pandit, A. S., Eisenhardt, N., Khavaran, A., Niskanen, E., Vos, S. M., Palvimo, J. J., Pichler, A., Cramer, P., & Sawarkar, R. (2021). Stress-induced nuclear condensation of NELF drives transcriptional downregulation. *Mol Cell*, *81*(5), 1013-1026.e1011. https://doi.org/10.1016/j.molcel.2021.01.016

Reijns, M. A., Alexander, R. D., Spiller, M. P., & Beggs, J. D. (2008). A role for Q/N-rich aggregation-prone regions in P-body localization. *J Cell Sci*, *121*(Pt 15), 2463-2472. https://doi.org/10.1242/jcs.024976

Reinle, K., Mogk, A., & Bukau, B. (2022). The Diverse Functions of Small Heat Shock Proteins in the Proteostasis Network. *J Mol Biol*, *434*(1), 167157. https://doi.org/10.1016/j.jmb.2021.167157

Riback, J. A., Katanski, C. D., Kear-Scott, J. L., Pilipenko, E. V., Rojek, A. E., Sosnick, T. R., & Drummond, D. A. (2017). Stress-Triggered Phase Separation Is an Adaptive, Evolutionarily Tuned Response. *Cell*, *168*(6), 1028-1040.e1019. https://doi.org/10.1016/j.cell.2017.02.027

Richter, K., Haslbeck, M., & Buchner, J. (2010). The heat shock response: life on the verge of death. *Mol Cell*, *40*(2), 253-266. https://doi.org/10.1016/j.molcel.2010.10.006

Riedl, M., Strauch, A., Catici, D. A., & Haslbeck, M. (2020). Proteinaceous transformers: Structural and functional variability of human sHsps. *International Journal of Molecular Sciences*, *21*(15), 5448.

Ritossa, F. (1962). A new puffing pattern induced by temperature shock and DNP in Drosophila. *Experientia*, *18*(12), 571-573.

Rosenzweig, R., Nillegoda, N. B., Mayer, M. P., & Bukau, B. (2019). The Hsp70 chaperone network. *Nature Reviews Molecular Cell Biology*, *20*(11), 665-680. https://doi.org/10.1038/s41580-019-0133-3

Ryu, K., Park, G., & Cho, W. K. (2024). Emerging insights into transcriptional condensates. *Exp Mol Med*, *56*(4), 820-826. https://doi.org/10.1038/s12276-024-01228-9

Sabari, B. R., Dall'Agnese, A., Boija, A., Klein, I. A., Coffey, E. L., Shrinivas, K., Abraham, B. J., Hannett, N. M., Zamudio, A. V., Manteiga, J. C., Li, C. H., Guo, Y. E., Day, D. S., Schuijers, J., Vasile, E., Malik, S., Hnisz, D., Lee, T. I., Cisse, II,…Young, R. A. (2018). Coactivator condensation at super-enhancers links phase separation and gene control. *Science*, *361*(6400). https://doi.org/10.1126/science.aar3958

Sabari, B. R., Dall'Agnese, A., & Young, R. A. (2020). Biomolecular Condensates in the Nucleus. *Trends Biochem Sci*, *45*(11), 961-977. https://doi.org/10.1016/j.tibs.2020.06.007

Sarge, K. D., Murphy, S. P., & Morimoto, R. I. (1993). Activation of heat shock gene transcription by heat shock factor 1 involves oligomerization, acquisition of DNA-binding activity, and nuclear localization and can occur in the absence of stress. *Mol Cell Biol*, *13*(3), 1392-1407. https://doi.org/10.1128/mcb.13.3.1392-1407.1993

Sawarkar, R. (2022). Transcriptional lockdown during acute proteotoxic stress. *Trends Biochem Sci*, *47*(8), 660-672. https://doi.org/10.1016/j.tibs.2022.03.020

Schmauder, L., Sima, S., Hadj, A. B., Cesar, R., & Richter, K. (2022). Binding of the HSF-1 DNA-binding domain to multimeric C. elegans consensus HSEs is guided by cooperative interactions. *Scientific Reports*, *12*(1), 8984. https://doi.org/10.1038/s41598-022-12736-x

Semenza, G. L. (2003). Targeting HIF-1 for cancer therapy. *Nat Rev Cancer*, *3*(10), 721-732. https://doi.org/10.1038/nrc1187

Sharma, R., Choi, K.-J., Quan, M. D., Sharma, S., Sankaran, B., Park, H., LaGrone, A., Kim, J. J., MacKenzie, K. R., Ferreon, A. C. M., Kim, C., & Ferreon, J. C. (2021). Liquid condensation of reprogramming factor KLF4 with DNA provides a mechanism for chromatin organization. *Nature Communications*, *12*(1), 5579. https://doi.org/10.1038/s41467-021-25761-7

Sharp, P. A., Chakraborty, A. K., Henninger, J. E., & Young, R. A. (2022). RNA in formation and regulation of transcriptional condensates. *Rna*, *28*(1), 52-57. https://doi.org/10.1261/rna.078997.121

Shen, P. S., Park, J., Qin, Y., Li, X., Parsawar, K., Larson, M. H., Cox, J., Cheng, Y., Lambowitz, A. M., Weissman, J. S., Brandman, O., & Frost, A. (2015). Rqc2p and 60S ribosomal subunits mediate mRNA-independent elongation of nascent chains. *Science*, *347*(6217), 75-78. https://doi.org/doi:10.1126/science.1259724

Shi, Y., Mosser, D. D., & Morimoto, R. I. (1998). Molecularchaperones as HSF1-specific transcriptional repressors. *Genes & development*, *12*(5), 654-666.

Shin, Y., & Brangwynne, C. P. (2017). Liquid phase condensation in cell physiology and disease. *Science*, *357*(6357). https://doi.org/10.1126/science.aaf4382

Shin, Y., Chang, Y. C., Lee, D. S. W., Berry, J., Sanders, D. W., Ronceray, P., Wingreen, N. S., Haataja, M., & Brangwynne, C. P. (2018). Liquid Nuclear Condensates Mechanically Sense and Restructure the Genome. *Cell*, *175*(6), 1481-1491.e1413. https://doi.org/10.1016/j.cell.2018.10.057

Shrinivas, K., Sabari, B. R., Coffey, E. L., Klein, I. A., Boija, A., Zamudio, A. V., Schuijers, J., Hannett, N. M., Sharp, P. A., Young, R. A., & Chakraborty, A. K. (2019). Enhancer Features that Drive Formation of Transcriptional Condensates. *Mol Cell*, *75*(3), 549-561.e547. https://doi.org/10.1016/j.molcel.2019.07.009

Singh, M. K., Shin, Y., Han, S., Ha, J., Tiwari, P. K., Kim, S. S., & Kang, I. (2024). Molecular Chaperonin HSP60: Current Understanding and Future Prospects. *Int J Mol Sci*, *25*(10). https://doi.org/10.3390/ijms25105483

Sitron, C. S., Park, J. H., Giafaglione, J. M., & Brandman, O. (2020). Aggregation of CAT tails blocks their degradation and causes proteotoxicity in S. cerevisiae. *PLoS One*, *15*(1), e0227841. https://doi.org/10.1371/journal.pone.0227841

Solís, Eric J., Pandey, Jai P., Zheng, X., Jin, Dexter X., Gupta, Piyush B., Airoldi, Edoardo M., Pincus, D., & Denic, V. (2016). Defining the Essential Function of Yeast Hsf1 Reveals a Compact Transcriptional Program for Maintaining Eukaryotic Proteostasis. *Molecular Cell*, *63*(1), 60-71. https://doi.org/10.1016/j.molcel.2016.05.014

Sorger, P. K., Lewis, M. J., & Pelham, H. R. (1987). Heat shock factor is regulated differently in yeast and HeLa cells. *Nature*, *329*(6134), 81-84. https://doi.org/10.1038/329081a0

Sorger, P. K., & Nelson, H. C. (1989). Trimerization of a yeast transcriptional activator via a coiled-coil motif. *Cell*, *59*(5), 807-813. https://doi.org/10.1016/0092-8674(89)90604-1

Sorger, P. K., & Pelham, H. R. (1987). Purification and characterization of a heat-shock element binding protein from yeast. *Embo j*, *6*(10), 3035-3041. https://doi.org/10.1002/j.1460-2075.1987.tb02609.x

Soto, C. (2003). Unfolding the role of protein misfolding in neurodegenerative diseases. *Nat Rev Neurosci*, *4*(1), 49-60. https://doi.org/10.1038/nrn1007

Sousa, R., & Lafer, E. M. (2015). The role of molecular chaperones in clathrin mediated vesicular trafficking. *Front Mol Biosci*, *2*, 26. https://doi.org/10.3389/fmolb.2015.00026

Specht, S., Miller, S. B., Mogk, A., & Bukau, B. (2011). Hsp42 is required for sequestration of protein aggregates into deposition sites in Saccharomyces cerevisiae. *Journal of Cell Biology*, *195*(4), 617-629.

Stortz, M., Pecci, A., Presman, D. M., & Levi, V. (2020). Unraveling the molecular interactions involved in phase separation of glucocorticoid receptor. *BMC Biol*, *18*(1), 59. https://doi.org/10.1186/s12915-020-00788-2

Strom, A. R., Emelyanov, A. V., Mir, M., Fyodorov, D. V., Darzacq, X., & Karpen, G. H. (2017). Phase separation drives heterochromatin domain formation. *Nature*, *547*(7662), 241-245. https://doi.org/10.1038/nature22989

Su, X., Ditlev, J. A., Hui, E., Xing, W., Banjade, S., Okrut, J., King, D. S., Taunton, J., Rosen, M. K., & Vale, R. D. (2016). Phase separation of signaling molecules promotes T cell receptor signal transduction. *Science*, *352*(6285), 595-599. https://doi.org/10.1126/science.aad9964

Sullivan, E. K., Weirich, C. S., Guyon, J. R., Sif, S., & Kingston, R. E. (2001). Transcriptional activation domains of human heat shock factor 1 recruit human SWI/SNF. *Mol Cell Biol*, *21*(17), 5826-5837. https://doi.org/10.1128/mcb.21.17.5826-5837.2001

Takaki, E., Fujimoto, M., Sugahara, K., Nakahari, T., Yonemura, S., Tanaka, Y., Hayashida, N., Inouye, S., Takemoto, T., Yamashita, H., & Nakai, A. (2006). Maintenance of olfactory neurogenesis requires HSF1, a major heat shock transcription factor in mice. *J Biol Chem*, *281*(8), 4931-4937. https://doi.org/10.1074/jbc.M506911200

Tang, Z., Dai, S., He, Y., Doty, Rosalinda A., Shultz, Leonard D., Sampson, Stephen B., & Dai, C. (2015). MEK Guards Proteome Stability and Inhibits Tumor-Suppressive Amyloidogenesis via HSF1. *Cell*, *160*(4), 729-744. https://doi.org/10.1016/j.cell.2015.01.028

Toivola, D. M., Strnad, P., Habtezion, A., & Omary, M. B. (2010). Intermediate filaments take the heat as stress proteins. *Trends Cell Biol*, *20*(2), 79-91. https://doi.org/10.1016/j.tcb.2009.11.004

Trojanowski, J., Frank, L., Rademacher, A., Mücke, N., Grigaitis, P., & Rippe, K. (2022). Transcription activation is enhanced by multivalent interactions independent of phase separation. *Mol Cell*, *82*(10), 1878-1893.e1810. https://doi.org/10.1016/j.molcel.2022.04.017

Tuite, M. F., Bossier, P., & Fitch, I. T. (1988). A highly conserved sequence in yeast heat shock gene promoters. *Nucleic Acids Res*, *16*(24), 11845. https://doi.org/10.1093/nar/16.24.11845

Tye, B. W., & Churchman, L. S. (2021). Hsf1 activation by proteotoxic stress requires concurrent protein synthesis. *Mol Biol Cell*, *32*(19), 1800-1806. https://doi.org/10.1091/mbc.E21-01-0014

Uchida, S., Hara, K., Kobayashi, A., Fujimoto, M., Otsuki, K., Yamagata, H., Hobara, T., Abe, N., Higuchi, F., Shibata, T., Hasegawa, S., Kida, S., Nakai, A., & Watanabe, Y. (2011). Impaired hippocampal spinogenesis and neurogenesis and altered affective behavior in mice lacking heat shock factor 1. *Proc Natl Acad Sci U S A*, *108*(4), 1681-1686. https://doi.org/10.1073/pnas.1016424108

Ungelenk, S., Moayed, F., Ho, C.-T., Grousl, T., Scharf, A., Mashaghi, A., Tans, S., Mayer, M. P., Mogk, A., & Bukau, B. (2016). Small heat shock proteins sequester misfolding proteins in near-native conformation for cellular protection and efficient refolding. *Nature Communications*, *7*(1), 13673.

Vellai, T., & Takács-Vellai, K. (2010). Regulation of protein turnover by longevity pathways. *Adv Exp Med Biol*, *694*, 69-80. https://doi.org/10.1007/978-1-4419-7002-2_7

Vigh, L., Nakamoto, H., Landry, J., Gomez-Munoz, A., Harwood, J. L., & Horvath, I. (2007). Membrane regulation of the stress response from prokaryotic models to mammalian cells. *Ann N Y Acad Sci*, *1113*, 40-51. https://doi.org/10.1196/annals.1391.027

Voellmy, R., & Boellmann, F. (2007). Chaperone regulation of the heat shock protein response. *Adv Exp Med Biol*, *594*, 89-99. https://doi.org/10.1007/978-0-387-39975-1_9

Vujanac, M., Fenaroli, A., & Zimarino, V. (2005). Constitutive nuclear import and stress-regulated nucleocytoplasmic shuttling of mammalian heat-shock factor 1. *Traffic*, *6*(3), 214-229. https://doi.org/10.1111/j.1600-0854.2005.00266.x

Wang, B., Zhang, L., Dai, T., Qin, Z., Lu, H., Zhang, L., & Zhou, F. (2021). Liquid–liquid phase separation in human health and diseases. *Signal Transduction and Targeted Therapy*, *6*(1), 290. https://doi.org/10.1038/s41392-021-00678-1

Wang, L., Gao, Y., Zheng, X., Liu, C., Dong, S., Li, R., Zhang, G., Wei, Y., Qu, H., Li, Y., Allis, C. D., Li, G., Li, H., & Li, P. (2019). Histone Modifications Regulate Chromatin Compartmentalization by Contributing to a Phase Separation Mechanism. *Molecular Cell*, *76*(4), 646-659.e646. https://doi.org/10.1016/j.molcel.2019.08.019

Wei, M. T., Chang, Y. C., Shimobayashi, S. F., Shin, Y., Strom, A. R., & Brangwynne, C. P. (2020). Nucleated transcriptional condensates amplify gene expression. *Nat Cell Biol*, *22*(10), 1187-1196. https://doi.org/10.1038/s41556-020-00578-6

Weindling, E., & Bar-Nun, S. (2015). Sir2 links the unfolded protein response and the heat shock response in a stress response network. *Biochemical and Biophysical Research Communications*, *457*(3), 473-478. https://doi.org/https://doi.org/10.1016/j.bbrc.2015.01.021

Wendt, K. S., & Grosveld, F. G. (2014). Transcription in the context of the 3D nucleus. *Current Opinion in Genetics & Development*, *25*, 62-67. https://doi.org/https://doi.org/10.1016/j.gde.2013.11.020

Widłak, W., Benedyk, K., Vydra, N., Głowala, M., Scieglińska, D., Małusecka, E., Nakai, A., & Krawczyk, Z. (2003). Expression of a constitutively active mutant of heat shock factor 1 under the control of testis-specific hst70 gene promoter in transgenic mice induces degeneration of seminiferous epithelium. *Acta Biochim Pol*, *50*(2), 535-541.

Wong Po Foo, C. T., Lee, J. S., Mulyasasmita, W., Parisi-Amon, A., & Heilshorn, S. C. (2009). Two-component protein-engineered physical hydrogels for cell encapsulation. *Proc Natl Acad Sci U S A*, *106*(52), 22067-22072. https://doi.org/10.1073/pnas.0904851106

Yang, P., Mathieu, C., Kolaitis, R. M., Zhang, P., Messing, J., Yurtsever, U., Yang, Z., Wu, J., Li, Y., Pan, Q., Yu, J., Martin, E. W., Mittag, T., Kim, H. J., & Taylor, J. P. (2020). G3BP1 Is

a Tunable Switch that Triggers Phase Separation to Assemble Stress Granules. *Cell*, *181*(2), 325-345.e328. https://doi.org/10.1016/j.cell.2020.03.046

Yoo, H., Bard, J. A. M., Pilipenko, E. V., & Drummond, D. A. (2022). Chaperones directly and efficiently disperse stress-triggered biomolecular condensates. *Mol Cell*, *82*(4), 741-755.e711. https://doi.org/10.1016/j.molcel.2022.01.005

Zaffagnini, G., Savova, A., Danieli, A., Romanov, J., Tremel, S., Ebner, M., Peterbauer, T., Sztacho, M., Trapannone, R., Tarafder, A. K., Sachse, C., & Martens, S. (2018). p62 filaments capture and present ubiquitinated cargos for autophagy. *Embo j*, *37*(5). https://doi.org/10.15252/embj.201798308

Zamudio, A. V., Dall'Agnese, A., Henninger, J. E., Manteiga, J. C., Afeyan, L. K., Hannett, N. M., Coffey, E. L., Li, C. H., Oksuz, O., Sabari, B. R., Boija, A., Klein, I. A., Hawken, S. W., Spille, J. H., Decker, T. M., Cisse, II, Abraham, B. J., Lee, T. I., Taatjes, D. J.,…Young, R. A. (2019). Mediator Condensates Localize Signaling Factors to Key Cell Identity Genes. *Mol Cell*, *76*(5), 753-766.e756. https://doi.org/10.1016/j.molcel.2019.08.016

Zhao, C., Hashiguchi, A., Kondoh, K., Du, W., Hata, J.-i., & Yamada, T. (2002). Exogenous expression of heat shock protein 90kDa retards the cell cycle and impairs the heat shock response. *Experimental cell research*, *275*(2), 200-214.

Zheng, X., Beyzavi, A., Krakowiak, J., Patel, N., Khalil, A. S., & Pincus, D. (2018). Hsf1 Phosphorylation Generates Cell-to-Cell Variation in Hsp90 Levels and Promotes Phenotypic Plasticity. *Cell Reports*, *22*(12), 3099-3106. https://doi.org/10.1016/j.celrep.2018.02.083

Zheng, X., Krakowiak, J., Patel, N., Beyzavi, A., Ezike, J., Khalil, A. S., & Pincus, D. (2016). Dynamic control of Hsf1 during heat shock by a chaperone switch and phosphorylation. *Elife*, *5*. https://doi.org/10.7554/eLife.18638

Zou, J., Guo, Y., Guettouche, T., Smith, D. F., & Voellmy, R. (1998). Repression of heat shock transcription factor HSF1 activation by HSP90 (HSP90 complex) that forms a stress-sensitive complex with HSF1. *Cell*, *94*(4), 471-480. https://doi.org/10.1016/s0092-8674(00)81588-3

Zuiderweg, E. R., Hightower, L. E., & Gestwicki, J. E. (2017). The remarkable multivalency of the Hsp70 chaperones. *Cell Stress Chaperones*, *22*(2), 173-189. https://doi.org/10.1007/s12192-017-0776-y

CHAPTER 2

Preserve or destroy: orphan proteins and the heat shock response

This chapter is a full reprint of Ali et al 2024 on which I am an author. This work is has been accepted at Journal of Cell Biology and will be published before the end of the year. It is included with permission from all the authors. I wrote the first draft of this review, except the last section which was done by Asif Ali. I also performed revisions before final publication.

2.1 Abstract

Most eukaryotic genes encode polypeptides that are either obligate members of hetero-stoichiometric complexes or clients of organelle targeting pathways. Proteins in these classes can be released from the ribosome as "orphans"—newly synthesized proteins not associated with their stoichiometric binding partner(s) and/or not targeted to their destination organelle. Here we integrate recent findings suggesting that, although cells selectively degrade orphan proteins under homeostatic conditions, they can preserve them in chaperone-regulated biomolecular condensates during stress. These orphan protein condensates activate the heat shock response (HSR) and represent subcellular sites where the chaperones induced by the HSR execute their functions. Reversible condensation of orphan proteins may broadly safeguard labile precursors during stress.

2.2 Main

2.2.1 Orphan protein quality control and the heat shock response

Few proteins are islands. Most genes in the model eukaryote *Saccharomyces cerevisiae* encode proteins designated for specific trafficking to membrane-enclosed subcellular compartments or assembly with other cellular factors into stoichiometric complexes (Gavin et al., 2006; Krogan

et al., 2006). Analyses of protein-protein interactions indicate that more than 50% of proteins have the propensity to engage in heteromeric complexes of defined stoichiometry, although membrane proteins tend to exhibit a slightly lower degree of interaction (Aebersold and Mann, 2016; Michaelis et al., 2023). Even under the most well balanced homeostatic cellular conditions, the lack of operonic structure to eukaryotic genes and the inherent stochasticity of gene expression inevitably results in stoichiometric imbalances. Substituent polypeptides in a protein complex not associated with their binding partner(s), and newly synthesized membrane or organellar proteins not targeted to their destinations, are termed "orphan" proteins (Juszkiewicz and Hegde, 2018).

Under nonstress conditions, cells employ degradation mechanisms to recognize and remove orphan proteins, giving the cell a buffering capacity to counter small imbalances in stoichiometry. Even in aneuploid cells, in which protein complexes with members on different chromosomes have constitutive stoichiometric imbalances with substantial numbers of orphan proteins, protein homeostasis pathways maintain cell viability via degradation and adaptive aggregate/condensate formation (Ben-David and Amon, 2020; Brennan et al., 2019; Oromendia et al., 2012). However, saturation of this buffering capacity, through mutations or environmental perturbations, triggers an evolutionarily conserved transcriptional program known as the Heat Shock Response (HSR) (Alford et al., 2021; Brandman et al., 2012; Pincus, 2020) (Figure 1A). The HSR enhances the ability of cells to cope with the build-up of aggregation-prone orphan proteins by increasing the production of chaperones via the transcriptional activator Hsf1. Under prolonged stress, the HSR feeds forward to upregulate proteasomal machinery via Rpn4 (Boos et al., 2019; Work and Brandman, 2021).

The observation that orphan proteins trigger cells to produce both chaperones and degradation machinery underscores the key regulatory decision that cells confront when orphans accumulate: to preserve or destroy them. Here, we will highlight recent discoveries describing

dedicated proteostasis mechanisms that route orphans for degradation or preservation. In addition to specific ubiquitin-proteasome pathways to degrade different classes of orphan proteins under nonstress conditions, we discuss novel roles for the Hsp70 chaperone system in preserving orphan proteins in reversible biomolecular condensates during stress and how these orphan protein condensates serve as subcellular hubs that regulate – and are regulated by – the HSR (Figure 1A).

2.2.2 Orphan protein degradation and accumulation during stress

Cells deploy specific ubiquitin-proteasome pathways to degrade different classes of orphan proteins. For example, cells use the mitochondrial protein translocation-associated degradation (mitoTAD) pathway and nuclear quality control factors to continuously survey the translocation through the outer membrane (TOM) complex and prevent clogging of the TOM channel with mitochondrial precursor proteins (Mårtensson et al., 2019; Shakya et al., 2021). When this safeguard is overwhelmed, such as via the acute blockage of mitochondrial import by engineered clogger proteins, orphan mitochondrial proteins (oMPs) accumulate in the cytosol in reversible condensates and selectively induce the HSR among all cellular stress responses (Boos et al., 2019; Krämer et al., 2023). Since these mitochondrial precursors require cytosolic chaperones to initiate targeting, their accumulation in the cytosol appropriates Hsp70, titrating Hsp70 away from repressing Hsf1 in the nucleus and thereby inducing the HSR (Feder et al., 2021; Krakowiak et al., 2018; Masser et al., 2019; Zheng et al., 2016) (Figure 1A). In further support of this mitochondria-to-HSR signalling axis, the mitochondrial unfolded protein response (UPR^{mito}) in mammalian cells was recently shown to be similarly triggered by oMPs accumulating in the cytosol and activating the HSR by Hsp70 sequestration (Sutandy et al., 2023).

The most heterotypic complex in the cell is the ribosome, which in yeast requires the stoichiometric assembly of 79 different proteins and 4 RNAs (Lempiainen and Shore, 2009; Shore and Albert, 2022; Shore et al., 2021). When there is a moderate excess of ribosomal protein production, such as when a single protein is overexpressed, the E3 ubiquitin ligase Tom1 targets the orphan ribosomal proteins (oRPs) for degradation by the proteasome (Sung et al., 2016a; Sung et al., 2016b). In human cells, Huwe1 and UBE2O have been implicated in degradation of orphan proteins including oRPs (Nguyen et al., 2017; Xu et al., 2016; Yanagitani et al., 2017). However, in cases when this clearance mechanism is inundated via genetic mutation or chemical perturbation, oRPs form nuclear condensates with chaperones and the ribosomal protein gene transcriptional activator Ifh1 (Albert et al., 2019; Tye et al., 2019). As when the oMP degradation system is overwhelmed, accumulated oRPs activate the HSR by sequestering Hsp70 (Albert et al., 2019; Ali et al., 2023; Tye et al., 2019) (Figure 1A). Tail anchored proteins represent a third class of orphan proteins known to activate the HSR. Like mitochondrial import, tail anchor membrane insertion is mediated by a chaperone cascade that begins with Hsp70 delivering clients to the guided entry of tail anchored proteins (GET) pathway (Brandman et al., 2012; Cho et al., 2024; Shan, 2019; Wang et al., 2014). Glucose depletion and deletion of GET pathway factors results in accumulation of orphan tail anchored proteins (oTAPs) in cytosolic clusters that in current parlance would be termed condensates (Powis et al., 2013; Wang et al., 2014). While it remains unclear whether these oTAP condensates form as HSR signalling hubs during physiological heat shock, their formation upon glucose depletion – a condition known to activate the HSR (Hahn and Thiele, 2004; Zid and O'Shea, 2014) – suggests that they may serve as physiological HSR ligands under some conditions (Figure 1A).

In addition to oMPs, oRPs, and oTAPs, other classes of orphan proteins have been found to have dedicated E3 ligases to enforce stoichiometries in mammalian cells, including kinases,

transcription factors, the CCT chaperonin, and the proteasome itself (Mark et al., 2023; Mena et al., 2018; Padovani et al., 2022; Yagita et al., 2023; Zavodszky et al., 2021). Whether these classes of orphan proteins form condensates and activate the HSR during stress is not currently known.

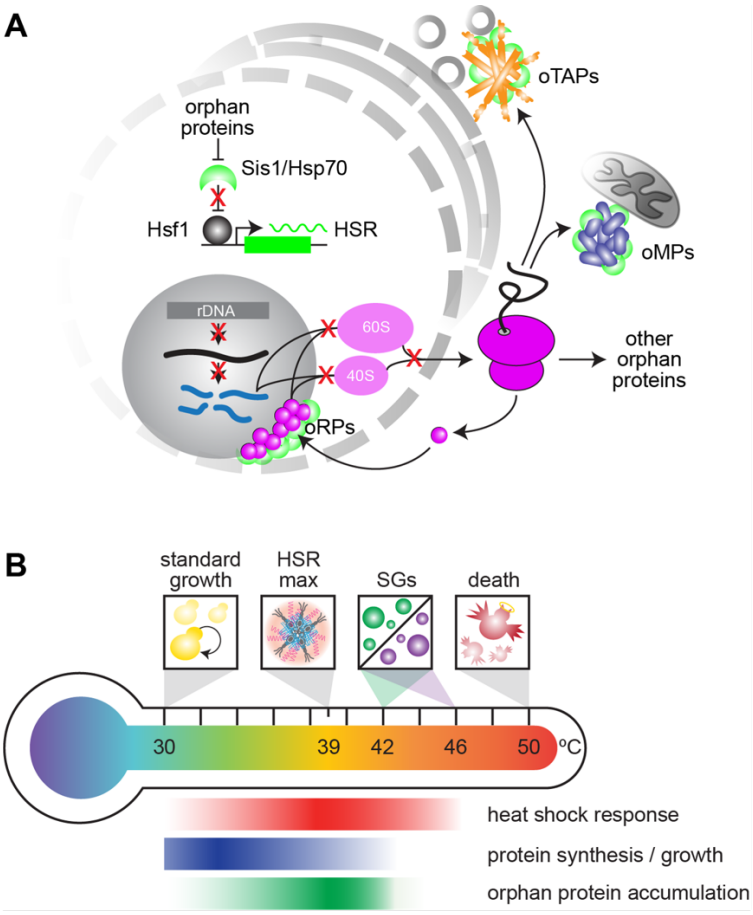

Figure 2.1. Orphan proteins and the heat shock response.
A. Accumulation of orphan ribosomal proteins (oRPs), orphan mitochondrial proteins (oMPs), and orphan tail anchored proteins (oTAPs) titrate the chaperone Hsp70 and its coregulator, the J-domain protein Sis1, away from Hsf1, activating the heat shock response (HSR).
B. Variation in the activity of the HSR, global protein synthesis, and the putative accumulation of orphan proteins as a function of temperature, highlighting key temperatures associated with growth, HSR maximal activity, condensation of different stress granule (SG) components, and cell death.

2.2.3 Orphan protein condensates as physiological ligands of the heat shock response

The stress conditions under which orphan protein condensates may form to signal the HSR, while potentially numerous, are physically constrained. Heat shock, as perhaps the best studied

environmental stress, presents an illustrative example. Yeast cells grow readily at 30°C with no signatures of stress evident in the transcriptome or proteome, and they die by lysis after a few minutes at 50°C. As the temperature rises above the standard growth condition – i.e., as the magnitude of stress increases – the HSR is induced, while overall protein synthesis and growth are concomitantly repressed. The magnitude of the HSR peaks at 39°C, when Hsf1 forms transcriptional condensates, and begins to decrease as the temperature is further increased due to the formation of stress granules that enforce the shutdown of translation (Chowdhary et al., 2022; Iserman et al., 2020; Kik et al., 2023; Riback et al., 2017) (Figure 1B). This loss of HSR output at temperatures above which stress granules form and global translation is reduced is consistent with observations that Hsf1 activity is also impaired at mild and moderate heat shock if translation is inhibited by cycloheximide or rocaglamide treatment or amino acid depletion (Masser et al., 2019; Santagata et al., 2013; Triandafillou et al., 2020; Tye and Churchman, 2021). Since production of orphan proteins requires translation, this tight correlation of HSR output and ongoing protein synthesis further supports the notion that orphan protein accumulation activates the HSR during physiological stress.

2.2.4 Reversible condensation of labile proteins in the nucleus during stress

While initially generated by cytosolic ribosomes, oRPs – which constitute a substantial fraction of all orphan proteins due to their high abundance – are subsequently imported into the nucleus for assembly with rRNA in the nucleolus. With the help a nuclear-specific proteostasis network and specialized phase-separated sites devoted to quality control, the nucleus helps to maintain the many metastable proteins that make up its proteome (Miller et al., 2015a; Miller et al., 2015b; Park et al., 2013; Prasad et al., 2018; Samant et al., 2018; Sontag et al., 2023; Sontag et al., 2017).

The most prominent membrane-free compartment in the nucleus is the nucleolus, the site of ribosome biogenesis (Feric et al., 2016; Lafontaine et al., 2021). The outer granular component (GC) of the nucleolus in human cells is densely packed with the negatively charged protein nucleophosmin (NPM1) that scaffolds the phase separation of the GC and has long been implicated in cancer (Grisendi et al., 2006; Mitrea et al., 2018). This GC component has been found to host ~200 stress-sensitive endogenous proteins during acute heat shock, affording these proteins from both outside and within the nucleolus protection during stress (Frottin et al., 2019). Hsp70 and cofactors localize to this site as well, maintaining proteins in a soluble state until stress recovery, suggesting an adaptive role for the nucleolar compartment. If the cells undergo prolonged stress, the GC solidifies and is no longer able to carry out its proteostasis function (Frottin et al., 2019).

Similarly, in *S. pombe* cells during heat stress, nuclear and nucleolar proteins segregate to the nucleolar periphery and rearrange to form rings that isolate essential proteins required for cellular transcription, processing, and cell cycle regulators, both inhibiting and protecting these proteins during acute stress (Gallardo et al., 2020). Upon release from heat stress, the nucleolar rings disassembled, allowing the proteins to revert to their previous locations. Hsp70 is present in these nucleolar rings during heat shock, and the disaggregase Hsp104 was found to be required for the efficient dissolution of these rings upon recovery (Cabrera et al., 2020; Gallardo et al., 2020).

During nutrient depletion, budding yeast cells enter a quiescent state where cells exit the cell cycle, translation rates decline and there is low metabolic activity, essentially placing the cells in a state of stress as they must work to protect their proteomes and maintain function (Sagot and Laporte, 2019; Sun and Gresham, 2021). Multiple studies have identified the presence of stress granules and P-bodies in the cytosol that sequester and maintain essential components of the proteostasis and translation machinery during quiescence, allowing them to be reactivated

when protein synthesis is once again resumed (Coller, 2011; Grousl et al., 2022; Liu et al., 2012; Marshall and Vierstra, 2018; Protter and Parker, 2016). Recently, the nucleus has also been shown to harbour reversible clusters of translation-associated proteins during prolonged stress and starvation (Kohler et al., 2024). Hsp104 likewise accumulates in the nucleus, safeguarding these factors for the rapid restart of protein synthesis upon refeeding. These nuclear localized translation factors qualify as orphan proteins due to their localization away from their functional home in the cytosol, and the chaperone-associated condensates they form preserve them rather than facilitating degradation.

2.2.5 Preservation of orphan ribosomal proteins in stress-induced condensates

Cells regulate the rate of ribosome production according to nutritional cues, and ribosomal protein gene transcription by RNA Pol II is tightly coordinated with rRNA synthesis by RNA Pol I (Lempiainen and Shore, 2009; Shore and Albert, 2022; Shore et al., 2021; Woolford and Baserga, 2013). Across a wide range of environmental conditions, a common transcriptional response to the stress is to repress transcription of rRNA and mRNAs encoding ribosomal proteins and biogenesis factors (Gasch et al., 2000; Gasch and Werner-Washburne, 2002). However, as described above in the case of case of heat shock, protein translation remains active at intermediate levels of stress (Iserman et al., 2020; Muhlhofer et al., 2019). To the extent that pre-existing mRNAs encoding ribosomal proteins continue to be translated during stress, they produce orphan ribosomal proteins as there is no rRNA for them to bind to. In the absence of rRNA, oRPs require chaperones and nuclear import factors to maintain their solubility and prevent aggregation (Pillet et al., 2022; Seidel et al., 2023; Tye et al., 2019).

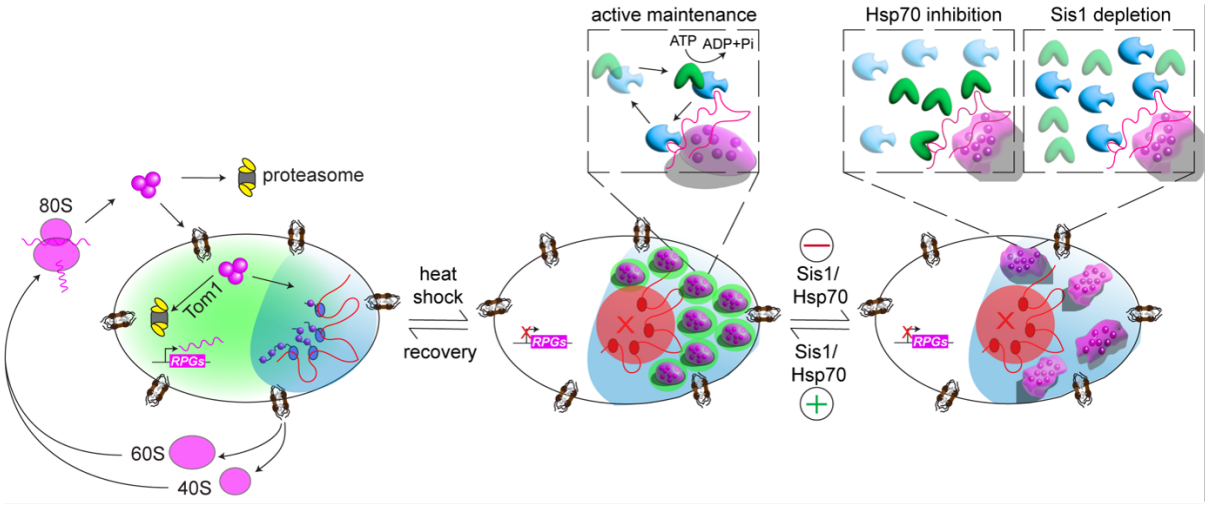

Figure 2.2. Preservation of orphan ribosomal proteins in chaperone-regulated condensates.
The ribosome biogenesis cycle is disrupted during stress, resulting in the formation of oRP condensates at the nucleolar periphery, the reversibility of which is maintained by the activity of Hsp70 and Sis1. Even solid oRP condensates are reversible if Sis1 and Hsp70 are allowed to resume their activity.

As described above, cells target oRPs for proteasomal degradation when expressed ectopically (Sung et al., 2016a; Sung et al., 2016b). By contrast, during heat shock, endogenous oRPs form adaptive, reversible condensates localized to the outer region of the nucleolus in yeast and human cells that preserve the oRPs for usage once the cell is no longer under stress (Ali et al., 2023) (Figure 2). As with previously described adaptive condensates such as stress granules, oRP condensates interact with chaperone proteins, most prominently the J-domain protein (JDP) Sis1/DnaJB6 and Hsp70. Sis1 is an essential JDP and co-chaperone for Hsp70 required for biogenesis of mTORC1-like kinase complexes and for partial repression of the HSR under nonstress conditions by targeting Hsp70 to bind to Hsf1 and (Feder et al., 2021; Garde et al., 2023; Klaips et al., 2020; Luke et al., 1991; Schilke and Craig, 2022). When Sis1 was depleted or Hsp70 was inhibited, oRP condensates solidified, showing that these chaperones are required for the maintenance of the dynamic state of these condensates. Without Sis1 or Hsp70, the reversibility of the condensates was also delayed, and recovery from heat shock and resumption of cell growth was postponed (Figure 2). This example represents a case where the biophysical properties of the oRP condensates – the liquid-like fluidity enforced by interactions

with Sis1 and Hsp70 – serves an adaptive advantage of preserving oRP functionality, allowing them to be readily incorporated into nascent ribosomes once rRNA synthesis resumes (Ali et al., 2023).

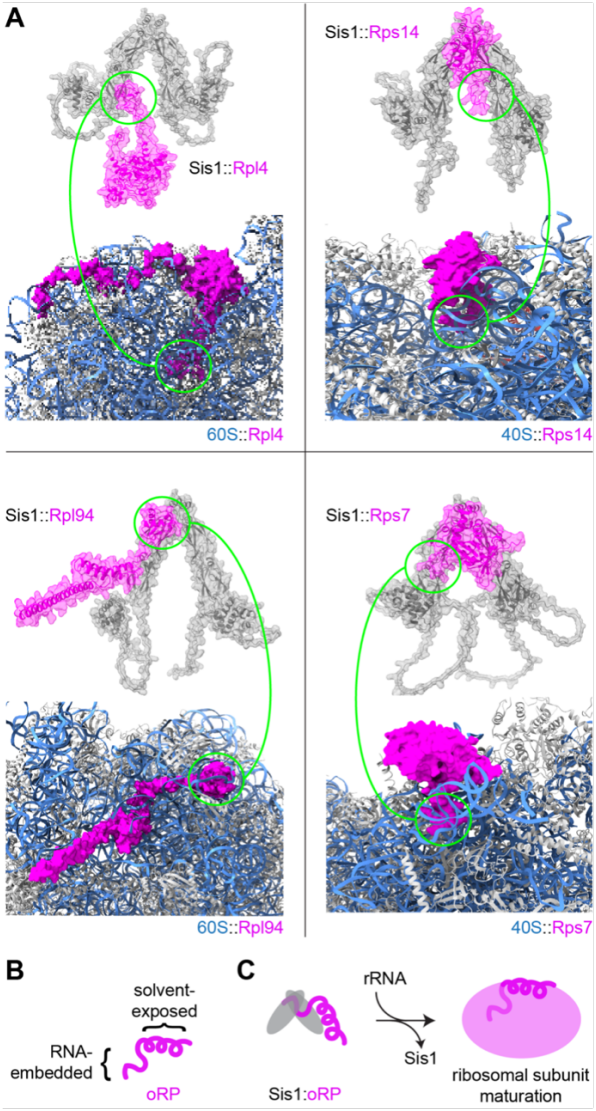

Figure 2.3. Predicted structures of Sis1 interacting with orphan ribosomal proteins.
A. AlphaFold multimer structure of Sis1 dimers with orphan ribosomal proteins depicted above the region of the ribosome containing each mature ribosomal protein (Evans et al., 2021). The regions that interact with Sis1, circled in green, are buried in the mature ribosome. These RPs are each integrated into the ribosome at different assembly steps.
B. Schematic of a single oRP.
C. Schematic for how RPs bind in a mutually exclusive manner to Sis1 and rRNA.

Using AlphaFold Multimer (Evans et al., 2021), we have generated high confidence model structures of the complex of Sis1 dimers with four different oRPs to guide our molecular

interpretation (Figure 3A). Importantly, these artificial intelligence-based models do not necessarily represent reality and have not been experimentally validated. Two of the modeled oRPs are constituents of the 60S subunit, two of the 40S, and each of the four are incorporated at different ribosome assembly steps (Woolford and Baserga, 2013). The models uniformly predicted that Sis1 interacts with regions of the oRPs that would be buried away from the surface of the ribosome and the surrounding solvent by interacting directly with rRNA (Figure 3B). These regions where Sis1 is predicted to bind are also predicted to interact with Hsp70 (Rudiger et al., 2001). This suggests a simple mechanism by which the reappearance of rRNA would outcompete Sis1 and Hsp70 to release the oRPs from the chaperones to resume ribosome biogenesis (Figure 3C).

2.2.6 Outlook: Who needs a chaperone more than an orphan?

In this perspective, we draw a through line connecting orphan proteins, stress induced adaptive condensates, and the HSR. Since the discovery of the HSR, the endogenous ligands that activate the response following heat shock and other stressors were long presumed to be toxic aggregates of denatured proteins (Lindquist, 1986; Zheng et al., 2016). However, much recent work has provided evidence in support of a different paradigm in which the protein aggregates that form during heat shock are nontoxic and programmed by evolution as adaptive mechanisms under specific conditions (Franzmann et al., 2018; Iserman et al., 2020; Riback et al., 2017; Wallace et al., 2015; Yoo et al., 2019).

From the perspective of HSR activation, two major classes of proteins have been implicated as the physiological ligands: heat- and pH-dependent condensates such as stress granules and newly synthesized proteins (Garde et al., 2023; Santiago et al., 2020; Triandafillou et al., 2020; Tye and Churchman, 2021). As oRPs have directly been shown to be a subset of the newly synthesized proteins that activate the HSR (Ali et al., 2023), and oMPs and oTAPs have been

strongly implicated (Boos et al., 2019; Brandman et al., 2012; Krämer et al., 2023; Wang et al., 2014), we speculate that different classes of orphan proteins will serve as physiological ligands of the HSR across diverse conditions. From the perspective of the orphan proteins, the chaperones provide binding partners and protection against promiscuous interactions. Moreover, the condensates they form function as nurseries to provide distributed coverage for precursor proteins by a limited number of chaperone proteins, signaling the HSR to increase chaperone production all the while. The notion that newly synthesized proteins are being "chaperoned" in an "orphanage" to conserve limited resources during stress is a powerful metaphor to describe these recently discovered preservation mechanisms.

2.3 Acknowledgments

We thank members of the Pincus lab for their ideas and input. This work was supported by NIH grants R01 GM138689, RM1 GM153533, and NSF QLCI QuBBE grant OMA-2121044.

Aebersold, R., and M. Mann. 2016. Mass-spectrometric exploration of proteome structure and function. *Nature*. 537:347-355.

Albert, B., I.C. Kos-Braun, A.K. Henras, C. Dez, M.P. Rueda, X. Zhang, O. Gadal, M. Kos, and D. Shore. 2019. A ribosome assembly stress response regulates transcription to maintain proteome homeostasis. *Elife*. 8.

Alford, B.D., E. Tassoni-Tsuchida, D. Khan, J.J. Work, G. Valiant, and O. Brandman. 2021. ReporterSeq reveals genome-wide dynamic modulators of the heat shock response across diverse stressors. *Elife*. 10.

Ali, A., R. Garde, O.C. Schaffer, J.A.M. Bard, K. Husain, S.K. Kik, K.A. Davis, S. Luengo-Woods, M.G. Igarashi, D.A. Drummond, A.H. Squires, and D. Pincus. 2023. Adaptive preservation of orphan ribosomal proteins in chaperone-dispersed condensates. *Nature Cell Biology*. 25:1691-1703.

Ben-David, U., and A. Amon. 2020. Context is everything: aneuploidy in cancer. *Nature Reviews Genetics*. 21:44-62.

Boos, F., L. Krämer, C. Groh, F. Jung, P. Haberkant, F. Stein, F. Wollweber, A. Gackstatter, E. Zöller, M. van der Laan, M.M. Savitski, V. Benes, and J.M. Herrmann. 2019. Mitochondrial protein-induced stress triggers a global adaptive transcriptional programme. *Nature Cell Biology*. 21:442-451.

Brandman, O., J. Stewart-Ornstein, D. Wong, A. Larson, C.C. Williams, G.W. Li, S. Zhou, D. King, P.S. Shen, J. Weibezahn, J.G. Dunn, S. Rouskin, T. Inada, A. Frost, and J.S. Weissman. 2012. A ribosome-bound quality control complex triggers degradation of nascent peptides and signals translation stress. *Cell*. 151:1042-1054.

Brennan, C.M., L.P. Vaites, J.N. Wells, S. Santaguida, J.A. Paulo, Z. Storchova, J.W. Harper, J.A. Marsh, and A. Amon. 2019. Protein aggregation mediates stoichiometry of protein complexes in aneuploid cells. *Genes & development*. 33:1031-1047.

Cabrera, M., S. Boronat, L. Marte, M. Vega, P. Perez, J. Ayte, and E. Hidalgo. 2020. Chaperone-facilitated aggregation of thermo-sensitive proteins shields them from degradation during heat stress. *Cell Reports*. 30:2430-2443. e2434.

Cho, H., Y. Liu, S. Chung, S. Chandrasekar, S. Weiss, and S.-o. Shan. 2024. Dynamic stability of Sgt2 enables selective and privileged client handover in a chaperone triad. *Nature Communications*. 15:134.

Chowdhary, S., A.S. Kainth, S. Paracha, D.S. Gross, and D. Pincus. 2022. Inducible transcriptional condensates drive 3D genome reorganization in the heat shock response. *Mol Cell*. 82:4386-4399 e4387.

Coller, H.A. 2011. The essence of quiescence. *Science*. 334:1074-1075.

Evans, R., M. O'Neill, A. Pritzel, N. Antropova, A. Senior, T. Green, A. Žídek, R. Bates, S. Blackwell, and J. Yim. 2021. Protein complex prediction with AlphaFold-Multimer. *biorxiv*:2021.2010. 2004.463034.

Feder, Z.A., A. Ali, A. Singh, J. Krakowiak, X. Zheng, V.P. Bindokas, D. Wolfgeher, S.J. Kron, and D. Pincus. 2021. Subcellular localization of the J-protein Sis1 regulates the heat shock response. *J Cell Biol*. 220.

Feric, M., N. Vaidya, T.S. Harmon, D.M. Mitrea, L. Zhu, T.M. Richardson, R.W. Kriwacki, R.V. Pappu, and C.P. Brangwynne. 2016. Coexisting liquid phases underlie nucleolar subcompartments. *Cell*. 165:1686-1697.

Franzmann, T.M., M. Jahnel, A. Pozniakovsky, J. Mahamid, A.S. Holehouse, E. Nüske, D. Richter, W. Baumeister, S.W. Grill, and R.V. Pappu. 2018. Phase separation of a yeast prion protein promotes cellular fitness. *Science*. 359:eaao5654.

Frottin, F., F. Schueder, S. Tiwary, R. Gupta, R. Korner, T. Schlichthaerle, J. Cox, R. Jungmann, F.U. Hartl, and M.S. Hipp. 2019. The nucleolus functions as a phase-separated protein quality control compartment. *Science*. 365:342-347.

Gallardo, P., P. Real-Calderón, I. Flor-Parra, S. Salas-Pino, and R.R. Daga. 2020. Acute heat stress leads to reversible aggregation of nuclear proteins into nucleolar rings in fission yeast. *Cell reports*. 33.

Garde, R., A. Singh, A. Ali, and D. Pincus. 2023. Transcriptional regulation of Sis1 promotes fitness but not feedback in the heat shock response. *Elife*. 12.

Gasch, A.P., P.T. Spellman, C.M. Kao, O. Carmel-Harel, M.B. Eisen, G. Storz, D. Botstein, and P.O. Brown. 2000. Genomic expression programs in the response of yeast cells to environmental changes. *Mol Biol Cell*. 11:4241-4257.

Gasch, A.P., and M. Werner-Washburne. 2002. The genomics of yeast responses to environmental stress and starvation. *Funct Integr Genomics*. 2:181-192.

Gavin, A.-C., P. Aloy, P. Grandi, R. Krause, M. Boesche, M. Marzioch, C. Rau, L.J. Jensen, S. Bastuck, B. Dümpelfeld, A. Edelmann, M.-A. Heurtier, V. Hoffman, C. Hoefert, K. Klein, M. Hudak, A.-M. Michon, M. Schelder, M. Schirle, M. Remor, T. Rudi, S. Hooper, A. Bauer, T. Bouwmeester, G. Casari, G. Drewes, G. Neubauer, J.M. Rick, B. Kuster, P. Bork, R.B. Russell, and G. Superti-Furga. 2006. Proteome survey reveals modularity of the yeast cell machinery. *Nature*. 440:631-636.

Grisendi, S., C. Mecucci, B. Falini, and P.P. Pandolfi. 2006. Nucleophosmin and cancer. *Nature Reviews Cancer*. 6:493-505.

Grousl, T., J. Vojtova, J. Hasek, and T. Vomastek. 2022. Yeast stress granules at a glance. *Yeast*. 39:247-261.

Hahn, J.-S., and D.J. Thiele. 2004. Activation of the Saccharomyces cerevisiae heat shock transcription factor under glucose starvation conditions by Snf1 protein kinase. *Journal of Biological Chemistry*. 279:5169-5176.

Iserman, C., C. Desroches Altamirano, C. Jegers, U. Friedrich, T. Zarin, A.W. Fritsch, M. Mittasch, A. Domingues, L. Hersemann, M. Jahnel, D. Richter, U.P. Guenther, M.W. Hentze, A.M. Moses, A.A. Hyman, G. Kramer, M. Kreysing, T.M. Franzmann, and S. Alberti. 2020. Condensation of Ded1p Promotes a Translational Switch from Housekeeping to Stress Protein Production. *Cell*. 181:818-831 e819.

Juszkiewicz, S., and R.S. Hegde. 2018. Quality Control of Orphaned Proteins. *Mol Cell*. 71:443-457.

Kik, S.K., D. Christopher, H. Glauninger, C.W. Hickernell, J.A.M. Bard, M. Ford, T.R. Sosnick, and D.A. Drummond. 2023. An adaptive biomolecular condensation response is conserved across environmentally divergent species. *bioRxiv*.

Klaips, C.L., M.H.M. Gropp, M.S. Hipp, and F.U. Hartl. 2020. Sis1 potentiates the stress response to protein aggregation and elevated temperature. *Nat Commun*. 11:6271.

Kohler, V., A. Kohler, L.L. Berglund, X. Hao, S. Gersing, A. Imhof, T. Nyström, J.L. Höög, M. Ott, and C. Andréasson. 2024. Nuclear Hsp104 safeguards the dormant translation machinery during quiescence. *Nature Communications*. 15:315.

Krakowiak, J., X. Zheng, N. Patel, Z.A. Feder, J. Anandhakumar, K. Valerius, D.S. Gross, A.S. Khalil, and D. Pincus. 2018. Hsf1 and Hsp70 constitute a two-component feedback loop that regulates the yeast heat shock response. *Elife*. 7.

Krämer, L., N. Dalheimer, M. Räschle, Z. Storchová, J. Pielage, F. Boos, and J.M. Herrmann. 2023. MitoStores: chaperone-controlled protein granules store mitochondrial precursors in the cytosol. *The EMBO Journal*. 42:e112309.

Krogan, N.J., G. Cagney, H. Yu, G. Zhong, X. Guo, A. Ignatchenko, J. Li, S. Pu, N. Datta, A.P. Tikuisis, T. Punna, J.M. Peregrín-Alvarez, M. Shales, X. Zhang, M. Davey, M.D. Robinson, A. Paccanaro, J.E. Bray, A. Sheung, B. Beattie, D.P. Richards, V. Canadien, A. Lalev, F. Mena, P. Wong, A. Starostine, M.M. Canete, J. Vlasblom, S. Wu, C. Orsi, S.R. Collins, S. Chandran, R. Haw, J.J. Rilstone, K. Gandi, N.J. Thompson, G. Musso, P. St Onge, S. Ghanny, M.H.Y. Lam, G. Butland, A.M. Altaf-Ul, S. Kanaya, A. Shilatifard, E. O'Shea, J.S. Weissman, C.J. Ingles, T.R. Hughes, J. Parkinson, M. Gerstein, S.J. Wodak, A. Emili, and J.F. Greenblatt. 2006. Global landscape of protein complexes in the yeast Saccharomyces cerevisiae. *Nature*. 440:637-643.

Lafontaine, D.L., J.A. Riback, R. Bascetin, and C.P. Brangwynne. 2021. The nucleolus as a multiphase liquid condensate. *Nature reviews Molecular cell biology*. 22:165-182.

Lempiainen, H., and D. Shore. 2009. Growth control and ribosome biogenesis. *Curr Opin Cell Biol*. 21:855-863.

Lindquist, S. 1986. The heat-shock response. *Annu Rev Biochem*. 55:1151-1191.

Liu, I.-C., S.-W. Chiu, H.-Y. Lee, and J.-Y. Leu. 2012. The histone deacetylase Hos2 forms an Hsp42-dependent cytoplasmic granule in quiescent yeast cells. *Molecular biology of the cell*. 23:1231-1242.

Luke, M.M., A. Sutton, and K.T. Arndt. 1991. Characterization of SIS1, a Saccharomyces cerevisiae homologue of bacterial dnaJ proteins. *J Cell Biol*. 114:623-638.

Mark, K.G., S. Kolla, J.D. Aguirre, D.M. Garshott, S. Schmitt, D.L. Haakonsen, C. Xu, L. Kater, G. Kempf, and B. Martínez-González. 2023. Orphan quality control shapes network dynamics and gene expression. *Cell*. 186:3460-3475. e3423.

Marshall, R.S., and R.D. Vierstra. 2018. Proteasome storage granules protect proteasomes from autophagic degradation upon carbon starvation. *elife*. 7.

Mårtensson, C.U., C. Priesnitz, J. Song, L. Ellenrieder, K.N. Doan, F. Boos, A. Floerchinger, N. Zufall, S. Oeljeklaus, B. Warscheid, and T. Becker. 2019. Mitochondrial protein translocation-associated degradation. *Nature*. 569:679-683.

Masser, A.E., W. Kang, J. Roy, J.M. Kaimal, J. Quintana-Cordero, M.R. Friedlander, and C. Andreasson. 2019. Cytoplasmic protein misfolding titrates Hsp70 to activate nuclear Hsf1. *Elife*. 8.

Mena, E.L., R.A. Kjolby, R.A. Saxton, A. Werner, B.G. Lew, J.M. Boyle, R. Harland, and M. Rape. 2018. Dimerization quality control ensures neuronal development and survival. *Science*. 362:eaap8236.

Michaelis, A.C., A.-D. Brunner, M. Zwiebel, F. Meier, M.T. Strauss, I. Bludau, and M. Mann. 2023. The social and structural architecture of the yeast protein interactome. *Nature*. 624:192-200.

Miller, S.B., C.T. Ho, J. Winkler, M. Khokhrina, A. Neuner, M.Y. Mohamed, D.L. Guilbride, K. Richter, M. Lisby, E. Schiebel, A. Mogk, and B. Bukau. 2015a. Compartment-specific aggregases direct distinct nuclear and cytoplasmic aggregate deposition. *EMBO J*. 34:778-797.

Miller, S.B., A. Mogk, and B. Bukau. 2015b. Spatially organized aggregation of misfolded proteins as cellular stress defense strategy. *J Mol Biol*. 427:1564-1574.

Mitrea, D.M., J.A. Cika, C.B. Stanley, A. Nourse, P.L. Onuchic, P.R. Banerjee, A.H. Phillips, C.-G. Park, A.A. Deniz, and R.W. Kriwacki. 2018. Self-interaction of NPM1 modulates multiple mechanisms of liquid–liquid phase separation. *Nature communications*. 9:842.

Muhlhofer, M., E. Berchtold, C.G. Stratil, G. Csaba, E. Kunold, N.C. Bach, S.A. Sieber, M. Haslbeck, R. Zimmer, and J. Buchner. 2019. The Heat Shock Response in Yeast Maintains Protein Homeostasis by Chaperoning and Replenishing Proteins. *Cell Rep*. 29:4593-4607 e4598.

Nguyen, A.T., M.A. Prado, P.J. Schmidt, A.K. Sendamarai, J.T. Wilson-Grady, M. Min, D.R. Campagna, G. Tian, Y. Shi, and V. Dederer. 2017. UBE2O remodels the proteome during terminal erythroid differentiation. *Science*. 357:eaan0218.

Oromendia, A.B., S.E. Dodgson, and A. Amon. 2012. Aneuploidy causes proteotoxic stress in yeast. *Genes & development*. 26:2696-2708.

Padovani, C., P. Jevtić, and M. Rapé. 2022. Quality control of protein complex composition. *Molecular Cell*.

Park, S.H., Y. Kukushkin, R. Gupta, T. Chen, A. Konagai, M.S. Hipp, M. Hayer-Hartl, and F.U. Hartl. 2013. PolyQ proteins interfere with nuclear degradation of cytosolic proteins by sequestering the Sis1p chaperone. *Cell*. 154:134-145.

Pillet, B., A. Mendez-Godoy, G. Murat, S. Favre, M. Stumpe, L. Falquet, and D. Kressler. 2022. Dedicated chaperones coordinate co-translational regulation of ribosomal protein production with ribosome assembly to preserve proteostasis. *Elife*. 11.

Pincus, D. 2020. Regulation of Hsf1 and the Heat Shock Response. *Adv Exp Med Biol*. 1243:41-50.

Powis, K., B. Schrul, H. Tienson, I. Gostimskaya, M. Breker, S. High, M. Schuldiner, U. Jakob, and B. Schwappach. 2013. Get3 is a holdase chaperone and moves to deposition sites for aggregated proteins when membrane targeting is blocked. *Journal of Cell Science*. 126:473-483.

Prasad, R., C. Xu, and D.T.W. Ng. 2018. Hsp40/70/110 chaperones adapt nuclear protein quality control to serve cytosolic clients. *J Cell Biol*. 217:2019-2032.

Protter, D.S., and R. Parker. 2016. Principles and properties of stress granules. *Trends in cell biology*. 26:668-679.

Riback, J.A., C.D. Katanski, J.L. Kear-Scott, E.V. Pilipenko, A.E. Rojek, T.R. Sosnick, and D.A. Drummond. 2017. Stress-Triggered Phase Separation Is an Adaptive, Evolutionarily Tuned Response. *Cell*. 168:1028-1040 e1019.

Rudiger, S., J. Schneider-Mergener, and B. Bukau. 2001. Its substrate specificity characterizes the DnaJ co-chaperone as a scanning factor for the DnaK chaperone. *EMBO J*. 20:1042-1050.

Sagot, I., and D. Laporte. 2019. Quiescence, an individual journey. *Current genetics*. 65:695-699.

Samant, R.S., C.M. Livingston, E.M. Sontag, and J. Frydman. 2018. Distinct proteostasis circuits cooperate in nuclear and cytoplasmic protein quality control. *Nature*. 563:407-411.

Santagata, S., M.L. Mendillo, Y.C. Tang, A. Subramanian, C.C. Perley, S.P. Roche, B. Wong, R. Narayan, H. Kwon, M. Koeva, A. Amon, T.R. Golub, J.A. Porco, Jr., L. Whitesell, and S. Lindquist. 2013. Tight coordination of protein translation and HSF1 activation supports the anabolic malignant state. *Science*. 341:1238303.

Santiago, A.M., D.L. Goncalves, and K.A. Morano. 2020. Mechanisms of sensing and response to proteotoxic stress. *Exp Cell Res*. 395:112240.

Schilke, B.A., and E.A. Craig. 2022. Essentiality of Sis1, a J-domain protein Hsp70 cochaperone, can be overcome by Tti1, a specialized PIKK chaperone. *Molecular Biology of the Cell*. 33:br3.

Seidel, M., N. Romanov, A. Obarska-Kosinska, A. Becker, N. Trevisan Doimo de Azevedo, J. Provaznik, S.R. Nagaraja, J.J. Landry, V. Benes, and M. Beck. 2023. Co-translational binding of importins to nascent proteins. *Nature Communications*. 14:3418.

Shakya, V.P.S., W.A. Barbeau, T. Xiao, C.S. Knutson, M.H. Schuler, and A.L. Hughes. 2021. A nuclear-based quality control pathway for non-imported mitochondrial proteins. *eLife*. 10:e61230.

Shan, S.-o. 2019. Guiding tail-anchored membrane proteins to the endoplasmic reticulum in a chaperone cascade. *Journal of Biological Chemistry*. 294:16577-16586.

Shore, D., and B. Albert. 2022. Ribosome biogenesis and the cellular energy economy. *Curr Biol*. 32:R611-R617.

Shore, D., S. Zencir, and B. Albert. 2021. Transcriptional control of ribosome biogenesis in yeast: links to growth and stress signals. *Biochem Soc Trans*. 49:1589-1599.

Sontag, E.M., F. Morales-Polanco, J.H. Chen, G. McDermott, P.T. Dolan, D. Gestaut, M.A. Le Gros, C. Larabell, and J. Frydman. 2023. Nuclear and cytoplasmic spatial protein quality control is coordinated by nuclear-vacuolar junctions and perinuclear ESCRT. *Nat Cell Biol*. 25:699-713.

Sontag, E.M., R.S. Samant, and J. Frydman. 2017. Mechanisms and Functions of Spatial Protein Quality Control. *Annu Rev Biochem*. 86:97-122.

Sun, S., and D. Gresham. 2021. Cellular quiescence in budding yeast. *Yeast*. 38:12-29.

Sung, M.-K., J.M. Reitsma, M.J. Sweredoski, S. Hess, and R.J. Deshaies. 2016a. Ribosomal proteins produced in excess are degraded by the ubiquitin–proteasome system. *Molecular Biology of the Cell*. 27:2642-2652.

Sung, M.K., T.R. Porras-Yakushi, J.M. Reitsma, F.M. Huber, M.J. Sweredoski, A. Hoelz, S. Hess, and R.J. Deshaies. 2016b. A conserved quality-control pathway that mediates degradation of unassembled ribosomal proteins. *Elife*. 5.

Sutandy, F.X.R., I. Gossner, G. Tascher, and C. Munch. 2023. A cytosolic surveillance mechanism activates the mitochondrial UPR. *Nature*. 618:849-854.

Triandafillou, C.G., C.D. Katanski, A.R. Dinner, and D.A. Drummond. 2020. Transient intracellular acidification regulates the core transcriptional heat shock response. *Elife*. 9.

Tye, B.W., and L.S. Churchman. 2021. Hsf1 activation by proteotoxic stress requires concurrent protein synthesis. *Mol Biol Cell*. 32:1800-1806.

Tye, B.W., N. Commins, L.V. Ryazanova, M. Wuhr, M. Springer, D. Pincus, and L.S. Churchman. 2019. Proteotoxicity from aberrant ribosome biogenesis compromises cell fitness. *Elife*. 8.

Wallace, E.W., J.L. Kear-Scott, E.V. Pilipenko, M.H. Schwartz, P.R. Laskowski, A.E. Rojek, C.D. Katanski, J.A. Riback, M.F. Dion, A.M. Franks, E.M. Airoldi, T. Pan, B.A. Budnik, and D.A. Drummond. 2015. Reversible, Specific, Active Aggregates of Endogenous Proteins Assemble upon Heat Stress. *Cell*. 162:1286-1298.

Wang, F., C. Chan, N.R. Weir, and V. Denic. 2014. The Get1/2 transmembrane complex is an endoplasmic-reticulum membrane protein insertase. *Nature*. 512:441-444.

Woolford, J.L., Jr., and S.J. Baserga. 2013. Ribosome biogenesis in the yeast Saccharomyces cerevisiae. *Genetics*. 195:643-681.

Work, J.J., and O. Brandman. 2021. Adaptability of the ubiquitin-proteasome system to proteolytic and folding stressors. *J Cell Biol*. 220.

Xu, Y., D.E. Anderson, and Y. Ye. 2016. The HECT domain ubiquitin ligase HUWE1 targets unassembled soluble proteins for degradation. *Cell discovery*. 2:1-16.

Yagita, Y., E. Zavodszky, S.-Y. Peak-Chew, and R.S. Hegde. 2023. Mechanism of orphan subunit recognition during assembly quality control. *Cell*. 186:3443-3459. e3424.

Yanagitani, K., S. Juszkiewicz, and R.S. Hegde. 2017. UBE2O is a quality control factor for orphans of multiprotein complexes. *Science*. 357:472-475.

Yoo, H., C. Triandafillou, and D.A. Drummond. 2019. Cellular sensing by phase separation: Using the process, not just the products. *J Biol Chem*. 294:7151-7159.

Zavodszky, E., S.-Y. Peak-Chew, S. Juszkiewicz, A.J. Narvaez, and R.S. Hegde. 2021. Identification of a quality-control factor that monitors failures during proteasome assembly. *Science*. 373:998-1004.

Zheng, X., J. Krakowiak, N. Patel, A. Beyzavi, J. Ezike, A.S. Khalil, and D. Pincus. 2016. Dynamic control of Hsf1 during heat shock by a chaperone switch and phosphorylation. *Elife*. 5.

Zid, B.M., and E.K. O'Shea. 2014. Promoter sequences direct cytoplasmic localization and translation of mRNAs during starvation in yeast. *Nature*. 514:117-121.

CHAPTER 3

Emergent 3D genome reorganization from the stepwise assembly of transcriptional condensates

This chapter is a reprint of the current draft of Chowdhary et al 2024 on which I am a primary author. This work is in preparation to be submitted at the end of this year. It is included with permission from all the authors. I contributed equally (with Surabhi Chowdhary) to the conceptualization, methodology and investigations performed in this study. I wrote this draft of the paper, and will contribute to the revision and editing of the final product before it is submitted.

3.1 Abstract

Transcriptional condensates are clusters of transcription factors, coactivators, and RNA Pol II associated with high-level gene expression. It remains unknown whether transcriptional condensates assemble cooperatively, via mutually dependent interactions among components, or serially, via discrete recruitment steps. Here we reveal that during the heat shock response (HSR) in budding yeast, assembly proceeds in a stepwise manner. To initiate condensation, the transcription factor Hsf1 partially dissociates from the chaperone Hsp70. Next, to recruit the Mediator coactivator, Hsf1 unleashes multi-valent interaction surfaces upon further Hsp70 dissociation and hyperphosphorylation. However, constitutive co-condensates of Hsf1 and Mediator are unable to attract Pol II, which condenses only upon an independent environmental cue. Rather than a cooperative ON/OFF switch, HSR condensates assemble in a series of regulated steps, enabling dynamically tunable gene control. Beyond transcription, fully assembled condensates with Pol II drive the emergence of long-range intergenic interactions, spatially repositioning HSR target genes during stress.

3.2 Introduction

Compartmentalization of transcriptional machinery in biomolecular condensates at specific genomic loci is associated with robust expression of developmental, disease-linked, and stress-induced genes (Boija et al., 2018; Cho et al., 2018; Hnisz et al., 2017). Hypothesized to be nucleated via the cooperative binding of sequence-specific transcription factors (Ferrie et al., 2022; Wei et al., 2020), transcriptional condensates additionally involve the concerted cooperative association of coactivators and RNA Polymerase II (Pol II) (Banani et al., 2017; Banani et al., 2016). Intrinsically disordered regions (IDRs), frequently present in constituent proteins, contribute to cooperative assemblies via low-affinity, multivalent interactions among regions with compatible blocks of surface charge (Boija et al., 2018; Cai et al., 2019; Cho et al., 2018; Sabari et al., 2018; Sabari et al., 2020). However, embedded within the network of disordered interactions, there exist allosteric regulatory interactions among structured domains, proscribing complex kinetic control. It remains unclear the extent to which the assembly and activity of transcriptional condensates differentially depend on cooperative interactions among multiple components versus specific pairwise interactions (Figure 1A).

The heat shock response (HSR) provides an experimental system to dissect the functional regulation of transcriptional condensates. The HSR is a conserved transcriptional program controlling the expression of molecular chaperones and other components of the protein homeostasis (proteostasis) network. In yeast and human cells, Hsf1, the master regulator of the HSR, forms transcriptional condensates at its target gene loci upon activation by heat shock (Chowdhary et al., 2022; Zhang et al., 2022). Like canonical transcriptional condensates at super-enhancers (Sabari et al., 2018), HSR condensates colocalize with the Mediator transcriptional coactivator and Pol II (Figure 1B). Unlike canonical transcriptional condensates, HSR condensates form rapidly upon heat shock, providing the opportunity to dissect the dynamics of the assembly process. Moreover, HSR condensates in yeast promote intergenic

interactions between unlinked Hsf1 target genes (Chowdhary et al., 2019), thereby reorganizing the 3D genome during stress and endowing HSR condensates with an emergent property beyond transcriptional activation (Chowdhary et al., 2022) (Figure 1B).

In this study, we leverage the yeast HSR system to delineate cooperative versus stepwise assembly mechanisms in the formation of transcriptional condensates. Our findings support a stepwise assembly model for HSR condensates, characterized by cooperative interactions at each stage. Specifically, we show that Hsf1 is essential for Mediator and Pol II condensation; Mediator is necessary for Pol II condensation but not for Hsf1; and Pol II is not required for the condensation of Hsf1 or Mediator. Hsf1 condensation is initiated by release from Hsp70 and relies on phosphorylation, allowing for a graded transcriptional response of HSR genes rather than a simple on/off switch.

Interestingly, while each step in the condensate assembly process is associated with increased transcription, Hsf1 condensate formation is not strictly required for HSR transcriptional activation. Using separation-of-function Hsf1 mutants that fail to form condensates but still robustly induce HSR gene transcription during heat shock, we find that even constitutively active Hsf1-Mediator co-condensates are insufficient to recruit Pol II. Although cells achieve high levels of inducible HSR transcription in the absence of full condensate assembly, intergenic interactions between HSR genes become apparent only when fully assembled condensates containing Pol II are present. These interactions significantly enhance cellular fitness under stress.

We propose that the stepwise assembly of HSR condensates allows precise tuning of gene expression, while cooperative interactions within fully assembled condensates enable adaptive 3D genome reconfiguration, enhancing cellular resilience during stress.

3.3 Results

3.3.1 Ordered assembly of HSR condensates during heat shock

To investigate whether HSR condensates assemble cooperatively or in a stepwise manner, we generated rapamycin-resistant yeast strains, and used the "anchor-away" (AA) system to conditionally deplete Hsf1, the Mediator subunits Med15 and Ssn3/Cdk8, and the RNA Pol II subunit Rpb3 from the nucleus upon rapamycin treatment (Figure 1C, D, E) (Haruki et al., 2008). Med15, known to directly associate with Hsf1 (Kim & Gross, 2013) was tagged with mCherry in Hsf1-AA strains to monitor condensate formation upon heat shock. Under non-stress conditions, Med15 and Rpb3 were diffusely localized in the nucleus, and rapamycin-induced depletion of Hsf1 did not alter this distribution. Upon heat shock, however, both Med15 and Rpb3 condensed in the nucleus—an effect that was abolished if cells were depleted of Hsf1.

In Med15-AA strains with Hsf1-GFP and Rpb3-mCherry, both Hsf1 and Rpb3 condensed upon heat shock in the absence of rapamycin, but only Hsf1 condensed when Med15 was depleted, leaving Rpb3 diffuse. Conversely, in the Ssn3/Cdk8-AA strain, both Hsf1 and Rpb3 condensed in response to heat shock regardless of rapamycin treatment (Figure S1A). This indicates that the core Mediator complex, which includes Med15, is essential for Pol II condensation upon heat shock, whereas the kinase module containing Ssn3/Cdk8 is not. In the Rpb3-AA background, strains tagged with Hsf1-GFP and Med15-mCherry showed condensation of both Hsf1 and Med15 irrespective of Rpb3 depletion. These findings suggest an ordered assembly of HSR condensates in which Hsf1 first condenses upon heat shock, recruits Mediator for co-condensation, and then Mediator recruits Pol II.

Functionally, nuclear depletion of Hsf1, Med15, and Rpb3 each reduced transcriptional induction of HSR target genes during heat shock, with Hsf1 and Rpb3 depletion having

stronger effects than Med15 depletion (Figure 1G). Depletion of any of these three factors also reduced the frequency of both intragenic and intergenic 3D interactions among HSR target genes, as measured by chromosome conformation capture (3C), with a more pronounced effect seen in Hsf1-AA and Rpb3-AA cells compared to Med15-AA (Figure 1F, S1B). Together, the imaging and molecular assays in these AA strains reveal that while HSR condensate assembly occurs in distinct stages, full condensate formation is required for effective transcription and 3D genome reorganization.

3.3.2 Multivalent repression of Hsf1 condensate formation by Hsp70

Since Hsf1 is essential for initiating HSR condensate formation, we hypothesized that mechanisms known to regulate Hsf1's transcriptional activity would similarly influence its condensation upon heat shock. Specifically, we focused on Hsp70, which directly binds to Hsf1 to repress its transcriptional activity (Krakowiak et al., 2018), and hyper-phosphorylation of IDRs on Hsf1, which positively regulates Hsf1 transactivation (Anckar & Sistonen, 2011; Guettouche et al., 2005; Zheng et al., 2018). We assessed the roles of Hsp70 binding and phosphorylation through mutational analyses of Hsf1.

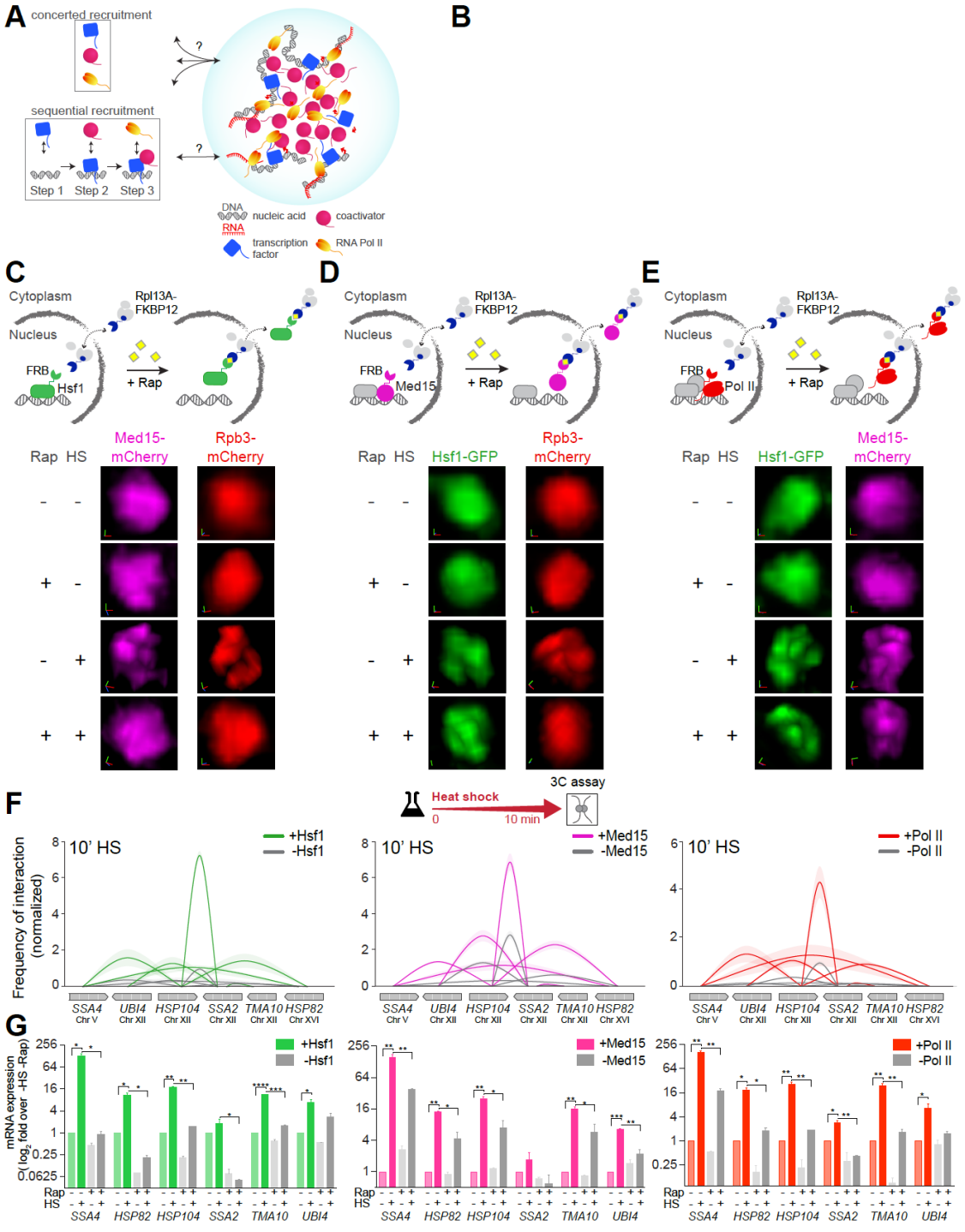

Figure 3.1 *Serial assembly of Hsf1, Mediator, and Pol II in transcriptional condensates.* **(A)** Cartoon depicting the two methods of condensate assembly. **(C-E)** Anchor-away experiments to determine sequence of HSR condensate assembly; Hsf1 (green), Med15 (magenta), Rpb3 (red). **(F)** Gene interaction analysis during HS (color) and NHS (grey), using chromosome conformation capture (3C). **(G)** Bar graphs depicting relative mRNA expression in HS (color) and NHS (grey) conditions.

To further explore these interactions, we generated Hsf1 mutants with disruptions in NE1, CE2, and both sites combined (Figure 2B, bottom), tagging each with GFP and expressing them from the endogenous HSF1 promoter as the sole source of Hsf1 in the cell. Imaging revealed that, unlike wildtype Hsf1, which is diffusely localized in the nucleus under NHS conditions, all three mutants – Hsf1-ne1, Hsf1-ce2, and the double mutant Hsf1-ne1ce2 – constitutively formed subnuclear foci in a similar number of cells as wildtype Hsf1 does under heat shock (Figure 2C, D, S2A). Consistent with previous findings, these mutants displayed elevated expression of HSR target genes under non-stress conditions. However, even the double mutant Hsf1-ne1ce2 retained substantial inducible transcriptional activity upon heat shock, indicating that additional regulatory mechanisms for Hsf1 are still active (Figure 2E, S2B).

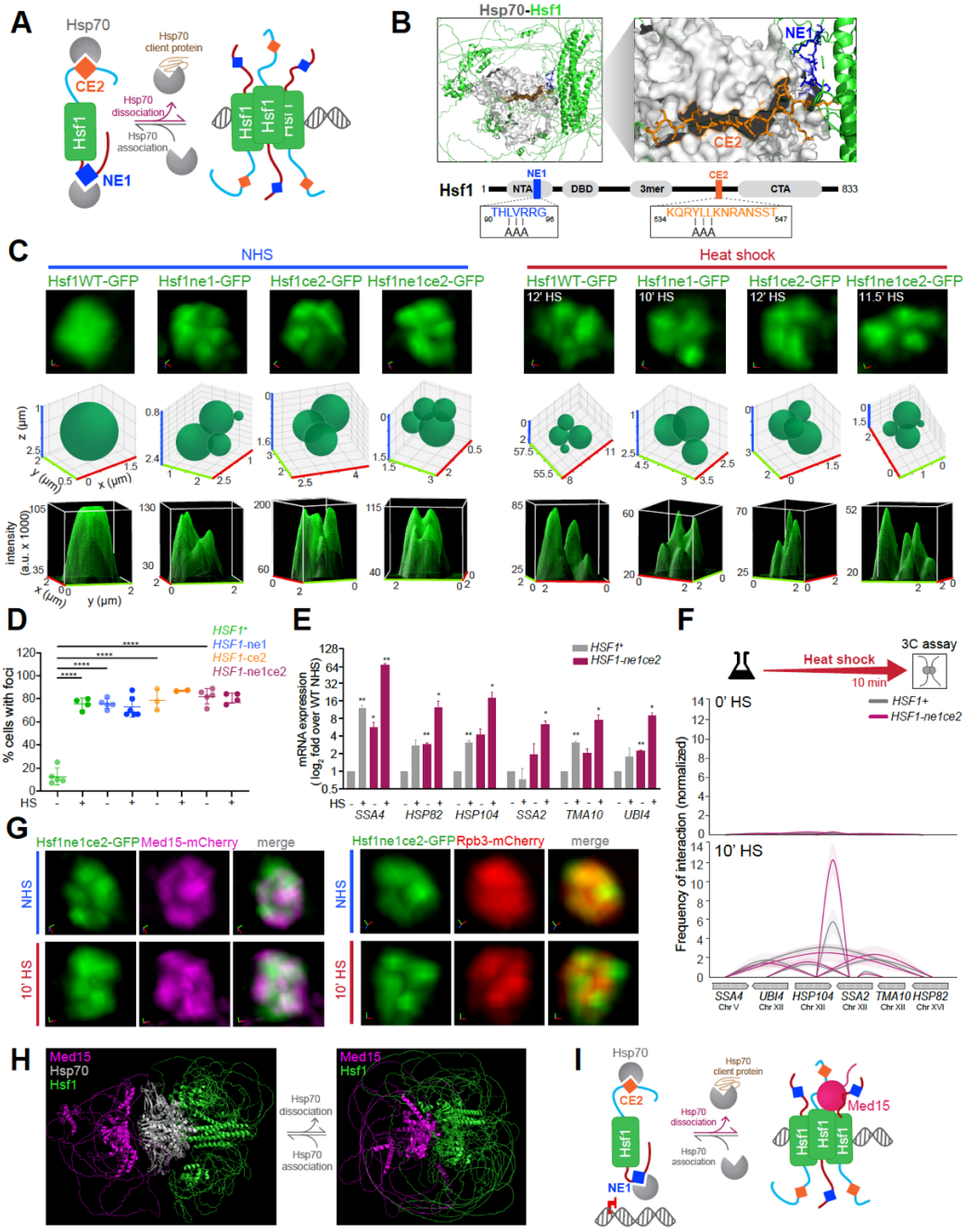

Figure 3.2 *Multivalent interaction sites on Hsf1 for Hsp70 and Mediator* **(A)** Model depicting Hsp70 binding and repression of Hsf1. **(B)** Depiction of NE1 and CE2 sites on Hsf1 generated with AlphaFold. **(C and G)** Characterization of Hsf1, Med15, and Rpb3 condensates in Hsf1-ne1, Hsf1-ce2, and Hsf1-ne1ce2 in NHS and HS conditions. **(D)** Quantification of foci for each Hsf1 variant with and without HS. **(E)** mRNA expression of five HSR genes for Hsf1-ne1ce2 in NHS (grey) and HS (maroon). **(F)** Interaction analysis of Hsf1-ne1ce2 at NHS (grey) and HS (maroon). **(G)** Structure of Hsf1-Hsp70 complex dissociation and interaction with Mediator, rendered using AlphaFold. **(I)** Model depicting multivalent regulation of Hsf1 and Mediator condensation by Hsp70.

3.3.3 Hsf1-Mediator condensates lack Pol II and intergenic interactions

To test whether constitutively condensed Hsf1 is sufficient to drive the condensation of Mediator and Pol II, we generated strains with Hsf1-GFP variants in which either Med15 or Rpb3 was tagged with mCherry. While Hsf1 was constitutively condensed in all mutants, Med15 showed continuous condensation only in the Hsf1-ne1ce2 double mutant, and Rpb3 remained diffuse across all mutants under non-stress conditions (Figure 2F, S2C). Under heat shock, however, all Hsf1 mutants, like wildtype, co-condensed with both Med15 and Rpb3. This reveals that while these Hsf1 condensates appear phenotypically similar, they are actually molecularly distinct: Hsf1 with a single mutated Hsp70 binding site condenses independently of Mediator and Pol II; Hsf1 with disrupted multivalent Hsp70 binding condenses with Mediator but not Pol II; and heat shock-activated Hsf1 condenses with both Mediator and Pol II.

We then examined the 3D configuration of HSR genes. Mutating Hsp70 binding sites, whether singly or in combination, did not lead to constitutive intergenic interactions as assessed by 3C (Figure 2F, S2D, E). However, consistent with heat shock driving the full assembly of HSR condensates with Mediator and Pol II, all mutants retained the ability to induce 3D genome reorganization under heat shock. Notably, the Hsf1-ne1ce2 double mutant displayed increased interaction frequencies between certain genes under thermal stress (Figure 2G, S2D, E). The mutants' ability to recover these functions during heat shock is further supported by the absence of any fitness deficits (Figure S2F).

These findings suggest that while Hsp70 binding restricts Mediator recruitment, loss of Hsp70 association alone is not sufficient to drive Pol II condensation or promote intergenic interactions. AlphaFold multimer modeling further supports this conclusion, indicating mutually exclusive interactions between Hsf1 and Hsp70, and Hsf1 and Med15. Models of

Hsf1, Hsp70, and Med15 (3:2:1 stoichiometry) and Hsf1 and Med15 (3:1 stoichiometry) suggest that Hsp70 sterically occludes Med15 binding (Figure 2H, I).

3.3.4 Regulation of Hsf1 condensate formation by phosphorylation

Post-translational modifications, such as phosphorylation, are known to modulate transcriptional condensate components, regulating their formation and dissolution (Guo et al., 2019; Henninger et al., 2021). Multiple phosphorylation sites have been identified on the Hsf1 protein (Figure 3B), but the roles of specific regulatory sites have yet to be clearly defined (Budzyński et al., 2015; Cho et al., 2014; Dai et al., 2015; Kline & Morimoto, 1997). To investigate how Hsf1 phosphorylation affects HSR condensate formation, we used previously established phospho-mutant strains: the phosphomimetic Hsf1-PO4* mutant, where 116 serine/threonine residues are converted to aspartate to mimic the negative charge of phosphorylation, and the phospho-null Hsf1-Δpo4 mutant, where 152 serine/threonine residues are converted to alanine, retaining only the phospho-site required for Hsf1 DNA binding (Figure 3C).

To analyse condensate dynamics, we created strains in which the mutated Hsf1 was tagged with GFP as the sole Hsf1 source, with either Med15 or Rpb3 tagged with mCherry. Under non-stress conditions, Hsf1-Δpo4-GFP remained diffuse, similar to wildtype Hsf1-GFP, while Hsf1-PO4*-GFP displayed constitutive condensation, forming foci in a similar proportion of cells to those observed under heat shock (Figure 3D). Surprisingly, under heat shock, neither Hsf1-Δpo4-GFP nor Mediator or Pol II condensed (Figure 3H), although these cells showed an increase in Hsf1 target gene mRNA expression, comparable to wildtype Hsf1 under stress (Figure 3F). This suggests that condensate formation—and thus stable, cooperative interactions among Hsf1, Mediator, and Pol II—is not required for transcriptional activation, effectively decoupling the processes of condensation and transcription. Notably, Hsf1-PO4*-GFP, similar to the Hsp70-binding double mutant, promotes constitutive Mediator condensation under both

non-stress and stress conditions (Figure 3H). However, Pol II does not condense in these mutants, even under heat shock, yet transcription of the HSR regulon occurs at higher levels than with wildtype Hsf1 (Figure 3F, H), further supporting the decoupling of transcription from complete condensate formation.

Neither phosphorylation mutant triggered 3D rearrangement of Hsf1 target genes in the absence of heat shock. Upon heat shock, both mutants exhibited reduced gene interactions, aligning with our previous observation that wildtype Hsf1-induced gene clustering is a consequence of complete HSR condensate formation (Figure 3G, S3C). Additionally, although the Hsf1-Δpo4-GFP mutant appears similar under non-stress and heat shock conditions, its gene expression response differs between these states, likely due to diminished gene interactions during heat shock. These findings demonstrate that while phosphorylation is essential for Hsf1 activation, it does not drive Pol II condensation.

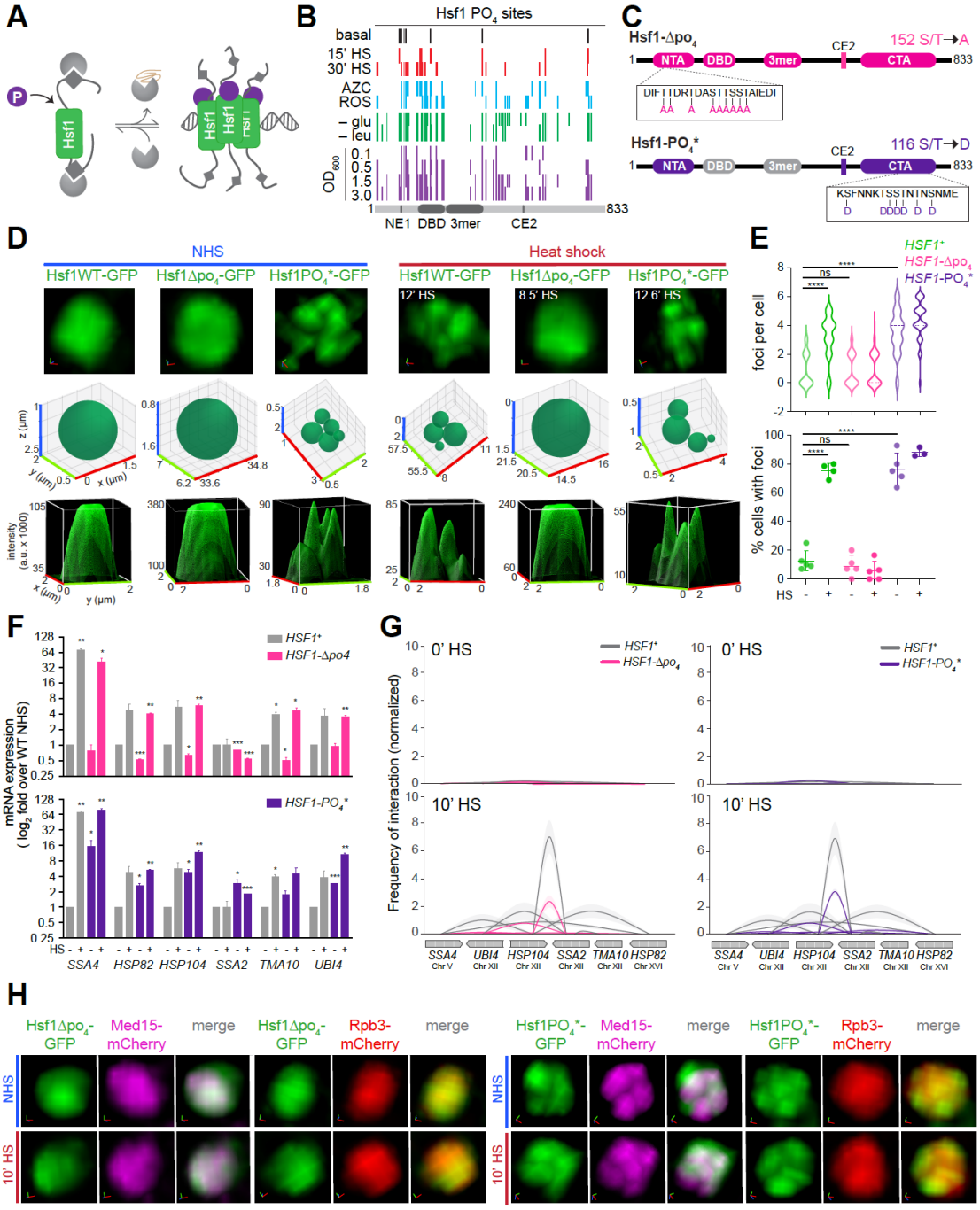

Figure 3.3 *Phospho-regulation of Hsf1condensate formation* **(A)** Model depicting activation of Hsf1 when phosphorylated **(B)** Map of reported phosphorylation sites on yeast Hsf1 in different conditions **(C)** Domain map of Hsf1- -Δpo$_4$ and Hsf1-PO4* **(D)** Characterization of Hsf1- -Δpo$_4$ and Hsf1-PO4*-GFP condensates at NHS and HS **(E)** Quantification of foci of each Hsf1-mutant **(F)** mRNA expression of 5 HSR genes in Hsf1- -Δpo$_4$ and Hsf1-PO4* at NHS (grey) and HS (color) **(G)** Gene interaction maps for Hsf1- -Δpo$_4$ and Hsf1-PO4* at NHS (grey) and HS (color) **(H)** Characterization of Med15 and Rpb3 condensation in Hsf1- -Δpo$_4$ and Hsf1-PO4* at NHS and HS conditions.

3.3.5 Dominance of phosphorylation over Hsp70 binding in regulating Hsf1 condensation

Since neither loss of Hsp70 binding nor hyperphosphorylation alone was sufficient to drive Pol II condensation, we generated mutant strains in which both the NE1 and CE2 sites of Hsf1 were mutated, combined with either hypo- or hyperphosphorylation. This allowed us to test whether these Hsf1 triple mutants could recruit Pol II and complete HSR condensate assembly under non-stress conditions. In the hypophosphorylated Hsf1-Δpo4-GFP strain, the Hsf1-ne1Δpo4-GFP and Hsf1-ce2Δpo4-GFP double mutants remained diffuse, even when exposed to acute heat stress (Figure S3A). Similarly, the Hsf1-ne1ce2Δpo4-GFP triple mutant did not form condensates upon heat shock, with both Mediator and Pol II remaining dispersed (Figure 4B, left; Figure 4E, top). Although the Hsf1-ne1ce2-GFP mutant exhibits constitutive condensation of Hsf1 and Mediator, hypophosphorylation has a stronger impact on Hsf1 activity than loss of Hsp70 binding. The triple mutant achieved wildtype levels of gene activation under both non-stress and heat shock conditions, indicating that hypophosphorylation overrides the effects of Hsp70 binding loss (Figure 4C, top).

In contrast, the hyperphosphorylated Hsf1-ne1PO4*-GFP and Hsf1-ce2PO4*-GFP double mutants displayed constitutive condensates under both non-stress and stress conditions (Figure S3B), as did the Hsf1-ne1ce2-PO4*-GFP triple mutant (Figure 4B, right). Like the Hsf1-PO4* single mutant, the triple mutant showed Mediator condensation and a hyperactive HSR at basal conditions, but no Pol II condensation (Figure 4E, bottom). Upon heat shock, Hsf1-ne1ce2-PO4* was able to further increase HSR gene expression, yet still failed to induce Pol II condensation, reinforcing the idea that transcriptional activation and condensation of the transcriptional machinery can be decoupled in these mutants. Unlike the Hsf1-ne1ce2Δpo4-GFP cells, hyperphosphorylation added to the Hsp70-binding mutations resulted in an overactive HSR under non-stress conditions, with gene expression levels comparable to those of wildtype Hsf1 during heat shock (Figure 4C, bottom).

Together, these results show that while mutations in phosphorylation and Hsp70-binding sites can mimic some aspects of HSR activity, they are insufficient to fully induce HSR condensate assembly under non-stress conditions. This highlights that complete condensate formation requires additional regulatory inputs beyond Hsp70 binding loss and phosphorylation to fully replicate the transcriptional and structural effects of heat shock.

In the Hsf1-ne1ce2Δpo4 strain, gene coalescence was absent under non-heat shock conditions, and heat shock led to reduced intergenic interactions (Figure 4D, left). Although Hsf1-ne1ce2Δpo4 shows a surge in gene transcription during heat shock, it does so without Mediator or Pol II condensation. Similar to the single Hsf1-Δpo4 mutant, this triple mutant achieves increased HSR gene expression levels upon heat shock, likely due to partial 3D reorganization of HSR genes. However, full gene coalescence cannot occur without transcriptional condensate formation, resulting in weaker intergenic interactions. Despite this functional limitation, these mutants do not display a growth defect, growing at rates comparable to wildtype Hsf1 strains at 37°C and in glucose-deficient media (Figure 4G).

The Hsf1-ne1ce2-PO4* mutant, like the hypophosphorylated variant, exhibits no gene coalescence under basal conditions and reduced induction of intergenic interactions between HSR genes during thermal stress (Figure 4D, right). In this case, the limited intergenic interactions and absence of Pol II condensation may be attributed to the highly negative charge of the Hsf1-PO4* mutant, which includes 116 negatively charged aspartate residues. To explore this, we generated 3D models of Mediator, Hsf1, and Pol II interactions for both wildtype and PO4* variants of Hsf1. The model of Hsf1-PO4* revealed a large negatively charged patch (in red) on its outer surface (Figure 4F), likely hindering interactions with Pol II's intrinsically disordered regions (IDRs) that are necessary for wildtype HSR condensate assembly, while Hsf1-Mediator interactions remain largely intact. Without Pol II recruitment,

full gene coalescence cannot occur, as all condensate components are required for the complete 3D genome rearrangements seen in wildtype cells.

3.3.6 Compromised fitness and intergenic interactions in constitutively condensed Hsf1

While Hsf1-ne1ce2-PO4* grows at basal temperatures similarly to wildtype cells, at 37°C this mutant strain exhibits a slight growth decrease and cell death in glucose-deficient media. These results demonstrate that transcriptional activation, condensate formation, and gene coalescence can be functionally separated in the HSR system without significant fitness costs in the hypophosphorylated state. However, the survival and adaptability of the PO4* triple mutant are compromised, suggesting that the mutant's negative charge impacts more than just Pol II recruitment.

3.3.7 Independent control of Hsf1 transcriptional activity by Hsp70 binding and phosphorylation

To investigate whether Hsp70 repression and Hsf1 phosphorylation act independently or within the same regulatory pathway, we conducted a quantitative genetic interaction analysis. Genetic interactions between two loci can be assessed by examining how the phenotype of the double mutant compares to the expected outcome based on the single mutants' phenotypes. For Hsf1-ne1, -ce2, and -ne1ce2 mutants, if the combined fold change in Hsf1 activity under non-heat shock conditions for each single mutant equals the observed fold change in the double mutant, it suggests that these sites function independently. We used a YFP reporter, integrated into the genome under a promoter with four heat shock element (HSE) repeats, to measure Hsf1 activity: when Hsf1 binds and activates these HSEs, YFP fluorescence reflects the level of Hsf1 activity. In our analysis, the expected fold change (if the two Hsp70 binding sites act independently) is shown as the striped bar, while the actual fold change for the double mutant is indicated in pink (Figure 5C). No significant difference between these values confirms that these two sites independently regulate Hsf1 activity (Figure 5A-C).

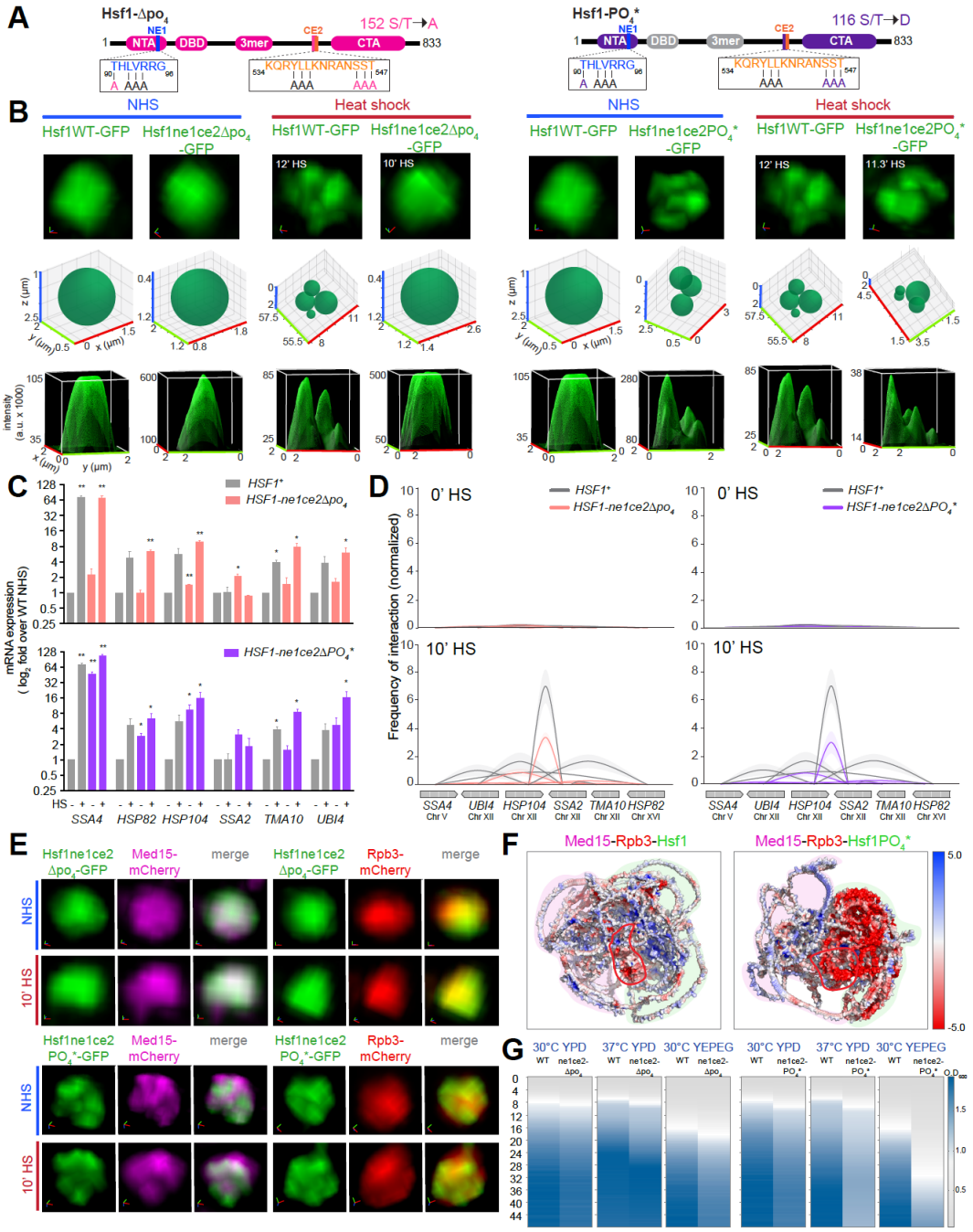

Figure 3.4 *Decoupling of condensate formation and transcriptional activity* **(A)** Domain map of Hsf1-ne1ce2Δpo4 and Hsf1-ne1ce2PO4* **(B)** Characterization of Hsf1-ne1ce2Δpo4 and Hsf1-ne1ce2PO4* condensates at NHS and HS conditions **(C)** mRNA expression of five HSR genes in Hsf1-ne1ce2Δpo4 and Hsf1-ne1ce2PO4* at NHS (grey) and HS (color) **(D)** gene interaction map of Hsf1-ne1ce2Δpo4 and Hsf1-ne1ce2PO4* at NHS (grey) and HS (color) **(E)** Characterization of Med15 and Rpb3 in Hsf1-ne1ce2Δpo4 and Hsf1-ne1ce2PO4* cells during NHS and HS **(F)** Model depicting interaction between Hsf1, Med15, and Rpb3 **(G)** Growth assay of Hsf1-ne1ce2Δpo4 and Hsf1-ne1ce2PO4* cells at 30C, 37C, and reduced glucose.

We extended this analysis to test interactions between Hsf1-Δpo4 and Hsf1-ne1ce2, and between Hsf1-PO4* and Hsf1-ne1ce2, to determine if hypophosphorylation and Hsp70-binding function independently in regulating Hsf1. Using the average gene expression levels induced by Hsf1-Δpo4 and Hsf1-ne1ce2 mutants, we found that gene expression in the Hsf1-ne1ce2Δpo4 double mutant matched the expected value from combining the single mutants, supporting that hypophosphorylation and Hsp70-binding regulate Hsf1 activity through separate pathways (Figure 5D-F). Although hypophosphorylation can mask the condensation phenotype of Hsp70-binding mutants, it does not alter their independent regulatory roles.

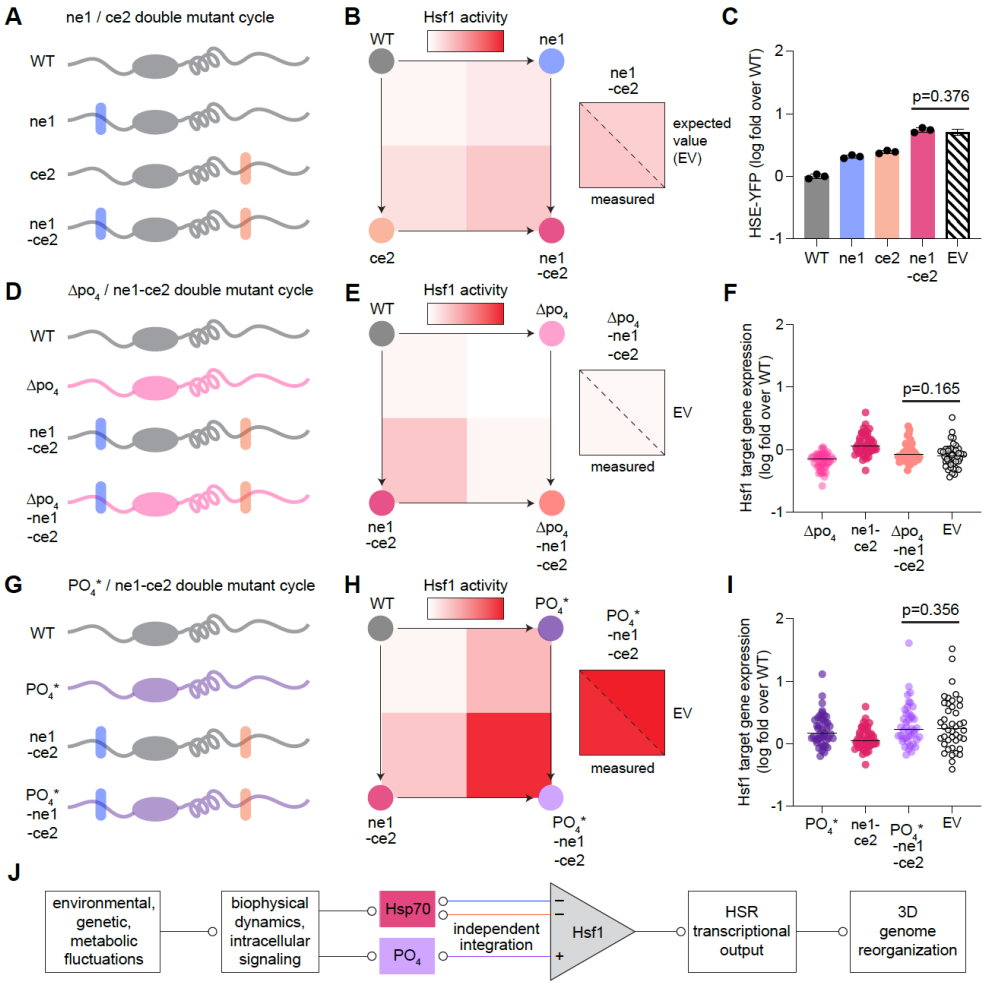

Figure 3.5 *Independent tuning of Hsf1 activity by Hsp70 binding and phosphorylation* **(A, D, G)** Cartoons depicting mutants used in each genetic interaction analysis **(B, E, H)** Heat map of Hsf1 activity for each mutant observed, color coding to compare the expected value and the actual value of the double mutants **(C, F, I)** Plots showing the Hsf1 activity and Hsf1 target gene expression for each mutant used in analysis **(J)** Schematic depicting the independent integration of the regulation of Hsf1 activity levels in response to different extracellular stimuli.

For the Hsf1-PO4* and Hsf1-ne1ce2 mutants, we similarly assessed HSR target gene expression by comparing the observed and expected values for Hsf1-ne1ce2PO4*. Consistent with previous results, there was no significant difference, indicating that hyperphosphorylation operates independently of Hsp70 repression (Figure 5G-I). This aligns with our earlier findings, where hyperphosphorylation exhibited an additive effect on the loss of Hsp70, further supporting the conclusion that Hsp70 binding and phosphorylation independently regulate Hsf1 activity.

Taken together, these results suggest that different environmental fluctuations can modulate a variable cellular response involving Hsf1 via the separate regulatory pathways of Hsp70 repression and Hsf1 phosphorylation. We hypothesize that, depending on the degree of stress, the intensity of these independent regulatory signals can adapt and then integrate to produce a corresponding level of Hsf1 activity, that can then induce the HSR accordingly and trigger 3D genome reorganization if needed (Figure 5J). This is vastly different to the historical concept of Hsf1 as an on/off switch where any amount of stress above a certain threshold will result in the same level of HSR activation.

3.3.8 Graded transcriptional output across the Hsf1 allelic series

To support our hypothesis from the previous section, we plotted the gene expression levels, under non-heat shock conditions, of all yeast HSR target genes for each of the Hsf1 variants we studied in this investigation (Figure 6A). The activity increases gradually with each mutation introduced, starting at its lowest with Hsf1-Δpo_4 and moving serially up to the Hsf1-ne1ce2-PO4* triple mutant, ending with wild type heat shock promoting the highest level of expression of HSR genes (Figure 6A). With each increasing step in activity, an emergent feature presents itself in terms of condensate formation (Figure 6B). Loss of one Hsp70 binding site induces Hsf1 condensation, while loss of both results in Mediator condensation as well. While

phosphorylation increases Hsf1 activity, it does not result in the final two properties of the HSR condensate, that is Pol II recruitment and 3D genome reorganization, even when combined with loss of Hsp70 binding ability. As of the time of this study, only heat shock triggers these last two steps, implicating that there is some characteristic of heat shock that we have not yet considered that allows Pol II to be released from the promoters of other genes and condense, thereby leading to intergenic interactions to push the full activation of the HSR. Given that the cell undergoes a number of changes during the HSR, there is most likely a regulatory element outside of Hsf1 that is involved in coordinating the final assembly stages of the condensate. These results support the finding that a complete HSR condensate is not needed for increased expression of the Hsf1 target genes, while also exhibiting that Hsf1 is able to produce a graded transcriptional output, similar to that hypothesized in the previous section.

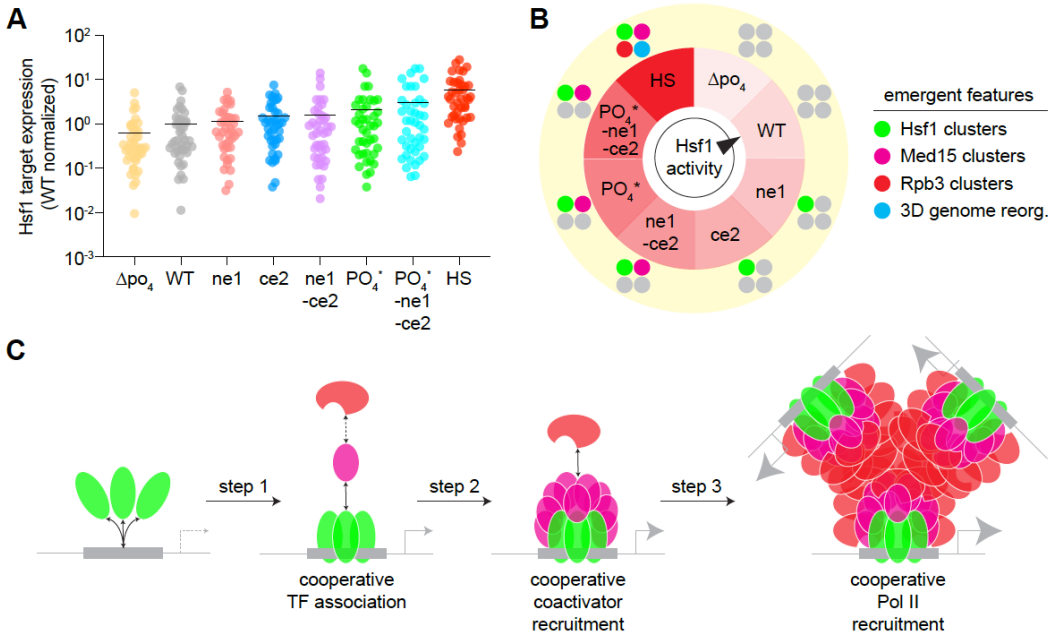

Figure 3.6 *Emergent 3D genome reorganization from fully assembled HSR condensates* **(A)** Hsf1 target gene expression for each mutant, each dot represents one gene **(B)** Schematic of Hsf1 activity, and its correlative position associated with HSR condensate assembly **(C)** Model of stepwise HSR condensate formation; Hsf1 (green), Mediator (magenta), Pol II (red).

3.4 Discussion

In this report, we establish that condensates form in a serial manner, starting with the concentration and cooperative inter-molecular interaction of Hsf1 IDRs, followed by the condensation of Mediator. Pol II cannot condense unless both Hsf1 and Mediator are present. This eventually leads to gene coalescence, an emergent function of the transcriptional condensate. Hsp70's multivalent binding to Hsf1 and the phosphorylation status of Hsf1 govern its ability to concentrate and recruit Mediator, while the coordination of RNA Pol II concentration and 3D genome interactions remains unclear. This inducible stepwise assembly pathway diverges from the previous model in the field, which suggests that the IDRs of DNA-bound transcription factors and those of other co-activator proteins interact cooperatively and without a specific sequence to partition into transcriptional condensates (Hnisz et al., 2017).

In wildtype Hsf1 cells exposed to thermal stress, we are able to detect the appearance of inter- and intrachromosomal interactions between Hsf1 target genes immediately after heat shock, correlating with the observation of Pol II condensates at this time point. This, along with our previous observations, implies that the concentration of Pol II molecules, and how they interact with Hsf1 and Mediator, triggers the on-switch of 3D genome reorganization. This is contrary to earlier reports using mammalian cells which have suggested that chromatin looping, enabled by CTCF and cohesin, drive the formation of condensates (Lee et al., 2021), or that transcriptional condensates occur at previously established super-enhancer sites where topologically associated domains (TADs) behave as a scaffold for transcriptional machinery to assemble and condense (Sabari et al., 2018). We show that the induction of intergenic interactions is the endpoint of assembly of the HSR condensate.

Hsf1, Mediator, and RNA Pol II condensates appear as distinct entities rather than as a single intermixing mass, as described in most representations of transcriptional condensates (Figure 2, 3, 4). This suggests that these regulatory molecules may condense individually instead of with

each other. While this could be true, these foci are still highly dynamic, trafficking quickly across the nucleoplasm and eventually contacting and interacting with one another. To this end, we previously demonstrated that colocalization of Mediator with Hsf1, and Pol II with Hsf1, occurs over 70% of the time in complete HSR condensates in cells expressing wildtype Hsf1 (Chowdhary et al., 2022). Therefore, HSR transcriptional condensates may not be present as a single intermixing mass in the nucleus, but as discrete entities that interact frequently to enhance the expression of specific gene groups. Clustering of both the transcriptional machinery and the genes to be transcribed still occurs, resulting in a more efficient and robust transcriptional output.

As we were unable to recreate complete HSR condensates in non-heat shock conditions by the modification of Hsf1, an additional layer of regulation in assembly is likely. The Hsf1 variants we implemented in our experiments are the only source of Hsf1 in these cells, meaning the cells have likely stabilized and adapted to this hyperactive form of Hsf1. There is likely something unique to acute heat shock that allows the release of Pol II from the promoters of the basal regulome and allows it to stably interact with Hsf1 and Mediator. As previously established, a large portion of the genome is repressed during heat shock (Rawat et al., 2021; Sawarkar, 2022), and this repression is Hsf1-independent (Duarte et al., 2016; Gasch & Werner-Washburne, 2002; Mahat et al., 2016). In these Hsf1-mutant cells, transcriptional activation and Pol II usage is no longer attenuated, creating competition between TFs of constitutively expressed genes and Hsf1 for Pol II recruitment. When the mutant strains undergo acute heat shock, the Hsf1 variants are able to recruit Pol II, further suggesting that Pol II must be liberated from other gene promoters before it can stably interact with Hsf1 and Mediator at HSR target genes.

Beyond transcriptional attenuation and gene coalescence, the components of the variant Hsf1 condensates that we observed must also be considered. The composition and induced activity of the Hsf1 condensates in these mutant strains may differ from those formed during a wildtype

HSR. Although these Hsf1 mutants were functional, promoting the transcription of the HSR regulon and supporting robust growth at basal temperatures, these differences must impact the interactions between Hsf1 and other proteins and nucleic acids. The Hsf1 phosphorylation variants are especially of concern, as their charge distributions are completely different compared to wildtype Hsf1. As described in the previous sections, the negative patch that forms on the surface of Hsf1-PO4* precludes interaction with Pol II, so it likely also prevents interactions with other wildtype HSR condensate components. Thus, we must further characterize not only these mutant Hsf1 condensates, but the wildtype condensates as well.

This is not to suggest that these mutants lack biological relevance. We were able to uncover a previously unknown mechanism of the regulation of Hsf1 by Hsp70 and phosphorylation in yeast, demonstrating their role in condensate assembly and HSR activity. Using prediction software like AlphaFold, we can also infer how Hsp70 impairs Hsf1 function. Multivalent binding of Hsp70 appears to suppress Hsf1 by creating a steric block that prevents interaction with Mediator but not with heat shock elements (Figure 2H). Mutating the NE1 and CE2 sites removes this block, allowing Mediator to perpetually associate with Hsf1. Notably, both sites must be mutated for Mediator recruitment, indicating that Hsp70 must be fully removed from these sites to allow Mediator engagement and condensate formation. This illustrates the tuneable nature of Hsf1 activity, where losing one Hsp70 molecule results in basal Hsf1-induced transcription, while losing both leads to higher levels of HSR gene expression.

We ascertain that there is increased transcriptional activity at each step of condensate assembly and Hsf1 can form transcriptionally active condensates without consistently associating with Mediator or Pol II. Since transcription of any gene requires these molecular complexes, the Hsf1 mutants we studied must still transiently engage Mediator and Pol II rather than form constant, enduring interactions. This suggests that sequentially concentrating each molecule that is part of the HSR condensate enhances transcription at each step, and maximum

transcription occurs only when all steps are completed, as in heat shock conditions. While this theory provides a coherent explanation for our results, it requires further investigation to determine what governs the final steps of HSR condensate assembly.

Although the HSR is conserved across eukaryotes, transcriptionally active HSR condensates like those in yeast have yet to be confirmed in mammalian cells. Human Hsf1 has been shown to form foci, similar to stress granules, in tumour cells, but their dissolution, rather than their formation, triggers heat shock protein transcription (Gaglia et al., 2020). However, in a recent study, it has been reported that in addition to these stress granules, small nuclear condensates of HSF1 and the transcription apparatus, including Mediator and BRD4, can form at target gene loci in HeLa cells and drive transcription (Zhang et al., 2022). The formation of these condensates is inhibited by Hsp70, with phosphorylation fine-tuning HSF1 activity, similar to what has been observed in yeast (Zhang et al., 2022; Zheng et al., 2018; Zheng et al., 2016). Gene coalescence, an emergent property of yeast HSR condensates, remains unstudied in mammalian cells. While topologically associated domains (TADs) in mammalian cells have been decoupled from gene expression (Ghavi-Helm et al., 2019), the mechanisms driving gene reorganization in human HSR condensates may differ due to the unique regulation of mammalian Hsf1.

3.4.1 Limitations of the study

The major limitation of this study is the spatiotemporal resolution of the live imaging data we generated to monitor the HSR condensates in yeast cells. The principal challenge is the small size of the yeast nucleus (<3 μm^3), which means that the HSR condensates are distributed and must rearrange in a very compact space. The low abundance of the components (on the order of 10^3 molecules of endogenously tagged Hsf1 or Med15 per cell), the rapid kinetics of formation and dissolution of HSR condensates, and the spatial distribution of the condensates across multiple z-planes presented further technical challenges. We relied on relatively long

exposures, requiring 15 seconds to capture each z-stack at each time point, and we were limited by photobleaching in the total number of timepoints we could collect. Together, these challenges made it difficult to discern whether the HSR condensates in budding yeast are discrete foci like transcriptional condensates in mammalian cells. Although HSR condensates share components and properties with mammalian transcriptional condensates, we do not rule out the possibility that HSR condensates might be qualitatively distinct given their transient nature and their ability to cluster HSR target genes. Perhaps, HSR condensates are constantly ebbing and flowing, forming mobile regions of local enrichment of the transcriptional machinery that rapidly recruit and release target genes as they dynamically survey the genome.

3.5 References

Anckar, J., & Sistonen, L. (2011). Regulation of HSF1 function in the heat stress response: implications in aging and disease. *Annu Rev Biochem*, *80*, 1089-1115. https://doi.org/10.1146/annurev-biochem-060809-095203

Banani, S. F., Lee, H. O., Hyman, A. A., & Rosen, M. K. (2017). Biomolecular condensates: organizers of cellular biochemistry. *Nat Rev Mol Cell Biol*, *18*(5), 285-298. https://doi.org/10.1038/nrm.2017.7

Banani, S. F., Rice, A. M., Peeples, W. B., Lin, Y., Jain, S., Parker, R., & Rosen, M. K. (2016). Compositional Control of Phase-Separated Cellular Bodies. *Cell*, *166*(3), 651-663. https://doi.org/10.1016/j.cell.2016.06.010

Boija, A., Klein, I. A., Sabari, B. R., Dall'Agnese, A., Coffey, E. L., Zamudio, A. V., Li, C. H., Shrinivas, K., Manteiga, J. C., Hannett, N. M., Abraham, B. J., Afeyan, L. K., Guo, Y. E., Rimel, J. K., Fant, C. B., Schuijers, J., Lee, T. I., Taatjes, D. J., & Young, R. A. (2018). Transcription Factors Activate Genes through the Phase-Separation Capacity of Their Activation Domains. *Cell*, *175*(7), 1842-1855.e1816. https://doi.org/10.1016/j.cell.2018.10.042

Budzyński, M. A., Puustinen, M. C., Joutsen, J., & Sistonen, L. (2015). Uncoupling Stress-Inducible Phosphorylation of Heat Shock Factor 1 from Its Activation. *Mol Cell Biol*, *35*(14), 2530-2540. https://doi.org/10.1128/mcb.00816-14

Cai, D., Feliciano, D., Dong, P., Flores, E., Gruebele, M., Porat-Shliom, N., Sukenik, S., Liu, Z., & Lippincott-Schwartz, J. (2019). Phase separation of YAP reorganizes genome topology for long-term YAP target gene expression. *Nat Cell Biol*, *21*(12), 1578-1589. https://doi.org/10.1038/s41556-019-0433-z

Cho, B. R., Lee, P., & Hahn, J. S. (2014). CK2-dependent inhibitory phosphorylation is relieved by Ppt1 phosphatase for the ethanol stress-specific activation of Hsf1 in Saccharomyces cerevisiae. *Mol Microbiol*, *93*(2), 306-316. https://doi.org/10.1111/mmi.12660

Cho, W. K., Spille, J. H., Hecht, M., Lee, C., Li, C., Grube, V., & Cisse, II. (2018). Mediator and RNA polymerase II clusters associate in transcription-dependent condensates. *Science*, *361*(6400), 412-415. https://doi.org/10.1126/science.aar4199

Chowdhary, S., Kainth, A. S., & Gross, D. S. (2017). Heat Shock Protein Genes Undergo Dynamic Alteration in Their Three-Dimensional Structure and Genome Organization in Response to Thermal Stress. *Mol Cell Biol*, *37*(24). https://doi.org/10.1128/mcb.00292-17

Chowdhary, S., Kainth, A. S., & Gross, D. S. (2020). Chromosome conformation capture that detects novel cis- and trans-interactions in budding yeast. *Methods*, *170*, 4-16. https://doi.org/10.1016/j.ymeth.2019.06.023

Chowdhary, S., Kainth, A. S., Paracha, S., Gross, D. S., & Pincus, D. (2022). Inducible transcriptional condensates drive 3D genome reorganization in the heat shock response. *Mol Cell*, *82*(22), 4386-4399.e4387. https://doi.org/10.1016/j.molcel.2022.10.013

Chowdhary, S., Kainth, A. S., Pincus, D., & Gross, D. S. (2019). Heat Shock Factor 1 Drives Intergenic Association of Its Target Gene Loci upon Heat Shock. *Cell Rep*, *26*(1), 18-28.e15. https://doi.org/10.1016/j.celrep.2018.12.034

Dai, S., Tang, Z., Cao, J., Zhou, W., Li, H., Sampson, S., & Dai, C. (2015). Suppression of the HSF1-mediated proteotoxic stress response by the metabolic stress sensor AMPK. *Embo j*, *34*(3), 275-293. https://doi.org/10.15252/embj.201489062

Duarte, F. M., Fuda, N. J., Mahat, D. B., Core, L. J., Guertin, M. J., & Lis, J. T. (2016). Transcription factors GAF and HSF act at distinct regulatory steps to modulate stress-induced gene activation. *Genes Dev*, *30*(15), 1731-1746. https://doi.org/10.1101/gad.284430.116

Ferrie, J. J., Karr, J. P., Tjian, R., & Darzacq, X. (2022). "Structure"-function relationships in eukaryotic transcription factors: The role of intrinsically disordered regions in gene regulation. *Mol Cell*, *82*(21), 3970-3984. https://doi.org/10.1016/j.molcel.2022.09.021

Gaglia, G., Rashid, R., Yapp, C., Joshi, G. N., Li, C. G., Lindquist, S. L., Sarosiek, K. A., Whitesell, L., Sorger, P. K., & Santagata, S. (2020). HSF1 phase transition mediates stress adaptation and cell fate decisions. *Nature Cell Biology*, *22*(2), 151-158. https://doi.org/10.1038/s41556-019-0458-3

Gasch, A. P., & Werner-Washburne, M. (2002). The genomics of yeast responses to environmental stress and starvation. *Funct Integr Genomics*, *2*(4-5), 181-192. https://doi.org/10.1007/s10142-002-0058-2

Ghavi-Helm, Y., Jankowski, A., Meiers, S., Viales, R. R., Korbel, J. O., & Furlong, E. E. M. (2019). Highly rearranged chromosomes reveal uncoupling between genome topology and gene expression. *Nature Genetics*, *51*(8), 1272-1282. https://doi.org/10.1038/s41588-019-0462-3

Guettouche, T., Boellmann, F., Lane, W. S., & Voellmy, R. (2005). Analysis of phosphorylation of human heat shock factor 1 in cells experiencing a stress. *BMC Biochem*, *6*, 4. https://doi.org/10.1186/1471-2091-6-4

Guo, Y. E., Manteiga, J. C., Henninger, J. E., Sabari, B. R., Dall'Agnese, A., Hannett, N. M., Spille, J. H., Afeyan, L. K., Zamudio, A. V., Shrinivas, K., Abraham, B. J., Boija, A., Decker, T. M., Rimel, J. K., Fant, C. B., Lee, T. I., Cisse, II, Sharp, P. A., Taatjes, D. J., & Young, R. A. (2019). Pol II phosphorylation regulates a switch between transcriptional and splicing condensates. *Nature*, *572*(7770), 543-548. https://doi.org/10.1038/s41586-019-1464-0

Haruki, H., Nishikawa, J., & Laemmli, U. K. (2008). The anchor-away technique: rapid, conditional establishment of yeast mutant phenotypes. *Mol Cell*, *31*(6), 925-932. https://doi.org/10.1016/j.molcel.2008.07.020

Henninger, J. E., Oksuz, O., Shrinivas, K., Sagi, I., LeRoy, G., Zheng, M. M., Andrews, J. O., Zamudio, A. V., Lazaris, C., Hannett, N. M., Lee, T. I., Sharp, P. A., Cissé, II, Chakraborty, A. K., & Young, R. A. (2021). RNA-Mediated Feedback Control of Transcriptional Condensates. *Cell*, *184*(1), 207-225.e224. https://doi.org/10.1016/j.cell.2020.11.030

Hnisz, D., Shrinivas, K., Young, R. A., Chakraborty, A. K., & Sharp, P. A. (2017). A Phase Separation Model for Transcriptional Control. *Cell*, *169*(1), 13-23. https://doi.org/10.1016/j.cell.2017.02.007

Kim, S., & Gross, D. S. (2013). Mediator recruitment to heat shock genes requires dual Hsf1 activation domains and mediator tail subunits Med15 and Med16. *J Biol Chem*, *288*(17), 12197-12213. https://doi.org/10.1074/jbc.M112.449553

Kline, M. P., & Morimoto, R. I. (1997). Repression of the heat shock factor 1 transcriptional activation domain is modulated by constitutive phosphorylation. *Mol Cell Biol*, *17*(4), 2107-2115. https://doi.org/10.1128/mcb.17.4.2107

Krakowiak, J., Zheng, X., Patel, N., Feder, Z. A., Anandhakumar, J., Valerius, K., Gross, D. S., Khalil, A. S., & Pincus, D. (2018). Hsf1 and Hsp70 constitute a two-component feedback loop that regulates the yeast heat shock response. *Elife*, *7*. https://doi.org/10.7554/eLife.31668

Lee, R., Kang, M.-K., Kim, Y.-J., Yang, B., Shim, H., Kim, S., Kim, K., Yang, C. M., Min, B.-g., Jung, W.-J., Lee, E.-C., Joo, J.-S., Park, G., Cho, W.-K., & Kim, H.-P. (2021). CTCF-mediated chromatin looping provides a topological framework for the formation of phase-separated transcriptional condensates. *Nucleic Acids Research*, *50*(1), 207-226. https://doi.org/10.1093/nar/gkab1242

Mahat, D. B., Salamanca, H. H., Duarte, F. M., Danko, C. G., & Lis, J. T. (2016). Mammalian Heat Shock Response and Mechanisms Underlying Its Genome-wide Transcriptional Regulation. *Mol Cell*, *62*(1), 63-78. https://doi.org/10.1016/j.molcel.2016.02.025

Peffer, S., Gonçalves, D., & Morano, K. A. (2019). Regulation of the Hsf1-dependent transcriptome via conserved bipartite contacts with Hsp70 promotes survival in yeast. *J Biol Chem*, *294*(32), 12191-12202. https://doi.org/10.1074/jbc.RA119.008822

Rawat, P., Boehning, M., Hummel, B., Aprile-Garcia, F., Pandit, A. S., Eisenhardt, N., Khavaran, A., Niskanen, E., Vos, S. M., Palvimo, J. J., Pichler, A., Cramer, P., & Sawarkar, R. (2021). Stress-induced nuclear condensation of NELF drives transcriptional downregulation. *Mol Cell*, *81*(5), 1013-1026.e1011. https://doi.org/10.1016/j.molcel.2021.01.016

Sabari, B. R., Dall'Agnese, A., Boija, A., Klein, I. A., Coffey, E. L., Shrinivas, K., Abraham, B. J., Hannett, N. M., Zamudio, A. V., Manteiga, J. C., Li, C. H., Guo, Y. E., Day, D. S., Schuijers, J., Vasile, E., Malik, S., Hnisz, D., Lee, T. I., Cisse, II,…Young, R. A. (2018). Coactivator condensation at super-enhancers links phase separation and gene control. *Science*, *361*(6400). https://doi.org/10.1126/science.aar3958

Sabari, B. R., Dall'Agnese, A., & Young, R. A. (2020). Biomolecular Condensates in the Nucleus. *Trends Biochem Sci*, *45*(11), 961-977. https://doi.org/10.1016/j.tibs.2020.06.007

Sawarkar, R. (2022). Transcriptional lockdown during acute proteotoxic stress. *Trends Biochem Sci*, *47*(8), 660-672. https://doi.org/10.1016/j.tibs.2022.03.020

Wei, M. T., Chang, Y. C., Shimobayashi, S. F., Shin, Y., Strom, A. R., & Brangwynne, C. P. (2020). Nucleated transcriptional condensates amplify gene expression. *Nat Cell Biol*, *22*(10), 1187-1196. https://doi.org/10.1038/s41556-020-00578-6

Zhang, H., Shao, S., Zeng, Y., Wang, X., Qin, Y., Ren, Q., Xiang, S., Wang, Y., Xiao, J., & Sun, Y. (2022). Reversible phase separation of HSF1 is required for an acute transcriptional response during heat shock. *Nature Cell Biology*, *24*(3), 340-352. https://doi.org/10.1038/s41556-022-00846-7

Zheng, X., Beyzavi, A., Krakowiak, J., Patel, N., Khalil, A. S., & Pincus, D. (2018). Hsf1 Phosphorylation Generates Cell-to-Cell Variation in Hsp90 Levels and Promotes Phenotypic Plasticity. *Cell Reports*, *22*(12), 3099-3106. https://doi.org/10.1016/j.celrep.2018.02.083

Zheng, X., Krakowiak, J., Patel, N., Beyzavi, A., Ezike, J., Khalil, A. S., & Pincus, D. (2016). Dynamic control of Hsf1 during heat shock by a chaperone switch and phosphorylation. *Elife*, *5*. https://doi.org/10.7554/eLife.18638

3.6 Methods

Resource availability

Lead contact for reagent and resource sharing

Further information and requests for resources and reagents should be directed to and will be fulfilled by the Lead Contact, Dr. David Pincus (pincus@uchicago.edu).

Materials availability

S. cerevisiae strains and plasmids generated in this study are available from the lead contact upon request.

Experimental models and subject details

All *S. cerevisiae* strains were grown in YPD (yeast extract-peptone-dextrose) or SDC (synthetic dextrose complete) media at 30°C as indicated below.

3.6.1 Yeast Strains

For tagging Hsf1, Med15 and Rpb3 with mCherry, PCR amplicons with mCherry coding sequence and homology to 3'-ends of either *HSF1*, *MED15* and *RPB3* were amplified from plasmid pFA6a-mCherry-hphMX6. The amplicons were transformed into the respective strains for in-frame insertion of mCherry. Primers used in strain construction are listed in Table S6.

For Myc x 9 tagging of Med15, genomic DNA of a previously myc9-tagged *MED15* strain (ASK201) (Anandhakumar et al., 2016) was used as template to amplify MYCx 9::TRP1 cassette flanked by DNA homologous to 3'-end of *MED15*. This amplicon was transformed in strains DSG144 and LRY003 to obtain strains ASK213 and ASK214, respectively. LRY003 is a derivative of previously described strain ASK804 (Chowdhary et al., 2019) in which TRP1 was deleted by replacing with KAN-MX.

For Myc x 13 tagging of Med15, plasmid pFA6a-13Myc-His3MX was used as template to obtain MYC13-HIS3 amplicon with homology to 3'-end of *MED15*. This amplicon was transformed in strains DPY144, DPY417 and DPY418 to obtain strains ASK215, ASK216 and ASK217, respectively.

For MS2-MCP labelling of *HSP12* mRNA, MCP-mCherry-URA3 cassette was amplified from plasmid pSH100 with primers Fw MCP-mCherry-Ura3 and Rv MCP-mCherry-Ura3. This cassette was inserted at the endogenous *URA3* locus in strain DPY032 to obtain strain SCY008. Next, 24xMS2-loxP-KANMX6-loxP cassette was amplified from plasmid pDZ415 using primers Fw HSP12-MS2-loxp-KanMX6-loxp and Rv HSP12-MS2-loxp-KanMX6-loxp. This cassette was inserted in the 3'-UTR region of *HSP12* (immediately after stop codon) of strain SCY008 to obtain strain SCY009. Finally, plasmid pSH69 was transformed to express Cre recombinase in strain SCY010 that led to the removal of KANMX in strain SCY011.

The diploid strain ASK741 was created by crossing a MATα derivative of strain DSG200 (Chowdhary et al., 2019) with MATa DSG200.

Plasmids pNH604-HSF1pr-HSF1-GFP and pNH604-HSF1pr-HSF1(147-833)-GFP were used as templates for quick change PCR (Primers, Fw subCE2-AAA and Rv subCE2-AAA) to create CE2->AAA mutation in WT and ΔNTA HSF1, respectively. These plasmids were linearized with Pme I (New England Biolabs) and transformed in strain DPY034 for integration at the *TRP1* locus to obtain strains *DPY1805* and DPY1818. Loss of parental HSF1 plasmid was confirmed by growth on 5-FOA media.

A complete list of strains is provided in Table S1. PCR primer sequences are provided in Table S6.

3.6.2 Culture Conditions

For microscopy, cells were grown at 30°C in SDC (synthetic dextrose complete) media to early-log density (A_{600} = 0.4-0.5).

For 3C, ChIP and RT-qPCR analyses, cells were grown at 30°C in YPD (yeast extract-peptone-dextrose) to a mid-log density (A_{600} = 0.65-0.8). A portion of the culture was maintained at 30°C as non-heat-shocked (NHS) sample while the remainder (heat-shocked (HS) sample) was subjected to an instantaneous 30°C to 39°C thermal upshift for the indicated duration.

For spot dilution analysis**,** cells were grown to stationary phase in YPD media. Master suspensions were prepared by diluting the saturated cultures to a uniform cell density (A_{600}=0.3) and were transferred to a 96-well microtiter plate. These were then serially diluted (five-fold). 4 µl of each dilution were transferred onto solid YPDA plates. Cells were grown at either 30° or 37°C for 30 h.

3.6.3 Chromosome Conformation Capture

TaqI-3C was conducted essentially as previously described (Chowdhary et al., 2017, 2020; Chowdhary et al., 2019). Briefly, cells were cultured to a mid-log density (A_{600} = 0.8) at 30°C. They were either maintained at 30°C or heat-shocked at 39°C for 10 min (or as indicated), and then crosslinked with formaldehyde (1% final concentration). For 3C assay involving hexanediol treatment, cells were heat-shocked at 39°C for 2.5 min followed by treatment with either 2,5- or 1,6-hexanediol (5% final concentration), and then crosslinked with formaldehyde. Crosslinked cells were harvested and lysed in FA lysis buffer (50 mM HEPES pH 7.9, 140 mM NaCl, 1% Triton X-100, 0.1% Sodium deoxycholate, 1 mM EDTA, 1 mM PMSF) for two cycles (20 min each) of vortexing at 4°C. A 10% fraction of the chromatin lysate was digested

using 200 U of Taq I (New England Biolabs) at 60°C for 7 h. Taq I was heat-inactivated at 80°C for 20 min. The digested chromatin fragments were centrifuged, and the pellet was resuspended in 100 µl of 10 mM Tris-HCl (pH 7.5). The Taq I-digested chromatin was diluted 7-fold to which 10,000 cohesive end units of Quick T4 DNA ligase (New England Biolabs) were added. Proximity ligation was performed at 25°C for 2h. The ligated sample was digested with RNase at 37°C for 20 min and then Proteinase K at 65°C for 12 h. The 3C DNA template was extracted using phenol-chloroform and then precipitated.

The interaction frequencies were quantified using qPCR. Quantitative PCR was performed on a CFX Real-Time PCR system (Bio-Rad) using Power SYBR Green PCR master mix (Fisher Scientific). Sequences of 3C primers used in this study are provided in Table S2. Normalization controls were used to account for the following: (i) variation in primer pair efficiencies; (ii) primer dimer background; (iii) variation in the recovery of 3C templates; and (iv) to ensure a ligation-dependent 3C signal. For detailed algorithms to calculate normalized 3C interaction frequencies, see below and (Chowdhary et al., 2020).

3.6.4 Chromatin Immunoprecipitation (ChIP)

ChIP was conducted essentially as previously described (Chowdhary et al., 2019). Briefly, the cells were heat-shocked at 39°C for 7.5 min (or maintained at 30°C) and crosslinked with 1% formaldehyde. Cells were then harvested and subjected to glass bead lysis in lysis buffer (50 mM HEPES pH 7.5, 140 mM NaCl, 1% Triton X-100, 0.1% Sodium deoxycholate, 1 mM EDTA, 2 mM PMSF, and 250 µg/ml cOmplete™, EDTA-free Protease Inhibitor Cocktail) for 30 min at 4°C. The chromatin lysate was sonicated to an average size of ~250 bp using 40 cycles of sonication (30 sec on/off High-Power setting; Diagenode Biorupter Plus). A 20% fraction of the sonicated chromatin was incubated with one of the following antibodies: 1 µl of anti-Rpb1; 1 µl of anti-Hsf1 (Chowdhary et al., 2019) or 2.5 µl of anti-Myc (Santa Cruz Biotechnology) for

16 h at 4°C. Antibody-chromatin complexes were immobilized on Protein A-Sepharose beads (GE Healthcare) for 16 h at 4°C, then washed sequentially with lysis buffer, high salt buffer (50 mM HEPES pH 7.5, 500 mM NaCl, 1% Triton X-100, 0.1% Sodium Deoxycholate, 1 mM EDTA), wash buffer (10 mM Tris pH 8.0, 250 mM LiCl, 0.5% NP-40, 0.5% Sodium Deoxycholate, 1 mM EDTA) and finally 1x TE (10 mM Tris-HCl pH 8.0, 0.5 mM EDTA). Chromatin was eluted by incubating the beads in elution buffer (50 mM Tris pH 8.0, 1% SDS, 10 mM EDTA) at 65°C for 30 min. RNA and proteins were removed by DNase-free RNase (final concentration of 200 µg/ml; incubation at 37°C for 1 h) and Proteinase K (final concentration of 50 µg/ml; incubation at 60°C for 16 h). The ChIP template was extracted using phenol-chloroform and precipitated in presence of ethanol.

ChIP occupancy signals were quantified using qPCR. Sequences of ChIP primers used in this study are provided in Table S4. The ChIP DNA quantities were deduced from interpolation of a standard curve generated using genomic DNA template. The qPCR signal for each primer combination was normalized to the corresponding signal from the input DNA. The input DNA control was incorporated to correct for variation in the recovery of ChIP DNA templates.

3.6.5 Reverse Transcription-qPCR (RT-qPCR)

Cells were cultured to a mid-log density (A_{600} = 0.8) at 30°C and were either maintained at 30°C or heat-shocked at 39°C for times indicated. 20 mM sodium azide was added at appropriate times to terminate transcription. Cells were then harvested and subjected to glass bead lysis in presence of TRIzol (Invitrogen) and chloroform for 10 min at 4°C. Total RNA was precipitated in ethanol. A fraction of total RNA (~20 µg) was treated with DNase I (RNase-free; New England Biolabs) at 37°C for 15 min. DNase I was heat-inactivated at 75°C for 10 min. RNA was purified using the RNA clean and concentrator kit (Zymo Research). 2-3 µg of

the purified RNA template and random hexamers were used for preparing cDNA (Superscript IV first-strand synthesis system; Invitrogen).

The cDNA reaction mix was diluted 2-fold, and 2 µl of the diluted cDNA template was used for qPCR reaction. Sequences of primers used for RT-qPCR analysis in this study are provided in Table S5. Relative cDNA levels were quantified using the ΔΔCt method (Chowdhary et al., 2017). qPCR signal from *SCR1* Pol III transcript was used as a normalization control. This accounted for variation in the recovery of cDNA templates. Relative fold change per minute in mRNA expression was calculated by dividing mean mRNA levels (derived from two independent biological samples) for a given time point by previous time point, and then by the time elapsed in minutes.

3.6.6 Fluorescence microscopy

For live-cell imaging, cells were grown at 30°C to early log phase (A_{600} = 0.5) in synthetic dextrose complete (SDC) medium. An aliquot of living cells was immobilized onto concanavalin A-coated glass bottom dish. Fresh SDC medium was added in the dish before imaging. Images were taken on Leica TCS SP5 II STED-CW laser scanning confocal microscope (Leica Microsystems, Inc., Buffalo Grove, IL) equipped with GaAsP hybrid detector and STED mode turned off. Samples were subjected to heat shock at 39°C by heating the objective (HCX PL APOCS 63x/1.4 oil UV) with Bioptechs objective heater system and by controlling the temperature of air flowing through the incubator chamber enclosing the microscope. Argon laser was used at lines 488 and 514 nm for excitation of GFP and mVenus. The orange HeNe laser light source was used for excitation of mCherry at 594 nm. STED laser (592 nm) was turned off for all live imaging experiments, except during STED imaging in Figures 2A, B (see below for details). For experiments involving hexanediol treatment, cells were heat-shocked and imaged for ~8 min. Immediately after this, the SDC media in the dish

was replaced with pre-warmed (39°C) SDC supplemented with either 2,5- or 1,6-hexanediol (5% final concentration), and cells were imaged at 39°C for the times indicated.

The images were acquired in xyz scan mode, covering 8 to 10 planes on the z-axis with an interplanar distance of 0.25 µm. For dual-color imaging of live cells, fluorophores were sequentially scanned in two channels with scanning modes switched on between lines. The sequential capture allowed rapid scanning of fluorophores in both channels while minimizing bleed-through or channel crosstalk. Post-acquisition, images were deconvolved by YacuDecu function that utilizes Richardson-Lucy algorithm for calculating theoretical Point Spread Functions (PSFs) (https://github.com/bnorthan) (Rueden et al., 2017). The PSFs were computed each time based on the set of microscopy parameters used in the imaging analyses. Custom plugins for Fiji (Schindelin et al., 2012) were used to colorize, split or merge channels, make composites and adjust brightness of the images. 3D rendering and visualization were performed using either ClearVolume (Royer et al., 2015) or arivis Vision 4D software v. 3.1 (render mode: maximum intensity; arivis AG, Rostok, Germany). For images processed without deconvolution (Figure S2A-D), images were acquired as above and custom plugins for Fiji were used to colorize, split or merge channels, subtract background and apply gaussian blur.

For colocalization analyses, the fractional overlap metric scores (Manders' colocalization coefficients) were calculated using JACoP plugin implemented in ImageJ (Bolte and Cordelieres, 2006; Schneider et al., 2012). The average intensity plots were generated using the plot profile feature in ImageJ. Intensities of pixels were obtained along the line path (as indicated in Figure 1G) for each z-section. Intensities across nine individual z-sections were combined and the average was plotted for each channel.

For analysis of gene coalescence, nine z-planes with an interplanar distance of 0.5 µm, covering the entire depth of the nucleus, were inspected for location of tagged genomic loci. The relative

nuclear positions of the tagged loci were assessed by measuring 3D distances between them. 3D distances were measured as 3D polyline lengths between the signal centroids of tagged gene loci. A cell was scored positive for coalescence if the 3D distance between the centroids was between 0.3 and 0.7 µm. 3D distance measurements, 3D rendering, and visualization were performed in arivis Vision4D.

3.6.7 Stimulated emission depletion (STED) super-resolution microscopy in live cells

Samples for STED imaging were prepared as described for live imaging, except live cells were subjected to heat shock at 39°C by heating the objective (STED rated HCX PL APO 100x/1.4 oil) and incubator chamber enclosing the microscope. High-resolution STED images of cells expressing Hsf1-mVenus were acquired in xyz scan mode (z=9; interplanar distance=0.25 µm) on Leica TCS SP5 II STED-CW laser scanning confocal microscope with STED mode turned on. The 514 nm line from argon ion laser light source was used to excite mVenus. Emission depletion was accomplished with 592 nm continuous wave STED laser. Images were deconvolved as above, then rendered (render mode: volumetric) and visualized in arivis Vision4D. STED microscopy was used for acquiring images analyzed and presented in Figure 2A, B.

3.7 Quantification and statistical analysis

3.7.1 Hsf1, Med15 and Rpb1 ChIP-seq data analysis

Hsf1 ChIP-seq data were obtained from GSE117653 (Pincus et al., 2018). Med15 data are from PRJNA657372 (Sarkar et al., 2022). Rpb1 ChIP-seq data were obtained from GSE125226 (Albert et al., 2019). Reads were aligned to the *S. cerevisiae* reference genome (SacCer3) using Bowtie 2 (Langmead and Salzberg, 2012). SAM files were converted to BAM format using SAMtools (Li et al., 2009). BAM files were then converted to bigWig and

bedGraph format at bin size of 1 (-bs 1) and normalized to the library size (--normalizeUsing CPM) using bamCoverage function of deepTools2 (Ramirez et al., 2016). The bigWig files were used to obtain genome browser tracks in Integrative Genomics Viewer (IGV) browser (Robinson et al., 2011), and to make metagene plots. Metagene profiles were created using computeMatrix and plotProfile function tools in deepTools2. The plots are scaled +/-1 kb of ORFs of the Hsf1-dependent genes (Pincus et al., 2018). Occupancy of Hsf1, Med15 and Rpb1 (Pol II) were computed using the bedtools map function. The occupancy of Hsf1 and Med15 were obtained as sum of signals across 1 kb region upstream of ORFs of protein-coding genes. For occupancy of Pol II, sum of signals across ORFs were normalized to length of the ORFs.

For analysis of co-occupancy between Hsf1 and Med15, peaks were called using MACS2 algorithm (Zhang et al., 2008) with -g 1.2e7 --keep-dup auto flags. Peaks identified on repetitive regions of telomeres and rDNA were excluded from the analysis. The overlap of Med15 and Hsf1 peaks was computed using intersect Bed -wa -u -a Med15_peaks.bed -b Hsf1_peaks.bed option.

For analysis of Pol II distribution at Hsf1 genes, CPKM of Pol II reads were obtained for all non-overlapping, verified ORFs archived in SGD (Cherry et al., 2012) using the bedtools map function. These normalized counts were then used to calculate % Pol II reads at Hsf1 gene targets in comparison to all other genes in the yeast genome.

3.7.2 Nascent transcript sequencing data analysis

NAC-seq data were obtained from GSE117653 (Pincus et al., 2018). Reads were aligned to the *S. cerevisiae* reference genome (SacCer3) using TopHat2 (Kim et al., 2013) with --segment-length 20 -I 2500 options. Wiggle files were generated by normalizing to the library size (--normalizeUsing CPM) using the bamCoverage function of deepTools2 and visualized in IGV genome browser.

3.7.3 Foci counting and characterization

Hsf1, Med15 and Rpb3 foci were detected and quantified within 3D live-cell images using the automated FindFoci plugin (Herbert et al., 2014) in ImageJ. For foci detection in 3D, a region of interest was marked around the nucleus of each cell and then foci within the marked regions were identified across all z planes (z=9). We used the optimizer function in the plugin submenu to train FindFoci algorithm and predict optimum parameter settings for foci assignment. The following set of optimized parameters were applied to all images in this study: (a) background, one standard deviation above mean; (b) search method, above background with an optimal value of 0.3; and (c) merge option, relative above background with peak parameter of 0.2 and minimum size as 1. Finally, we used the x, y, z position coordinates and sizes of peak intensity regions to present foci as 3D bubble charts. The 3D bubble charts were created by calling bubblechart3 function in MATLAB (MATLAB, 2021. *version 9.11.0.1873467* (R2021b), Natick, MA: The MathWorks, Inc.).

For visualizing images as 3D surface plots, a square of 10 × 10 pixels was marked around the nucleus of each cell type in each condition (as indicated in Figure 1D). Representative planes of each cell were analyzed and displayed as 3D surface plots using the Interactive 3D Surface Plot plugin in ImageJ (contributing author: Kai Uwe Barthel, Germany). Appropriate parameter settings for scale, rotation, smoothing, and lightning were adapted for the display of 3D surface plots. Note that for each cell type, similar parameter settings were used in both non-heat shock and heat shock conditions.

3.7.4 Analysis of average relative localization of factors

Foci of LacO-tagged *HSP104* gene locus or MS2-tagged *HSP12* mRNA locus were manually identified in a specific *z* plane and centered within a square of 12 × 12 pixels. Distribution of signal from another channel, depicting nuclear distribution of the secondary factor, was

gathered from corresponding 12 × 12 squares in the same *z* plane. A composite text image was created by computing average of centered images from roughly 30 cells per condition. The intensity of each pixel was scaled from 0 to 100 using a formula for uniform scaling: [(intensity-minimum) / (maximum-minimum)] × 100. For negative control, fifteen 12 × 12 arrays were generated with random numbers from 0 to 100. A composite text image was then created by computing an average of the corresponding values. For positive control, kernel density of a 2D Gaussian distribution was generated in an array and computed using the following formula: $e^{\wedge}(-z^2/(2\sigma^2)) / \sigma (2p)^{-1/2}$. Here, z is in range (-k, k+1) and $\sigma = 1$. This array was then used to create a text image with a scale ranging between 0 and 100. Finally, text images of controls or test samples were used to generate contour plots using the Plotly function (Plotly Technologies Inc., 2015) in R (R Core Team, 2020). The intensity minima and maxima were split into 800 steps for all contour plots.

3.7.5 Quantification of overall and pixel-to-pixel variation within STED-acquired images

For demonstration of internal dynamics of Hsf1 foci, the variation between corresponding pixels of Hsf1 foci was compared against overall variation in the images. For this analysis, we used STED-acquired images of cells expressing Hsf1-mVenus captured at every minute over the intermixing phase of heat shock (8 to 12 min-HS). We marked 12 × 12 pixel squares bounding the nuclei of six individual cells imaged every minute between t1 (8min) and t5 (12min). Next, we obtained maximum intensity projections of the 3D images stacks for each individual nuclei at each of five heat shock time points. All pixel intensities were scaled from 0 to 100 to account for variation in image brightness by computing into the following formula: [(intensity-minimum) / (maximum-minimum)] × 100. Standard deviation was calculated for the min-max normalized pixels to determine pixel-to-pixel variation in Hsf1 levels at the given nuclear locations. Overall standard deviation was computed from average intensities of each

image in the time course. The overall standard deviation was then used to populate a 12 ×12-pixel square for comparison to pixel-to-pixel variation of Hsf1 intensity and presented as heat maps. Six such distributions, each of overall variation and pixel-to-pixel variation, were used to plot cumulative frequency of pixels as a function of standard deviation.

3.7.6 Quantification of 3C

TaqI-3C data was quantified as described in (Chowdhary et al., 2020; Chowdhary et al., 2019). The percent digestion efficiency was determined by amplifying a region across Taq I restriction site using a pair of convergent primers (sequences provided in Table S3). The percent digestion efficiencies were determined for each primer combination and incorporated into the following formula:

$$\% \text{ digestion} = 100 - \frac{100}{2^{[(Ct_R - Ct_{ARS504})^{\mathbf{DO}} - (Ct_R - Ct_{ARS504})^{\mathbf{UND}}]}}$$

Here, Ct_R is the cycle threshold (Ct) quantification of the digested only (DO) or undigested (UND) templates, and Ct_{ARS504} the cycle threshold quantification of the *ARS504* locus (a region lacking a Taq I site).

For measurement of normalized frequency of intragenic or intergenic interactions, the Ct values for digested only (DO_{3C}) and ligated (Lig_{3C}) templates for crosslinked chromatin, and digested only and ligated genomic DNA (Lig_{gDNA} and DO_{gDNA}, respectively) were incorporated into the following formula:

Normalized Frequency of Interaction =

$$\frac{[(2^{-\Delta Ct_{Lig_{3C}}/ARS504_{Lig_{3C}}})/(2^{-\Delta Ct_{DO_{3C}}/ARS504_{DO_{3C}}})]\Big/_{[(Digestion\ site\ 1)\times(Digestion\ site\ 2)]}}{[(2^{-\Delta Ct_{Lig_{gDNA}}}\Big/_{ARS504_{Lig_{gDNA}}})\Big/(2^{-\Delta Ct_{DO_{gDNA}}}\Big/_{ARS504_{DO_{gDNA}}})]\Big/_{[(Digestion\ site\ 1)\times(Digestion\ site\ 2)]}}$$

(i): ΔCt values were obtained by subtracting Ct (no-template) from those of Lig_{3C}, DO_{3C}, or gDNA templates.

(ii): $2^{-\Delta Ct}/ARS504$ are the fold-over signals normalized to *ARS504* locus.

(iii): Ligation-dependent signals (LDS) are determined as ratio of fold-over normalized signals of Lig_{3C} and DO_{3C} templates $(2^{-\Delta Ct_{Lig_{3C}}}/ARS504_{Lig_{3C}})/(2^{-\Delta Ct_{DO_{3C}}}/ARS504_{DO_{3C}})$; also applicable to the gDNA control.

(iv): LDS were corrected for variation in Taq I digestion efficiencies of sites 1 and 2 (as detailed above).

(v): Normalized Frequency of Interaction is defined as the ratio of ligation-dependent signals of 3C and gDNA control templates after correcting for differences in their digestion efficiencies.

3.7.7 Statistical tests used

Student's *t* test (two-tailed) was used to calculate statistical significance between all pairwise comparisons (as assumptions of parametric distributions were fulfilled), except in Figure 2B and D, two sample Kolmogorov–Smirnov test and one-way ANOVA followed by Tukey's post hoc analysis were used, respectively.

Each pairwise comparison is done with means of two independent biological samples (N=2) +SD. n.s., $P>0.05$; *, $P<0.05$; **, $P<0.01$; ***, $P<0.001$.

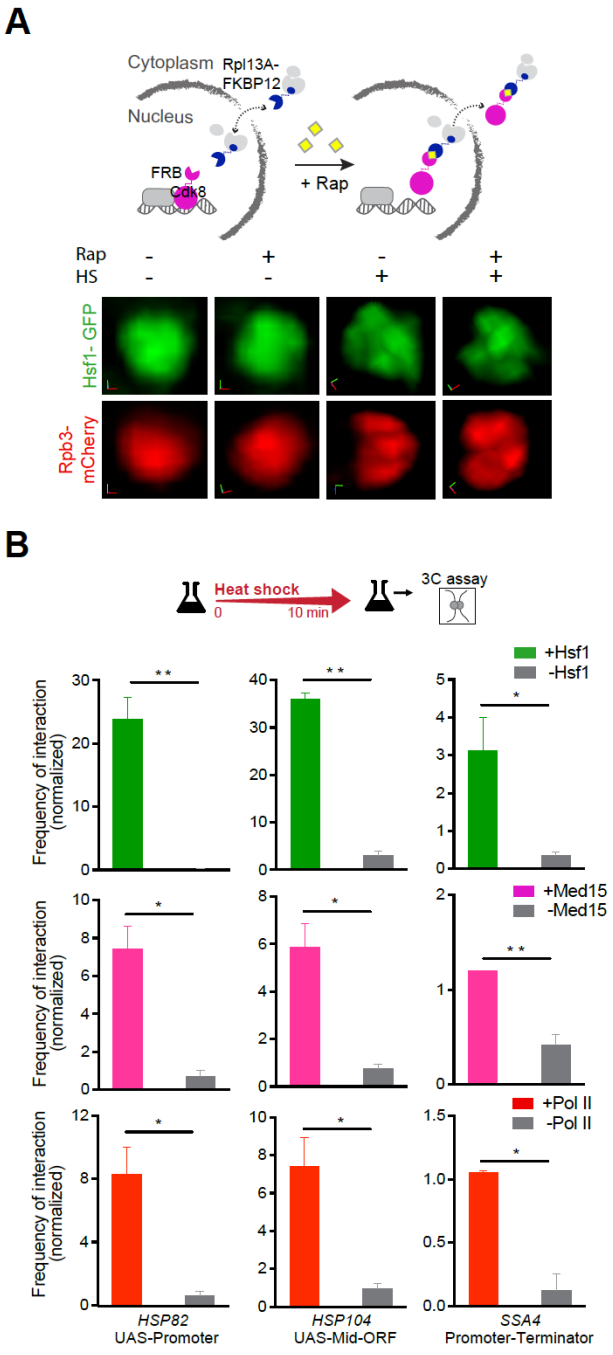

Figure 3.7.1 (A) Anchor-away assay for Ssn3/Cdk8; Hsf1 (green), Rpb3 (red) **(B)** Quantification of frequency of intragenic contacts detected within three HSR genes with and with either Hsf1, Med15, or Rpb3 depleted from the nucleus after 10 min of HS.

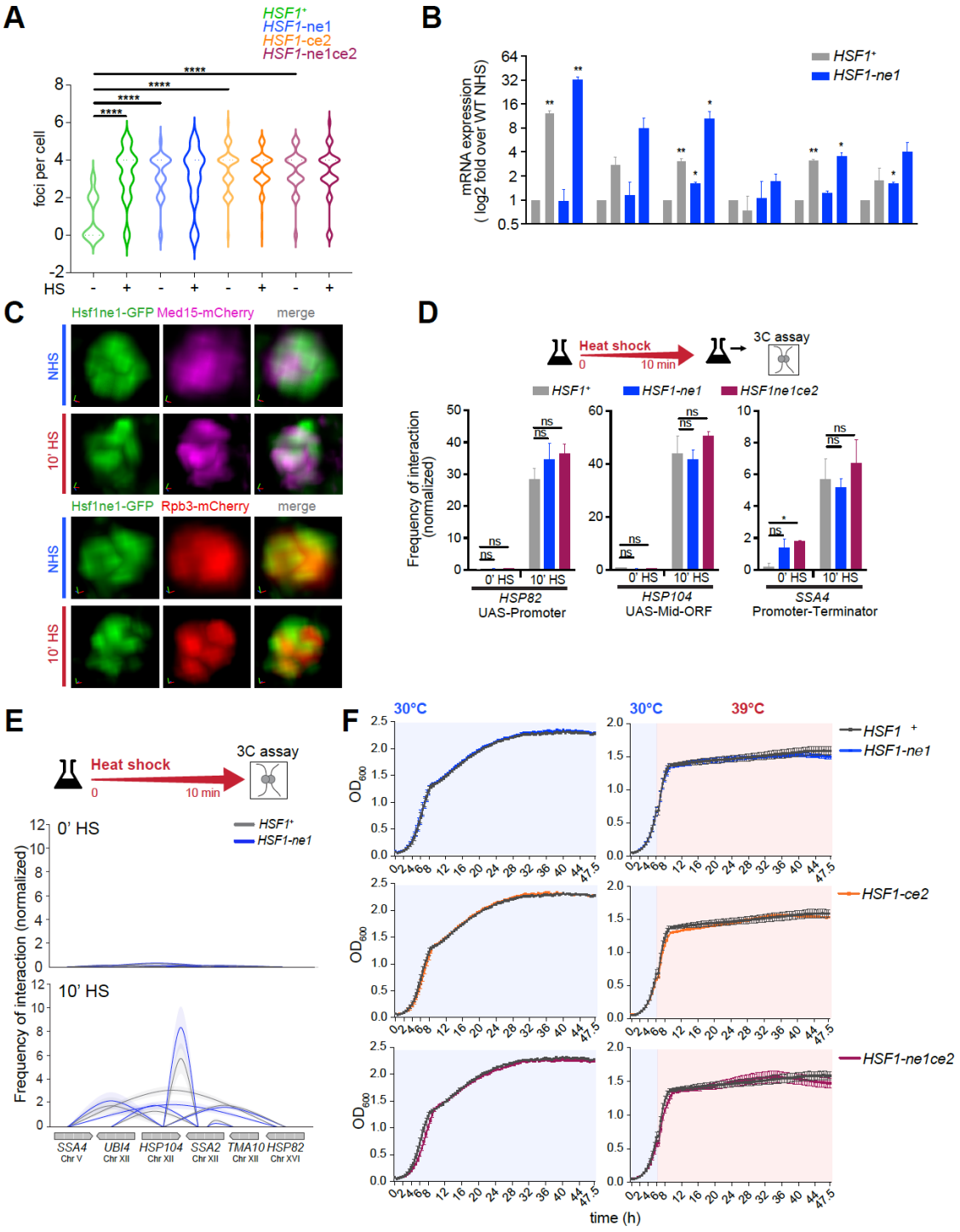

Figure 3.7.2 (**A**) Distribution of quantification of foci per cell in Hsp70-binding mutant strains (**B**) mRNA expression of 5 HSR genes in Hsf1-ne1 cells at NHS (grey) and HS (blue) (**C**) Characterization of Hsf1, Med15, and Rpb3 condensation in Hsf1-ne1 cells at NHS and HS (**D**) Quantification of frequency of intragenic contacts detected within three HSR genes in Hsf1, Hsf1-ne1, and Hsf1-ne1ce2 (**E**) Intergenic interactions between five HSR genes in Hs1-ne1 (blue) cells before and after HS (**F**) Growth curves for all three Hsp70 binding mutants at 30C and 39C.

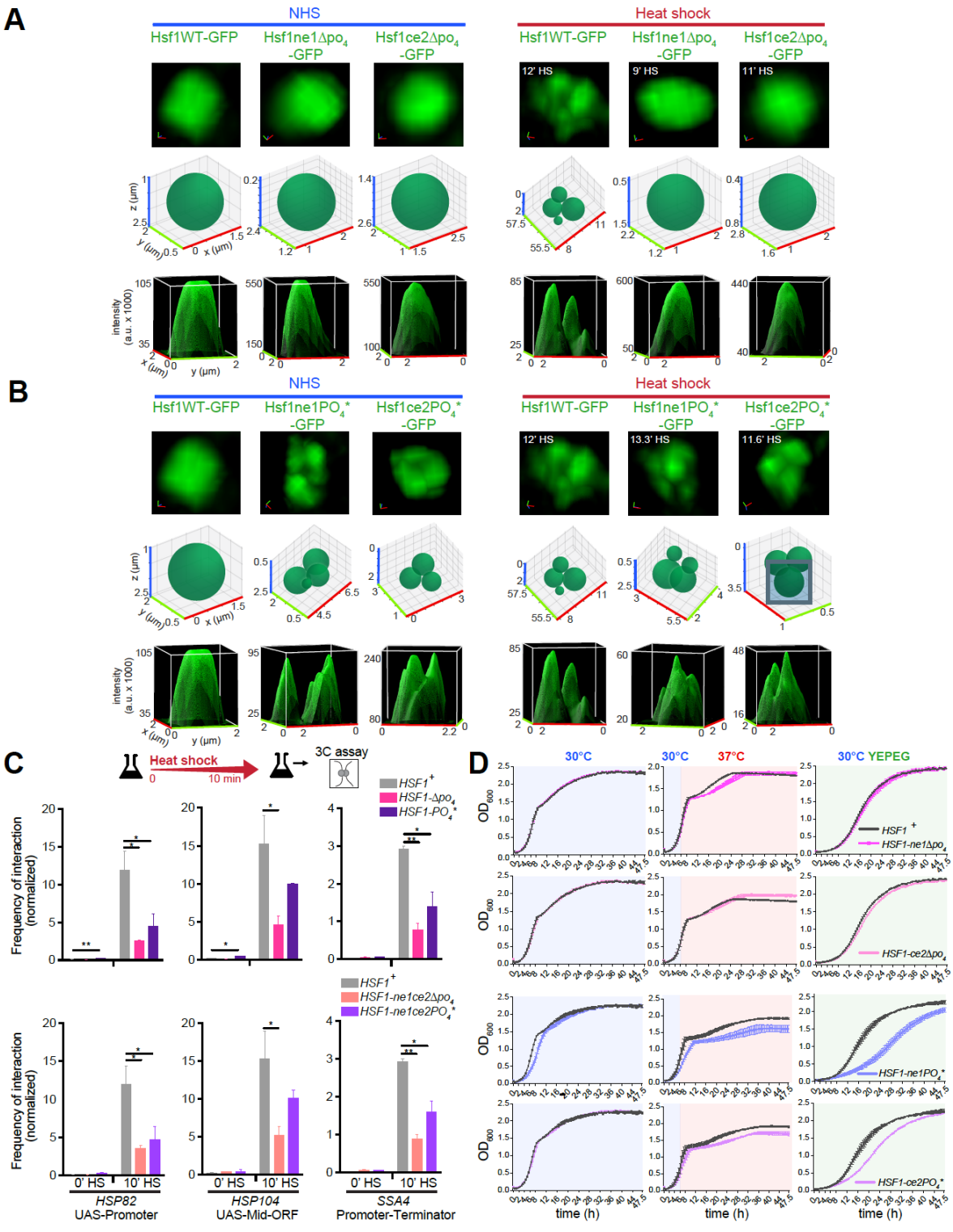

Figure 3.7.3 (A and B) Characterization of Hsf1-ne1Δpo4 (top) and Hsf1-ne1PO4* (bottom) condensation before and after a 10 min HS. **(C)** Intragenic contact frequencies detected within *HSP82*, *HSP104* and *SSA4* in cells heat-shocked for 10 min **(D)** Growth curves for Hsf1-ne1Δpo4, Hsf1-ce2Δpo4, Hsf1-ne1PO4*, and Hsf1-ce2PO4* at 30C, 37C, and reduced glucose.

CHAPTER 4

DISCUSSION AND FUTURE DIRECTIONS

4.1 Discussion

In this study, I demonstrate that Hsf1 can rapidly and inducibly form transcriptional condensates in response to thermal stress. These condensates are dynamic and transient, aligning with the timing of the heat shock response (HSR) and dissolving as Hsf1 deactivates and the cell returns to a steady state. Both Mediator and RNA Pol II are recruited to HSR condensates, with gene coalescence of Hsf1 target genes strongly correlating with the presence of these condensates. The N-terminal activation (NTA) domain of Hsf1 is essential for condensate formation, highlighting the role of Hsf1's intrinsically disordered regions (IDRs) in driving condensate assembly. This study presents a novel mode of transcriptional regulation in yeast, suggesting that transcriptional condensates, previously only described in mammalian cells, are evolutionarily conserved structures fundamental to eukaryotic gene control.

4.1.1 Induced HSR condensates form in a sequential manner

We show that these condensates form in a stepwise manner, with the cooperative interaction of Hsf1 molecules being the first step, followed by the condensation of Mediator. RNA Pol II cannot condense unless Hsf1 and Mediator are present, and we believe that this eventually leads to gene coalescence, as an emergent function of the transcriptional condensate. This is in contrast to the prevailing model in the field that implies the IDRs of TFs and other regulatory factors interact cooperatively and with no sequential preference to form transcriptional condensates. Previous theories also do not really mention how changes in chromatin conformation can influence the assembly of these structures, or if gene interactions occur due

to the presence of the condensate (Sabari et al., 2018; Sharp et al., 2022; Shrinivas et al., 2019). Multivalent binding of Hsp70 to the Hsf1 molecule and phosphorylation determine the ability of Hsf1 to concentrate and then recruit Mediator to condensates, while what governs the coordination of RNA Pol II recruitment and 3D genome interaction is yet to determined.

In many of the images included in this document, we show condensates of Hsf1, Mediator, and Pol II that look like separate entities rather than intermixing in a large singular blob, as is described in most texts about transcriptional condensates. This implies that these regulatory molecules may condense separately. While this may be true, these foci are incredibly dynamic, moving around the nucleus quickly, and thus they will eventually interact with one another. To reiterate this, we showed that colocalization of Med and Hsf1, and Pol II and Hsf1 in complete WT HSR condensates occurs >70% of the time. All of this is to suggest that perhaps we have been thinking of transcriptional condensates incorrectly and instead one big group of intermixing molecules, we have discrete condensates of each that interact frequently to induce faster genetic expression of specific gene groups. Concentration of not only transcriptional machinery but the genes that must be transcribed still occurs, leading to more efficient, rapid and robust expression.

4.1.2 Stress-specific events are required for Pol II recruitment and 3D genome reorganization

Because we could not reproduce a complete condensate in NHS conditions by mutating Hsf1 alone, it is possible there is another layer of modulation involved. The Hsf1 mutants that we used were the only copies present, and therefore the cells had adapted and stabilized to this form of hyperactive Hsf1. It is likely that there is something exclusive to acute HS that releases Pol II and allows it to stably interact with Hsf1 and Mediator at these sites. A large fraction of the genome is repressed during HS (Sawarkar, 2022), and this repression is Hsf1-independent (Duarte et al., 2016; Gasch & Werner-Washburne, 2002; Mahat et al., 2016). In these Hsf1-

mutant cells, perhaps transcriptional activation, and in turn Pol II usage, is no longer attenuated, setting up competition between TFs of constitutively expressed genes and Hsf1 for Pol II recruitment. Indeed, when the mutant strains undergo acute HS, they are able to recruit Pol II, further supporting the argument that Pol II needs to be released by transcriptional machinery at other sites to be able to stably interact with Hsf1 at its target genes.

4.1.3 An emergent property of fully assembled HSR condensates is 3D genome reorganization

Since we theorize that the function of a fully formed condensate is what drives gene coalescence at sites of Hsf1-induced transcription, Pol II must be recruited for the chromosome conformation to be altered. Therefore, in the Hsf1 mutants employed in this investigation, Pol II was not recruited when cells were at NHS conditions and thus intergenic interactions did not occur. However, HS did induce chromatin remodeling in all strains observed, though these intergenic interactions were reduced in the phosphorylation mutants and the ΔNTA mutants. This may be due to a number of factors that could affect the protein structure of the Hsf1 molecule. With the ΔNTA mutants, the loss of one of the IDRs of Hsf1 is most likely the reasoning behind loss of condensation, as interactions between the IDRs of proteins are what drives the assembly of these transcriptional structures. Thus, a lack of the NTA leads to a reduction in intergenic interactions as well, since the recruitment of the regulatory machinery is generally impaired. Additionally, the phosphorylation mutants possess a vastly different charge compared to WT Hsf1, with Hsf1-PO_4* being incredibly negatively charged, while the Hsf1-Δpo_4 may not possess the charge necessary to implement condensation. This change in protein charge conceivably influences the interactions of the mutant Hsf1 with not only Mediator and RNA Pol II but also the DNA itself.

Beyond transcriptional attenuation and gene coalescence, the components of the variant Hsf1 condensates that we observed must also be considered. The composition and induced activity

of the Hsf1 condensates in these mutant strains may differ from those formed during a wildtype HSR. Although these Hsf1 mutants were functional, promoting the transcription of the HSR regulon and supporting robust growth at basal temperatures, these differences must impact the interactions between Hsf1 and other proteins and nucleic acids. The Hsf1 phosphorylation variants are especially of concern, as their charge distributions are completely different compared to wildtype Hsf1. As described in the previous sections, the negative patch that forms on the surface of Hsf1-PO4* precludes interaction with Pol II, so it likely also prevents interactions with other wildtype HSR condensate components. Thus, we must further characterize not only these mutant Hsf1 condensates, but the wildtype condensates as well.

4.1.4 Hsp70 binding and phosphorylation of Hsf1 independently modulate Hsf1 to tune the HSR

This is not to say that these mutants are not biologically relevant. We were able to discern an unexpected mechanism of Hsf1 regulation by Hsp70 and phosphorylation in yeast, exhibiting their involvement in condensate assembly, and therefore HSR activity. Additionally, through the use of computational tools, like AlphaFold, we can biochemically infer how Hsp70 is impairing Hsf1 function. Hsp70 seems to passively suppress Hsf1, as binding creates a steric occlusion on the Hsf1 trimer that prevents interaction with Mediator, but not HSEs. Mutating the NE1 and CE2 sites rids Hsf1 of this structural impairment and therefore Mediator is free to associate with it for a longer timescale. Interestingly, the mutation of both sites must occur for Med to be recruited, suggesting that only a complete loss of bound Hsp70 at these specific loci on Hsf1 can create the space for Mediator engagement and condensation. This is evidence for the tunability of Hsf1 activity, as two bound Hsp70s results in basal levels of Hsf1-induced transcription, but the loss of one or both Hsp70s results in different levels of activation. Hence, Hsf1 itself can interact and condense with the loss of one Hsp70, but the loss of two Hsp70s results in Mediator recruitment and comparatively higher levels of HSR gene expression.

To add to this observation, we noted an increase in transcriptional activity at every step of condensate assembly and discerned that Hsf1 can form transcriptionally active condensates without a consistent association with Med and Pol II. Since transcription cannot occur without these molecular complexes, the Hsf1 mutants we used must only transiently employ them rather than form stable interactions that result in recruitment to the condensate. To continue the theory previously mentioned of interacting condensates, perhaps the concentration of each molecule leads to more efficient transcription at each step, and when all the necessary steps have occurred, as in HS conditions, the transcription is highest. This is a tidy way to consolidate the results we see, but it definitely requires further investigation, especially to determine what governs the last steps of HSR condensate assembly.

4.1.5 HSR transcriptional condensates in mammals

Though the HSR is largely conserved among eukaryotes, the presence of transcriptionally active HSR condensates similar to those in yeast is yet to be determined in mammalian cells. HSF1 has been shown to form foci in human tumor cells, however, their dissolution is what triggered the transcription of Hsps rather than their formation (Gaglia et al., 2020). Conversely, a recent study reported that in addition to the previously mentioned HSF1 stress granules, small nuclear condensates of Hsf1 and the transcription apparatus, including Mediator and BRD4, assemble at target gene loci and drive their transcription in HeLa cells (Zhang et al., 2022). Furthermore, the formation of these condensates is inhibited by Hsp70 with additional fine-tuning of HSF1 activity by phosphorylation, similar to what we have observed in yeast (Zhang et al., 2022). However, directing gene coalescence, which we have determined as an emergent property of yeast HSR condensates, has yet to be examined in mammalian cells. The presence of topologically associated domains (TADs) in mammalian cells has been uncoupled from gene expression (Ghavi-Helm et al., 2019), so these regions may not be the genomic restructuring we are interested in for HSR condensates. That being said, the mammalian HSF1 is regulated

in a different manner to its yeast counterpart, and this may also influence the dynamics of condensate assembly.

4.2 Future directions

As stated above, investigating the specific events of HS could aid us in discerning what exactly is required for RNA Pol II recruitment and condensation. Additionally, we could investigate the differential interactions of the Hsf1-mutants we have designed during NHS and HS to determine if there are any specific associations that will lead us to a greater understanding of this stress response. Here, I outline some experiments that can further elucidate HSR condensate assembly.

4.2.1 Transcriptional attenuation during heat shock

Transcriptional attenuation is a major characteristic of HS and ribosome biogenesis is one of the main processes that is shut down during stress. Ribosome biogenesis is an intensive cellular program which employs an incredible number of cellular resources, including RNA polymerase II (Warner, 1999). During thermal stress, ribosomal protein synthesis is halted, freeing up RNA Pol II molecules to preferentially express HSR genes (Ali et al., 2023; Chowdhary et al., 2022; Kainth et al., 2021). And so, to recruit RNA Pol II to the NHS foci we need to inhibit this "competition" between transcription factors of ribosomal biogenesis genes and Hsf1 to engage Pol II to their targets. Previous studies have shown that disrupting ribosome biogenesis can induce the HSR (Tye et al., 2019), further lending evidence to the idea that this will allow us to free up RNA Pol II for recruitment to Hsf1 condensates.

In the mutant yeast strains we have been investigating so far, there is no acute stress and steady state has been reached. The cells have acclimatized to higher Hsf1 activity and no longer need to prioritize Hsf1 targets. Inhibiting the expression of ribosome biogenesis (RiBi) genes, and

ribosomal protein genes (RPGs) in these strains, could allow the release of RNA Pol II. Our mutant Hsf1 will then be able to enlist Pol II to the NHS foci, completing the formation of the Hsf1 transcriptional condensate under NHS conditions. This can be done by building a strain that has an analog sensitive Tpk1/2/3, a major component in both the PKA and TORC1 pathways, both of which are involved in the regulation of ribosome biogenesis in yeast (Kunkel et al., 2019). Once these cells have been dosed, ribosome production will be halted and the dynamics of Hsf1, Mediator and RNA Pol II can be observed. This should be done in the Hsp70-binding mutant strains, as well as the Hsf1 phosphorylation strains. RNA Pol II should then likely be able to condense, specifically in the nuclei of the mutants which already allow Mediator condensation.

In the case that there are too many pleiotropic effects by inhibiting Tpk1/2/3, the downstream effectors in the PKA and TORC1 pathways can also be manipulated, particularly Dot6 and Tod6, both of which are negative regulators of ribosome biogenesis. Dot6 and Tod6 are phosphorylated by Tpk1/2/3 and Sch9, which in turn impedes their activity, allowing ribosome production to occur (Kunkel et al., 2019). Inducible mutant copies of these proteins can be created that are not able to be phosphorylated and will thus, inhibit ribosome biogenesis at a more specific level. If we see Pol II condensation in these mutants at NHS conditions, intergenic interactions can be determined, and since we believe Pol II recruitment is what drives this process, we should likely see gene coalescence in these mutants.

4.2.2 Intracellular pH changes during the HSR

A decrease in cytosolic pH accompanies the transcriptional changes of stress response (Kroschwald et al., 2015; Munder et al., 2016; Weitzel et al., 1987). This stress-driven acidification is conserved across eukaryotic species (Triandafillou et al., 2020), and stress-induced condensation has been shown to be dependent on this pH change (Kroschwald et al.,

2015; Petrovska et al., 2014; Riback et al., 2017). The change in pH in our mutant strains was not examined and so this may very well be a factor that is involved in Pol II recruitment to HSR condensates. To measure cellular pH, the method implemented by Triandafillou et al. could be used, in which yeast are engineered to express pHluorin, a pH biosensor (Miesenböck et al., 1998) that can then be calibrated to measure cytosolic pH in our mutants, as well as during stress. The acidification that is observed in WT yeast cells at HS is transient and the cell is brought back to resting pH (~7.5) quickly once it has reached steady state. Therefore, it is unlikely that these Hsf1-mutant strains exhibit a consistent acidic cytosol as this could disrupt a number of cellular processes and impair cell growth. And so, perhaps manipulating intracellular pH in the Hsf1 mutant cells could provide us with more insight into HSR condensate formation. To do this, nigericin, an ionophore that temporarily destroys the electrochemical gradient by allowing ions to penetrate the cellular membrane (Valkonen et al., 2013), could be used to induce different pHs in mutant cells at NHS conditions and condensate assembly could be observed. Again, if Pol II condensation and gene coalescence is observed after acidification then reconstitution of HSR condensates at NHS conditions will have been successful.

4.2.3 Determining other factors involved in HSR condensate assembly and composition

To determine other proteins or nucleic acids that are present in these HSR condensates, a pull-down assay followed by mass spectrometry could prove to be useful. Because many interactions of Hsf1 may be transient, it can be difficult to determine them by biochemical methods. To bypass this issue, proximity labelling mass spectrometry can be used. In this method, Hsf1 will be fused with a peroxidase (ascorbic acid peroxidase; APEX). When treated with hydrogen peroxide, APEX can convert biotin-phenol provided to the cells to biotin-phenol radicals that result in proteins that are present within a radius of 20nm to be covalently labelled. These labelled proteins can then be purified using Streptavidin-labelled beads, essentially capturing a

snapshot of protein interactions with the APEX-labelled Hsf1. Samples can be taken at different time points during HS and compared to the interactions of NHS Hsf1. Similarly, all the Hsf1 mutant interactions can also be characterized and compared to WT HS to determine if there are any differences that could help to decipher the assembly of the HSR condensates.

Along the same lines, a genetic approach could also be used. By using a CRISPRi library in conjunction with the triple mutant, Hsf1-mNE1mCE2PO$_4$*, any gain-of-function mutations that result in Pol II recruitment can be isolated. This could lead to the elucidation of any factors that influence HSR condensate formation, and their functions with the HSR and beyond can then be further examined.

4.2.4 Elucidating the Hsf1 phosphorylation sites necessary for HSR regulation

Lastly, determining which phosphorylation sites are the most important for HSR induction could also lend some insight in how phosphorylation plays a role in Hsf1 function. Like human cells, there could be specific Ser or Thr residues that are involved in the activation and inhibition of Hsf1. A good starting point could be determining what part of the Hsf1 protein the essential PO4 site could be. To do this, Hsf1 mutants in which only the Ser/Thr residues of a specific portion of Hsf1, like the NTA, can be mutated to alanine or aspartate and Hsf1 activity, as well as condensate formation can then be investigated. Using prediction software like AlphaFold could also help to narrow down which phosphorylation sites are likely to play a role in inducing interactions with other Hsf1 molecules and Mediator. Like the Hsf1-Hsp70-Mediator complex mentioned previously, illustrating any structural changes that may be prompted by the phosphorylation of Hsf1 residues could provide insight into how this PTM modulates Hsf1 activity in yeast.

In this thesis, we elucidate the founding inducible transcriptional condensate in yeast cells and determine how its assembly is regulated. We uncover that the formation of the HSR condensate

occurs in a stepwise manner, and we uncouple transcriptional activity and the presence of Mediator and Pol II at these structures. Lastly, we establish that not only is Hsf1 induced activity adjustable, suggesting that it can be modified according to the stimulus, the recruitment of transcriptional apparatus can also be modulated based on the strength of the stress. This reiterates the argument that HSR condensates are adaptive and provide a means of protection against environmental triggers.

Ali, A., Garde, R., Schaffer, O. C., Bard, J. A. M., Husain, K., Kik, S. K., Davis, K. A., Luengo-Woods, S., Igarashi, M. G., Drummond, D. A., Squires, A. H., & Pincus, D. (2023). Adaptive preservation of orphan ribosomal proteins in chaperone-dispersed condensates. *Nat Cell Biol*, *25*(11), 1691-1703. https://doi.org/10.1038/s41556-023-01253-2

Chowdhary, S., Kainth, A. S., Paracha, S., Gross, D. S., & Pincus, D. (2022). Inducible transcriptional condensates drive 3D genome reorganization in the heat shock response. *Mol Cell*, *82*(22), 4386-4399.e4387. https://doi.org/10.1016/j.molcel.2022.10.013

Duarte, F. M., Fuda, N. J., Mahat, D. B., Core, L. J., Guertin, M. J., & Lis, J. T. (2016). Transcription factors GAF and HSF act at distinct regulatory steps to modulate stress-induced gene activation. *Genes Dev*, *30*(15), 1731-1746. https://doi.org/10.1101/gad.284430.116

Gaglia, G., Rashid, R., Yapp, C., Joshi, G. N., Li, C. G., Lindquist, S. L., Sarosiek, K. A., Whitesell, L., Sorger, P. K., & Santagata, S. (2020). HSF1 phase transition mediates stress adaptation and cell fate decisions. *Nature Cell Biology*, *22*(2), 151-158. https://doi.org/10.1038/s41556-019-0458-3

Gasch, A. P., & Werner-Washburne, M. (2002). The genomics of yeast responses to environmental stress and starvation. *Funct Integr Genomics*, *2*(4-5), 181-192. https://doi.org/10.1007/s10142-002-0058-2

Ghavi-Helm, Y., Jankowski, A., Meiers, S., Viales, R. R., Korbel, J. O., & Furlong, E. E. M. (2019). Highly rearranged chromosomes reveal uncoupling between genome topology and gene expression. *Nature Genetics*, *51*(8), 1272-1282. https://doi.org/10.1038/s41588-019-0462-3

Kainth, A. S., Chowdhary, S., Pincus, D., & Gross, D. S. (2021). Primordial super-enhancers: heat shock-induced chromatin organization in yeast. *Trends Cell Biol*, *31*(10), 801-813. https://doi.org/10.1016/j.tcb.2021.04.004

Kroschwald, S., Maharana, S., Mateju, D., Malinovska, L., Nüske, E., Poser, I., Richter, D., & Alberti, S. (2015). Promiscuous interactions and protein disaggregases determine the material state of stress-inducible RNP granules. *Elife*, *4*, e06807. https://doi.org/10.7554/eLife.06807

Kunkel, J., Luo, X., & Capaldi, A. P. (2019). Integrated TORC1 and PKA signaling control the temporal activation of glucose-induced gene expression in yeast. *Nat Commun*, *10*(1), 3558. https://doi.org/10.1038/s41467-019-11540-y

Mahat, D. B., Salamanca, H. H., Duarte, F. M., Danko, C. G., & Lis, J. T. (2016). Mammalian Heat Shock Response and Mechanisms Underlying Its Genome-wide Transcriptional Regulation. *Mol Cell*, *62*(1), 63-78. https://doi.org/10.1016/j.molcel.2016.02.025

Miesenböck, G., De Angelis, D. A., & Rothman, J. E. (1998). Visualizing secretion and synaptic transmission with pH-sensitive green fluorescent proteins. *Nature*, *394*(6689), 192-195. https://doi.org/10.1038/28190

Munder, M. C., Midtvedt, D., Franzmann, T., Nüske, E., Otto, O., Herbig, M., Ulbricht, E., Müller, P., Taubenberger, A., Maharana, S., Malinovska, L., Richter, D., Guck, J., Zaburdaev,

V., & Alberti, S. (2016). A pH-driven transition of the cytoplasm from a fluid- to a solid-like state promotes entry into dormancy. *Elife*, *5*. https://doi.org/10.7554/eLife.09347

Petrovska, I., Nüske, E., Munder, M. C., Kulasegaran, G., Malinovska, L., Kroschwald, S., Richter, D., Fahmy, K., Gibson, K., Verbavatz, J. M., & Alberti, S. (2014). Filament formation by metabolic enzymes is a specific adaptation to an advanced state of cellular starvation. *Elife*, *3*. https://doi.org/10.7554/eLife.02409

Riback, J. A., Katanski, C. D., Kear-Scott, J. L., Pilipenko, E. V., Rojek, A. E., Sosnick, T. R., & Drummond, D. A. (2017). Stress-Triggered Phase Separation Is an Adaptive, Evolutionarily Tuned Response. *Cell*, *168*(6), 1028-1040.e1019. https://doi.org/10.1016/j.cell.2017.02.027

Sabari, B. R., Dall'Agnese, A., Boija, A., Klein, I. A., Coffey, E. L., Shrinivas, K., Abraham, B. J., Hannett, N. M., Zamudio, A. V., Manteiga, J. C., Li, C. H., Guo, Y. E., Day, D. S., Schuijers, J., Vasile, E., Malik, S., Hnisz, D., Lee, T. I., Cisse, II,…Young, R. A. (2018). Coactivator condensation at super-enhancers links phase separation and gene control. *Science*, *361*(6400). https://doi.org/10.1126/science.aar3958

Sawarkar, R. (2022). Transcriptional lockdown during acute proteotoxic stress. *Trends Biochem Sci*, *47*(8), 660-672. https://doi.org/10.1016/j.tibs.2022.03.020

Sharp, P. A., Chakraborty, A. K., Henninger, J. E., & Young, R. A. (2022). RNA in formation and regulation of transcriptional condensates. *Rna*, *28*(1), 52-57. https://doi.org/10.1261/rna.078997.121

Shrinivas, K., Sabari, B. R., Coffey, E. L., Klein, I. A., Boija, A., Zamudio, A. V., Schuijers, J., Hannett, N. M., Sharp, P. A., Young, R. A., & Chakraborty, A. K. (2019). Enhancer Features that Drive Formation of Transcriptional Condensates. *Mol Cell*, *75*(3), 549-561.e547. https://doi.org/10.1016/j.molcel.2019.07.009

Triandafillou, C. G., Katanski, C. D., Dinner, A. R., & Drummond, D. A. (2020). Transient intracellular acidification regulates the core transcriptional heat shock response. *Elife*, *9*, e54880. https://doi.org/10.7554/eLife.54880

Tye, B. W., Commins, N., Ryazanova, L. V., Wühr, M., Springer, M., Pincus, D., & Churchman, L. S. (2019). Proteotoxicity from aberrant ribosome biogenesis compromises cell fitness. *Elife*, *8*. https://doi.org/10.7554/eLife.43002

Valkonen, M., Mojzita, D., Penttilä, M., & Bencina, M. (2013). Noninvasive high-throughput single-cell analysis of the intracellular pH of Saccharomyces cerevisiae by ratiometric flow cytometry. *Appl Environ Microbiol*, *79*(23), 7179-7187. https://doi.org/10.1128/aem.02515-13

Warner, J. R. (1999). The economics of ribosome biosynthesis in yeast. *Trends Biochem Sci*, *24*(11), 437-440. https://doi.org/10.1016/s0968-0004(99)01460-7

Weitzel, G., Pilatus, U., & Rensing, L. (1987). The cytoplasmic pH, ATP content and total protein synthesis rate during heat-shock protein inducing treatments in yeast. *Exp Cell Res*, *170*(1), 64-79. https://doi.org/10.1016/0014-4827(87)90117-0

Zhang, H., Shao, S., Zeng, Y., Wang, X., Qin, Y., Ren, Q., Xiang, S., Wang, Y., Xiao, J., & Sun, Y. (2022). Reversible phase separation of HSF1 is required for an acute transcriptional

response during heat shock. *Nature Cell Biology*, *24*(3), 340-352. https://doi.org/10.1038/s41556-022-00846-7

APPENDIX 1

Inducible transcriptional condensates drive 3D genome reorganization in the heat shock response

This chapter is a full reprint of Chowdhary et al 2022 on which I am an author. This work is included with permission from all the authors. I made the yeast strains used in this study, performed growth curve experiments, and helped write some of the methods section.

A1.1 Abstract

Mammalian developmental and disease-associated genes concentrate large quantities of the transcriptional machinery by forming membrane-less compartments known as transcriptional condensates. However, it is unknown whether these structures are evolutionarily conserved or involved in 3D genome reorganization. Here, we identify inducible transcriptional condensates in the yeast heat shock response (HSR). HSR condensates are biophysically dynamic spatiotemporal clusters of the sequence-specific transcription factor Heat shock factor 1 (Hsf1) with Mediator and RNA Pol II. Uniquely, HSR condensates drive intergenic interactions between multiple Hsf1 target genes, even those located on different chromosomes, resulting in their coalescence. Binding of the chaperone Hsp70 to a site on Hsf1 represses clustering, while an intrinsically disordered region on Hsf1 promotes condensate formation and intergenic interactions. Mutation of both Hsf1 determinants reprograms HSR condensates to become constitutively active without intergenic coalescence, which comes at a fitness cost. These results suggest that transcriptional condensates are ancient and flexible compartments of eukaryotic gene control.

A1.2 Introduction

Eukaryotes have evolved specialized mechanisms to ensure robust expression of critically important genes such as those activated to specify cell lineage and in response to stress. Mammalian cells utilize clusters of transcription factor binding sites, termed "super-enhancers" (SEs), to drive high-level gene expression by concentrating a large fraction of transcriptional activators and coactivators such as the Mediator complex (Hnisz et al., 2013; Whyte et al., 2013). SEs are interwoven by an extensive DNA looping network constituted by enhancer elements and target gene promoters (Beagrie et al., 2017; Dowen et al., 2014; Huang et al., 2018). Recent studies suggest that SEs function through cooperative assembly of the transcriptional apparatus into "biomolecular condensates" (Boija et al., 2018; Guo et al., 2019; Sabari et al., 2018), defined as self-organized membrane-free compartments that concentrate specific biomolecules (Banani et al., 2017). Transcriptional condensates at SEs are hypothesized to drive transcriptional bursting and stabilize expression of associated genes (Henninger et al., 2021; Hnisz et al., 2017; Sabari et al., 2018).

Biomolecular condensates in general – and transcriptional condensates in particular – are commonly established and maintained by multivalent interactions. In many cases, multivalent interactions driven by intrinsically disordered regions (IDRs) appear to be important for establishing and maintaining condensates (Banani et al., 2017; Shin and Brangwynne, 2017). Some IDRs can engage in a network of weak and transient "fuzzy" interactions with other proteins and nucleic acids and are often subject to reversible post-translational modifications that can regulate these interactions (Boehning et al., 2018; Boija et al., 2018; Chong et al., 2018; Guo et al., 2019; Hnisz et al., 2017; Sabari et al., 2018; Sanborn et al., 2021; Shin and Brangwynne, 2017; Tuttle et al., 2021; Wei et al., 2020; Sanders et al., 2020; Lu et al., 2019). Multivalent biomolecules can undergo a spontaneous phase transition. In its simplest form, this means that above a concentration known as the saturation concentration, the components can

demix into two distinct phases: a dense, macromolecule-enriched phase and a dilute, macromolecule-depleted phase (Banani et al., 2017; Shin and Brangwynne, 2017). The nature and strength of intermolecular interactions and the number of participant molecules are likely to influence the dynamics inside the condensates (Brangwynne et al., 2009; Hnisz et al., 2017). In the case of transcriptional condensates, intermediate concentrations of transcriptional activators can lead to formation of active hubs that are not necessarily phase separated (Chong et al., 2018; Baek et al., 2021), suggesting biophysical diversity among different transcriptional condensates.

To date, transcriptional condensates have been best characterized at stably expressed loci in mammalian cells (Boija et al., 2018; Cho et al., 2018; Sabari et al., 2018). However, signalling factors have been shown to concentrate within transcriptional condensates in response to specific stimuli (Lu et al., 2020; Nair et al., 2019; Stortz et al., 2021; Zamudio et al., 2019).

Whether transcriptional condensates are conserved features of eukaryotic gene transcription remains unknown. Moreover, it is unclear how they conduct gene control in a three-dimensional (3D) context and whether transcriptional condensates influence 3D genomic organization. In this study, we address these questions by employing the highly dynamic heat shock response (HSR) system of budding yeast.

Recent studies in budding yeast have revealed profound remodelling of the 3D chromatin architecture following activation of the HSR by Hsf1 (Chowdhary et al., 2017; Chowdhary et al., 2019), and we speculated that transcriptional condensates may drive this 3D genomic reorganization (Kainth et al., 2021). Indeed, the HSR shares several key features with mammalian SEs, such as recruitment of high levels of the transcriptional machinery at the associated genes and extensive DNA looping interactions. A key distinction is that, as opposed to the stable gene expression enforced by SEs, HSR activation in yeast is induced in a

remarkably rapid yet transient manner: large increases in occupancy of Hsf1 and the transcriptional machinery at HSR genes accompany transcriptional activation within 60 seconds of temperature upshift and return to pre-heat shock levels within 30 to 60 minutes (Chowdhary et al., 2017; Chowdhary et al., 2019; Kim and Gross, 2013; Kremer and Gross, 2009; Pincus et al., 2018; Vinayachandran et al., 2018). Beyond the enhancer-promoter loops found in SEs, HSR genes engage in physical interactions with other HSR genes separated by large distances and even located on different chromosomes (Chowdhary et al., 2017; Chowdhary et al., 2019). Both intragenic and intergenic rearrangements of HSR genes are dynamic and concur with transcriptional output (Chowdhary et al., 2017). Thus, induction of the yeast HSR may involve transient condensates that form intergenic hubs of transcriptional activity.

Here we provide experimental evidence implicating biomolecular condensation as the underlying mechanism of 3D gene control during the yeast HSR. We show that Hsf1, together with Mediator and RNA Pol II, forms transcriptional condensates at HSR genes in response to heat shock. These condensates are inducible, highly dynamic, transient, and promote intergenic chromatin interactions among genes in the Hsf1 regulon. We identify the N-terminal IDR of Hsf1 and a C-terminal binding site for the chaperone Hsp70 as molecular determinants that promote condensation with intergenic interactions and inhibit cluster formation, respectively. Finally, we generate a separation-of-function mutant of Hsf1 by mutating both of these determinants that forms constitutive condensates but fails to drive intergenic interactions. This double mutant displays a strong growth defect at elevated temperature, suggesting that formation of constitutive condensates that lack intergenic interactions comes at a fitness cost in this system. Together, our work reveals that transcriptional condensates are a conserved feature of eukaryotic gene control that can be induced and dissolved as a means to reversibly reconfigure the 3D genome.

A1.3 Results

A1.3.1 Inducible high-level occupancy of the transcriptional machinery at HSR genes

To determine whether yeast HSR genes – defined as genes under the control of Hsf1 – share key features with genes that drive lineage specification and disease progression in mammalian cells, we assessed the extent to which HSR genes concentrate the transcriptional machinery. Using a consistent bioinformatic pipeline, we reanalyzed chromatin immunoprecipitation sequencing (ChIP-seq) data of Hsf1, Med15 (subunit of the Mediator complex known to interact with Hsf1) and Rpb1 (subunit of RNA Pol II) across the genome under basal and acute heat shock conditions (Albert et al., 2019; Anandhakumar et al., 2016; Kim and Gross, 2013; Pincus et al., 2018; Sarkar et al., 2022). We found strong enrichment of all three factors at HSR genes upon heat shock and observed that the Hsf1 and Med15 peaks colocalize at heat shock elements (HSEs), the known binding sites for Hsf1 (Figures 1A, S1A-D).

Although HSR genes constitute <1% of the yeast genome, 30% of Med15 and 20% of Pol II ChIP-seq reads overlapped with Hsf1 reads upon heat shock (Figure S1C). Rank order analysis of protein-coding genes (n=5983) by change in Med15 occupancy during acute heat shock revealed that all HSR genes are in the top 20%, with the majority residing above the inflection point of the curve (Figure 1B). To determine if Hsf1 binding is sufficient to recruit high levels of Mediator upon heat shock, we performed ChIP of Hsf1 and Med15 at the non-HSR gene *BUD3* in a wild type strain and a strain harboring a chromosomal integration of a high-affinity HSE at the *BUD3* locus (Chowdhary et al., 2019). While neither Hsf1 nor Med15 were detectable at the wild type *BUD3* locus, a brief heat shock induced massive recruitment of Hsf1 and Med15 to *BUD3* with the engineered HSE (Figure S1E), suggesting that Mediator is robustly and selectively recruited by Hsf1 at its gene targets. Together, these data demonstrate that HSR genes disproportionately concentrate the transcriptional machinery upon activation.

A1.3.2 Hsf1, Mediator and RNA Pol II colocalize in subnuclear clusters upon heat shock

We hypothesized that HSR genes engage a large fraction of transcriptional machinery by spatially concentrating the requisite factors within the nucleus. Therefore, we investigated the spatiotemporal distributions of Hsf1, Mediator and RNA Pol II in live single cells upon heat shock (Figures 1C, D). In unstressed cells, endogenously tagged Hsf1-mVenus was predominantly nuclear and diffusely localized (Figure 1C, NHS). However, Hsf1 formed semi-discrete subnuclear clusters within 6 min of heat shock that persisted for 20-25 min, after which Hsf1 returned to its diffuse localization pattern (Figure 1C, heat shock). Hsf1 clusters were identified within 3D images of live cells using the automated FindFoci algorithm in ImageJ that detects above background peak intensity regions within images (Figure 1D, E). Here, we have interpreted inhomogeneities in signal distribution as foci (or clusters) of locally enriched target molecules. This analysis revealed the presence of Hsf1 clusters in >80% cells subjected to 9, 13, or 18-min heat shock; fewer cells (20-50%) evinced clusters when induced for 28 min or longer (Figure 1E). We typically observed 4 clusters of Hsf1 per individual nucleus, although the number varied between 2 and 6 over the course of heat shock (Figure 1C, D, E). These results are consistent for both the deconvolved images and those processed without deconvolution (Figure S2A, C).

Clusters of Hsf1 were not always in a single plane but were spatially distributed across multiple planes along the z-axis. To provide the best representation of the number and position of clusters in each nucleus, we rendered images in 3D and displayed foci assignments as 3D bubble plots (Figure 1C, D). For further characterization and improved clarity, we also visualized images as 3D surface plots that display inhomogeneities within images as peaks of signal intensity. 3D surface plots of images of acutely heat-shocked cells showed 3-4 distinct peaks, confirming presence of clusters under such conditions (Figure 1D). We could detect inhomogeneities within images processed without deconvolution, and these images displayed

the same number of foci and peaks as deconvolved images, which rules out processing or deconvolution-related artifacts in our image analyses (Figure S2B). Analysis of diploid cells expressing Hsf1-GFP gave virtually identical results; neither kinetics nor number of clusters changed significantly, indicating that the number of Hsf1 clusters does not correlate with ploidy (Figure S3C). To distinguish whether redistribution of Hsf1 into clusters is a physical consequence of elevated temperature or a regulatory consequence of Hsf1 activation, we imaged Hsf1-mVenus expressing cells following treatment with azetidine-2-carboxylic acid (AZC), a proline analogue that incorporates into nascent proteins, impairs protein folding, and activates Hsf1 (Trotter et al., 2001; Zheng et al., 2018). Following AZC treatment, Hsf1 formed intranuclear clusters in a majority of cells (Figure S3D). Therefore, Hsf1 clustering appears to be driven by activation rather than heat per se.

We next tested whether Mediator and RNA Pol II also formed intranuclear clusters during heat shock by imaging haploid cells expressing either endogenously tagged Med15-mCherry or Rpb3-mCherry. In the absence of heat shock, Med15 and Rpb3 were diffusely localized within the nucleus (Figure 1C and D, NHS). However, like Hsf1, both formed an average of 4 subnuclear clusters in >80% of cells upon heat shock that emerged and dissolved with similar kinetics to Hsf1 (Figures 1C, D and S3A, B). Moreover, live cell 3D imaging of cells co-expressing Med15-mCherry or Rpb3-mCherry with Hsf1-mVenus revealed that the clusters formed by both factors co-localized with Hsf1 during heat shock with a fractional overlap of at least 70% (Figures 1F, G and S3E). These data provide evidence of spatiotemporal interactions between Hsf1, Mediator and RNA Pol II inside living cells following heat shock.

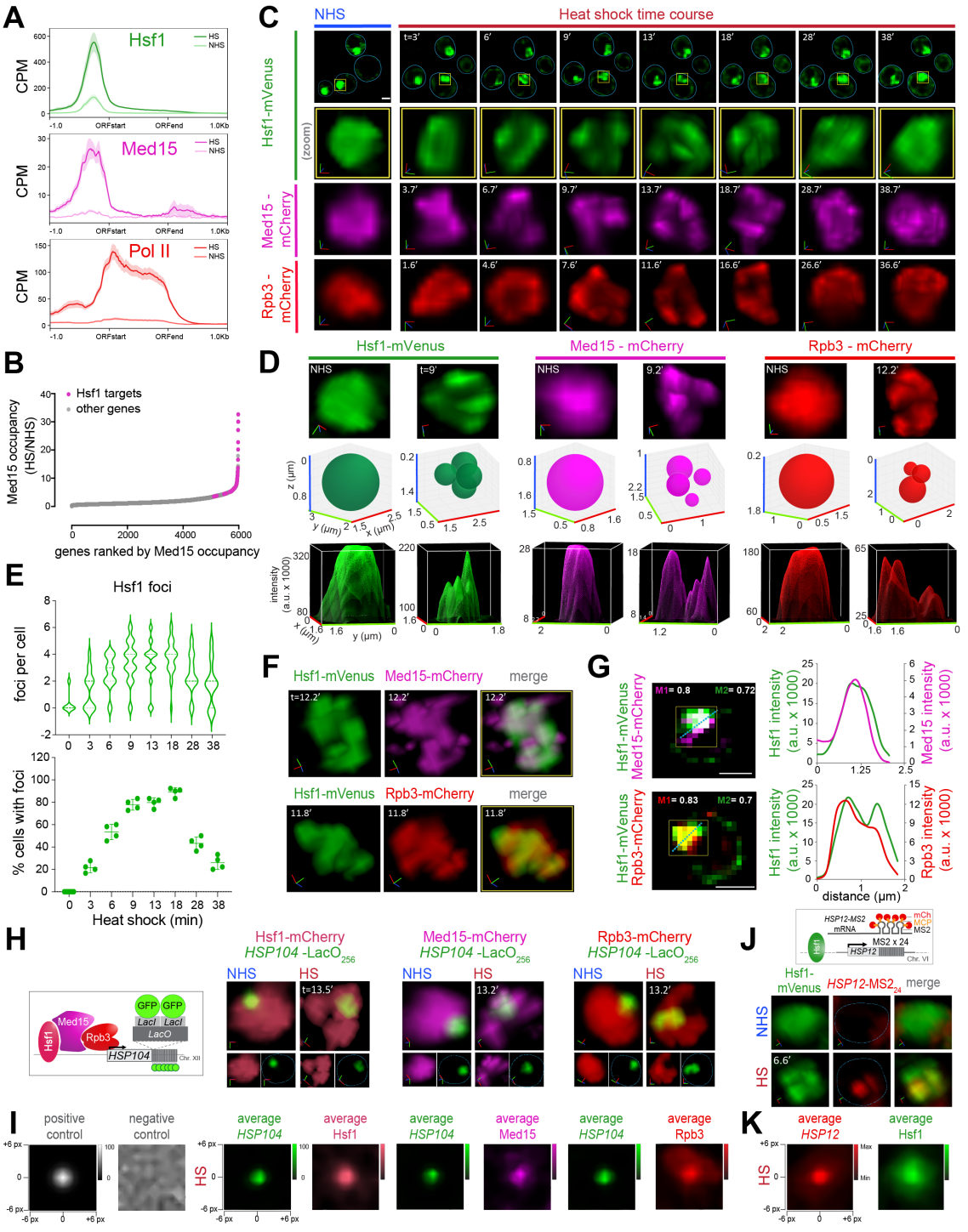

Figure A1.1. Hsf1, Mediator and RNA Pol II form transcriptionally active clusters at HSR genes upon heat shock

A) Metagene plots of Hsf1 (top), Med15 (middle) and Pol II (Rpb1; bottom) normalized ChIP-seq reads of Hsf1-dependent genes in *S. cerevisiae* (n=42) centered over ORFs with 1 kb surrounding region. Shown are means +/- SE (shaded region). NHS, non-heat shock; HS, heat shock; CPM, counts per million reads.

B) Fold change in Med15 occupancy across Pol II-transcribed genes (0 to -1 kb from +1 ATG) upon heat shock, arranged according to their rank order.

C) Time lapse live-cell imaging of three individual cell types expressing either Hsf1-mVenus (rows 1, 2), or Med15-mCherry (row 3), or Rpb3-mCherry (row 4) before (NHS, 24-26°C) and following HS (39°C) for the times (t) indicated. For each cell type, a single cell is followed throughout the heat shock time course. Row 1: images of cells expressing Hsf1-mVenus. Representative planes are shown. Blue line highlights cell boundary. Scale bar is 2 µm. Row 2: enlarged view of the nucleus (see yellow box in Row 1). Shown is the 3D volumetric rendering of each nucleus; x (red), y (green) and z (blue) axes are indicated. Rows 3 and 4: 3D volumetric rendering of nuclei of cells expressing Med15-mCherry and Rpb3-mCherry, respectively.
D) Characterization of Hsf1, Med15 and Rpb3 foci in live cells. Top row: 3D volumetric rendering of cells expressing Hsf1-mVenus, Med15-mCherry and Rpb3-mCherry before (NHS) and following HS for the times (t) indicated. Middle row: 3D bubble charts of Hsf1, Med15 and Rpb3 foci that were detected and quantified using the automated FindFoci algorithm in cells shown in the top row. Bottom row: Visualization of Hsf1, Med15 and Rpb3 foci of cells shown in top row as 3D surface plots. Height of the plot corresponds to luminance of pixels within the image. x (red), y (green) and z (blue) axes are indicated.
E) Top: number of Hsf1 foci per cell quantified from live imaging of cells expressing Hsf1-mVenus before (0 min) and following HS for the times (t) indicated. Bottom: percentage of cells expressing Hsf1 foci. Foci were identified and counted using the automated FindFoci algorithm. 40-60 cells were evaluated per time point. Cells with >2 foci are counted as those containing foci for percentage evaluation. Shown are means +/- SD.
F) Live imaging of cells co-expressing Hsf1-mVenus and Med15-mCherry (top), or Hsf1-mVenus and Rpb3-mCherry (bottom). Cells were heat-shocked for the indicated time (t).
G) Left: Quantification of colocalization using Mander's Overlay Coefficient of Hsf1-mVenus and Med15-mCherry (top), or Hsf1-mVenus and Rpb3-mCherry (bottom). M1 indicates the fraction of mCherry that overlaps mVenus; M2, fraction overlap of mVenus with mCherry. Scale bar is 2 µm. Right: average intensity profiles along blue dotted lines are indicated in the images.
H) 3D rendered micrographs of Hsf1-mCherry (left), Med15-mCherry (middle) or Rpb3-mCherry (right) and the *HSP104-LacO*$_{256}$ gene locus as depicted in the schematic (leftmost) under NHS and following heat shock for the indicated times (t). Blue dotted line highlights nuclear boundary.
I) Contour plots of Hsf1-mCherry (left), Med15-mCherry (middle) or Rpb3-mCherry (right) showing averaged signal intensities centred at the *HSP104-LacO*$_{256}$ gene locus 13 minutes following heat shock. The negative and positive controls (left) were generated from simulation analysis of an array of numbers arranged either randomly (negative control) or as 2D gaussian distribution (positive control).
J) Top: schematic of Hsf1 (green) and the MCP-mCherry labelled *HSP12-MS2*$_{24}$ mRNA (red). Bottom: 3D rendered micrographs of representative cells heat-shocked for ~7 min or not (NHS). Blue dotted line highlights nuclear boundary.
K) Contour plot of Hsf1-mVenus (right) showing averaged intensity signal centred at *HSP12-MS2*$_{24}$ mRNA (left). Cells were imaged at 5 minutes of heat shock.

A1.3.3 Hsf1 clusters activate transcription of HSR genes

To determine whether HSR genes associate with the Hsf1/Med15/Rpb3 clusters in yeast, we created three individual strains bearing 3′-flanking arrays of 256 *lacO*-repeats at the *HSP104* locus – a canonical HSR gene bound by these factors (Figure S1D) – and co-expressing LacI-GFP with either Hsf1-, Med15- or Rpb3-mCherry (Figure 1H). Live-cell imaging revealed that under basal conditions, *HSP104-lacO*$_{256}$ minimally overlapped with Hsf1-, Med15- and Rpb3-

mCherry but consistently co-localized with these factors during acute heat shock (Figure 1H and S3F). Across a population of cells, the average fluorescence intensities of Hsf1, Med15 and Rpb3 were enriched at the center of the *HSP104-lacO$_{256}$* focus (Figure 1I). These results indicate that the Hsf1, Mediator and Pol II clusters associate with a canonical HSR gene.

To directly test whether Hsf1 clusters are sites of active transcription, we employed the MS2 RNA imaging system to visualize nascent transcript production (Hocine et al., 2013; Lenstra and Larson, 2016). We inserted 24 repeats of the MS2 stem loop into the genome in the 3′ untranslated region of the *HSP12* gene, another HSR target (Figure S1D), in a strain expressing the MS2 coat protein fused to mCherry (MCP-mCherry) and co-expressing Hsf1-mVenus. We observed no *HSP12-MS$_{24}$* fluorescence under non-heat shock conditions, indicating a lack of transcription of *HSP12* mRNA, while heat shock induced the transient appearance of a concentrated focus of nascent *HSP12-MS$_{24}$* mRNA that colocalized with Hsf1-mVenus (Figures 1J and S3G). The average fluorescence intensity of Hsf1 was enriched at the center of the *HSP12-MS2$_{24}$* mRNA focus across a population of acutely heat-shocked cells (Figure 1K). These data demonstrate that, upon heat shock, Hsf1 forms subnuclear clusters with the transcriptional machinery that mark sites of nascent mRNA production.

A1.3.4 Hsf1 clusters exhibit properties of biomolecular condensates

As shown above, HSR genes concentrate high levels of the transcriptional machinery and are activated in spatial clusters, reminiscent of SE-associated transcriptional condensates that drive expression of mammalian cell identity genes. Transcriptional condensates display the hallmark property of rapid exchange and reorganization of constituent biomolecules (Boija et al., 2018; Cho et al., 2018; Sabari et al., 2018). To investigate the dynamics of Hsf1 clusters in living cells, we employed the stimulated emission depletion (STED) super-resolution imaging technique. We took time-series images of live cells expressing Hsf1-mVenus every minute and found that

the Hsf1 clusters exhibited a stereotyped temporal signature along the course of heat shock: (1) an early demixing phase; (2) an intermediate intermixing phase; and (3) a late remixing phase (Figure 2A).

The demixing phase is marked by formation of semi-discrete clusters of Hsf1 during the first 6-7 min of heat shock induction. During the demixing phase, Hsf1 nuclear distribution transitions from a homogenous to a heterogenous regime. In the intermixing phase (8-27 min), Hsf1 clusters rearrange continuously within the nucleus, demonstrating exchange of contents among the clusters. During the intermixing phase, Hsf1 signal intensity displayed substantial pixel-to-pixel variation across the time points – underscoring its spatial dynamics – while overall Hsf1 signal in the nuclei remained nearly constant (Figure 2B). Moreover, as displayed in 3D bubble charts, varying numbers, sizes and positions of Hsf1 foci reveal rapid and intricate rearrangements among clusters in the intermixing phase (Figure 2A, bottom). Finally, in the remixing phase (28-32 min), Hsf1 clusters disperse to the pre-heat shocked diffuse form, transitioning from heterogenous to a more uniformly distributed regime. These results demonstrate that Hsf1 clusters are remarkably dynamic: they form quickly, rearrange rapidly, and dissolve abruptly.

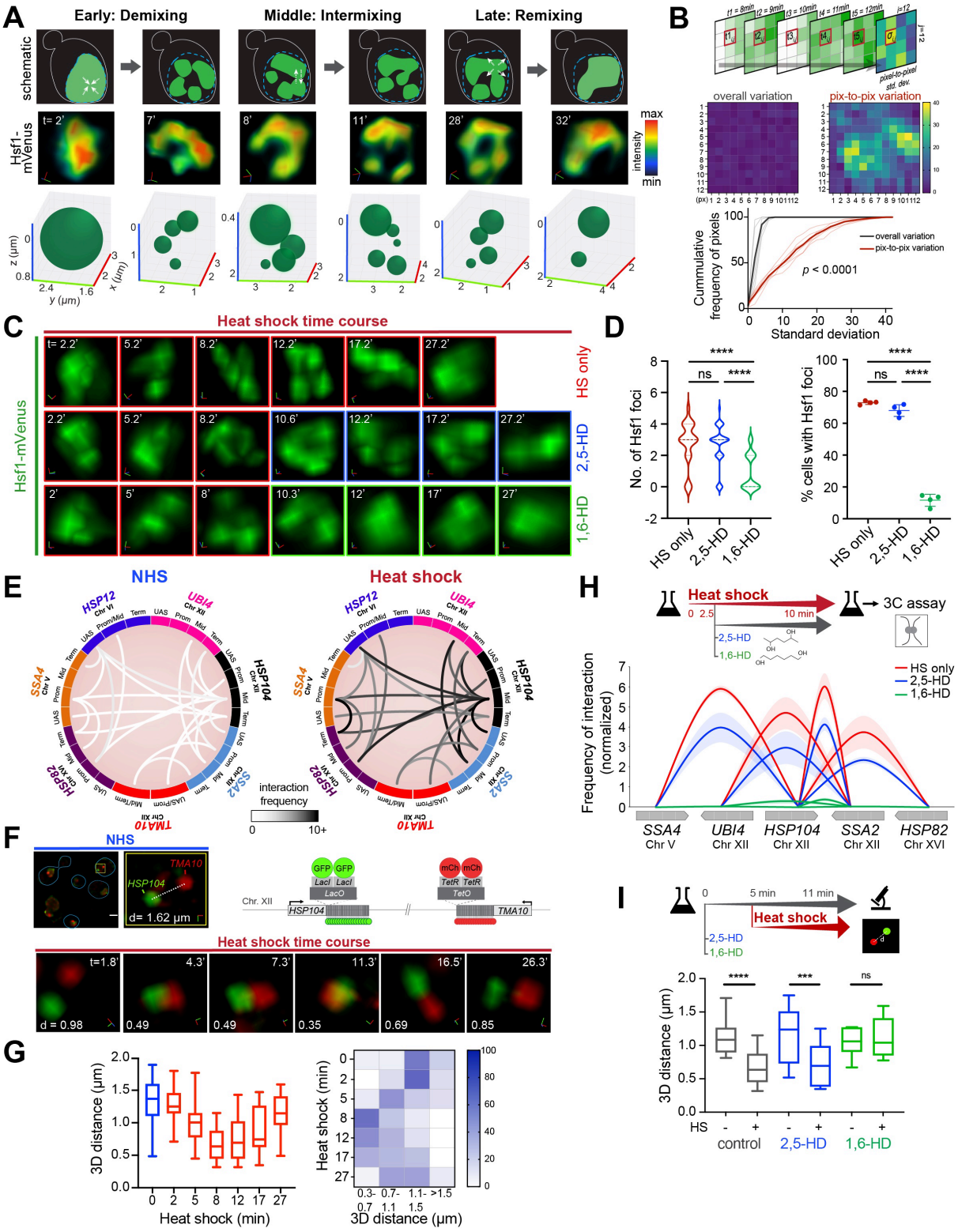

Figure A1.2. Hsf1 clusters are dynamic and associated with HSR gene coalescence

A) Schematic (top), STED super-resolution imaging (middle) and 3D bubble plots (bottom) depicting Hsf1-mVenus foci dynamics at different stages of heat shock: Early, demixing (2 and 7 min-HS); Middle, intermixing (8 and 11 min-HS); and Late, remixing (28 and 32 min-HS). 3D rendering axes: x (red), y (green) and z (blue) are shown.

B) Demonstration of internal dynamics of Hsf1 foci identified within STED images acquired each minute over the intermixing phase of heat shock. Top: schematic of the method used for computing

variation between pixels. Pixel-to-pixel variation (σ) was calculated for each pixel in a 12 (i) x 12 (j) square bounding the nucleus across time points between t1 (8min) and t5 (12min). Middle: Heatmap comparison of pixel-to-pixel variation in a representative nucleus against overall variation within the image. Bottom: Cumulative frequency distribution of standard deviations for pixel-to-pixel (red) and overall (black) variation within six individual cells. *P* value between means of the two distributions is indicated.

C) 3D rendered micrographs of a representative cell subjected to heat shock for times (t) indicated in the absence of hexanediol (top) or treated with either 2,5-HD (middle) or 1,6-HD (bottom) after 9 min of HS. Note that a different cell was imaged after alcohol treatment.

D) Number of Hsf1 foci per cell and the percentage of cells showing >2 Hsf1 foci (n=110-140 cells/condition) following heat shock for 9 minutes +/- the indicated HD. Cells were imaged approximately 3 minutes after adding HD. Foci were identified and counted using the automated FindFoci algorithm ****P <0.0001; ns (not significant), P >0.05. *P* values were calculated by ANOVA followed by Tukey's post hoc analysis.

E) Circos plots depicting intergenic interactions between indicated gene pairs as determined by Taq I-3C derived from (Chowdhary et al., 2017; Chowdhary et al., 2019). Arc shades depict the frequencies of chromatin interactions between indicated regions. For each gene pair, top two interactions are shown.

F) Time lapse live-cell imaging of a diploid strain expressing *HSP104-lacO*$_{256}$, *TMA10-tetO*$_{200}$, *LacI-GFP* and *TetR-mCherry* (schematic, top right). Top left: micrographs of representative cells under NHS conditions (blue line highlights cell boundary) and an enlarged 3D view of the nuclear region indicated within the yellow box. Bottom: enlarged 3D micrographs of a representative cell subjected to heat shock for the times (t) indicated (axes: x (red), y (green) and z (blue)). d, 3D distances measured between signal centroids.

G) Distribution of 3D distances between *lacO*-tagged *HSP104* and *tetO*-tagged *TMA10* gene loci in cells subjected to heat shock for times indicated (n=13 for NHS; n=20-30 for HS time points). Bottom: Heat map depicting percentage of cells with tagged gene loci within indicated 3D distances binned at intervals of 0.4 μm.

H) Intergenic contacts (solid arcs) between indicated Hsf1 target gene pairs as determined by TaqI-3C in presence and absence of hexanediol. Values indicate normalized interaction frequencies. Genes are segmented as UAS, promoter, mid-ORF and terminator (from blunt to arrowhead direction). Data are derived from two independent biological replicates; qPCR =4. Depicted are means +/- SD (shaded region around solid arcs).

I) Distribution of 3D distances between tagged gene loci under conditions as indicated. Cells were left untreated or pre-treated for 5 min with either 2,5- or 1,6-hexanediol followed by no heat shock or heat shock for 6 min and then imaged. n =13-22. ****P <0.0001; ***P <0.001; ns (not significant), P >0.05 (calculated using two-tail t test).

To further probe the material properties of Hsf1 clusters, we tested their sensitivity to an aliphatic alcohol, 1,6-hexanediol (1,6-HD). 1,6-HD has historically been used to disrupt liquid-like biomolecular condensates, including transcriptional condensates in mammalian cells. While the exact mechanism of action remains unclear, evidence suggests that it impacts hydrophobic and aromatic interactions more strongly than electrostatic effects (Cho et al., 2018; Kroschwald et al., 2015; Patel et al., 2015; Sabari et al., 2018). Extended treatment of cells with 1,6-HD can impact membrane integrity and cause blebbing – which could be an

early sign of autophagy or cell death – as well as disrupt chromatin architecture and inhibit kinase and phosphatase activity (Duster et al., 2021; Itoh et al., 2021; Kroschwald et al., 2017). To minimize the pleiotropic and aberrant effects of 1,6-HD, we optimized the concentration and duration of hexanediol treatment for the two most widely studied examples of nuclear biomolecular condensates: the nucleolus and the nuclear pore complex (NPC) (Banani et al., 2017; Kato and McKnight, 2018). To this end, we applied 1,6-HD to living cells expressing endogenous Nop56-mRFP (nucleolar component) and Pom34-GFP (nuclear pore component) at three different concentrations (3, 5 and 10%) for 20-30 minutes (Figure S4A, B). While it took more than 15 minutes to disintegrate the nucleolus and NPC with 3% 1,6-HD, similar effects were evident in less than 4 minutes when 10% 1,6-HD was applied. Moreover, membrane blebbing was prominent following addition of 10% 1,6-HD. Treatment with 5% 1,6-HD resulted in dissolution of the nucleolus and NPC after 7 minutes with no signs of membrane blebbing until after 20 minutes (Figure S4B). We also scored the effects of 2,5-hexanediol (2,5-HD), a less hydrophobic alcohol with the same atomic composition as 1,6-HD. 2,5-HD had minimal effect on nucleolar and NPC integrity when used at lower concentrations (3 or 5%). However, at 10%, the effects of 2,5-HD were the same as observed with 1,6-HD (Figure S4A, B). Based on these observations, we identified 5% for less than 20 minutes as the optimum concentration and treatment duration for both hexanediols.

To determine the effect of hexanediols on Hsf1 clusters, we first heat shocked cells for 8 minutes to allow cluster formation and then treated cells expressing Hsf1-mVenus with either 5% 1,6-HD or 2,5-HD. Hsf1 clusters were dissolved within 4 minutes upon addition of 1,6-HD but were unaffected by 2,5-HD treatment and mimicked cells that were only heat-shocked (Figure 2C, D). We observed similar effects on Med15 clusters, except they were even more rapidly dissolved upon 1,6-HD treatment (Figure S4C, D). Together, these data indicate that the transcriptionally active Hsf1 clusters display properties characteristic of biomolecular

condensates: they continuously intermix and exchange contents, and they are potentially held together by weak, hydrophobic interactions. We will hereon refer to them as HSR condensates.

A1.3.5 HSR condensates drive intergenic interactions among HSR genes

HSR genes engage in selective intra- and inter-chromosomal interactions upon heat shock-induced activation (Chowdhary et al., 2017; Chowdhary et al., 2019), and we hypothesized that these interactions are driven by condensate formation (Kainth et al., 2021). Using a highly sensitive chromosome conformation capture technique (TaqI-3C) (Chowdhary et al., 2020), we have demonstrated interactions among seven Hsf1-dependent genes spanning distinct chromosomes (Chowdhary et al., 2019) (Figure 2E). The intergenic interactions between Hsf1-dependent genes occur with low frequency under non-heat shock conditions but increase many -fold upon acute heat shock, coincident with their increased transcription. To complement this molecular assay, we directly imaged intergenic coalescence of HSR genes in live cells by utilizing a heterozygous diploid strain bearing operator arrays chromosomally linked to HSR genes, *HSP104-lacO*$_{256}$ and *TMA10-tetO*$_{200}$, that co-expresses LacI-GFP and TetR-mCherry (Chowdhary et al., 2019) (Figure 2F). Under non-heat shock conditions, *HSP104-lacO*$_{256}$ and *TMA10-tetO*$_{200}$ were spatially separated, as indicated by a large 3D distance between the two loci (d =1.6 μm). This is consistent with the respective locations of *HSP104* and *TMA10* on the far left and right arms of chromosome XII, as well as their physical isolation from each other due to the nucleolar barrier between them. However, upon heat shock, *HSP104-lacO*$_{256}$ and *TMA10-tetO*$_{200}$ came in close proximity within 5 minutes of thermal exposure, coalescing into a partially-overlapping focus after 10 minutes that ultimately dissipated after 16 minutes (Figure 2F). We obtained consistent results for images processed with or without deconvolution (Figure S2D). Across a population of cells, *HSP104-lacO*$_{256}$ and *TMA10-tetO*$_{200}$ were separated by much larger 3D distances under non-inducing and chronic heat shock conditions (17 min and later),

while the distribution was skewed toward shorter distances in acutely heat-shocked cells (Figure 2G).

As a control, we imaged a heterozygous diploid strain bearing operator arrays chromosomally linked to an HSR gene, *HSP104-lacO*$_{256}$, and an Hsf1-independent, Msn2/4-regulated gene, *PGM2-lacO*$_{128}$ (Figure S4G; (Chowdhary et al., 2019)). In contrast to the above observations of two HSR genes, *HSP104-lacO*$_{256}$ and *PGM2-lacO*$_{128}$ remain spatially separated by 3D distances of >1.1 μm in both the presence and absence of heat shock (Figure S4G, H). This result corroborates our previous findings that intergenic interactions are distinct properties of genes regulated by Hsf1, and Msn2/4 regulated genes fail to coalesce with Hsf1 targets despite their strong activation in response to thermal stress (Chowdhary et al., 2019). Taken together, the above observations indicate that coalescence of Hsf1-dependent genes is specific and highly dynamic with kinetics closely paralleling that of Hsf1 cluster formation and dissolution.

To determine if HSR condensates are involved in driving intergenic coalescence, we perturbed Hsf1 clusters and assayed for coalescence using the TaqI-3C and live single cell imaging analyses. First, we induced Hsf1 clusters by subjecting cells to brief heat shock treatment for 2.5 minutes before adding 1,6-HD or 2,5-HD and performed TaqI-3C (Figures 2H, S4E). We detected strong chromatin interactions between HSR genes in cells heat-shocked for 2.5 minutes. The 3C interactions were only moderately reduced in the presence of 2,5-HD, including intragenic interactions within the HSR genes. By contrast, addition of 1,6-HD reduced the contact frequencies to background levels. Next, we treated cells with 1,6-HD or 2,5-HD prior to heat shock and performed single cell imaging of the strain bearing fluorescently tagged alleles of *HSP104* and *TMA10*. The coalescence of *HSP104-lacO*$_{256}$ and *TMA10-tetO*$_{200}$ was abolished in cells that were pretreated for 5 min with 5% 1,6-HD before heat shock but occurred normally in cells treated with 5% 2,5-HD, matching the cells with no alcohol pretreatment (Figure S4F). Quantification revealed that the mean 3D distance decreased from

>1.1 μm to <0.7 μm upon heat shock over a population of cells subjected to either 5% 2,5-HD or no pre-treatment, whereas the loci remained separated by >1.1 μm in 1,6-HD-treated cells (Figure 2I). Collectively, these results indicate that 1,6-HD not only dissolves the clusters of Hsf1, but also disrupts intergenic interactions between HSR genes.

A1.3.6 Hsp70 binding represses Hsf1 cluster formation

Do the molecular mechanisms that control Hsf1 activity also regulate HSR condensate formation? Hsf1 activity is repressed when it is bound by the chaperone Hsp70 (Figure 3A) (Krakowiak et al., 2018; Masser et al., 2019; Peffer et al., 2019; Zheng et al., 2016), so we wondered if Hsp70 binding would also repress HSR condensate formation. To test this, we disrupted the Hsp70 binding site located in the C-terminal segment of Hsf1, known as "conserved element 2" (CE2), by introducing alanine substitutions at residues known to be required for Hsp70 association (Krakowiak et al., 2018; Peffer et al., 2019) (Figure 3A, B). We expressed GFP-tagged Hsf1-ce2AAA as the only copy of Hsf1 and imaged its localization. In contrast to the diffuse nuclear localization of wild type Hsf1, we observed constitutive clustering of Hsf1-ce2AAA in unstressed cells that persisted during heat shock (Figure 3C).

To determine whether the constitutive clusters formed by Hsf1-ce2AAA are transcriptionally active, we measured mRNA levels of representative HSR genes in cells expressing wild type Hsf1 and Hsf1-ce2AAA (Figure 3D). In agreement with the known repressive role for Hsp70 binding, we detected a significant increase in the basal mRNA levels of some targets in Hsf1-ce2AAA cells compared to cells expressing wild type Hsf1. However, the basal levels of most target transcripts in the mutant were lower than their respective levels in wild type cells following heat shock, suggesting that the constitutive clusters formed by Hsf1-ce2AAA are less active than those formed by wild type Hsf1 upon activation. Further supporting a lack of full activation in the mutant, both Med15 and Rpb3 were diffusely localized under basal conditions

in Hsf1-ce2AAA cells and only formed clusters with Hsf1-ce2AAA upon heat shock (Figure 3F). Moreover, HSR genes showed no detectable intergenic interactions as measured by TaqI-3C under basal conditions in Hsf1-ce2AAA cells, but both intra- and intergenic interactions were induced upon heat shock to the same degree as in wild type cells (Figures 3E and S5D). Thus, mutation of the CE2 binding site for Hsp70 results in constitutive Hsf1 cluster formation, but this is not sufficient to trigger formation of HSR condensates that drive intergenic interactions.

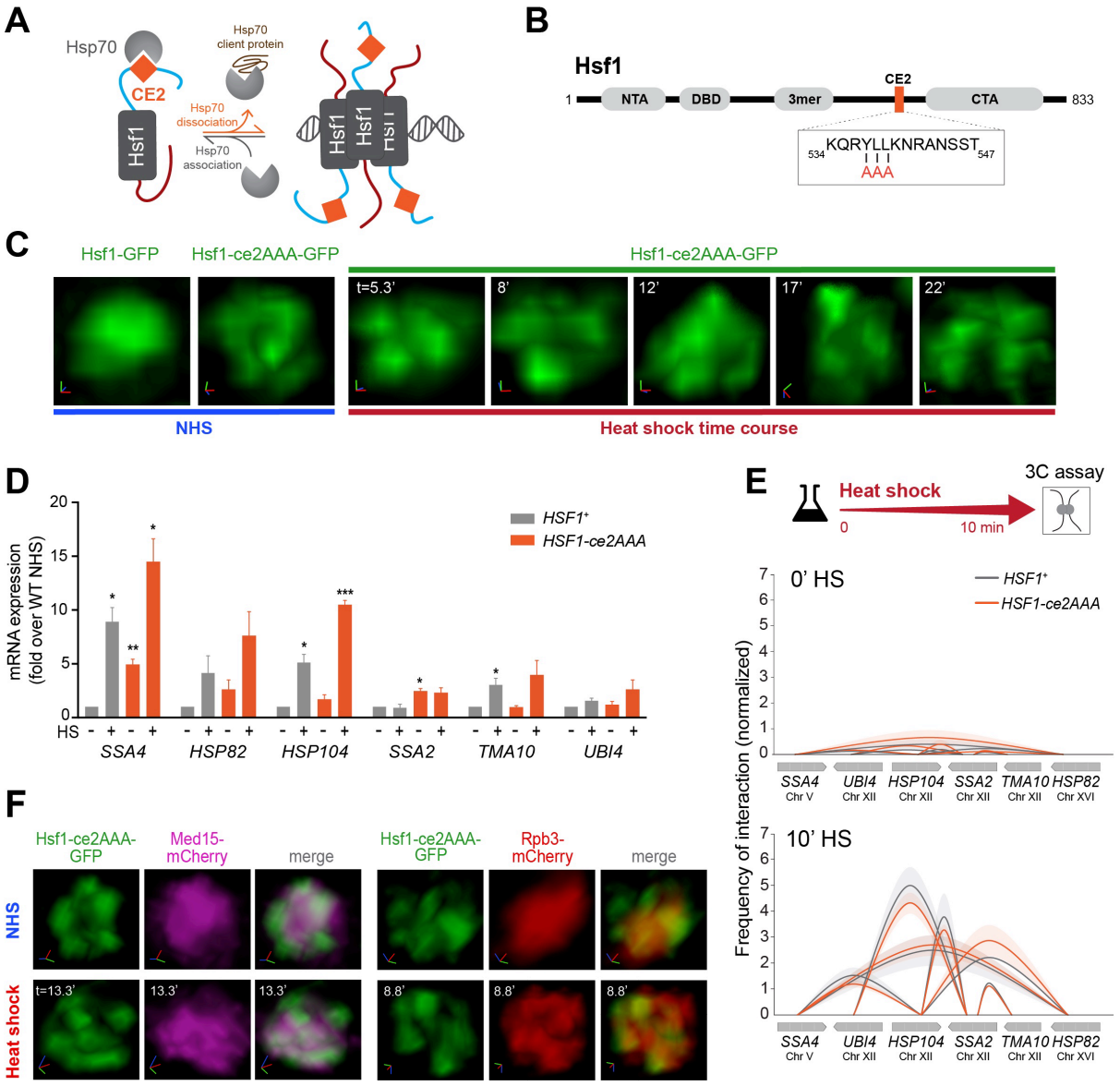

Figure A1.3. Hsp70 binding to Hsf1 represses cluster formation

A) Schematic of the Hsp70 titration model of Hsf1 regulation. Hsp70 binds to Hsf1 via the CE2 domain and inactivates Hsf1. Accumulation of chaperone clients sequesters Hsp70, leaving Hsf1 free to activate transcription.

B) Domain map of Hsf1. NTA, N-terminal activation domain; DBD, DNA binding domain; 3mer, trimerization domain; CE2, conserved element 2 domain (orange); CTA, C-terminal activation domain. Box: CE2 sequence and alanine substitutions in the Hsf1-ce2AAA mutant.

C) 3D rendered images of wild type and Hsf1-ce2AAA mutant cells in NHS or HS conditions.

D) mRNA expression measured by RT-qPCR of representative Hsf1-regulated genes in *HSF1*$^{+}$ and *HSF1-ce2AAA* strains under NHS and 10 min-HS conditions. ***P <0.001; **P <0.01; *P <0.05 (calculated using multiple unpaired t tests)

E) Intergenic contacts (solid arcs) between indicated Hsf1 target gene pairs under NHS and 10 min-HS conditions as determined by TaqI-3C.

F) Live imaging of cells co-expressing Hsf1 ce2AAA-GFP and Med15-mCherry (left), or Hsf1 ce2AAA-GFP and Rpb3-mCherry (right) under NHS or HS conditions.

A1.3.7 The N-terminal domain of Hsf1 promotes formation of HSR condensates

Hsf1 contains large functional N-terminal and C-terminal activation domains referred to as NTA and CTA (Figure 4A). The NTA both represses Hsf1 under basal conditions – likely due to a second Hsp70 binding site – and plays a positive role in transactivation, while the CTA simply constitutes a strong transactivation domain (Kim and Gross, 2013; Krakowiak et al., 2018; Peffer et al., 2019; Sorger, 1990). The NTA and CTA are highly disordered (Figures 4B and S5G), as predicted by Metapredict V2 (Emenecker et al., 2022). Both regions act synergistically to stably recruit Mediator to the HSR gene promoters, facilitating interactions between Hsf1 and the Mediator complex; either domain alone can do so only weakly (Figure 4A) (Kim and Gross, 2013). To address whether they play a role in intergenic interactions and HSR condensate formation is not known, we separately removed both regions.

We observed that Hsf1-ΔNTA-GFP failed to form clusters even upon heat shock (Figure 4C, D). Moreover, Rpb3 and Med15 also could not re-distribute into clusters in the Hsf1-ΔNTA mutant, suggesting that interactions between Hsf1, Mediator and Pol II are required for clustering during heat shock (Figure 4C, D). These data further support the interpretation that clustering of Hsf1, and additionally Med15 and Rpb3, is driven by regulatory activation rather than heat per se. At the molecular level, we found that while Hsf1-ΔNTA was able to robustly bind to the promoter of the target gene *HSP104* and recruit RNA Pol II upon heat shock, it was unable to recruit high levels of Med15 (Figure 4F). We obtained virtually identical results for two other HSR genes, *HSP82* and *SSA4* (Figure S5B). The rate of inducible transcription of HSR genes and the appearance of intragenic 3D interactions were largely unaffected in the Hsf1-ΔNTA cells relative to wild type (Figures 4E, S5A, C). Since Mediator is indispensable for transcriptional activation (Anandhakumar et al., 2016), the lack of detectable Med15 in the ChIP assay suggests that Hsf1-ΔNTA is only able to transiently recruit but not stably interact

with Mediator. Along with the lack of Med15 recruitment, we observed a substantial decrease in intergenic interactions between *HSP104* and other HSR genes in Hsf1-ΔNTA cells compared to wild type (Figure 4G). Loss of the CTA likewise decreased Mediator recruitment and ablated heat shock-induced intergenic interactions among HSR genes, but it also impaired fitness under all growth conditions, rendering it too severe a mutation to interpret specifically (Figure S5H-J) (Krakowiak et al., 2018; Sorger, 1990). These data indicate that the NTA promotes the ability of Hsf1 to cluster with Mediator and Pol II upon heat shock and drive intergenic interactions among HSR genes.

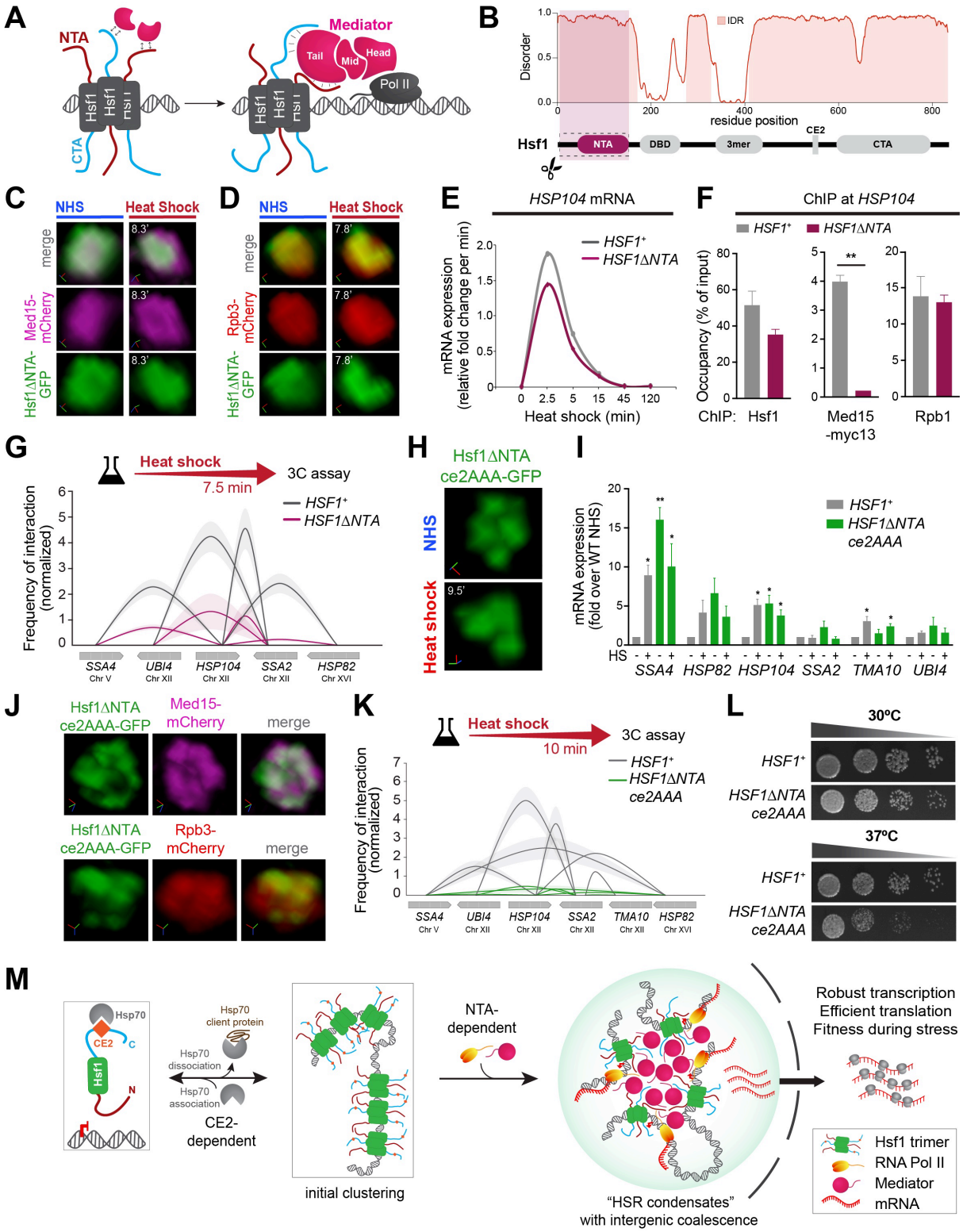

Figure A1.4. HSR condensates drive inducible intergenic coalescence by the combined actions of the CE2 and NTA regions of Hsf1

A) Cartoon depiction of Mediator recruitment at HSR genes via dual Hsf1 activation domains.

B) Domain map and prediction of disorder in Hsf1 by Metapredict V2 (Emenecker et al., 2022).

C) Live imaging of cells expressing Hsf1ΔNTA -GFP and Med15-mCherry under NHS or HS conditions.

D) Live imaging of cells expressing Hsf1ΔNTA -GFP and Rpb3-mCherry under NHS or HS conditions.
E) Transcription rates of *HSP104* in *HSF1*$^{+}$ and *HSF1-ΔNTA* isogenic strains during a heat shock time course, as deduced from RT-qPCR.
F) Hsf1 and Med15-myc13 ChIP at the UASs and Rpb1 ChIP at the promoter region of *HSP104* in wild type and Hsf1-ΔNTA strains heat-shocked for 7.5 min. Depicted are means + SD. **, $P < 0.01$ (calculated using two-tail t-test).
G) Intergenic contacts (solid arcs) between indicated Hsf1 target gene pairs in 7.5 min-HS conditions as determined by TaqI-3C.
H) Representative 3D rendered micrographs of cells expressing Hsf1-GFP and Hsf1-ΔNTA-ce2AAA-GFP under NHS and HS (axes: x (red), y (green) and z (blue)).
I) mRNA expression measured by RT-qPCR of representative Hsf1-regulated genes in *HSF1*$^{+}$ and *HSF1-ΔNTAce2AAA* strains under NHS and 10 min-HS conditions. **$P < 0.01$; *$P < 0.05$ (calculated using multiple unpaired t tests)
J) Live imaging of cells co-expressing Hsf1ΔNTAce2AAA -GFP with Med15-mCherry (top) or Rpb3-mCherry (bottom) under NHS conditions.
K) Intergenic contacts (solid arcs) between indicated Hsf1 target gene pairs following 10 min-HS conditions as determined by TaqI-3C.
L) Spot dilution analysis of *HSF1*$^{+}$ and *HSF1-ΔNTAce2AAA* cells. Plates were incubated at 30°C or 37°C for 30 h.
M) Schematic depiction of HSR condensation. In unstressed cells, Hsp70 binds to Hsf1 via the CE2 domain and inactivates Hsf1. Accumulation of misfolded proteins sequesters Hsp70 and frees Hsf1 which then binds to its gene targets and forms initial clusters. The activated Hsf1 recruits Mediator via the NTA domain. Hsf1, together with Mediator and RNA Pol II, forms dynamic transcriptional condensates (HSR condensates) that localize multiple Hsf1 target genes engaging in specific interactions with each other. The HSR condensates with intergenic coalescence promote high transcriptional activity, maximal gene expression and cellular fitness during stress.

A1.3.8 Inducible HSR condensates promote cellular fitness under stress

HSR condensates share biophysical properties and molecular constituents with mammalian transcriptional condensates that form at SEs, yet HSR condensates are distinct in their transient kinetics and their ability to drive intergenic interactions between chromosomally linked and unlinked genes. Since loss of CE2 resulted in constitutive Hsf1 clustering, and loss of the NTA reduced intergenic interactions, we reasoned that combining these mutations would reprogram Hsf1 to be constitutively clustered but unable to drive intergenic interactions. To test this, we generated a double mutant, Hsf1-ΔNTAce2AAA, GFP-tagged it and expressed it as the only copy of Hsf1 from the endogenous *HSF1* promoter.

Indeed, Hsf1-ΔNTAce2AAA-GFP formed constitutive clusters (Figure 4H, NHS) and was fully activated, driving transcription of some target genes under basal conditions to levels exceeding their expression during heat shock in wild type cells (Figure 4I). In contrast to the constitutive clusters of Hsf1-ce2AAA single mutant, Hsf1-ΔNTAce2AAA-GFP colocalized in clusters with Med15- and Rpb3-mCherry under basal conditions (Figure 4J). Upon heat shock, the double mutant showed no further increase in transcription of HSR genes, and levels of several HSR targets even decreased (Figure S5E). While Hsf1-ΔNTAce2AAA-GFP clusters persisted during heat shock (Figure 4H, heat shock), Med15- and Rpb3-mCherry clusters were diminished (Figure S5F). Despite its constitutive transcriptional activity and clustering, Hsf1-ΔNTAce2AAA was unable to drive intergenic interactions among HSR genes, even during heat shock (Figure 4K). Finally, Hsf1-ΔNTAce2AAA cells showed impaired growth at elevated temperature (Figure 4L), suggesting that the ability to form inducible transcriptional condensates that are capable of driving intergenic interactions promotes fitness during stress. Thus, the CE2 and NTA are determinants that endow HSR condensates with inducibility and the capacity to drive intergenic interactions, features necessary for cell survival under stress.

A1.4 Discussion

Here we have shown that activation of the HSR in budding yeast involves the formation of inducible biomolecular condensates that localize multiple target genes into subnuclear compartments with high transcriptional activity. These HSR condensates form and dissolve over the course of heat shock and contain biophysically dynamic clusters of the transcription factor Hsf1 along with Mediator and RNA Pol II (Figure 4M). Importantly, Hsf1 also forms clusters when cells are treated with AZC to activate the HSR, demonstrating that condensate formation, is driven by regulatory activation and can be decoupled from the physical process of heating. Our discovery of HSR condensates in yeast demonstrates that transcriptional

condensates exist outside of the mammalian lineage and suggests that these structures are likely an ancient and conserved feature of eukaryotic gene control.

The distinguishing features of HSR condensates – their inducible kinetics and intergenic interactions – indicate that transcriptional condensates are capable of rapidly and reversibly remodeling the 3D genome in response to environmental cues. HSR condensates encode these unique properties within the primary sequence of Hsf1 via Hsp70 binding sites and the intrinsically disordered NTA. As such, genetic disruption of the CE2 binding site for Hsp70 combined with ablation of the NTA was sufficient to reprogram HSR condensates to be constitutive structures that lack intergenic coalescence. Thus, relatively simple genetic changes can have dramatic consequences in the regulatory properties of transcriptional condensates, endowing these structures with evolutionary plasticity.

In many biomolecular condensates, especially those forming at gene regulatory elements, the constituent biomolecules contain intrinsically disordered regions (IDRs) that assemble cooperatively (Banani et al., 2017; Boehning et al., 2018; Boija et al., 2018; Chong et al., 2018; Hnisz et al., 2017; Nair et al., 2019; Sabari et al., 2018; Shin and Brangwynne, 2017; Lu et al, 2019). Given that deletion of the NTA domain of Hsf1 results in loss of condensates and intergenic coalescence (Figure 4C, G), it is likely that cooperative binding among the IDRs of Hsf1, Mediator and RNA Pol II (Figure S5K, L) could serve to nucleate the HSR condensates and bring HSR genes in 3D proximity (Figure 4M). The other possibility is that Hsf1 initiates the condensation. This initiation mechanism could entail cooperative binding of Hsf1 trimers to multiple HSEs of canonical gene targets (Erkine et al., 1999), with each activator molecule then tethering or engaging one or more polymerases and/or Mediator subunits (Baek et al., 2021). These local multivalent interactions between Hsf1 and Mediator at individual HSR genes could then intermix with other such local assemblies leading to intergenic coalescence.

The role of the chaperone Hsp70 in repressing Hsf1 clustering represents a cell biological manifestation of the known role of Hsp70 in repressing Hsf1 transcriptional activity (Kmiecik et al., 2020; Krakowiak et al., 2018; Masser et al., 2019; Zheng et al., 2016). While we do not elucidate the biochemical basis of this repression in the current study, two mechanisms are possible: Hsp70 could passively block clustering by steric occlusion, and/or Hsp70 could mechanically pull Hsf1 out of the clusters. Precedents exist for both of these putative mechanisms in repression of cytosolic condensates (Ruff et al., 2021; Yoo et al., 2022). Hsp70 could also mask one or both IDRs, thereby inhibiting nucleation events described above. Regardless of the specific mechanisms, Hsp70 may generally function as a "molecular stir bar" to antagonize condensates both within and outside the nucleus. Expanding on this notion, Hsf1 may have evolved to form condensates upon activation that mimic other condensates recognized by Hsp70 in order to peg its activity – and therefore the expression of the HSR regulon – to the availability of Hsp70. Other chaperones such as Hsp90, which is known to associate with nuclear hormone receptors that also condense with the transcriptional machinery (Frank et al., 2021; Nair et al., 2019; Picard et al., 1990), may also remodel transcriptional condensates.

Are HSR condensates likely to be conserved in mammalian cells? In human cells, HSF1 does indeed form large stress-induced subnuclear foci upon heat shock (Jolly et al., 1997). However, rather than driving transcription of HSR genes, these large HSF1 foci have been shown to localize to noncoding satellite DNA regions and are anti-correlated with HSR gene expression (Gaglia et al., 2020; Jolly et al., 2004). In addition to these large HSF1-containing clusters, a recent study provides compelling evidence that smaller HSF1 foci represent transcriptionally active condensates at HSR genes (Zhang et al., 2022). Beyond HSF1, the mammalian Pol II-pausing factor NELF (negative elongation factor), which is associated with transcriptional dowregulation during stress, also forms condensates upon heat shock that are distinct from

HSF1 foci (Rawat et al., 2021). NELF condensates may liberate transcriptional machinery from housekeeping genes that can then be recruited by HSF1 to drive high-level induction of the HSR (Kainth et al., 2021; Mahat et al., 2016). It remains unclear whether mammalian HSF1 condensates play a role in 3D genome organization as neither large nor small HSF1 foci have been tested in this regard. Although the organization of mammalian genomes into topologically associated domains (TADs) (Dixon et al., 2012) would seem to preclude the ability of HSR genes to coalesce upon activation like they do in yeast, multiple HSR genes are endogenously clustered adjacent to each other in the human genome, which may potentially allow intergenic interactions among HSR genes to occur (Kainth et al., 2021). Thus, it is possible that inducible intergenic transcriptional condensates are conserved features of the HSR across the eukaryotic lineage.

HSR condensates may provide several advantages to cells under stress (Figure 4M). First, condensation serves to concentrate large quantities of the transcriptional machinery to enable robust induction of Hsf1-regulated genes critical to counteracting the stress. Second, the coalescence of multiple Hsf1 target genes, separated by large distances on and between chromosomes, could reduce search time for repeated transcriptional firing events and coordinate transcriptional bursting across the HSR regulon. Third, the localized transcription of multiple HSR genes could promote mRNA clustering into "transperons" that may bypass normal mRNA quality control processes and increase efficiency of post-transcriptional steps of gene expression such as nuclear export (Nair et al., 2021; Zander et al., 2016). Fourth, HSR condensates may enable target messages to avoid cytosolic stress granules and thereby promote their privileged translation (Zid and O'Shea, 2014), perhaps by recruiting translation factors or mRNA modifying enzymes. HSR condensates may thus promote cell survival under stress by controlling both transcriptional and post-transcriptional events. HSR condensates represent the founding example of inducible transcriptional clusters with an ability to drive intergenic

interactions between stress-responsive genes. Given these attributes, it may be the case that analogous structures have evolved to execute other stimulus-regulated transcriptional programs within budding yeast and beyond.

A1.4.1 Limitations of the study

The major limitation of this study is the spatiotemporal resolution of the live imaging data we generated to monitor the HSR condensates in yeast cells. The principal challenge is the small size of the yeast nucleus (<3 μm^3), which means that the HSR condensates are distributed and must rearrange in a very compact space. The low abundance of the components (on the order of 10^3 molecules of endogenously tagged Hsf1 or Med15 per cell), the rapid kinetics of formation and dissolution of HSR condensates, and the spatial distribution of the condensates across multiple z-planes presented further technical challenges. We relied on relatively long exposures, requiring 15 seconds to capture each z-stack at each time point, and we were limited by photobleaching in the total number of timepoints we could collect. Together, these challenges made it difficult to discern whether the HSR condensates in budding yeast are discrete foci like transcriptional condensates in mammalian cells. Although HSR condensates share components and properties with mammalian transcriptional condensates, we do not rule out the possibility that HSR condensates might be qualitatively distinct given their transient nature and their ability to cluster HSR target genes. Perhaps, HSR condensates are constantly ebbing and flowing, forming mobile regions of local enrichment of the transcriptional machinery that rapidly recruit and release target genes as they dynamically survey the genome.

In addition to the condensates themselves, the same constraints apply to the LacO and TetR arrays we used to image and quantify the distance between genomic loci in single cells. Perhaps due to the long acquisition times, these arrays – which typically appear as diffraction-limited spots in the literature – spanned multiple pixels in our high-resolution deconvolved images,

limiting the precision of our 3D distance measurements. Although we cannot precisely quantify distance with the arrays in single cells, our TaqI-3C data complement the microscopy-based analyses. Together, these orthogonal approaches support the model that Hsf1 target genes preferentially get closer to one another upon heat shock in a manner that requires Hsf1 to form inducible condensates.

A1.5 Acknowledgments

We would like to thank Vytas Bindokas and Christine Labno at the University of Chicago Integrated Light Microscopy Core (RRID: SCR_019197) for imaging assistance and technical support. We thank Rama Ranganathan and Alex Ruthenburg for sharing reagents and equipment. We also thank Luke Dyer for help with strain construction and Pincus and Gross lab members for helpful discussions. This work was supported by NIH grants R01 GM138689 to D.P. and R01 GM138988 and R15 GM128065 to D.S.G, and the NSF Quantum Leap Challenge Institute for Quantum Sensing for Biophysics and Bioengineering OMA-2121044 to D.P.

A1.6 Author contributions

Conceptualization: S. C., D. S. G. and D. P.; Methodology: S. C., A. S. K., D. S. G. and D. P; Formal Analysis: S. C. and A. S. K.; Investigation: S. C. and A. S. K.; Resources: S. C., A. S. K., S. P.; Writing – original draft: S. C. and D. P.; Writing – Review and Editing: S. C., A. S. K., S. P., D. S. G. and D. P.; Visualization: S. C., A. S. K. and D. P.; Supervision: D. S. G. and D. P.; Funding Acquisition: D. S. G. and D. P.

Declaration of interests

The authors declare no competing interests.

REFERENCES

Albert, B., Kos-Braun, I.C., Henras, A.K., Dez, C., Rueda, M.P., Zhang, X., Gadal, O., Kos, M., and Shore, D. (2019). A ribosome assembly stress response regulates transcription to maintain proteome homeostasis. Elife *8*. 10.7554/eLife.45002.

Anandhakumar, J., Moustafa, Y.W., Chowdhary, S., Kainth, A.S., and Gross, D.S. (2016). Evidence for Multiple Mediator Complexes in Yeast Independently Recruited by Activated Heat Shock Factor. Mol Cell Biol *36*, 1943-1960. 10.1128/MCB.00005-16.

Baek, I., Friedman, L.J., Gelles, J., and Buratowski, S. (2021). Single-molecule studies reveal branched pathways for activator-dependent assembly of RNA polymerase II pre-initiation complexes. Mol Cell 81, 3576-3588 e3576. 10.1016/j.molcel.2021.07.025.

Banani, S.F., Lee, H.O., Hyman, A.A., and Rosen, M.K. (2017). Biomolecular condensates: organizers of cellular biochemistry. Nat Rev Mol Cell Biol *18*, 285-298. 10.1038/nrm.2017.7.

Beagrie, R.A., Scialdone, A., Schueler, M., Kraemer, D.C., Chotalia, M., Xie, S.Q., Barbieri, M., de Santiago, I., Lavitas, L.M., Branco, M.R., et al. (2017). Complex multi-enhancer contacts captured by genome architecture mapping. Nature *543*, 519-524. 10.1038/nature21411.

Boehning, M., Dugast-Darzacq, C., Rankovic, M., Hansen, A.S., Yu, T., Marie-Nelly, H., McSwiggen, D.T., Kokic, G., Dailey, G.M., Cramer, P., et al. (2018). RNA polymerase II clustering through carboxy-terminal domain phase separation. Nat Struct Mol Biol *25*, 833-840. 10.1038/s41594-018-0112-y.

Boija, A., Klein, I.A., Sabari, B.R., Dall'Agnese, A., Coffey, E.L., Zamudio, A.V., Li, C.H., Shrinivas, K., Manteiga, J.C., Hannett, N.M., et al. (2018). Transcription Factors Activate Genes through the Phase-Separation Capacity of Their Activation Domains. Cell *175*, 1842-1855 e1816. 10.1016/j.cell.2018.10.042.

Bolte, S., and Cordelieres, F.P. (2006). A guided tour into subcellular colocalization analysis in light microscopy. J Microsc *224*, 213-232. 10.1111/j.1365-2818.2006.01706.x.

Brangwynne, C.P., Eckmann, C.R., Courson, D.S., Rybarska, A., Hoege, C., Gharakhani, J., Julicher, F., and Hyman, A.A. (2009). Germline P granules are liquid droplets that localize by controlled dissolution/condensation. Science *324*, 1729-1732. 10.1126/science.1172046.

Cherry, J.M., Hong, E.L., Amundsen, C., Balakrishnan, R., Binkley, G., Chan, E.T., Christie, K.R., Costanzo, M.C., Dwight, S.S., Engel, S.R., et al. (2012). Saccharomyces Genome Database: the genomics resource of budding yeast. Nucleic Acids Res 40, D700-705. 10.1093/nar/gkr1029.

Cho, W.K., Spille, J.H., Hecht, M., Lee, C., Li, C., Grube, V., and Cisse, II (2018). Mediator and RNA polymerase II clusters associate in transcription-dependent condensates. Science *361*, 412-415. 10.1126/science.aar4199.

Chong, S., Dugast-Darzacq, C., Liu, Z., Dong, P., Dailey, G.M., Cattoglio, C., Heckert, A., Banala, S., Lavis, L., Darzacq, X., and Tjian, R. (2018). Imaging dynamic and selective low-

complexity domain interactions that control gene transcription. Science *361*. 10.1126/science.aar2555.

Chowdhary, S., Kainth, A.S., and Gross, D.S. (2017). Heat Shock Protein Genes Undergo Dynamic Alteration in Their Three-Dimensional Structure and Genome Organization in Response to Thermal Stress. Mol Cell Biol *37*. 10.1128/MCB.00292-17.

Chowdhary, S., Kainth, A.S., and Gross, D.S. (2020). Chromosome conformation capture that detects novel cis- and trans-interactions in budding yeast. Methods *170*, 4-16. 10.1016/j.ymeth.2019.06.023.

Chowdhary, S., Kainth, A.S., Pincus, D., and Gross, D.S. (2019). Heat Shock Factor 1 Drives Intergenic Association of Its Target Gene Loci upon Heat Shock. Cell Rep *26*, 18-28 e15. 10.1016/j.celrep.2018.12.034.

Dixon, J.R., Selvaraj, S., Yue, F., Kim, A., Li, Y., Shen, Y., Hu, M., Liu, J.S., and Ren, B. (2012). Topological domains in mammalian genomes identified by analysis of chromatin interactions. Nature *485*, 376-380.

Dosztanyi, Z., Csizmok, V., Tompa, P., and Simon, I. (2005). IUPred: web server for the prediction of intrinsically unstructured regions of proteins based on estimated energy content. Bioinformatics 21, 3433-3434. 10.1093/bioinformatics/bti541.

Dowen, J.M., Fan, Z.P., Hnisz, D., Ren, G., Abraham, B.J., Zhang, L.N., Weintraub, A.S., Schuijers, J., Lee, T.I., Zhao, K., and Young, R.A. (2014). Control of cell identity genes occurs in insulated neighborhoods in mammalian chromosomes. Cell *159*, 374-387. 10.1016/j.cell.2014.09.030.

Duster, R., Kaltheuner, I.H., Schmitz, M., and Geyer, M. (2021). 1,6-Hexanediol, commonly used to dissolve liquid-liquid phase separated condensates, directly impairs kinase and phosphatase activities. J Biol Chem *296*, 100260. 10.1016/j.jbc.2021.100260.

Emenecker, R.J., Griffith, D., Holehouse, A.S. (2022). Metapredict V2: An update to metapredict, a fast, accurate, and easy-to-use predictor of consensus disorder and structure. bioRxiv, 2022.06.06.494887. 10.1101/2022.06.06.494887.

Erkine, A.M., Magrogan, S.F., Sekinger, E.A., and Gross, D.S. (1999). Cooperative binding of heat shock factor to the yeast HSP82 promoter in vivo and in vitro. Mol Cell Biol *19*, 1627-1639.

Frank, F., Liu, X., and Ortlund, E.A. (2021). Glucocorticoid receptor condensates link DNA-dependent receptor dimerization and transcriptional transactivation. Proc Natl Acad Sci U S A *118*. 10.1073/pnas.2024685118.

Gaglia, G., Rashid, R., Yapp, C., Joshi, G.N., Li, C.G., Lindquist, S.L., Sarosiek, K.A., Whitesell, L., Sorger, P.K., and Santagata, S. (2020). HSF1 phase transition mediates stress adaptation and cell fate decisions. Nat Cell Biol *22*, 151-158. 10.1038/s41556-019-0458-3.

Guo, Y.E., Manteiga, J.C., Henninger, J.E., Sabari, B.R., Dall'Agnese, A., Hannett, N.M., Spille, J.H., Afeyan, L.K., Zamudio, A.V., Shrinivas, K., et al. (2019). Pol II phosphorylation

regulates a switch between transcriptional and splicing condensates. Nature *572*, 543-548. 10.1038/s41586-019-1464-0.

Hegemann, J.H., and Heick, S.B. (2011). Delete and repeat: a comprehensive toolkit for sequential gene knockout in the budding yeast Saccharomyces cerevisiae. Methods Mol Biol *765*, 189-206. 10.1007/978-1-61779-197-0_12.

Henninger, J.E., Oksuz, O., Shrinivas, K., Sagi, I., LeRoy, G., Zheng, M.M., Andrews, J.O., Zamudio, A.V., Lazaris, C., Hannett, N.M., et al. (2021). RNA-Mediated Feedback Control of Transcriptional Condensates. Cell *184*, 207-225 e224. 10.1016/j.cell.2020.11.030.

Herbert, A.D., Carr, A.M., and Hoffmann, E. (2014). FindFoci: a focus detection algorithm with automated parameter training that closely matches human assignments, reduces human inconsistencies and increases speed of analysis. PLoS One 9, e114749. 10.1371/journal.pone.0114749.

Hnisz, D., Abraham, B.J., Lee, T.I., Lau, A., Saint-Andre, V., Sigova, A.A., Hoke, H.A., and Young, R.A. (2013). Super-enhancers in the control of cell identity and disease. Cell *155*, 934-947. 10.1016/j.cell.2013.09.053.

Hnisz, D., Shrinivas, K., Young, R.A., Chakraborty, A.K., and Sharp, P.A. (2017). A Phase Separation Model for Transcriptional Control. Cell *169*, 13-23. 10.1016/j.cell.2017.02.007.

Hocine, S., Raymond, P., Zenklusen, D., Chao, J.A., and Singer, R.H. (2013). Single-molecule analysis of gene expression using two-color RNA labeling in live yeast. Nat Methods *10*, 119-121. 10.1038/nmeth.2305.

Huang, J., Li, K., Cai, W., Liu, X., Zhang, Y., Orkin, S.H., Xu, J., and Yuan, G.C. (2018). Dissecting super-enhancer hierarchy based on chromatin interactions. Nat Commun *9*, 943. 10.1038/s41467-018-03279-9.

Itoh, Y., Iida, S., Tamura, S., Nagashima, R., Shiraki, K., Goto, T., Hibino, K., Ide, S., and Maeshima, K. (2021). 1,6-hexanediol rapidly immobilizes and condenses chromatin in living human cells. Life Sci Alliance *4*. 10.26508/lsa.202001005.

Jolly, C., Metz, A., Govin, J., Vigneron, M., Turner, B.M., Khochbin, S., and Vourc'h, C. (2004). Stress-induced transcription of satellite III repeats. J Cell Biol *164*, 25-33. 10.1083/jcb.200306104.

Jolly, C., Morimoto, R., Robert-Nicoud, M., and Vourc'h, C. (1997). HSF1 transcription factor concentrates in nuclear foci during heat shock: relationship with transcription sites. J Cell Sci *110 (Pt 23)*, 2935-2941.

Kainth, A.S., Chowdhary, S., Pincus, D., and Gross, D.S. (2021). Primordial super-enhancers: heat shock-induced chromatin organization in yeast. Trends in cell biology *31*, 801-813. 10.1016/j.tcb.2021.04.004.

Kato, M., and McKnight, S.L. (2018). A Solid-State Conceptualization of Information Transfer from Gene to Message to Protein. Annu Rev Biochem *87*, 351-390. 10.1146/annurev-biochem-061516-044700.

Kim, D., Pertea, G., Trapnell, C., Pimentel, H., Kelley, R., and Salzberg, S.L. (2013). TopHat2: accurate alignment of transcriptomes in the presence of insertions, deletions and gene fusions. Genome Biol *14*, R36. 10.1186/gb-2013-14-4-r36.

Kim, S., and Gross, D.S. (2013). Mediator recruitment to heat shock genes requires dual Hsf1 activation domains and mediator tail subunits Med15 and Med16. J Biol Chem *288*, 12197-12213. 10.1074/jbc.M112.449553.

Kmiecik, S.W., Le Breton, L., and Mayer, M.P. (2020). Feedback regulation of heat shock factor 1 (Hsf1) activity by Hsp70-mediated trimer unzipping and dissociation from DNA. The EMBO journal *39*, e104096. 10.15252/embj.2019104096.

Krakowiak, J., Zheng, X., Patel, N., Feder, Z.A., Anandhakumar, J., Valerius, K., Gross, D.S., Khalil, A.S., and Pincus, D. (2018). Hsf1 and Hsp70 constitute a two-component feedback loop that regulates the yeast heat shock response. Elife *7*. 10.7554/eLife.31668.

Kremer, S.B., and Gross, D.S. (2009). SAGA and Rpd3 chromatin modification complexes dynamically regulate heat shock gene structure and expression. J Biol Chem *284*, 32914-32931. 10.1074/jbc.M109.058610.

Kroschwald, S., Maharana, S., Mateju, D., Malinovska, L., Nuske, E., Poser, I., Richter, D., and Alberti, S. (2015). Promiscuous interactions and protein disaggregases determine the material state of stress-inducible RNP granules. Elife *4*, e06807. 10.7554/eLife.06807.

Kroschwald, S., Maharana, S., and Simon, A. (2017). Hexanediol: a chemical probe to investigate the material properties of membrane-less compartments.

Langmead, B., and Salzberg, S.L. (2012). Fast gapped-read alignment with Bowtie 2. Nat Methods *9*, 357-359. 10.1038/nmeth.1923.

Lenstra, T.L., and Larson, D.R. (2016). Single-Molecule mRNA Detection in Live Yeast. Curr Protoc Mol Biol *113*, 14 24 11-14 24 15. 10.1002/0471142727.mb1424s113.

Li, H., Handsaker, B., Wysoker, A., Fennell, T., Ruan, J., Homer, N., Marth, G., Abecasis, G., Durbin, R., and Genome Project Data Processing, S. (2009). The Sequence Alignment/Map format and SAMtools. Bioinformatics *25*, 2078-2079. 10.1093/bioinformatics/btp352.

Longtine, M.S., McKenzie, A., 3rd, Demarini, D.J., Shah, N.G., Wach, A., Brachat, A., Philippsen, P., and Pringle, J.R. (1998). Additional modules for versatile and economical PCR-based gene deletion and modification in Saccharomyces cerevisiae. Yeast *14*, 953-961. 10.1002/(SICI)1097-0061(199807)14:10<953::AID-YEA293>3.0.CO;2-U.

Lu, F., Portz, B., and Gilmour, D.S. (2019). The C-Terminal Domain of RNA Polymerase II Is a Multivalent Targeting Sequence that Supports Drosophila Development with Only Consensus Heptads. Mol Cell *73*, 1232-1242 e1234. 10.1016/j.molcel.2019.01.008.

Lu, Y., Wu, T., Gutman, O., Lu, H., Zhou, Q., Henis, Y.I., and Luo, K. (2020). Phase separation of TAZ compartmentalizes the transcription machinery to promote gene expression. Nat Cell Biol 22, 453-464. 10.1038/s41556-020-0485-0.

Mahat, D.B., Salamanca, H.H., Duarte, F.M., Danko, C.G., and Lis, J.T. (2016). Mammalian Heat Shock Response and Mechanisms Underlying Its Genome-wide Transcriptional Regulation. Mol. Cell *62*, 63-78. 10.1016/j.molcel.2016.02.025.

Masser, A.E., Kang, W., Roy, J., Mohanakrishnan Kaimal, J., Quintana-Cordero, J., Friedlander, M.R., and Andreasson, C. (2019). Cytoplasmic protein misfolding titrates Hsp70 to activate nuclear Hsf1. Elife *8*. 10.7554/eLife.47791.

Nair, R.R., Zabezhinsky, D., Gelin-Licht, R., Haas, B.J., Dyhr, M.C., Sperber, H.S., Nusbaum, C., and Gerst, J.E. (2021). Multiplexed mRNA assembly into ribonucleoprotein particles plays an operon-like role in the control of yeast cell physiology. Elife *10*. 10.7554/eLife.66050.

Nair, S.J., Yang, L., Meluzzi, D., Oh, S., Yang, F., Friedman, M.J., Wang, S., Suter, T., Alshareedah, I., Gamliel, A., et al. (2019). Phase separation of ligand-activated enhancers licenses cooperative chromosomal enhancer assembly. Nat Struct Mol Biol *26*, 193-203. 10.1038/s41594-019-0190-5.

Patel, A., Lee, H.O., Jawerth, L., Maharana, S., Jahnel, M., Hein, M.Y., Stoynov, S., Mahamid, J., Saha, S., Franzmann, T.M., et al. (2015). A Liquid-to-Solid Phase Transition of the ALS Protein FUS Accelerated by Disease Mutation. Cell *162*, 1066-1077. 10.1016/j.cell.2015.07.047.

Peffer, S., Goncalves, D., and Morano, K.A. (2019). Regulation of the Hsf1-dependent transcriptome via conserved bipartite contacts with Hsp70 promotes survival in yeast. J Biol Chem *294*, 12191-12202. 10.1074/jbc.RA119.008822.

Picard, D., Khursheed, B., Garabedian, M., Fortin, M., Lindquist, S., and Yamamoto, K. (1990). Reduced levels of hsp90 compromise steroid receptor action *in vivo*. Nature *348*, 166-168.

Pincus, D., Anandhakumar, J., Thiru, P., Guertin, M.J., Erkine, A.M., and Gross, D.S. (2018). Genetic and epigenetic determinants establish a continuum of Hsf1 occupancy and activity across the yeast genome. Mol Biol Cell *29*, 3168-3182. 10.1091/mbc.E18-06-0353.

Plotly Technologies Inc. (2015). Collaborative data science. Plotly Technologies Inc.
R Core Team (2020). R: A Language and Environment for Statistical Computing. R Foundation for Statistical Computing.

Ramirez, F., Ryan, D.P., Gruning, B., Bhardwaj, V., Kilpert, F., Richter, A.S., Heyne, S., Dundar, F., and Manke, T. (2016). deepTools2: a next generation web server for deep-sequencing data analysis. Nucleic Acids Res *44*, W160-165. 10.1093/nar/gkw257.

Rawat, P., Boehning, M., Hummel, B., Aprile-Garcia, F., Pandit, A.S., Eisenhardt, N., Khavaran, A., Niskanen, E., Vos, S.M., Palvimo, J.J., et al. (2021). Stress-induced nuclear condensation of NELF drives transcriptional downregulation. Mol Cell 81, 1013-1026 e1011. 10.1016/j.molcel.2021.01.016.

Robinson, J.T., Thorvaldsdottir, H., Winckler, W., Guttman, M., Lander, E.S., Getz, G., and Mesirov, J.P. (2011). Integrative genomics viewer. Nat Biotechnol *29*, 24-26. 10.1038/nbt.1754.

Royer, L.A., Weigert, M., Gunther, U., Maghelli, N., Jug, F., Sbalzarini, I.F., and Myers, E.W. (2015). ClearVolume: open-source live 3D visualization for light-sheet microscopy. Nat Methods *12*, 480-481. 10.1038/nmeth.3372.

Rueden, C.T., Schindelin, J., Hiner, M.C., DeZonia, B.E., Walter, A.E., Arena, E.T., and Eliceiri, K.W. (2017). ImageJ2: ImageJ for the next generation of scientific image data. BMC Bioinformatics *18*, 529. 10.1186/s12859-017-1934-z.

Ruff, K.M., Choi, Y.H., Cox, D., Ormsby, A.R., Myung, Y., Ascher, D.B., Radford, S.E., Pappu, R.V., and Hatters, D.M. (2021). Sequence grammar underlying unfolding and phase separation of globular proteins. bioRxiv, 2021.2008.2020.457073. 10.1101/2021.08.20.457073.

Sabari, B.R., Dall'Agnese, A., Boija, A., Klein, I.A., Coffey, E.L., Shrinivas, K., Abraham, B.J., Hannett, N.M., Zamudio, A.V., Manteiga, J.C., et al. (2018). Coactivator condensation at super-enhancers links phase separation and gene control. Science *361*. 10.1126/science.aar3958.

Sabari, B.R., Dall'Agnese, A., and Young, R.A. (2020). Biomolecular Condensates in the Nucleus. Trends Biochem Sci *45*, 961-977. 10.1016/j.tibs.2020.06.007.

Sanborn, A.L., Yeh, B.T., Feigerle, J.T., Hao, C.V., Townshend, R.J., Lieberman Aiden, E., Dror, R.O., and Kornberg, R.D. (2021). Simple biochemical features underlie transcriptional activation domain diversity and dynamic, fuzzy binding to Mediator. Elife *10*. 10.7554/eLife.68068.

Sanders, D.W., Kedersha, N., Lee, D.S.W., Strom, A.R., Drake, V., Riback, J.A., Bracha, D., Eeftens, J.M., Iwanicki, A., Wang, A., et al. (2020). Competing Protein-RNA Interaction Networks Control Multiphase Intracellular Organization. Cell *181*, 306-324 e328. 10.1016/j.cell.2020.03.050.

Sarkar, D., Zhu, Z.I., Knoll, E.R., Paul, E., Landsman, D., and Morse, R.H. (2022). Mediator dynamics during heat shock in budding yeast. Genome Res 32, 111-123. 10.1101/gr.275750.121.

Schindelin, J., Arganda-Carreras, I., Frise, E., Kaynig, V., Longair, M., Pietzsch, T., Preibisch, S., Rueden, C., Saalfeld, S., Schmid, B., et al. (2012). Fiji: an open-source platform for biological-image analysis. Nat Methods *9*, 676-682. 10.1038/nmeth.2019.

Schneider, C.A., Rasband, W.S., and Eliceiri, K.W. (2012). NIH Image to ImageJ: 25 years of image analysis. Nat Methods *9*, 671-675. 10.1038/nmeth.2089.

Shin, Y., and Brangwynne, C.P. (2017). Liquid phase condensation in cell physiology and disease. Science *357*. 10.1126/science.aaf4382.

Sorger, P.K. (1990). Yeast heat shock factor contains separable transient and sustained response transcriptional activators. Cell *62*, 793-805.

Stortz, M., Presman, D.M., Pecci, A., and Levi, V. (2021). Phasing the intranuclear organization of steroid hormone receptors. Biochem J 478, 443-461. 10.1042/BCJ20200883.

Trotter, E.W., Berenfeld, L., Krause, S.A., Petsko, G.A., and Gray, J.V. (2001). Protein misfolding and temperature up-shift cause G1 arrest via a common mechanism dependent on heat shock factor in Saccharomyces cerevisiae. Proc Natl Acad Sci U S A *98*, 7313-7318. 10.1073/pnas.121172998.

Tuttle, L.M., Pacheco, D., Warfield, L., Wilburn, D.B., Hahn, S., and Klevit, R.E. (2021). Mediator subunit Med15 dictates the conserved "fuzzy" binding mechanism of yeast transcription activators Gal4 and Gcn4. Nat Commun *12*, 2220. 10.1038/s41467-021-22441-4.

Vinayachandran, V., Reja, R., Rossi, M.J., Park, B., Rieber, L., Mittal, C., Mahony, S., and Pugh, B.F. (2018). Widespread and precise reprogramming of yeast protein-genome interactions in response to heat shock. Genome Res. 10.1101/gr.226761.117.

Wang, N., Lo Presti, L., Zhu, Y.H., Kang, M., Wu, Z., Martin, S.G., and Wu, J.Q. (2014). The novel proteins Rng8 and Rng9 regulate the myosin-V Myo51 during fission yeast cytokinesis. J Cell Biol *205*, 357-375. 10.1083/jcb.201308146.

Wei, M.T., Chang, Y.C., Shimobayashi, S.F., Shin, Y., Strom, A.R., and Brangwynne, C.P. (2020). Nucleated transcriptional condensates amplify gene expression. Nat Cell Biol *22*, 1187-1196. 10.1038/s41556-020-00578-6.

Whyte, W.A., Orlando, D.A., Hnisz, D., Abraham, B.J., Lin, C.Y., Kagey, M.H., Rahl, P.B., Lee, T.I., and Young, R.A. (2013). Master transcription factors and Mediator establish super-enhancers at key cell identity genes. Cell *153*, 307-319. S0092-8674(13)00392-9 [pii] 10.1016/j.cell.2013.03.035.

Yoo, H., Bard, J.A.M., Pilipenko, E.V., and Drummond, D.A. (2022). Chaperones directly and efficiently disperse stress-triggered biomolecular condensates. Mol Cell 82, 741-755 e711. 10.1016/j.molcel.2022.01.005.

Zamudio, A.V., Dall'Agnese, A., Henninger, J.E., Manteiga, J.C., Afeyan, L.K., Hannett, N.M., Coffey, E.L., Li, C.H., Oksuz, O., Sabari, B.R., et al. (2019). Mediator Condensates Localize Signaling Factors to Key Cell Identity Genes. Mol Cell 76, 753-766 e756. 10.1016/j.molcel.2019.08.016.

Zander, G., Hackmann, A., Bender, L., Becker, D., Lingner, T., Salinas, G., and Krebber, H. (2016). mRNA quality control is bypassed for immediate export of stress-responsive transcripts. Nature *540*, 593-596. 10.1038/nature20572

Zhang, H., Shao, S., Zeng, Y., Wang, X., Qin, Y., Ren, Q., Xiang, S., Wang, Y., Xiao, J., and Sun, Y. (2022). Reversible phase separation of HSF1 is required for an acute transcriptional response during heat shock. Nat Cell Biol 24, 340-352. 10.1038/s41556-022-00846-7.

Zhang, Y., Liu, T., Meyer, C.A., Eeckhoute, J., Johnson, D.S., Bernstein, B.E., Nusbaum, C., Myers, R.M., Brown, M., Li, W., and Liu, X.S. (2008). Model-based analysis of ChIP-Seq (MACS). Genome Biol 9, R137. 10.1186/gb-2008-9-9-r137.

Zheng, X., Beyzavi, A., Krakowiak, J., Patel, N., Khalil, A.S., and Pincus, D. (2018). Hsf1 Phosphorylation Generates Cell-to-Cell Variation in Hsp90 Levels and Promotes Phenotypic Plasticity. Cell Rep *22*, 3099-3106. 10.1016/j.celrep.2018.02.083.

Zheng, X., Krakowiak, J., Patel, N., Beyzavi, A., Ezike, J., Khalil, A., and Pincus, D. (2016). Dynamic control of Hsf1 during heat shock by a chaperone switch and phosphorylation. Elife *5*. http://dx.doi.org/10.7554/eLife.18638.

Zid, B.M., and O'Shea, E.K. (2014). Promoter sequences direct cytoplasmic localization and translation of mRNAs during starvation in yeast. Nature *514*, 117-121. 10.1038/nature13578.

A1.8 Methods

Resource availability

Lead contact for reagent and resource sharing

Further information and requests for resources and reagents should be directed to and will be fulfilled by the Lead Contact, Dr. David Pincus (pincus@uchicago.edu).

Materials availability

S. cerevisiae strains and plasmids generated in this study are available from the lead contact upon request.

Experimental models and subject details

All *S. cerevisiae* strains were grown in YPD (yeast extract-peptone-dextrose) or SDC (synthetic dextrose complete) media at 30°C as indicated below.

A1.8.1 Yeast Strains

For tagging Hsf1, Med15 and Rpb3 with mCherry, PCR amplicons with mCherry coding sequence and homology to 3'-ends of either *HSF1*, *MED15* and *RPB3* were amplified from plasmid pFA6a-mCherry-hphMX6. The amplicons were transformed into the respective strains for in-frame insertion of mCherry. Primers used in strain construction are listed in Table S6.

For Myc x 9 tagging of Med15, genomic DNA of a previously myc9-tagged *MED15* strain (ASK201) (Anandhakumar et al., 2016) was used as template to amplify MYCx 9::TRP1 cassette flanked by DNA homologous to 3'-end of *MED15*. This amplicon was transformed in strains DSG144 and LRY003 to obtain strains ASK213 and ASK214, respectively. LRY003 is a derivative of previously described strain ASK804 (Chowdhary et al., 2019) in which TRP1 was deleted by replacing with KAN-MX.

For Myc x 13 tagging of Med15, plasmid pFA6a-13Myc-His3MX was used as template to obtain MYC13-HIS3 amplicon with homology to 3'-end of *MED15*. This amplicon was transformed in strains DPY144, DPY417 and DPY418 to obtain strains ASK215, ASK216 and ASK217, respectively.

For MS2-MCP labelling of *HSP12* mRNA, MCP-mCherry-URA3 cassette was amplified from plasmid pSH100 with primers Fw MCP-mCherry-Ura3 and Rv MCP-mCherry-Ura3. This cassette was inserted at the endogenous *URA3* locus in strain DPY032 to obtain strain SCY008. Next, 24xMS2-loxP-KANMX6-loxP cassette was amplified from plasmid pDZ415 using primers Fw HSP12-MS2-loxp-KanMX6-loxp and Rv HSP12-MS2-loxp-KanMX6-loxp. This cassette was inserted in the 3'-UTR region of *HSP12* (immediately after stop codon) of strain SCY008 to obtain strain SCY009. Finally, plasmid pSH69 was transformed to express Cre recombinase in strain SCY010 that led to the removal of KANMX in strain SCY011.

The diploid strain ASK741 was created by crossing a MATα derivative of strain DSG200 (Chowdhary et al., 2019) with MATa DSG200.

Plasmids pNH604-HSF1pr-HSF1-GFP and pNH604-HSF1pr-HSF1(147-833)-GFP were used as templates for quick change PCR (Primers, Fw subCE2-AAA and Rv subCE2-AAA) to create CE2->AAA mutation in WT and ΔNTA HSF1, respectively. These plasmids were linearized with Pme I (New England Biolabs) and transformed in strain DPY034 for integration at the *TRP1* locus to obtain strains *DPY1805* and DPY1818. Loss of parental HSF1 plasmid was confirmed by growth on 5-FOA media.

A complete list of strains is provided in Table S1. PCR primer sequences are provided in Table S6.

A1.8.2 Culture Conditions

For microscopy, cells were grown at 30°C in SDC (synthetic dextrose complete) media to early-log density (A_{600} = 0.4-0.5).

For 3C, ChIP and RT-qPCR analyses, cells were grown at 30°C in YPD (yeast extract-peptone-dextrose) to a mid-log density (A_{600} = 0.65-0.8). A portion of the culture was maintained at 30°C as non-heat-shocked (NHS) sample while the remainder (heat-shocked (HS) sample) was subjected to an instantaneous 30°C to 39°C thermal upshift for the indicated duration.

For spot dilution analysis**,** cells were grown to stationary phase in YPD media. Master suspensions were prepared by diluting the saturated cultures to a uniform cell density (A_{600}=0.3) and were transferred to a 96-well microtiter plate. These were then serially diluted (five-fold). 4 µl of each dilution were transferred onto solid YPDA plates. Cells were grown at either 30° or 37°C for 30 h.

A1.8.3 Chromosome Conformation Capture

TaqI-3C was conducted essentially as previously described (Chowdhary et al., 2017; 2020; Chowdhary et al., 2019). Briefly, cells were cultured to a mid-log density (A_{600} = 0.8) at 30°C. They were either maintained at 30°C or heat-shocked at 39°C for 10 min (or as indicated), and then crosslinked with formaldehyde (1% final concentration). For 3C assay involving hexanediol treatment, cells were heat-shocked at 39°C for 2.5 min followed by treatment with either 2,5- or 1,6-hexanediol (5% final concentration), and then crosslinked with formaldehyde. Crosslinked cells were harvested and lysed in FA lysis buffer (50 mM HEPES pH 7.9, 140 mM NaCl, 1% Triton X-100, 0.1% Sodium deoxycholate, 1 mM EDTA, 1 mM PMSF) for two cycles (20 min each) of vortexing at 4°C. A 10% fraction of the chromatin lysate was digested using 200 U of Taq I (New England Biolabs) at 60°C for 7 h. Taq I was heat-inactivated at

80°C for 20 min. The digested chromatin fragments were centrifuged, and the pellet was resuspended in 100 µl of 10 mM Tris-HCl (pH 7.5). The Taq I-digested chromatin was diluted 7-fold to which 10,000 cohesive end units of Quick T4 DNA ligase (New England Biolabs) were added. Proximity ligation was performed at 25°C for 2h. The ligated sample was digested with RNase at 37°C for 20 min and then Proteinase K at 65°C for 12 h. The 3C DNA template was extracted using phenol-chloroform and then precipitated.

The interaction frequencies were quantified using qPCR. Quantitative PCR was performed on a CFX Real-Time PCR system (Bio-Rad) using Power SYBR Green PCR master mix (Fisher Scientific). Sequences of 3C primers used in this study are provided in Table S2. Normalization controls were used to account for the following: (i) variation in primer pair efficiencies; (ii) primer dimer background; (iii) variation in the recovery of 3C templates; and (iv) to ensure a ligation-dependent 3C signal. For detailed algorithms to calculate normalized 3C interaction frequencies, see below and (Chowdhary et al., 2020).

A1.8.4 Chromatin Immunoprecipitation (ChIP)

ChIP was conducted essentially as previously described (Chowdhary et al., 2019). Briefly, the cells were heat-shocked at 39°C for 7.5 min (or maintained at 30°C) and crosslinked with 1% formaldehyde. Cells were then harvested and subjected to glass bead lysis in lysis buffer (50 mM HEPES pH 7.5, 140 mM NaCl, 1% Triton X-100, 0.1% Sodium deoxycholate, 1 mM EDTA, 2 mM PMSF, and 250 µg/ml cOmplete™, EDTA-free Protease Inhibitor Cocktail) for 30 min at 4°C. The chromatin lysate was sonicated to an average size of ~250 bp using 40 cycles of sonication (30 sec on/off High-Power setting; Diagenode Biorupter Plus). A 20% fraction of the sonicated chromatin was incubated with one of the following antibodies: 1 µl of anti-Rpb1; 1 µl of anti-Hsf1 (Chowdhary et al., 2019) or 2.5 µl of anti-Myc (Santa Cruz Biotechnology) for 16 h at 4°C. Antibody-chromatin complexes were immobilized on Protein A-Sepharose beads (GE Healthcare) for 16 h at 4°C, then washed sequentially with lysis buffer, high salt buffer (50

mM HEPES pH 7.5, 500 mM NaCl, 1% Triton X-100, 0.1% Sodium Deoxycholate, 1 mM EDTA), wash buffer (10 mM Tris pH 8.0, 250 mM LiCl, 0.5% NP-40, 0.5% Sodium Deoxycholate, 1 mM EDTA) and finally 1x TE (10 mM Tris-HCl pH 8.0, 0.5 mM EDTA). Chromatin was eluted by incubating the beads in elution buffer (50 mM Tris pH 8.0, 1% SDS, 10 mM EDTA) at 65°C for 30 min. RNA and proteins were removed by DNase-free RNase (final concentration of 200 µg/ml; incubation at 37°C for 1 h) and Proteinase K (final concentration of 50 µg/ml; incubation at 60°C for 16 h). The ChIP template was extracted using phenol-chloroform and precipitated in presence of ethanol.

ChIP occupancy signals were quantified using qPCR. Sequences of ChIP primers used in this study are provided in Table S4. The ChIP DNA quantities were deduced from interpolation of a standard curve generated using genomic DNA template. The qPCR signal for each primer combination was normalized to the corresponding signal from the input DNA. The input DNA control was incorporated to correct for variation in the recovery of ChIP DNA templates.

A1.8.5 Reverse Transcription-qPCR (RT-qPCR)

Cells were cultured to a mid-log density (A_{600} = 0.8) at 30°C, and were either maintained at 30°C or heat-shocked at 39°C for times indicated. 20 mM sodium azide was added at appropriate times to terminate transcription. Cells were then harvested and subjected to glass bead lysis in presence of TRIzol (Invitrogen) and chloroform for 10 min at 4°C. Total RNA was precipitated in ethanol. A fraction of total RNA (~20 µg) was treated with DNase I (RNase-free; New England Biolabs) at 37°C for 15 min. DNase I was heat-inactivated at 75°C for 10 min. RNA was purified using the RNA clean and concentrator kit (Zymo Research). 2-3 µg of the purified RNA template and random hexamers were used for preparing cDNA (Superscript IV first-strand synthesis system; Invitrogen).

The cDNA reaction mix was diluted 2-fold, and 2 µl of the diluted cDNA template was used for qPCR reaction. Sequences of primers used for RT-qPCR analysis in this study are provided in Table S5. Relative cDNA levels were quantified using the ΔΔCt method (see Chowdhary et al., 2017). qPCR signal from *SCR1* Pol III transcript was used as a normalization control. This accounted for variation in the recovery of cDNA templates. Relative fold change per minute in mRNA expression was calculated by dividing mean mRNA levels (derived from two independent biological samples) for a given time point by previous time point, and then by the time elapsed in minutes.

A1.8.6 Fluorescence microscopy

For live-cell imaging, cells were grown at 30°C to early log phase (A_{600} = 0.5) in synthetic dextrose complete (SDC) medium. An aliquot of living cells was immobilized onto concanavalin A-coated glass bottom dish. Fresh SDC medium was added in the dish before imaging. Images were taken on Leica TCS SP5 II STED-CW laser scanning confocal microscope (Leica Microsystems, Inc., Buffalo Grove, IL) equipped with GaAsP hybrid detector and STED mode turned off. Samples were subjected to heat shock at 39°C by heating the objective (HCX PL APOCS 63x/1.4 oil UV) with Bioptechs objective heater system and by controlling the temperature of air flowing through the incubator chamber enclosing the microscope. Argon laser was used at lines 488 and 514 nm for excitation of GFP and mVenus. The orange HeNe laser light source was used for excitation of mCherry at 594 nm. STED laser (592 nm) was turned off for all live imaging experiments, except during STED imaging in Figures 2A, B (see below for details). For experiments involving hexanediol treatment, cells were heat-shocked and imaged for ~8 min. Immediately after this, the SDC media in the dish

was replaced with pre-warmed (39°C) SDC supplemented with either 2,5- or 1,6-hexanediol (5% final concentration), and cells were imaged at 39°C for the times indicated.

The images were acquired in xyz scan mode, covering 8 to 10 planes on the z-axis with an interplanar distance of 0.25 µm. For dual-color imaging of live cells, fluorophores were sequentially scanned in two channels with scanning modes switched on between lines. The sequential capture allowed rapid scanning of fluorophores in both channels while minimizing bleed-through or channel crosstalk. Post-acquisition, images were deconvolved by YacuDecu function that utilizes Richardson-Lucy algorithm for calculating theoretical Point Spread Functions (PSFs) (https://github.com/bnorthan) (Rueden et al., 2017). The PSFs were computed each time based on the set of microscopy parameters used in the imaging analyses. Custom plugins for Fiji (Schindelin et al., 2012) were used to colorize, split or merge channels, make composites and adjust brightness of the images. 3D rendering and visualization were performed using either ClearVolume (Royer et al., 2015) or arivis Vision 4D software v. 3.1 (render mode: maximum intensity; arivis AG, Rostok, Germany). For images processed without deconvolution (Figure S2A-D), images were acquired as above and custom plugins for Fiji were used to colorize, split or merge channels, subtract background and apply gaussian blur.

For colocalization analyses, the fractional overlap metric scores (Manders' colocalization coefficients) were calculated using JACoP plugin implemented in ImageJ (Bolte and Cordelieres, 2006; Schneider et al., 2012). The average intensity plots were generated using the plot profile feature in ImageJ. Intensities of pixels were obtained along the line path (as indicated in Figure 1G) for each z-section. Intensities across nine individual z-sections were combined and the average was plotted for each channel.

For analysis of gene coalescence, nine z-planes with an interplanar distance of 0.5 µm, covering the entire depth of the nucleus, were inspected for location of tagged genomic loci. The relative

nuclear positions of the tagged loci were assessed by measuring 3D distances between them. 3D distances were measured as 3D polyline lengths between the signal centroids of tagged gene loci. A cell was scored positive for coalescence if the 3D distance between the centroids was between 0.3 and 0.7 µm. 3D distance measurements, 3D rendering, and visualization were performed in arivis Vision4D.

A1.8.7 Stimulated emission depletion (STED) super-resolution microscopy in live cells

Samples for STED imaging were prepared as described for live imaging, except live cells were subjected to heat shock at 39°C by heating the objective (STED rated HCX PL APO 100x/1.4 oil) and incubator chamber enclosing the microscope. High-resolution STED images of cells expressing Hsf1-mVenus were acquired in xyz scan mode (z=9; interplanar distance=0.25 µm) on Leica TCS SP5 II STED-CW laser scanning confocal microscope with STED mode turned on. The 514 nm line from argon ion laser light source was used to excite mVenus. Emission depletion was accomplished with 592 nm continuous wave STED laser. Images were deconvolved as above, then rendered (render mode: volumetric) and visualized in arivis Vision4D. STED microscopy was used for acquiring images analyzed and presented in Figure 2A, B.

A1.9 Quantification and statistical analysis

A1.9.1 Hsf1, Med15 and Rpb1 ChIP-seq data analysis

Hsf1 ChIP-seq data were obtained from GSE117653 (Pincus et al., 2018). Med15 data are from PRJNA657372 (Sarkar et al., 2022). Rpb1 ChIP-seq data were obtained from GSE125226 (Albert et al., 2019). Reads were aligned to the *S. cerevisiae* reference genome (SacCer3) using Bowtie 2 (Langmead and Salzberg, 2012). SAM files were converted to BAM format using SAMtools (Li et al., 2009). BAM files were then converted to bigWig and bedGraph format at bin size of 1 (-bs 1) and normalized to the library size (--normalizeUsing

CPM) using bamCoverage function of deepTools2 (Ramirez et al., 2016). The bigWig files were used to obtain genome browser tracks in Integrative Genomics Viewer (IGV) browser (Robinson et al., 2011), and to make metagene plots. Metagene profiles were created using computeMatrix and plotProfile function tools in deepTools2. The plots are scaled +/-1 kb of ORFs of the Hsf1-dependent genes (Pincus et al., 2018). Occupancy of Hsf1, Med15 and Rpb1 (Pol II) were computed using the bedtools map function. The occupancy of Hsf1 and Med15 were obtained as sum of signals across 1 kb region upstream of ORFs of protein-coding genes. For occupancy of Pol II, sum of signals across ORFs were normalized to length of the ORFs.

For analysis of co-occupancy between Hsf1 and Med15, peaks were called using MACS2 algorithm (Zhang et al., 2008) with -g 1.2e7 --keep-dup auto flags. Peaks identified on repetitive regions of telomeres and rDNA were excluded from the analysis. The overlap of Med15 and Hsf1 peaks was computed using intersect Bed -wa -u -a Med15_peaks.bed -b Hsf1_peaks.bed option.

For analysis of Pol II distribution at Hsf1 genes, CPKM of Pol II reads were obtained for all non-overlapping, verified ORFs archived in SGD (Cherry et al., 2012) using the bedtools map function. These normalized counts were then used to calculate % Pol II reads at Hsf1 gene targets in comparison to all other genes in the yeast genome.

A1.9.2 Nascent transcript sequencing data analysis

NAC-seq data were obtained from GSE117653 (Pincus et al., 2018). Reads were aligned to the *S. cerevisiae* reference genome (SacCer3) using TopHat2 (Kim et al., 2013) with --segment-length 20 -I 2500 options. Wiggle files were generated by normalizing to the library size (--normalizeUsing CPM) using the bamCoverage function of deepTools2 and visualized in IGV genome browser.

A1.9.3 Foci counting and characterization

Hsf1, Med15 and Rpb3 foci were detected and quantified within 3D live-cell images using the automated FindFoci plugin (Herbert et al., 2014) in ImageJ. For foci detection in 3D, a region of interest was marked around the nucleus of each cell and then foci within the marked regions were identified across all z planes (z=9). We used the optimizer function in the plugin submenu to train FindFoci algorithm and predict optimum parameter settings for foci assignment. The following set of optimized parameters were applied to all images in this study: (a) background, one standard deviation above mean; (b) search method, above background with an optimal value of 0.3; and (c) merge option, relative above background with peak parameter of 0.2 and minimum size as 1. Finally, we used the x, y, z position coordinates and sizes of peak intensity regions to present foci as 3D bubble charts. The 3D bubble charts were created by calling bubblechart3 function in MATLAB (MATLAB, 2021. *version 9.11.0.1873467* (R2021b), Natick, MA: The MathWorks, Inc.).

For visualizing images as 3D surface plots, a square of 10 × 10 pixels was marked around the nucleus of each cell type in each condition (as indicated in Figure 1D). Representative planes of each cell were analyzed and displayed as 3D surface plots using the Interactive 3D Surface Plot plugin in ImageJ (contributing author: Kai Uwe Barthel, Germany). Appropriate parameter settings for scale, rotation, smoothing, and lightning were adapted for the display of 3D surface plots. Note that for each cell type, similar parameter settings were used in both non-heat shock and heat shock conditions.

A1.9.4 Analysis of average relative localization of factors

Foci of LacO-tagged *HSP104* gene locus or MS2-tagged *HSP12* mRNA locus were manually identified in a specific *z* plane and centered within a square of 12 × 12 pixels. Distribution of signal from another channel, depicting nuclear distribution of the secondary factor, was

gathered from corresponding 12 × 12 squares in the same *z* plane. A composite text image was created by computing average of centered images from roughly 30 cells per condition. The intensity of each pixel was scaled from 0 to 100 using a formula for uniform scaling: [(intensity-minimum) / (maximum-minimum)] × 100. For negative control, fifteen 12 × 12 arrays were generated with random numbers from 0 to 100. A composite text image was then created by computing an average of the corresponding values. For positive control, kernel density of a 2D Gaussian distribution was generated in an array and computed using the following formula: $e^{\wedge}(-z^2/(2\sigma^2)) / \sigma (2p)^{-1/2}$. Here, z is in range (-k, k+1) and $\sigma = 1$. This array was then used to create a text image with a scale ranging between 0 and 100. Finally, text images of controls or test samples were used to generate contour plots using the Plotly function (Plotly Technologies Inc., 2015) in R (R Core Team, 2020). The intensity minima and maxima were split into 800 steps for all contour plots.

A1.9.5 Quantification of overall and pixel-to-pixel variation within STED-acquired images

For demonstration of internal dynamics of Hsf1 foci, the variation between corresponding pixels of Hsf1 foci was compared against overall variation in the images. For this analysis, we used STED-acquired images of cells expressing Hsf1-mVenus captured at every minute over the intermixing phase of heat shock (8 to 12 min-HS). We marked 12 × 12 pixel squares bounding the nuclei of six individual cells imaged every minute between t1 (8min) and t5 (12min). Next, we obtained maximum intensity projections of the 3D images stacks for each individual nuclei at each of five heat shock time points. All pixel intensities were scaled from 0 to 100 to account for variation in image brightness by computing into the following formula: [(intensity-minimum) / (maximum-minimum)] × 100. Standard deviation was calculated for the min-max normalized pixels to determine pixel-to-pixel variation in Hsf1 levels at the given nuclear locations. Overall standard deviation was computed from average intensities of each

image in the time course. The overall standard deviation was then used to populate a 12 ×12-pixel square for comparison to pixel-to-pixel variation of Hsf1 intensity and presented as heat maps. Six such distributions, each of overall variation and pixel-to-pixel variation, were used to plot cumulative frequency of pixels as a function of standard deviation.

A1.9.6 Quantification of 3C

TaqI-3C data was quantified as described in (Chowdhary et al., 2020; Chowdhary et al., 2019). The percent digestion efficiency was determined by amplifying a region across Taq I restriction site using a pair of convergent primers (sequences provided in Table S3). The percent digestion efficiencies were determined for each primer combination and incorporated into the following formula:

$$\% \text{ digestion} = 100 - \frac{100}{2^{[(Ct_R - Ct_{ARS504})^{\mathbf{DO}} - (Ct_R - Ct_{ARS504})^{\mathbf{UND}}]}}$$

Here, Ct_R is the cycle threshold (Ct) quantification of the digested only (DO) or undigested (UND) templates, and Ct_{ARS504} the cycle threshold quantification of the *ARS504* locus (a region lacking a Taq I site).

For measurement of normalized frequency of intragenic or intergenic interactions, the Ct values for digested only (DO_{3C}) and ligated (Lig_{3C}) templates for crosslinked chromatin, and digested only and ligated genomic DNA (Lig_{gDNA} and DO_{gDNA}, respectively) were incorporated into the following formula:

Normalized Frequency of Interaction =

$$\frac{\left[\left(2^{-\Delta Ct_{Lig_{3C}}}/ARS504_{Lig_{3C}}\right)/\left(2^{-\Delta Ct_{DO_{3C}}}/ARS504_{DO_{3C}}\right)\right]\Big/_{[(Digestion\ site\ 1)\times(Digestion\ site\ 2)]}}{\left[\left(2^{-\Delta Ct_{Lig_{gDNA}}}\Big/ARS504_{Lig_{gDNA}}\right)\Big/\left(2^{-\Delta Ct_{DO_{gDNA}}}\Big/ARS504_{DO_{gDNA}}\right)\right]\Big/_{[(Digestion\ site\ 1)\times(Digestion\ site\ 2)]}}$$

(i): ΔCt values were obtained by subtracting Ct (no-template) from those of Lig_{3C}, DO_{3C}, or gDNA templates.

(ii): $2^{-\Delta Ct}/ARS504$ are the fold-over signals normalized to *ARS504* locus.

(iii): Ligation-dependent signals (LDS) are determined as ratio of fold-over normalized signals of Lig_{3C} and DO_{3C} templates $(2^{-\Delta Ct_{Lig_{3C}}}/ARS504_{Lig_{3C}})/(2^{-\Delta Ct_{DO_{3C}}}/ARS504_{DO_{3C}})$; also applicable to the gDNA control.

(iv): LDS were corrected for variation in Taq I digestion efficiencies of sites 1 and 2 (as detailed above).

(v): Normalized Frequency of Interaction is defined as the ratio of ligation-dependent signals of 3C and gDNA control templates after correcting for differences in their digestion efficiencies.

A1.9.7 Statistical tests used

Student's *t* test (two-tailed) was used to calculate statistical significance between all pairwise comparisons (as assumptions of parametric distributions were fulfilled), except in Figure 2B and D, two sample Kolmogorov–Smirnov test and one-way ANOVA followed by Tukey's post hoc analysis were used, respectively.

Each pairwise comparison is done with means of two independent biological samples (N=2) +SD. n.s., $P>0.05$; *, $P<0.05$; **, $P<0.01$; ***, $P<0.001$.

A1.10 Supplemental tables

A1.10.1 Yeast strains

Strain name	**Genotype**	**Reference/ Source**
DPY001	*MATa ADE2 trp1-1 can1-100 leu2-3,112 his3-11,15 ura3-1*	El-Samad lab
DPY032	DPY001; *HSF1-mVenus::HIS3*	This study
SCY001	DPY001; *MED15-mCherry::hphMX6*	This study
SCY002	DPY001; *RPB3-mCherry::hphMX6*	This study
SCY003	DPY032; *MED15-mCherry::hphMX6*	This study
SCY004	DPY032; *RPB3-mCherry::hphMX6*	This study
DBY255	*MATa ade2-1 can1-100 leu2-3,112 trp1-1 ura3-1 his3-11,15::GFP-LacI::HIS3 HSP104-$LacO_{256}$::TRP1 SEC63-MYC×13::KAN-MX*	Brickner et al., 2012
SCY005	DBY255; *HSF1-mCherry::hphMX6*	This study
SCY006	DBY255; *MED15-mCherry::hphMX6*	This study
SCY007	DBY255; *RPB3-mCherry::hphMX6*	This study
SCY008	DPY032; *ura3-1::MCP-mCherry::URA3*	This study
SCY009	SCY008; *HSP12-$MS2_{24}$-loxp-KAN-MX6-loxp*	This study
SCY010	SCY009; *pSH69-Cre-hphMX6*	This study
SCY011	SCY010*; HSP12-$MS2_{24}$-loxp*	This study
BY4741	*MATa his3Δ1 leu2Δ0 met15Δ0 ura3Δ0*	Chowdhary et al., 2019
DSG144	BY4741; *trp1Δ::KAN-MX*	Gross Lab
ASK804	BY4741; *3xHSE-BUD3*	Chowdhary et al., 2019
LRY003	ASK804*; trp1Δ::KAN-MX*	This study
ASK213	DSG144; *MED15-MYCx9::TRP1*	This study
ASK214	LRY003; *MED15-MYCx9::TRP1*	This study
ASK741	MATα/*MATa; Hsf1-GFP::HIS3MX6/ Hsf1-GFP::HIS3MX6*	This study

ASK727	*MATa/MATa ade2-1/ ade2-1 CAN1^{+}/can1-100 ura3-1/ ura3-1 THR^{+}/thr1-4 leu2-3,112/ leu2-3,112 trp1-1/ trp1^{-} his3-11,15::GFP-LacI::HIS3/ his^{-} HSP104-LacO$_{256}$::TRP1/HSP104^{+} TMA10-tetO$_{200}$::LEU2/TMA10^{+} leu2::tetR-mCherry::hphMX::leu2 SEC63-MYC×13*	Chowdhary et al., 2019
IGY101	*MATa /MATa can1-100 / can1-100 leu2-3,112 / leu2-3,112 trp1-1 / trp1-1 ura3-1 / ura3-1 ade2-1/ ade2-1 ADE2 his3-11,15::GFP-LacI::HIS3/his3-11,15::GFP-LacI::HIS3 HSP104-LacO256::TRP1/HSP104+ PGM2-LacO128::URA3/PGM2+ pGPDmCherry-ER04::TRP1 SEC63-MYC 13:: KAN-MX/SEC63+*	Chowdhary et al., 2019
SCY712	*MATa/MATa his3Δ1/his3Δ1 leu2Δ0/leu2Δ0 lys2Δ0/LYS^{+} met15Δ0/MET^{+} ura3Δ0/ ura3Δ0 SIK1-mRFP::KanMX6/SIK1^{+} POM34-GFP::HIS3MX6/POM34^{+}*	Chowdhary et al., 2019
DPY182	DPY001; *hsf1Δ::KAN; HSF1pr-HSF1-GFP::TRP1*	This study
DPY034	DPY001; *hsf1Δ::KAN; pRS316-HSF1*	This study
DPY1805	DPY001; *trp1-1::HSF1pr-HSF1-ce2AAA-GFP::TRP1*	This study
SCY012	DPY1805; *MED15-mCherry::hphMX6*	This study
SCY013	DPY1805; *RPB3-mCherry::hphMX6*	This study
DPY144	DPY001*; HSE-YFP::LEU2*	Krakowiak et al., 2018
ASK215	DPY144; *MED15-MYCx13::HIS3*	This study
DPY304	DPY001*; HSE-YFP::LEU2 hsf1Δ::KAN HSF1pr-HSF1::TRP1*	Krakowiak et al., 2018
DPY417	DPY001*; HSE-YFP::LEU2 hsf1Δ::KAN HSF1pr-hsf1(147-833)::TRP1*	Krakowiak et al., 2018
ASK216	DPY417; *MED15-MYCx13::HIS3*	This study
DPY179	DPY001; *hsf1Δ::KAN HSF1pr-hsf1(147-833)-GFP::TRP1*	This study

SCY014	DPY179; *MED15-mCherry::hphMX6*	This study
SCY015	DPY179; *RPB3-mCherry::hphMX6*	This study
DPY1818	DPY001; *trp1-1::HSF1pr-hsf1(147-833)-ce2AAA-GFP::TRP1*	This study
SCY016	*DPY1818; MED15-mCherry::hphMX6*	This study
SCY017	DPY1818; *RPB3-mCherry::hphMX6*	This study
DPY418	DPY001*; HSE-YFP::LEU2 hsf1Δ::KAN HSF1pr-hsf1(1-424)::TRP1*	Krakowiak et al., 2018
ASK217	DPY418; *MED15-MYCx13::HIS3*	This study

A1.10.2 Forward primers used in 3C analysis

Name	Sequence (5' → 3')
UBI4 F+524	GTAAGCAGCTAGAAGATGGTAGAACC
UBI4 F+1624	TGATACGGATAGAATATTGTGACTACC
HSP104 F-63	AGGCATTGTAATCTTGCCTCAATTC
HSP104 F+782	GTAAGACCGCTATTATTGAAGGTG
HSP104 F+1550	CCCTTGATGCTGAACGTAGATATG
HSP104 F+2756	AGGTGATGACGATAATGAGGACAG
SSA2 F-242	CACTGCATTCTTACTCTCTCTTGG
SSA2 F+198	AGGTAACAGAACCACTCCATCTTTC
SSA2 F+1368	TCTCTACTTATGCTGACAACCAACC
SSA2 F+2297	AGTGACTTGAAGACTAGGAATATCG
TMA10 F+159	ACGAAGCAAAGTCTAACCCAAAG
TMA10 F+811	ATGCAAAAACACTTCCCAGAATAG
SSA4 F-268	ACACGAAAGATATCTCAACTCTAGCC
SSA4 F+198	GCCTTCTTATGTGGCTTTTACTGAC
SSA4 F+2255	ATAAGAAAGTCATCGCCAAACAAC
HSP12 F-47	ACGTATAAATAGGACGGTGAATTGC
HSP12 F+279	AAAAGGCAAGGATAACGCTGAAG
HSP82 F-290	CCTCTCTCAACACAGTAATCCATAAAC
HSP82 F+740	AATTAGTCGTCACCAAGGAAGTTG
HSP82 F+1445	GCCAGAACACCAAAAGAACATCTAC
HSP82 F+2189	ATGAGGATGAAGAAACAGAGACTGC
ARS504F (internal control)	GTCAGACCTGTTCCTTTAAGAGG

A1.10.3 Reverse primers used for percent digestion determination in 3C

Name	Sequence (5' → 3')
UBI4 R+524	TGAATTTTCGACTTAACGTTGTCG
UBI4 R+1624	ATCACCCAGTATCCCTGATTTCAC
HSP104 R-63	ATCGTTAGAGCCCTTTCTGTAAATTG
HSP104 R+782	TTCTTCGATTTCCTTCAAAACACC
HSP104 R+1550	CCACATTTTGGATCATGGAGTTG
HSP104 R+2756	TCTTTTGCTCGGGTGTCAAGTTC
SSA2 R-242	GATGGAATGTTCTAGAAAAAACTTC
SSA2 R+198	GCTTCATATCACCTTGGACTTCTG
SSA2 R+1368	TTCAATTTGTGGGACACCTCTTG
SSA2 R+2297	GACGCCCTTACGAATAGAACTTTAC
TMA10 R+159	TTTCATTGTTTTGGGAGTTAGAGC
TMA10 R+811	CCGGTTATAGGACCCTTATTGATG
SSA4 R-268	TGTTACTGTCGTCAAACTAAGGAG
SSA4 R+198	TTTACGTCCGATCAGACGCTTAG
SSA4 R+2255	GTGTTAAACTCCGGTCAAAAGAAAC
HSP12 R-47	TTCAGAAGCTTTTTCACCGAATC
HSP12 R+279	AAACCATGTAACTACAAAGAGTTCCG
HSP82 R-290	GAAGGACCTGGTTGGTATTAAGATG
HSP82 R+740	AATGCTTAACGTACAATGGGTCTTC
HSP82 R+1445	ATTCATCAATTGGGTCGGTCAAG
HSP82 R+2189	ACACACTAGACGCGTCGGAATAG
ARS504R (internal control)	CATACCCTCGGGTCAAACAC

A1.10.4 Primers used in ChIP analysis

Name	Sequence (5' → 3')
BUD3 UAS F (-294 to -72)	GCTCTTTGTCATACGCATAGAATTG
BUD3 UAS R	CAGTAGAATGCGAGTACAGACAAAC
HSP104 UAS F (-266 to -195)	CTTAAACGTTCCATAAGGGGC
HSP104 UAS R	TGCAGTTCTTTGAGATGGGCC
HSP104 PROM F (-132 to +41)	AGGCATTGTAATCTTGCCTC TTC
HSP104 PROM R	ATCGTTAGAGCCCTTTCTGTAAATTG

HSP82 UAS F (-393 to -155)	CCTCTCTCAACACAGTAATCCATAAAC
HSP82 UAS R	GAAGGACCTGGTTGGTATTAAGATG
HSP82 PROM F (-156 to -88)	TCCGCCACCCCCTAAAAC
HSP82 PROM R	TGAGGAGGTCACAGATGTTAA
SSA4 UAS F (-396 to -145)	ACACGAAAGATATCTCAACTCTAGCC
SSA4 UAS R	TGTTACTGTCGTCAAACTAAGGAG
SSA4 PROM F (-245 to +35)	AGTTCCTAGAACCTTATGGAAGCAC
SSA4 PROM R	GTTGTACCTAAATCAATACCAACAGC

A1.10.5 Primers used in RT-qPCR analysis

Name	Sequence (5' → 3')
HSP104 F+1922	TTAGCTAATCCAAGGCAACCAG
HSP104 ORF R+1922	ACCTTCATCGTACCCGACATAAC
HSP82 F+1838	ACATGGAAAGAATCATGAAGGCTC
HSP82 R +1838	AAGTCCTTGACAGTCTTGTCTTGAG
SSA4 F+1539	ATCTACTGGGTAAATTTGAGTTGAGC
SSA4 R+1539	CTAGCTGATTCTTAGCTTGAACACG
SSA2 F+1905	CTAAATTGTACCAAGCTGGTGGTG
SSA2 R+1905	AATACAGAGGAAAGCAAAAGTAAAAC
TMA10 F+159	ACGAAGCAAAGTCTAACCCAAAG
TMA10 R+159	TTTCATTGTTTTGGGAGTTAGAGC
UBI4 F+524	GTAAGCAGCTAGAAGATGGTAGAACC
UBI4 R+524	TGAATTTTCGACTTAACGTTGTCG
SCR1 F	CTCCACCTTCACCGCTGTTAG
SCR1 R	AAATATGGTTCAGGACACACTCC

A1.10.6 Primers used in construction of strains

Primer Name	**Sequence (5' → 3')**
Primers used in construction of strains: SCY005	
Fw Hsf1-mCherry-hphMX6	AGGACCCGACAGAGTACAACGATCACCGCCTGCCCAAACGAGCTAAGAAA CCAGCTGAAGCTTCGTAC
Rv Hsf1-mCherry-hphMX6	ACTATATTAAATGATTATATACGCTATTTAATGACCTTGCCCTGTGTA CCGCATAGGCCACTAGTG
Primers used in construction of strains: SCY001, SCY003, SCY006, SCY012, SCY014, SCY016	
Fw Med15-mCherry-hphMX6	GTTCAGAACAATTCAATGTATGGGATTGGAATAATTGGACAAGTGCTACT CCAGCTGAAGCTTCGTAC
Rv Med15-mCherry-hphMX6	CAAACGAAGTAACTTCAAAAGTATCAAAAGTATGGAAACTTCAAATGT CCGCATAGGCCACTAGTG
Primers used in construction of strains: SCY002, SCY004, SCY007, SCY013, SCY015, SCY017	
Fw Rpb3-mCherry-hphMX6	ATGCATCTCAAATGGGTAATACTGGATCAGGAGGGTATGATAATGCTTGG CCAGCTGAAGCTTCGTAC
Rv Rpb3-mCherry-hphMX6	TTCGGTTCGTTCACTTGTTTTTTTTCCTCTATTACGCCCACTTGAGAA CCGCATAGGCCACTAGTG
Primers used in construction of strains: SCY008 and SCY009	
Fw MCP-mCherry-Ura3	ATAAATCATGTCGAAAGCTACATATAAGG
Rv MCP-mCherry-Ura3	GCTCTAATTTGTGAGTTTAGTATACATGCATTTACTTATAATACAGTTTTTTA TTTTTTGCTTTTTCTCTTGAGGTCACATGATCG
Fw HSP12-MS2-loxp-KanMX6-loxp	TATGTTTCCGGTCGTGTCCACGGTGAAGAAGACCCAACCAAGAAGTAA GCCGCTCTAGAACTAGTGGATCC

Rv HSP12-MS2-loxp-KanMX6-loxp	ACACATCATAAAGAAAAAACCATGTAACTACAAAGAGTTCCGAAAGAT GCATAGGCCACTAGTGGATCTG
Primers used in construction of strains: ASK213 and ASK214	
Fw Med15-myc9	GATTCTCCTGATGACCCATTCATGAC
Rv Med15-myc9	CTGATGATAGTCAAGTCCATTGG
Primers used in construction of strains: ASK215, ASK216 and ASK217	
Fw Med15-myc13	GTTCAGAACAATTCAATGTATGGGATTGGAATAA TTGGACAAGTGCTACTCGGATCCCCGGGTTAATTAACG
Rv Med15-myc13	CACCAAACGAAGTAACTTCAAAAGTATCAAAAGT ATGGAAACTTCAAATGTGAATTCGAGCTCGTTTAAAC
Primers used in construction of strains: DPY1805 and DPY1818	
Fw subCE2-AAA	CCAATAAGGCCCTATAAACAAAGAGCTGCTGCTAAAAATA GAGCCAATTCCTCG
Rv subCE2-AAA	CGAGGAATTGGCTCTATTTTTAGCAGCAGCTCTTTGTTTA TAGGGCCTTATTGG

Figure S1

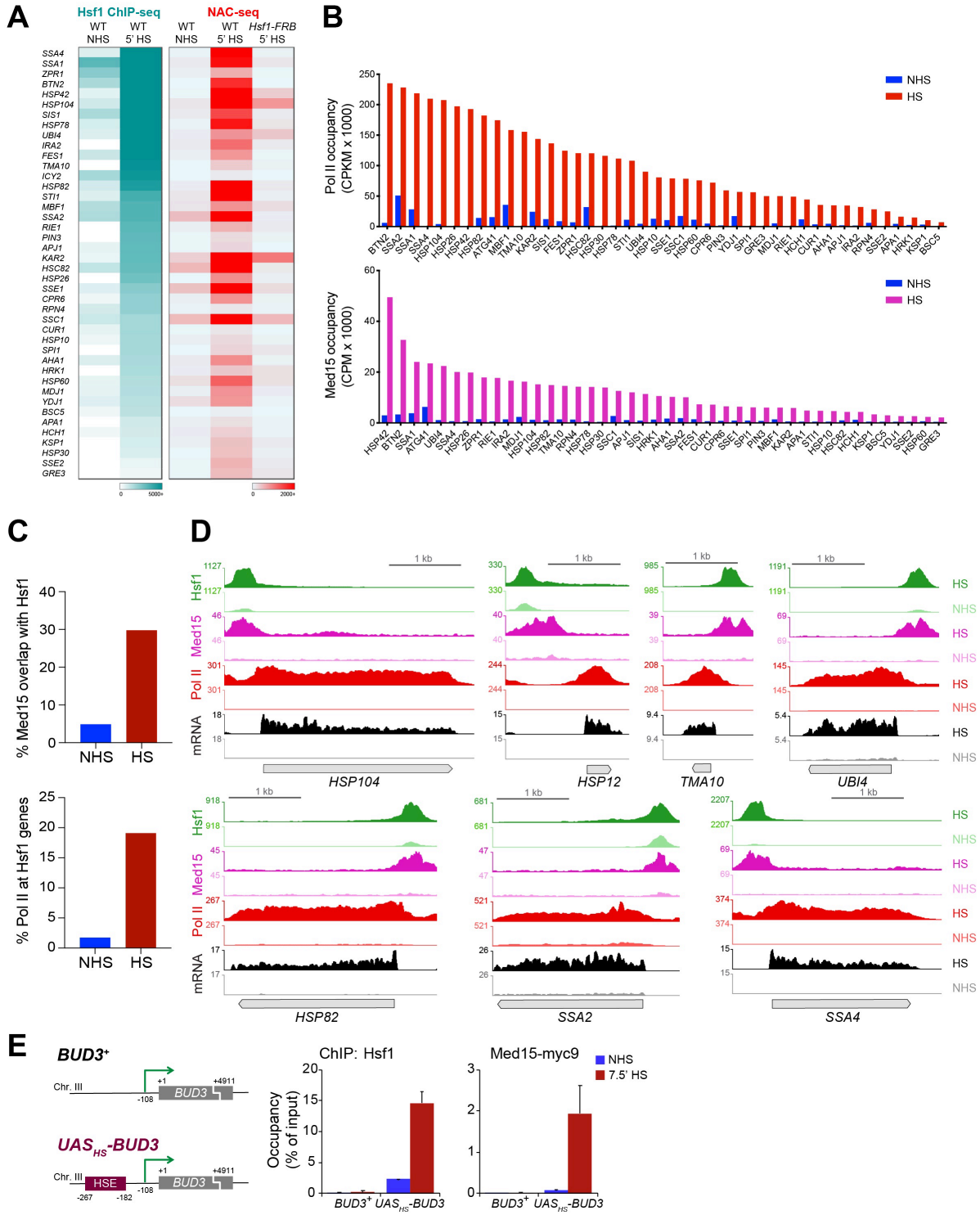

Figure A1.11.1. Heat shock genes associate with exceptionally high levels of Hsf1, Mediator and RNA Pol II

A) Heat Shock Factor 1 (Hsf1) occupancy and nascent-RNA transcription at genes bound and induced by Hsf1 in *S. cerevisiae* (n=42). Left: heatmaps depicting occupancy of Heat Shock Factor 1 (Hsf1) in non-

heat shock (NHS) and 5 min heat shock (HS) conditions, as determined by ChIP-seq (gray to teal). Right: heatmaps showing nascent-RNA densities in presence and absence of heat shock and Hsf1, as determined by NAC-seq (gray to red). Genes are sorted in the descending order of Hsf1 ChIP-seq counts (top to bottom). NAC-seq and Hsf1 ChIP-seq data were derived from (Pincus et al., 2018).
B) RNA Pol II (top) and Med15 (bottom) occupancy at Hsf1-dependent genes in NHS and HS conditions. For Med15 ChIP-seq analysis, cells were heat-shocked for 15 min at 37 ˚C (Sarkar et al., 2022). For Pol II, 5 min at 40 ˚C (Albert et al., 2019).
C) Top: percentage of overlap between Med15 ChIP-seq reads and Hsf1 in NHS and HS conditions. Bottom: percentage of Pol II distribution at Hsf1 target genes in NHS and HS conditions.
D) IGV browser views of Hsf1 (green), Med15 (magenta) and RNA Pol II (Rpb1; red) ChIP-seq densities as well as NAC-seq counts (black) at the indicated genes in NHS and HS conditions.
E) Left: physical maps of *BUD3* and the chromosomal transgene UAS_{HS}-*BUD3*. Right: Hsf1 and Med15-myc9 occupancy at $BUD3^{+}$ and UAS_{HS}-*BUD3* in NHS and 7.5 min HS conditions (n=2; qPCR=4).

Figure S2

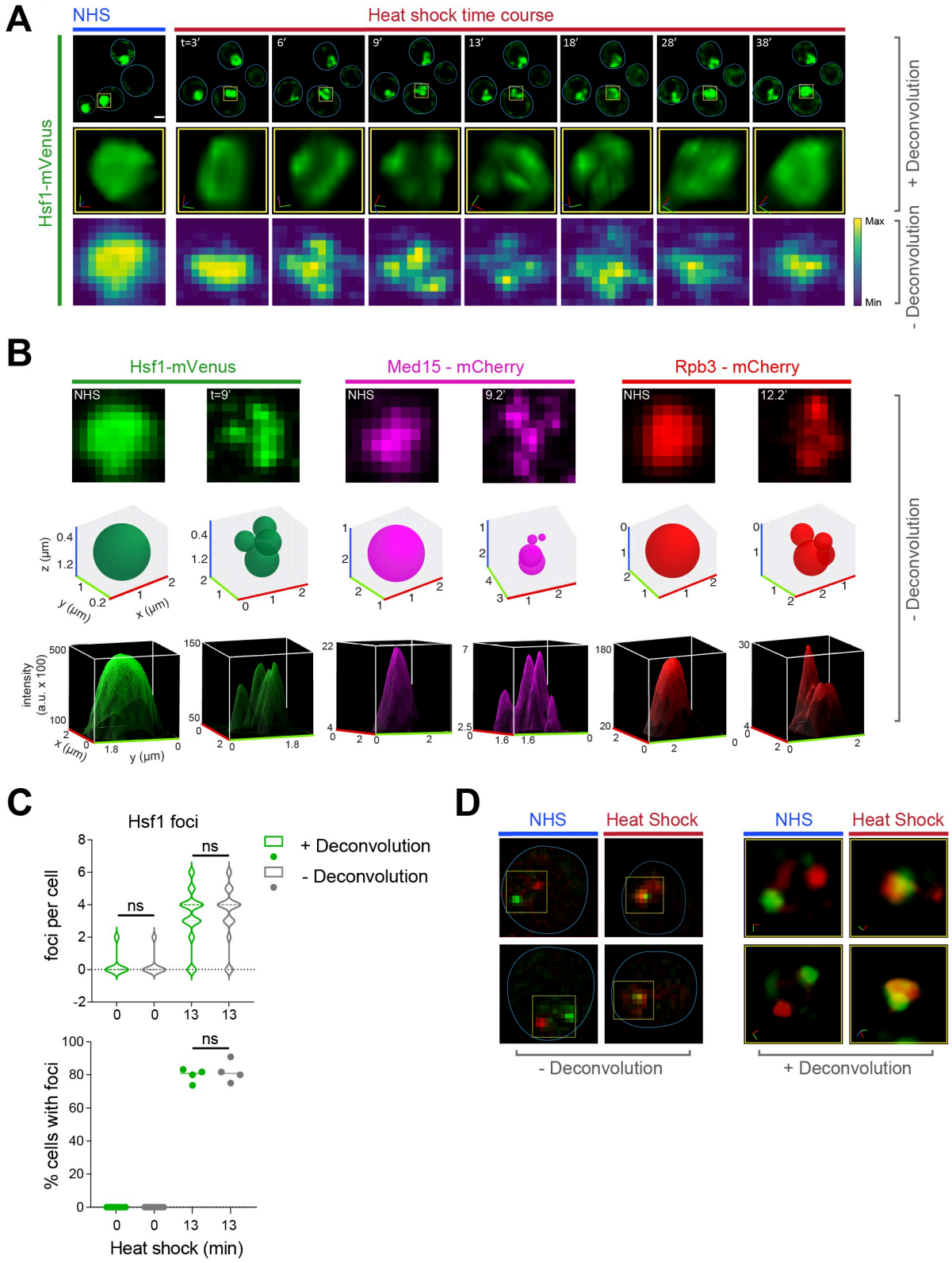

Figure A1.11.2. Deconvolution does not alter the results of image analysis

A) Time lapse live-cell imaging cells expressing Hsf1-mVenus before (NHS, 24-26°C) and following HS (39°C) for the times (t) indicated. Row 1: Representative planes are shown. Blue line highlights cell boundary. Scale bar is 2 µm. Row 2: enlarged view of the nucleus (see yellow box in Row 1). Shown is

the 3D volumetric rendering of each nucleus; x (red), y (green) and z (blue) axes are indicated. A single cell is followed throughout the heat shock time course. The images in top two rows are processed with deconvolution. Row 3: Images of cells shown in Row 2 processed without deconvolution.
B) Characterization of Hsf1, Med15 and Rpb3 foci in live cells. Top row: Representative planes of cells expressing Hsf1-mVenus, Med15-mCherry and Rpb3-mCherry before (NHS) and following HS for the times (t) indicated. Images are processed without deconvolution.
Middle row: 3D bubble charts of Hsf1, Med15 and Rpb3 foci that were detected and quantified using the automated FindFoci algorithm in cells shown in the top row. Bottom row: Visualization of Hsf1, Med15 and Rpb3 foci of cells shown in top row as 3D surface plots. Height of the plot corresponds to luminance of pixels within the image. x (red), y (green) and z (blue) axes are indicated. Analyses of the deconvolved images of the same cells are shown in Figure 1.
C) Top: number of Hsf1 foci per cell quantified from live imaging of cells expressing Hsf1-mVenus before (0 min) and following 13 min HS. Bottom: percentage of cells expressing Hsf1 foci. Foci were identified and counted using the automated FindFoci algorithm in images processed with or without deconvolution. 40-60 cells were evaluated per time point. Cells with >2 foci are counted as those containing foci for percentage evaluation. Shown are means +/- SD. ns (not significant), calculated using unpaired t test.
D) Live-cell imaging of a diploid strain expressing *HSP104-lacO$_{256}$*, *TMA10-tetO$_{200}$*, *LacI-GFP* and *TetR-mCherry*. Left: micrographs of representative cells under NHS and HS conditions. Blue line highlights cell boundary. A yellow bounding box indicates the nuclear region. Right: enlarged 3D renderings of representative cells shown in left (axes: x (red), y (green) and z (blue)). Images are processed with (right) or without (left) deconvolution.

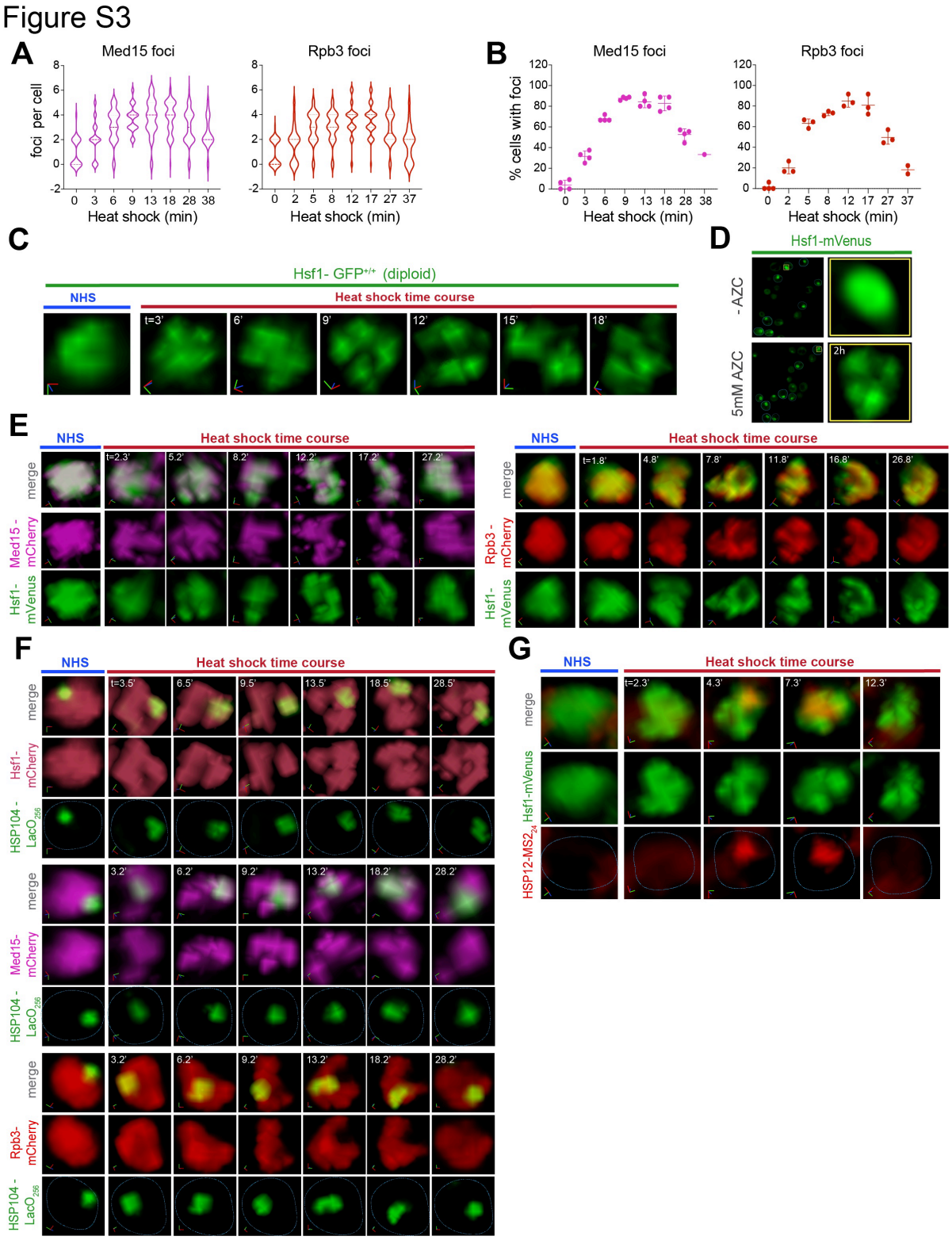

Figure A1.11.3. Hsf1 forms transcriptionally active clusters upon stress

A) Number of Med15 (left) and Rpb3 (right) foci per cell quantified from live imaging of cells expressing Med15-mCherry or Rpb3-mCherry before (0 min) and following HS for the times (t) indicated. Foci were detected and quantified using the automated FindFoci algorithm in ImageJ; 40-60 cells were evaluated per time point.

B) Percentage of cells expressing Med15-mCherry (left) and Rpb3-mCherry (right) foci. Foci were identified and counted as above. Cells with >2 foci were considered as those containing foci for percentage evaluation. Shown are means +/- SD.
C) Live-cell imaging of a diploid strain ASK741 expressing Hsf1-GFP before (NHS, 26.5°C) and following heat shock (39°C) for the times (t) indicated. A single cell is followed throughout the heat shock time course. Shown is the 3D volumetric rendering of each nucleus; x (red), y (green) and z (blue) axes are indicated. For HS images, z=11.
D) Live imaging of cells expressing Hsf1-mVenus in presence or absence of L-azetidine-2-carboxylic acid (AZC). Left: representative images before or following 2h of AZC treatment. Blue line highlights cell boundary. Right: enlarged view of the nucleus indicated in yellow boxes on the left. Cells were rendered and visualized by ClearVolume.
E) Live imaging of cells co-expressing Hsf1-mVenus and Med15-mCherry (left), or Hsf1-mVenus and Rpb3-mCherry (right). Shown are enlarged 3D rendered nuclei of representative cells that were imaged before (NHS) or following heat shock for the indicated times (t). Note that in each case, a single cell is followed through the heat shock time course. Images were rendered and visualized in arivis.
F) 3D rendered micrographs of Hsf1-mCherry (top), Med15-mCherry (middle) or Rpb3-mCherry (bottom) and the *HSP104-LacO*$_{256}$ gene locus before and following heat shock for the indicated times. For each cell type, a single cell is followed through the heat shock time course. Blue dotted line highlights nuclear boundary. 3D rendering and visualization was performed in arivis; x (red), y (green) and z (blue) axes are shown.
G) 3D rendered micrographs of Hsf1-mVenus and the MCP-mCherry labeled *HSP12-MS2*$_{24}$ mRNA before or following heat shock for the indicated times. Blue dotted line highlights nuclear boundary. A single cell is followed throughout the heat shock time course. 3D rendering and visualization was performed in arivis.

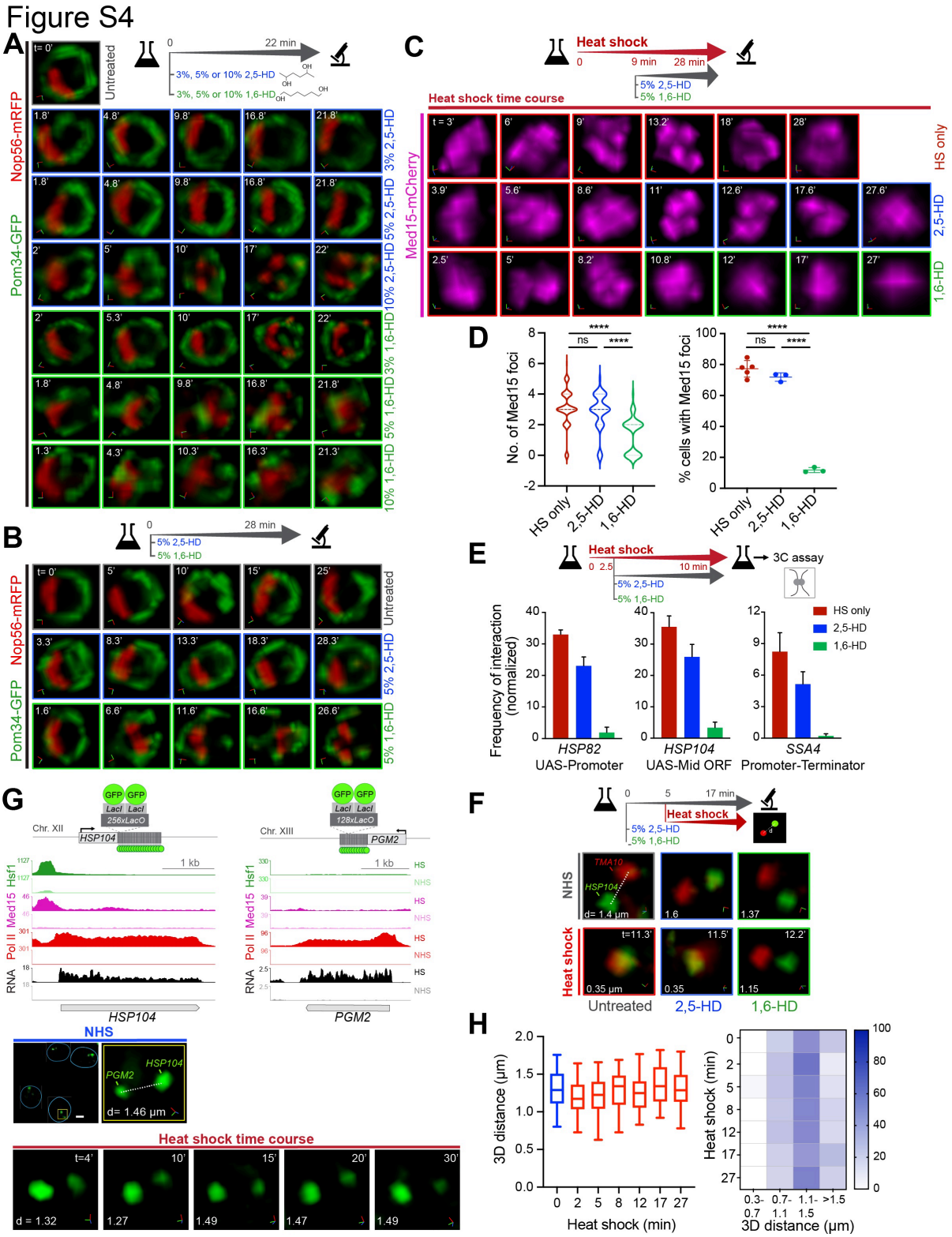

Figure A1.11.4. 1,6-hexanediol disrupts the Nucleolus, the nuclear pore complex, Mediator clusters and gene interactions within and between Hsf1 target genes

A) 3D rendered micrographs of representative cells in absence of alcohol (untreated) or treated with either 2,5-HD or 1,6-HD at 3, 5 or 10% concentrations. Row 1, right: experimental workflow. Rows 1-7: Live-cell imaging of diploid strain SCY712 (Nop56-RFP Pom34-GFP). Red, Nop56-RFP

(component of the nucleolus); Green, Pom34 (component of the nuclear pore complex). z =6. Note that in each row, a single cell is followed throughout the treatment.

B) Comparison of effects of 5% 2,5-HD vs. 5% 1,6-HD on the nucleolus and nuclear pore complex. Analysis and presentation as in A; z =7.

C) 3D rendered micrographs of a representative cell expressing Med15-mCherry subjected to heat shock for times (t) indicated in the absence of alcohol (top) or treated with either 2,5-HD (middle) or 1,6-HD (bottom) after 9 min of HS. Note that a different cell was imaged after alcohol treatment.

D) Number of Med15 foci (left) and the percentage of cells showing >2 foci (right) in presence or absence of HD. Cells expressing Med15-mCherry were heat-shocked for 9 min followed by treatment with either 2,5- or 1,6-hexanediol (or not). Cells were imaged after ~3 min of adding the drug. Foci were identified and counted using the automated FindFoci algorithm; 100-110 cells were evaluated per condition. ****P <0.0001; ns (not significant), P >0.05. P values were calculated by ANOVA followed by Tukey's post hoc analysis.

E) Intragenic interactions within indicated Hsf1 target genes as determined by TaqI-3C assay. Top: experimental workflow. Bottom: Intragenic contact frequencies detected within *HSP82*, *HSP104* and *SSA4* in cells heat-shocked and treated with either 2,5- or 1,6-hexanediol (or not). Depicted are means +SD (n=2; qPCR=4).

F) Intergenic interactions between *lacO*-tagged *HSP104* and *tetO*-tagged *TMA10* gene loci as determined by live-cell imaging analysis. Top: experimental workflow. Cells were pre-treated with either 5% 2,5- or 1,6-hexanediol (or not) for 5 min followed by heat shock of 12 min (or not) and imaged at times (t) indicated. Middle: representative images of cells that were pre-treated with either 1,6-HD or 2,5-HD or left untreated (right to left). Bottom: same as above, except cells were subjected to heat shock following treatment with alcohol (or not). Cells were rendered and visualized in arivis; x (red), y (green) and z (blue) axes are shown. d, 3D distances measured between signal centroids. Images were taken across 9 planes in z-direction; step size =0.5 µm.

G) Live-cell imaging of a diploid strain expressing *HSP104-lacO*$_{256}$, *PGM2-lacO*$_{128}$ and *LacI-GFP* (schematic, top). Middle: IGV browser views of Hsf1 (green), Med15 (magenta) and RNA Pol II (Rpb1; red) ChIP-seq densities as well as NAC-seq counts (black) at *HSP104* and *PGM2* in NHS and HS conditions; note the absence of significant Hsf1 and Med15 ChIP-seq peaks at *PGM2*. Bottom: time lapse live imaging of representative cells before and following heat shock for the times (t) indicated. Cell boundary is highlighted in blue. For NHS, an enlarged 3D view of the nuclear region is indicated within the yellow box. Axes x (red), y (green) and z (blue) are indicated. d is the 3D distance measured between signal centroids (two green spots).

H) Left: Distribution of 3D distances between *lacO*-tagged *HSP104* and *PGM2* gene loci in cells subjected to heat shock for times indicated. Right: Heat map depicting percentage of cells with tagged gene loci within indicated 3D distances binned at intervals of 0.4 µm. 45-60 cells were evaluated per condition.

Figure S5

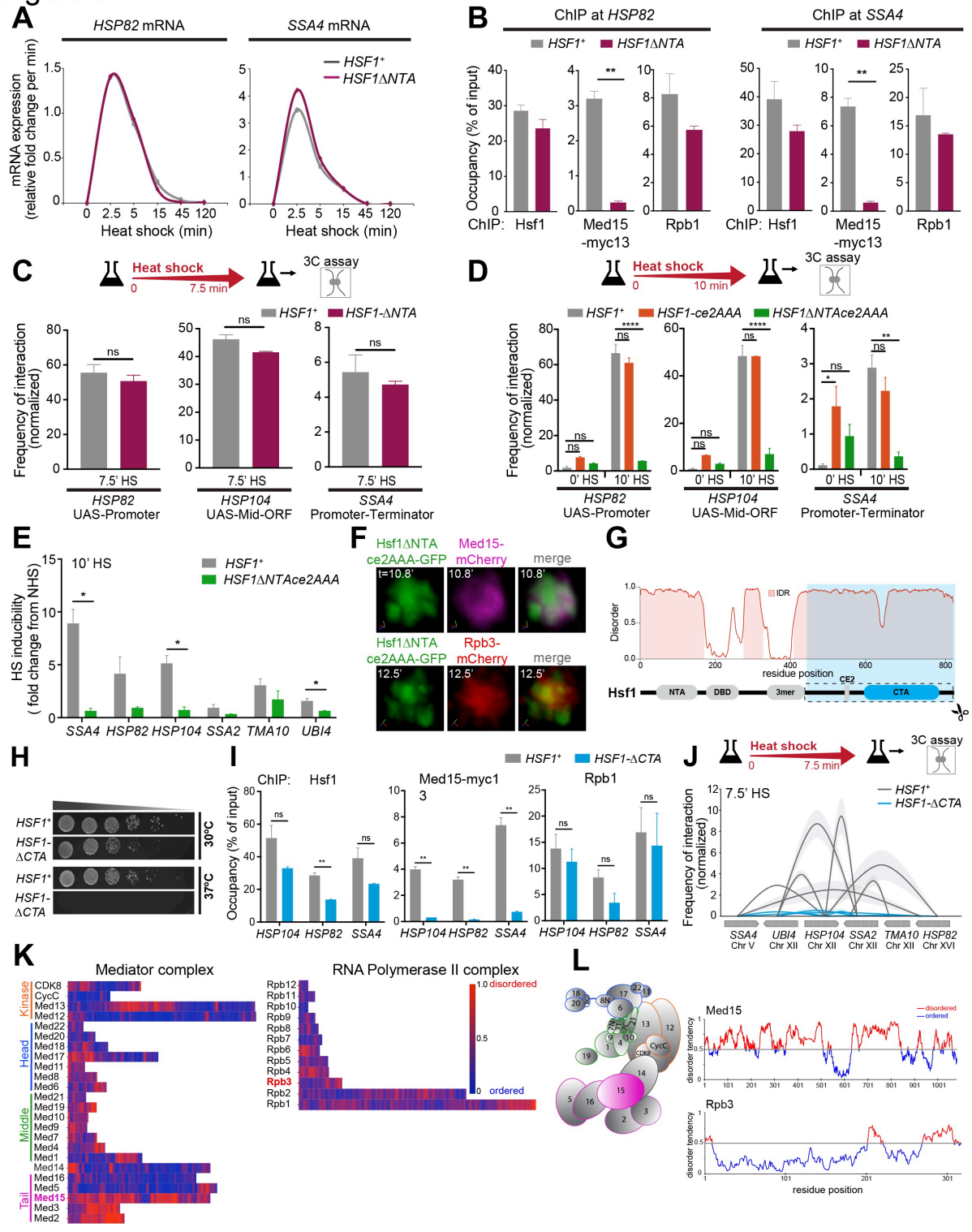

Figure A1.11.5. Stable Mediator occupancy is necessary for driving intergenic interactions between Hsf1-target genes

A) Transcription rates of *HSP82* and *SSA4* in *HSF1*$^+$ and *HSF1-ΔNTA* isogenic strains during a heat shock time course, as deduced from RT-qPCR.

B) Hsf1 and Med15-myc13 ChIP at the UASs and Rpb1 ChIP at promoters of *HSP82* and *SSA4* in wild type and Hsf1-ΔNTA strains heat-shocked for 7.5 min. Depicted are means + SD. **, P <0.01 (calculated using two-tail t-test).

C) Intragenic looping and crumpling interactions within indicated Hsf1 target genes in WT and *HSF1-ΔNTA* cells heat-shocked for 7.5 min. Top: experimental workflow of TaqI-3C assay. Bottom: Intragenic contact frequencies detected within *HSP82*, *HSP104* and *SSA4* in HS conditions. Depicted are means +SD (n=2; qPCR=4). ns (not significant), $P > 0.05$ (calculated using two-tail t test).
D) Intragenic interactions within indicated Hsf1 target genes in WT, *HSF1-ce2AAA* and *HSF1-ΔNTAce2AAA* cells under NHS and 10 min-HS conditions. Top: experimental workflow of TaqI-3C assay. Bottom: Intragenic contact frequencies detected within *HSP82*, *HSP104* and *SSA4* in NHS and HS conditions. Depicted are means +SD (n=2; qPCR=4) ****$P < 0.0001$; **$P < 0.01$; *$P < 0.05$; ns (not significant), $P > 0.05$. P values were calculated by ANOVA followed by Tukey's post hoc analysis.
E) Heat shock inducibility in WT and *HSF1-ΔNTAce2AAA* cells heat shocked for 10 min, as deduced from fold change mRNA expression of representative HSR genes. Depicted are means + SD (n=2; qPCR=4). *, $P < 0.05$ (calculated using two-tail t-test).
F) Live imaging of cells co-expressing Hsf1ΔNTAce2AAA-GFP with Med15-mCherry (top) or Rpb3-mCherry (bottom) under HS conditions (t=time point of HS).
G) Domain map and prediction of disorder in Hsf1. Top: predicted value of disorder tendency for each amino acid within Hsf1 obtained using Metapredict V2. Bottom: Domain map of Hsf1. NTA, N-terminal activation domain; DBD, DNA binding domain; 3mer, trimerization domain; CE2, conserved element 2 domain; CTA (blue), C-terminal activation domain. Box: truncation mutation in the Hsf1-ΔCTA mutant.
H) Spot dilution analysis of *HSF1*$^+$ and *HSF1-ΔCTA* cells. Five-fold serial dilutions of cells were spotted onto YPD. Plates were incubated at 30°C or 37°C for 30 h.
I) Hsf1 and Med15-myc13 ChIP at the UASs and Rpb1 ChIP at promoter regions of *HSP104*, *HSP82* and *SSA4*. Wild type and Hsf1-ΔCTA strains were heat-shocked for 7.5 min, then processed for ChIP. Depicted are means + SD (n=2; qPCR=4). **, $P < 0.01$; ns (not significant), $P > 0.05$ (calculated using two-tail t-test).
J) Intergenic contacts (solid arcs) between indicated Hsf1 target gene pairs for *HSF1*$^+$ and *HSF1-ΔNTA* strains. Cells were heat-shocked for 7.5 min, then processed for TaqI-3C. Values indicate normalized interaction frequencies. Gene regions are depicted as UAS, promoter, mid-ORF and terminator (from blunt to arrowhead direction). Data are derived from two independent biological replicates; qPCR=4. Depicted are means +/- SD (shaded region around solid arcs).
K) *In silico* analysis of disorder prediction in the Mediator and RNA Pol II subunits. Shown are heat maps of predicted values of disorder for each amino acid of a subunit. Heat maps are presented from amino to carboxyl terminus (left to right). Disorder tendencies were calculated using IUPRED. Values <0.5 (blue) are ordered and >0.5 (red) are disordered.
L) Left: yeast Mediator subunits in Head (blue), Middle (green), Tail (magenta) and Kinase (orange) modules. Med14 is a scaffold (black). Right: prediction of disorder in Med15 and Rpb3 protein subunits of the Mediator and RNA Pol II complexes, respectively. The plots score predicted values of disorder tendency for each amino acid within Med15 or Rpb3, as per IUPRED. Values <0.5 (blue) are ordered and >0.5 are disordered (red).